REACTIONS OF SILYLENES WITH CARBONYL COMPOUNDS

A STUDY OF THE REACTIONS OF TRANSIENT SILYLENES WITH CARBONYL COMPOUNDS IN SOLUTION

By: MICHAEL SON, B.Sc. (Honours)

A Thesis

Submitted to the School of Graduate Studies

in Partial Fulfillment of the Requirements

for the Degree Master of Science

McMaster University

MASTER OF SCIENCE (2019) McMaster University

(Chemistry and Chemical Biology) Hamilton, Ontario

TITLE: A Study of the Reactions of Transient Silylenes with Carbonyl Compounds in Solution

AUTHOR: Michael Son

B. Sc. (Honours, McMaster University)

SUPERVISOR: Professor William J. Leigh

NUMBER OF PAGES xxxiv, 159

ABSTRACT

The reactions of the transient silylenes $SiMe_2$, $SiPh_2$, and $SiMes_2$ with enolizable and non-enolizable carbonyl compounds have been studied in solution by steady state and laser flash photolysis methods.

These reactions have been shown to involve the initial formation of a silacarbonyl ylide intermediate, which has been detected directly in several cases and found to exhibit a broad absorption band in the $\lambda_{max} \approx 500 - 650$ nm range in solution. The ensuing chemistry of these intermediates depends on the nature of the carbonyl compound.

The reactions of silylenes with enolizable carbonyl compounds generate ene-adducts formed via H-migration in the silacarbonyl ylide. Kinetic isotope effects were investigated in the reactions of the three silylenes with acetone(-d_6) and camphor(-d_2). The results show an isotope effect for camphor, which indicates the H-migration step is the rate-determining step in the reaction. The effects of ring strain in the carbonyl compound were investigated with dicyclopropyl ketone, relative to diisopropyl ketone. The introduction of ring strain causes a systematic decrease in the rate constants.

On the other hand, the reactions of silylenes with non-enolizable carbonyl compounds proceed via cycloaddition. The reactions of $SiMes_2$ with 2,2,5,5-tetramethylcyclopentanone and $SiPh_2$ with 2-adamantanone afford [1+2] and [1+2+2]-cycloadducts, respectively. The kinetic behavior of the silylene and silacarbonyl ylide of these systems are reflective of their corresponding reaction mechanism. However, the kinetic behavior of the silacarbonyl ylides in the reactions of $SiMe_2$ with $SiPh_2$ with

2,2,5,5-tetramethylcyclopentanone and di-*tert*-butyl ketone are more complex to interpret because a stable cycloadduct is not observed.

The trends in the reactivity of the three silylenes, and in some cases the silacarbonyl ylides, with the series of enolizable and non-enolizable carbonyl compounds studied in our group are discussed in this thesis.

ACKNOWLEDGEMENTS:

I would like to express my deepest appreciation to my supervisor Professor William J. Leigh (Willie) for his patience, motivation, and immense knowledge. His guidance helped me throughout my research and has allowed me to grow as a researcher in the field. I could not imagine having had a better advisor and mentor.

I would like to thank my committee member Professor Michael A. Brook for his insightful comments. In addition, thank you to my external Professor Ignacio Vargas-Baca.

Thanks to all of the staff members in the department, Dr. Bob Berno and Dr. Hilary Jenkins of the NMR facility, Dr. Kirk Green and Dr. Fan Fei of the Mass Spec. facility, and Dr. Jim Britten of the X-Ray Diffraction facility for their experimental assistance.

To my colleagues - Dr. Ian R. Duffy and Ketha Jeyakanthan – I thank you for your scientific and "everyday life" discussions, guiding me in the right direction, and for all the fun we had together in the lab. Also, I am grateful to my close friends Peter Ho and Sam Ros for their friendship and advice.

I would like to thank Claire Browne and Alex Sever for their hard work and large contributions to the research. In addition, I would also like to thank all of the undergraduate students I had met that have kept me sane throughout my years and kept me in the loop of what is trending. All of you are lit!

And finally, I would like to thank my family for their love, support, and understanding which gave me strength to carry me through all the difficulties over the years.

Thanks for all your encouragement!

TABLE OF CONTENTS:

	List of Figures	xi
	List of Tables	xxiii
	List of Compound Numbers	xxvi
	List of Abbreviations and Symbols	xxxi
	Contributions to the Work	xxxiii
Chapter 1 – Introduction:		1
1.1	Overview	1
1.2	Nomenclature	1
1.3	Structure and Properties of Silylenes	2
1.4	Generation of Silylenes	4
1.5	Stability of Silylenes	6
1.6	Reactions of Silylenes	9
1.6.1	Dimerization	9
1.6.2	Bond Insertion Reactions	9
1.6.3	Addition to Unsaturated C-C Bonds	11
1.6.4	Complexation with Lewis Bases	13
1.6.5	Reactions with Carbonyl Compounds	14
1.7	Techniques Used for the Study of Transient Silylenes	22
1.8	Tools for Elucidation of Reaction Mechanisms	23
1.8.1	Kinetic Isotope Effect	23
1.8.2	Variable Temperature and Determination of Activation Parameters	24

1.9 Goals and Outline of the Thesis 26

1.10 References 29

Chapter 2 - Kinetic and Thermodynamic Studies of the Reactions of Silylenes with Enolizable Carbonyl Compounds: 34

2.1 Overview 34

2.2 Previous Studies in Our Group 35

2.3 Scope of the Study 46

2.4 Kinetic Isotope Effects 46

2.4.1 Reactions of Silylenes with Camphor-3,3-d_2 46

2.5 Reactions of Silylenes with Other Enolizable Carbonyl Compounds 50

2.5.1 Reaction of $SiPh_2$ with Cyclopentanone 50

2.5.2 Reaction of $SiMe_2$ with Norcamphor 51

2.5.3 Reactions of Silylenes with Dicyclopropyl Ketone 52

2.6 Discussion 57

2.7 Conclusion 63

2.8 Supporting Information 65

2.9 References 70

Chapter 3 – Kinetic and Thermodynamic Studies of the Reactions of Silylenes with Non-Enolizable Carbonyl Compounds 71

3.1 Overview 71

3.2 Previous Studies in Our Group 71

3.3 Scope of the Study 77

3.4 Product Studies 79

3.4.1	Reaction of $SiMes_2$ with 2,2,5,5-Tetramethylcyclopentanone (**8**)	79
3.4.2	Steady State Photolysis of **3** in the Presence of Di-*tert*-butyl Ketone	86
3.4.3	Reaction of $SiPh_2$ with 2-Adamantanone (**5**)	89
3.4.4	Reaction of $SiPh_2$ with 2,2,5,5-Tetramethylcyclopentanone (**8**)	94
3.5	Laser Flash Photolysis	96
3.5.1	Reactions of Silylenes with 2-Adamantanone (**5**)	96
3.5.2	Reactions of Silylenes with 2,2,5,5-Tetramethylcyclopentanone (**8**)	102
3.6	Laser Flash Photolysis of Oxasilirane (**10**)	114
3.6.1	Laser Flash Photolysis of Oxasilirane (**10**)	114
3.6.2	Reaction of $SiMes_2$ with 1,1,3,3-Tetramethyl-2-indanone (**7**)	116
3.7	Discussion	117
3.8	Conclusion	123
3.9	Supporting Information	125
3.10	References	139
Chapter 4 – Conclusions and Future Work		140
4.1	Conclusions	140
4.2	Future Work	142
Chapter 5 – Experimental		145
5.1	General	145
5.2	Solvents	146
5.3	Commercial Reagents	147
5.4	Laser Flash Photolysis	148

5.5	Steady State Photolysis	149
5.6	Synthesis	150
5.6.1	Synthesis of 2,2-Dimesityl-1,1,1,3,3,3-hexamethyltrisilane	150
5.6.2	*Synthesis of Camphor-3,3-d_2*	151
5.6.3	*Synthesis of 2,2,5,5-Tetramethylcyclopentanone*	152
5.6.4	*Synthesis of 1,1,3,3-Tetramethyl-2-indanone*	153
5.6.5	*Synthesis of 2',2'-Dimesityl-1,1,3,3-tetramethyl-1,3-dihydrospiro[indene-2,3'-[1,2]oxasilirane* (**7**)	154
5.6.6	*Synthesis of 3,5-Diadamantyl-2,4-dioxa-1,1-diphenylsilacyclopentane* (**8**)	154
5.6.7	*Synthesis of 2,2-Dimesityl-4,4,7,7-tetramethyl-1-oxa-2-silaspiro[2.4]heptane* (**9**)	155
5.7	Compounds Identified *in-situ*	157
5.8	References	159

LIST OF FIGURES

Figure 1.1.	Electronic structures of the lowest energy singlet and triplet states of tetrylenes	3
Figure 1.2.	The zero-point energy difference between C-H and C-D bonds between the reactant and transition state changes as a function of the potential energy of the reaction and the corresponding transition state of the H-transfer (a) endothermic reaction (b) exothermic reaction (c) thermoneutral reaction. Figures were obtained from ref	24
Figure 2.1.	^{1}H NMR spectra of a solution of **2** (0.05 M), camphor (**4a**) 0.05 M, and 0.01 M hexamethyldisilane in C_6D_{12} (a) before and (b) after 20 mins of photolysis. (*Data recorded by C. Browne*)	37
Figure 2.2.	The open squares are the spectra of the silylenes (a) $SiMe_2$, (b) $SiPh_2$, and (c) $SiMes_2$, while the insets are the individual traces of the decay of the corresponding silylene and the growth of the corresponding disilene. (a) Transient absorption spectra recorded 0.09 - 0.12 μs (○) and 1.4 - 1.5 μs (■) after the laser pulse by laser flash photolysis of a hexanes solution of **1**. The inset shows transient decay traces recorded at 360 and 470. (b) Transient absorption spectra recorded 0.19 - 0.26 μs (○) and 4.2 - 4.3 μs (■) after the laser pulse by laser flash photolysis of a hexanes solution of **2**. The inset shows transient decay traces recorded at 460 and 530. (c) Transient absorption spectra recorded 0.0 - 1.3 μs (○) and 107 - 108 μs (■) after the laser pulse, from laser flash photolysis of a hexanes solution of **3**. The inset shows transient decay traces recorded at 420 and 570.	38
Figure 2.3.	(a) Transient absorption spectra recorded 0.19 – 0.22 (○) and 0.56 – 0.59 μs (□) after the laser pulse by laser flash photolysis of **1** in the presence of 0.4 mM 2,4-dimethyl-3-pentanone (**7**) in deoxygenated hexanes at 25^{o}C. The inset shows a transient decay trace recorded at 470 nm. (b) Plot of k_{decay} vs. ketone concentration for $SiMe_2$ monitored at 470 nm. The solid line is the linear least-squares fit of the data to eq. 2.4. (*Data recorded by C. Browne*)	39
Figure 2.4.	(a) Transient absorption spectra recorded 0.11 – 0.12 μs (○) and 1.2 – 1.3 μs (□) after the laser pulse by laser flash	41

photolysis of **2** in the presence of 10 mM 2,4-dimethyl-3-pentanone (**7**) in deoxygenated hexanes at 25°C. The dashed line spectrum (-) shows the difference between the spectra recorded at 0.11 – 0.12 μs and 1.2 – 1.3 μs after the laser pulse. The inset shows transient decay traces recorded at 300 and 600 nm. (b) Plot of k_{decay} vs. ketone concentration for the $SiPh_2$-**7** silacarbonyl ylide monitored at 600 nm. The solid line is the non-linear least-squares analysis of the data according to eq. 2.6. (*Data recorded by C. Browne*)

Figure 2.5. Plots of k_{decay} vs. ketone concentration for (a) $SiMe_2$ monitored at 470 nm and (b) $SiPh_2$-**4a** silacarbonyl ylide monitored at 600 nm at 25°C. The solid line is the non-linear least-squares analysis of the data according to eq. 2.6. (*Data recorded by C. Browne*) 43

Figure 2.6. Eyring plots associated with the H-migration step from the silacarbonyl ylide in the reaction of $SiMe_2$ (□) and $SiPh_2$ (○) containing 5 mM camphor (**4a**), monitored at 600 nm, at temperatures of 0.0 – 50.0°C. The slopes and intercepts are as follows: (□): slope = $(-3.57 \pm 0.5) \times 10^3$ K^{-1} and intercept = $(2.30 \pm 0.1) \times 10^1$ and (○): slope = $(-3.09 \pm 0.2) \times 10^3$ K^{-1} and intercept = $(1.77 \pm 0.1) \times 10^1$. 44

Figure 2.7. Plot of k_{decay} vs. [camphor-L_2] (L = H or D) for the $SiMe_2$-(□ and ■) and $SiPh_2$- (❍ and ●) camphor-L_2-derived silacarbonyl ylide monitored at 600 nm. The solid line is the non-linear least-squares analysis of the data according to equation 2.6. 47

Figure 2.8. Plot of k_{decay} vs. [camphor-d_2] for the $SiMe_2$-camphor-d_2 silacarbonyl ylide, monitored at 600 nm. The solid line is the non-linear least-squares fit of the data to eq. 2.6. The inset shows the plot of k_{decay} vs. [camphor-d_2] from 0 – 100 mM. 49

Figure 2.9. (a) Transient absorption spectra recorded 0.15 – 0.16 (○) and 0.28 – 0.30 μs (□) after the laser pulse by laser flash photolysis of **2** in the presence of 1 mM cyclopentanone in deoxygenated hexanes at 25°C. The inset shows transient decay traces recorded at 530 nm. (b) Plot of k_{decay} vs. ketone concentration for $SiPh_2$ monitored at 530 nm. The solid line is the result of linear least-squares analysis of the data according to eq. 2.4. 51

Figure 2.10. (a) Transient absorption spectra recorded 0.15 – 0.16 (○) and 0.28 – 0.29 μs (□) after the laser pulse by laser flash photolysis of **1** in the presence of 1 mM norcamphor in deoxygenated hexanes at 25°C. The inset shows transient decay traces recorded at 470 and 600 nm. (*Data recorded by C. Browne*) (b) Plot of k_{decay} vs. ketone concentration for the $SiMe_2$-norcamphor silacarbonyl ylide monitored at 600 nm. The solid line is the non-linear least-squares fit of the data to eq. 2.6. 52

Figure 2.11. Concentration vs. time plots for the photolysis (254 nm) of **1** (23 mM) in the presence of **14** (50 mM) in cyclohexane-d_{12}. Shown is the depletion of **1** (●) and **14** (■) with time irradiated and the formation of **15** (○) and the silyl enol ether **16** (□). The slopes are as follows: (**1**; ●): (-0.43± 0.05) mM/min, (**14**; ■) :(-0.57 ± 0.05) mM/min, (**15**; ○):(0.29 ± 0.06) mM/min, (**16**; □): (0.23 ± 0.01) mM/min. 53

Figure 2.12. ^1H NMR spectra of a solution of **1** (0.023 M), 0.05 M dicyclopropyl ketone (**14**), and 0.01 M hexamethyldisilane in C_6D_{12} (a) before and (b) after 35 mins of photolysis (* unreactive impurity) 54

Figure 2.13. (a) Transient absorption spectra recorded 272 – 336 ns (○) and 1.39 – 1.47 μs (□) after the laser pulse by laser flash photolysis of **1** in the presence of 6 mM dicyclopropyl ketone (**14**) in deoxygenated hexanes at 25°C. The inset shows transient decay traces recorded at 300 and 600 nm. (b) Plot of k_{decay} vs. ketone concentration of the $SiMe_2$-**14** silacarbonyl ylide monitored at 600 nm. The solid line is the non-linear least-squares fit of the data to eq. 2.6. 55

Figure 2.14. (a) Transient absorption spectra recorded 0.16 – 0.80 ns (○) and 4.32 – 5.28 μs (□) after the laser pulse by laser flash photolysis of **2** in the presence of 1 mM dicyclopropyl ketone in deoxygenated hexanes at 25°C. The inset shows transient decay traces recorded at 300 and 600 nm. (b) Plot of k_{decay} vs. ketone concentration for the $SiPh_2$-**14** silacarbonyl ylide monitored at 600 nm. The dashed line is the average k_2 value. 56

Figure 2.15. (a) Transient absorption spectra recorded 0.14 – 0.15 (○) and 0.56 – 0.59 μs (□) after the laser pulse by laser flash photolysis of **3** in the presence of 10 mM dicyclopropyl ketone (**14**) in deoxygenated hexanes at 25°C. The dashed line 57

spectrum (-) shows the difference between the two spectra. The inset shows transient decay traces recorded at 300 and 580 nm. (b) Plot of k_{decay} vs. ketone concentration for $SiMes_2$, monitored at 580 nm. The solid line is the linear least-squares analysis of the data according to eq. 2.4.

Figure S2.1. Arrhenius plots associated with the product-forming step from the silacarbonyl ylide in the reactions of $SiMe_2$ (□) and $SiPh_2$ (○) with 5 mM camphor (**4a**), monitored at 600 nm, at temperatures of 0.0 – 50.0°C. The slopes of the lines are as follows:(□): $-E_a/R = (-1.68 \pm 0.11) \times 10^3$ K^{-1} and (○): $-E_a/R = (-1.48 \pm 0.11) \times 10^3$ K^{-1}. 65

Figure S2.2. (a) Transient absorption spectra recorded 0.12 – 0.13 (○) and 0.44 – 0.45 μs (□) after the laser pulse by laser flash photolysis of **2** in the presence of 0.8 mM acetone-d_6 in deoxygenated hexanes at 25°C. The inset shows transient decay traces recorded at 300 and 530 nm. (b) Plot of k_{decay} vs. ketone concentration for $SiPh_2$ monitored at 530 nm. The solid line is the linear least-squares fit of the data to eq. 2.4. 65

Figure S2.3. (a) Transient absorption spectra recorded 0.10 – 0.12 (○) and 0.44 – 0.45 μs (□) after the laser pulse by laser flash photolysis of **3** in the presence of 1 mM acetone-d_6 in deoxygenated hexanes at 25°C. The inset shows transient decay traces recorded at 300 and 580 nm. (b) Plot of k_{decay} vs. ketone concentration for $SiMes_2$ monitored at 580 nm. The solid line is the linear least-squares fit of the data to eq. 2.4. 66

Figure S2.4. (a) Transient absorption spectra recorded 0.12 – 0.15 (○) and 0.56 – 0.59 μs (□) after laser pulse by laser flash photolysis of **1** in the presence of 5 mM camphor-d_2 in deoxygenated hexanes at 25°C. The inset shows transient decay traces recorded at 470 and 600 nm. (b) Plot of k_{decay} vs. ketone concentration for the $SiMe_2$-**4b** silacarbonyl ylide monitored at 600 nm. The solid line is the non-linear least-squares fit of the data to eq. 2.6. 66

Figure S2.5. (a) Transient absorption spectra recorded 0.00 – 0.80 (○) and 13.92 – 14.72 μs (□) after laser pulse by laser flash photolysis of **2** in the presence of 4 mM camphor-d_2 in deoxygenated hexanes at 25°C. The inset shows transient decay traces recorded at 290 and 600 nm. (b) Plot of k_{decay} vs. ketone concentration for the $SiPh_2$-**4b** silacarbonyl ylide 67

monitored at 600 nm. The solid line is the non-linear least-squares fit of the data to eq. 2.6.

Figure S2.6. (a) Transient absorption spectra recorded 0.11 – 0.13 (○) and 2.80 – 2.83 μs (□) after laser pulse by laser flash photolysis of **3** in the presence of 3.90 mM camphor-d_2 in deoxygenated hexanes at 25°C. The dashed line spectrum (-) shows the difference between the two spectra. The inset shows transient decay trace recorded at 580 nm. (b) Plot of k_{decay} vs. ketone concentration for $SiMes_2$ monitored at 580 nm. The solid line is the linear least-squares fit of the data to eq. 2.4. 67

Figure 3.1. (a) Transient absorption spectra recorded 0.14 – 0.17 μs (○) and 0.56 – 0.59 μs (□) after the laser pulse by laser flash photolysis of **1** in the presence of 0.6 mM pivalaldehyde in deoxygenated hexanes at 25°C. The inset shows transient decay trace recorded at 470 nm. (b) Plot of k_{decay} vs ketone concentration for $SiMe_2$ monitored at 470 nm. The solid line is the linear least-squares regression of the data according to eq. 3.1. 73

Figure 3.2. Transient absorption spectra recorded 0.13 – 0.26 μs (○) and 1.66 – 1.86 μs (□) after laser pulse by laser flash photolysis of **1** in the presence of 10 mM 2-adamantanone in deoxygenated hexanes at 25°C. The inset shows transient decay traces recorded at 290 and 600 nm. (*Data recorded by C. Browne*) 74

Figure 3.3. (a) Plot of k_{decay} vs ketone concentration for $SiMe_2$ and the $SiMe_2$-**5** silacarbonyl ylide monitored at 470 (□) and 570 (○) nm. The solid line is the linear least-squares fit of the data to eq. 3.1. (b) Decay trace of the silylene (monitored at 470 nm) in the presence of 0 and 0.5 mM 2-adamantnone. The red solid line is the non-linear regression of the one-phase decay. (*Data recorded by C. Browne*) 75

Figure 3.4. Plot of k_{decay} vs ketone concentration from laser flash photolysis of **2** in the presence of **5**, monitoring transient absorption at 520 nm. 76

Figure 3.5. Plot of k_{decay} vs ketone concentration for $SiMes_2$ monitored at 580 nm. The solid line is the linear least-square fit to eq. 3.1. 77

Figure 3.6.	^{1}H NMR spectra of a solution of 0.025 M **3**, 0.05 M **8**, and 0.01 M bis(trimethylsilyl)methane in C_6D_{12} (a) before and (b) after 35 mins of photolysis. The inset shows the region of the ^{1}H NMR spectrum between 1.20 – 1.80 ppm.	80
Figure 3.7.	Concentration vs. time plots for the photolysis of **3** in the presence of 2,2,5,5-tetramethylcyclopentanone (**8**) in cyclohexane-d_{12}. Shown is the depletion of **3** (●) and **8** (■) over irradiation time, along with the formation of **11** (○) and oxasilirane **12** (□). Slopes are as follows: (**3**; ●): (-0.51± 0.05) mM/min, (**8**; ■): (-0.20 ± 0.03) mM/min, (**11**; ○): (0.36 ± 0.04) mM/min, **(12**; □): (0.18 ± 0.01) mM/min.	80
Figure 3.8.	^{1}H NMR spectrum of **12** in $CDCl_3$.	82
Figure 3.9.	The proton (left) and carbon (right) assignments, used for Tables 3.3 and 3.4, for compound **12**.	82
Figure 3.10.	DEPTQ ^{13}C NMR spectrum of **12** in $CDCl_3$ (-CH and -CH_3 groups are negatively phased and -C and -CH_2 groups are positively phased).	84
Figure 3.11.	ORTEP drawing and labeling scheme of **12**. Hydrogen atoms are omitted for clarity.	85
Figure 3.12.	^{1}H NMR spectra of a solution of 0.05 M **3**, 0.05 M **6**, and 0.01 M bis(trimethylsilyl)methane in C_6D_{12} (a) before and (b) after 60 mins of photolysis (*ca.* 70% conversion of **3**).	87
Figure 3.13.	Concentration vs. time plots for the photolysis of **3** in the presence of di-*tert*-butyl ketone (**6**) in cyclohexane-d_{12}. Shown is the depletion of **3** (●) and **6** (■) over irradiation time, along with the formation of **11** (○) and oxasilirane **13** (□). Slopes are as follows: (**3**; ●): (-0.62± 0.03) mM/min, (**6**; ■): (-0.39 ± 0.02) mM/min, (**11**; ○): (0.35 ± 0.02) mM/min, (**13**; □): (0.21 ± 0.01) mM/min.	88
Figure 3.14.	DEPTQ ^{13}C NMR spectrum of a solution of 0.05 M **3**, 0.05 M **6**, and 0.01 M bis(trimethylsilyl)methane in C_6D_{12} after 60 mins of photolysis.	88
Figure 3.15.	The proton (left) and carbon (right) assignments, used for Tables 3.5 and 3.6, for compound **13**.	89

Figure 3.16.	^{1}H NMR spectra of a C_6D_{12} solution of 0.053 M **2** containing 0.11 M of **5**, and 0.01 M hexamethyldisilane (a) before and (b) after 45 mins of photolysis (*ca.* 40% conversion of **2**). (*Data recorded by A. Sever*)	90
Figure 3.17.	Concentration vs. time plots for the photolysis of **2** in the presence of 2-adamantanone (**5**) in cyclohexane-d_{12}. Shown is the depletion of **2** (●) and **5** (■) with irradiation time and the formation of **14** (○) and dioxasilacyclopentane (**9c**) (□). Slopes are as follows: (**2**; ●): (-0.11± 0.01) mM/min, (**5**; ■): (-0.22 ± 0.01) mM/min, (**14**; ○): (0.11 ± 0.01) mM/min, (**9c**; □): (0.95 ± 0.01) x 10^{-1} mM/min. (*Data recorded by A. Sever*)	90
Figure 3.18	^{1}H NMR spectrum of **9c** in $CDCl_3$.	91
Figure 3.19	The proton (left) and carbon (right) assignments, used for Tables 3.7 and 3.8, for compound **9c**.	92
Figure 3.20.	DEPTQ ^{13}C NMR spectrum of **9c** in $CDCl_3$ (-CH and -CH_3 groups are negatively phased and -C and -CH_2 groups are positively phased).	93
Figure 3.21.	^{1}H NMR spectra of a C_6D_{12} solution of 0.05 M **1**, 0.12 M of **4**, and 0.01 M hexamethyldisilane (a) before and (b) after 60 mins of photolysis (*ca.* 40% conversion of **1**).	95
Figure 3.22.	Concentration vs. time plots for the photolysis of **2** in the presence of 2,2,5,5-tetramethylcyclopentanone (**8**) in cyclohexane-d_{12}. Shown is the depletion of **2** (●) and **8** (■) and the formation of **14** (○) over time irradiated. Slopes are as follows: (**2**; ●): (-0.90 ± 0.01) mM/min, (**8**; ■): (-0.28 ± 0.01) mM/min, (**14**;○): (0.95 ± 0.01) mM/min.	95
Figure 3.23.	(a) Transient absorption spectra recorded 0.13 – 0.26 μs (○) and 1.66 – 1.86 μs (□) after the laser pulse by laser flash photolysis of **1** in the presence of 10 mM 2-adamantanone in deoxygenated hexanes at 25°C. The inset shows transient decay traces recorded at 300 and 570 nm. (b) Plot of k_{decay} vs ketone concentration (0 – 5mM) for the $SiMe_2$-**5** silacarbonyl ylide monitored at 600 nm. The solid line is the non-linear least-squares fit of the data to eq. 3.9.	97

Figure 3.24. Plot of k_{decay} vs ketone concentration for the $SiMe_2$-**5** silacarbonyl ylide monitored at 600 nm. The solid line is the linear least-squares regression of the data according to eq. 3.11. 99

Figure 3.25. (a) Transient absorption spectra recorded 0.19 – 0.32 μs (○) and 3.65 – 4.03 μs (□) after the laser pulse by laser flash photolysis of **2** in the presence of 5 mM 2-adamantanone in deoxygenated hexanes at 25°C. The dashed line spectrum (-) shows the difference between the two spectra. The inset shows transient decay traces recorded at 300 and 570 nm. (b) Plot of k_{decay} vs ketone concentration (0 – 5mM) for the $SiPh_2$-**5** silacarbonyl ylide monitored at 600 nm. The solid line is the non-linear least-squares fit of the data to eq. 3.9. 100

Figure 3.26. Plot of k_{decay} vs ketone concentration for the $SiPh_2$-**5** silacarbonyl ylide monitored at 600 nm. The solid line is the linear least-squares regression of the data according to eq. 3.11. 100

Figure 3.27. (a) Transient absorption spectra recorded 0.26 – 0.51 μs (○) and 28.0 – 28.3 μs (□) after the laser pulse by laser flash photolysis of **3** in the presence of 5 mM 2-adamantanone in deoxygenated hexanes at 25°C. The dashed line spectrum (-) shows the difference between the two spectra. The inset shows transient decay traces recorded at 290 and 600 nm. (b) Plot of k_{decay} vs ketone concentration (0 – 5 mM) for the $SiMes_2$-**5** silacarbonyl ylide monitored at 650 nm. The solid line is the linear least-squares analysis of the data according to eq. 3.9. 101

Figure 3.28. Plot of k_{decay} vs ketone concentration (10 – 80 mM) for the $SiMes_2$-**5** silacarbonyl ylide monitored at 650 nm. The solid line is the linear least-squares analysis of the data according to eq. 3.11. 102

Figure 3.29. (a) Transient absorption spectra recorded 0.22 - 0.35 μs (○) and 2.8 - 2.9 μs (□) after the laser pulse from laser flash photolysis of **3** in the presence of 10 mM 2,2,5,5-tetramethylcyclopentanone in deoxygenated hexanes at 25°C. The dashed line spectrum (-) shows the difference between the spectra recorded at 0.22 – 0.35 and 2.8–2.9 μs after the laser pulse; the inset shows transient decay traces at 290 and 580 nm. (b) Plot of k_{decay} vs ketone concentration for $SiMes_2$, 103

monitored at 580nm. The solid line is the linear least-squares fit of the data to eq. 3.1.

Figure 3.30. (a) Transient absorption spectra recorded 0.22 - 0.35 μs (○) and 2.8 - 2.9 μs (□) after the laser pulse by laser flash photolysis of $SiMe_2$ precursor **1** in the presence of 10 mM 2,2,5,5-tetramethylcyclopentanone in deoxygenated hexanes at 25°C. The inset shows transient decay traces at 470 and 600 nm. (b) Plot of the average first-order decay rate coefficient of the 470 and 600 nm transient absorptions vs. ketone concentration (0 – 2mM). The solid line is the non-linear least-squares fit of the data to eq. 3.9. 104

Figure 3.31. (a) Plot of k_{decay} vs ketone concentration of $SiMe_2$ and $SiMe_2$-**8** ylide monitored at 470 (○) and 600 (□) nm over the 10 – 60 mM concentration range. The solid line is the linear least-squares analysis of the data, by analyzing the 470 and 600 nm data sets as a single data set, to eq. 3.11. (b) Expanded plot of the data of (a) over the 0 – 10 mM concentration range. The solid line is the non-linear least squares regression of the data, by analyzing the 470 and 600 nm data sets as a single data set, to eq. 3.9. 105

Figure 3.32. (a) (a) Transient absorption spectra recorded 0.16 – 0.80 μs (○) and 2.78 – 2.94 μs (□) after laser pulse by laser flash photolysis of **2** in the presence of 10 mM 2,2,5,5-tetramethylcyclopentanone in deoxygenated hexanes at 25°C. The dashed line spectrum (-) shows the difference between the two spectra. The inset shows transient decay traces recorded at 290 and 600 nm. (b) Plot of k_{decay} vs ketone concentration for the $SiPh_2$-**8** silacarbonyl ylide monitored at 600 nm. The solid line is the non-linear least-squares fit of the data to eq. 3.9 106

Figure 3.33. Plot of k_{decay} vs ketone concentration for the $SiPh_2$-**8** silacarbonyl ylide monitored at 600 nm. The solid line is the linear least-squares regression of the data to eq. 3.11. 107

Figure 3.34. (a) Transient absorption spectra recorded 0.16 – 0.22 μs (○) and 1.39 – 1.47 μs (□) after laser pulse by laser flash photolysis of **2** in the presence of 5 mM di-*tert*-butyl ketone in deoxygenated hexanes at 25°C. The dashed line spectrum (-) shows the difference between the two spectra. The inset shows transient decay traces recorded at 290 and 530 nm with 108

k_{decay} values of $(9.8 \pm 0.2) \times 10^5$ and $(8.8 \pm 0.5) \times 10^5$ s^{-1}, respectively. (b) Plot of k_{decay} vs ketone concentration for the $SiPh_2$-**6** silacarbonyl ylide monitored at 600 nm. The solid line is the linear least-squares fit of the data to eq. 3.11.

Figure 3.35. ^1H NMR spectra of a C_6D_{12} solution containing 0.045 M 2,2,5,5-tetramethylcyclopentanone (**8**) and 0.01 M hexamethyldisilane (a) before and (b) after 60 mins of photolysis. 110

Figure 3.36. Transient absorption spectra recorded 0.22 – 0.35 μs (○) and 2.78 – 2.94 μs (□) after laser pulse by laser flash photolysis of 40 mM 2,2,5,5-tetramethylcyclopentanone in deoxygenated hexanes at 25°C. The inset shows transient decay traces at 300 nm. 111

Figure 3.37. Plot of extinction coefficients vs. wavelength of the synthesized 2,2,5,5-tetramethylcyclopentanone. The solid line (─) is the synthesized ketone used for the experiments mentioned above (Figures 3.29 – 3.33), while the dashed line (---) is the ketone used for the experiment below (Figure 3.38). The inset shows the same plot zoomed in the 200 – 300 nm range. 113

Figure 3.38. Plots of k_{decay} vs ketone concentration of $SiMe_2$ and $SiMe_2$-**8** ylide monitored at 470 (○) and 640 (□) nm. (a) The solid line is the average linear least-squares fit of the data to eq. 3.11 over the 0 – 60 mM ketone concentration range. (b) The same plot zoomed in the 0 – 10 mM ketone concentration range. The solid line is the non-linear least-squares analysis of the data, by analyzing the 470 and 600 nm data sets as a single data set, to eq. 3.9. 114

Figure 3.39. Transient absorption spectra recorded 0.00 – 2.56 μs (○) and 55.68 – 58.88 μs (□) after the laser pulse by laser flash photolysis of **7** in deoxygenated hexanes at 25°C. The inset shows transient decay traces at 420 and 580 nm. 116

Figure 3.40. Plot of k_{decay} vs ketone concentration for $SiMes_2$ monitored at 580 nm. The solid line is the linear least-squares fit of the data to eq. 3.1. 117

Figure S3.1. ^{1}H-^{1}H COSY spectrum of the solution of **12** in $CDCl_3$, with the ^{1}H NMR spectrum from Figure 3.8 used as a projection for both axes. 125

Figure S3.2. ^{1}H-^{13}C HSQC spectrum of the solution of **12** in $CDCl_3$, with the ^{1}H NMR and ^{13}C NMR spectra from Figures 3.8 and 3.10, used as a projection for the axes. 126

Figure S3.3. ^{1}H-^{13}C HMBC spectrum of the solution of **12** in $CDCl_3$, with the ^{1}H NMR and ^{13}C NMR spectra from Figures 3.8 and 3.10, used as a projection for the axes, respectively. 127

Figure S3.4. ^{1}H-^{29}Si HMBC spectrum of the solution of **12**, containing TMS, in $CDCl_3$. 128

Figure S3.5. ^{1}H-^{13}C HSQC spectrum of the crude photolysate solution of 0.05 M **3**, 0.05 M **6**, and 0.01 M bis(trimethylsilyl)methane in C_6D_{12} photolyzed for 60 mins, with the ^{1}H NMR and ^{13}C NMR spectra from Figures 312 and 3.13, used as a projection for the axes. 129

Figure S3.6. ^{1}H-^{13}C HMBC spectrum of the crude photolysate solution of 0.05 M **3**, 0.05 M **6**, and 0.01 M bis(trimethylsilyl)methane in C_6D_{12} photolyzed for 60 mins, with the ^{1}H NMR and ^{13}C NMR spectra from Figures 3.12 and 3.13, used as a projection for the axes 130

Figure S3.7. ^{1}H-^{29}Si HMBC spectrum of the crude photolysate solution of 0.05 M **3**, 0.05 M **6**, and 0.01 M bis(trimethylsilyl)methane in C_6D_{12} photolyzed for 60 mins 131

Figure S3.8. ^{1}H-^{1}H COSY spectrum of the solution of **9c** in $CDCl_3$, with the ^{1}H NMR spectrum from Figure 3.18, used as the projection for the axes. The figure on the bottom is zoomed in the 1.1 – 2.7 ppm range on both axes. 132

Figure S3.9. ^{1}H-^{13}C HSQC spectrum of the solution of **9c** in $CDCl_3$, with the ^{1}H NMR and ^{13}C NMR spectra from Figures 3.18 and 3.20, used as the projection for the axes. The figure on the bottom is zoomed in the 1.1 – 2.7 ppm (^{1}H NMR) and 18 – 48 ppm (^{13}C NMR) range. 133

Figure S3.10. ^{1}H-^{13}C HMBC spectrum of the solution of **9c** in $CDCl_3$, with the ^{1}H NMR and ^{13}C NMR spectra from Figures 3.18 and 134

3.20, used as the projection for the axes. The figure on the right is zoomed in the 1.1 – 2.7 ppm (^{1}H NMR) and 13 – 50 ppm (^{13}C NMR) range.

Figure S3.11. ^{1}H-^{29}Si HMBC spectrum of the solution of **9c**, containing TMS, in $CDCl_3$. 135

Figure S3.12. (a) Transient absorption spectra recorded 0.27 – 0.34 μs (○) and 1.39 – 1.47 μs (□) after the laser pulse by laser flash photolysis of **1** in the presence of 5 mM di-*tert*-butyl ketone (**6**) in deoxygenated hexanes at 25°C. The inset shows transient decay traces recorded at 470 and 620 nm with k_{decay} = (1.2 ± 0.1) × 10^6 and (1.3 ± 0.1) × 10^6 s^{-1}, respectively. (b) Plot of k_{decay} vs ketone for the $SiMe_2$-**6** silacarbonyl ylide monitored at 620 nm. The solid line is the non-linear least-squares fit of the data to eq. 3.9. 135

Figure S3.13. Plot of k_{decay} vs ketone for the $SiMe_2$-**6** silacarbonyl ylide monitored at 620 nm. The solid line is the linear least-squares fit of the data to eq. 3.11. 136

Figure S3.14. (a) Transient absorption spectra recorded 0.51 – 0.67 μs (○) and 4.06 – 4.22 μs (□) after laser pulse by laser flash photolysis of **3** in the presence of 5 mM di-*tert*-butyl ketone (**6**) in deoxygenated hexanes at 25°C. The dashed line spectrum (-) shows the difference between the two spectra. The inset shows transient decay traces recorded at 290 and 530 nm. (b) Plot of k_{decay} vs ketone concentration for $SiMes_2$ monitored at 580 nm. The solid line is the linear least-squares fit of the data to eq. 3.1. 136

Figure S3.15. ^{1}H NMR spectra of 2,2,5,5-tetramethycyclopentanone in $CDCl_3$. (a) Sample used in the initial studies. (b) Synthesis and attempted further purification of ketone. 137

Figure S3.16. Concentration vs. time plots for the photolysis of 0.045 M 2,2,5,5-tetramethylcyclopentanone (**7**) in cyclohexane-d_{12}. Shown is the depletion of **7** (○) and the formation of 2,2,5-trimethyl-4-hexenal (**15**, □). The slope of the consumption of ketone is are as follows: (○):(-8.0 ± 0.2) × 10^{-2} mM/min. (□): (5.1 ± 0.4) × 10^{-2} mM/min. 137

LIST OF TABLES

Table 1.1.	Common nomenclature of group 14 compound derivatives	2
Table 1.2.	Absolute rate constants (in units of 10^9 $M^{-1}s^{-1}$) for the reactions of transient silylenes with alcohols in hexanes or cyclohexane solution at 25°C	11
Table 1.3.	Equilibrium (K_C) and forward rate (k_C) constants for complexation of transient silylenes with O-donors in hexanes at 25°C	14
Table 1.4.	Rate constants (k_Q) for the reactions of transient silylenes with carbonyl compounds in hydrocarbon solutions	22
Table 2.1.	Absolute rate constants (k_Q) for the reactions of $SiMe_2$, $SiPh_2$, and $SiMes_2$ with ketones in hexanes solution at 25°C	40
Table 2.2.	Equilibrium (K_1) and H-migration rate constants (k_2) for the reactions of $SiMe_2$ and $SiPh_2$ with carbonyl compounds in hexanes at 25°C	42
Table 2.3.	Activation parameters of the H-migration pathway for the $SiMe_2$- and $SiPh_2$-derived silacarbonyl ylide with camphor	45
Table 2.4.	Kinetic parameters for the two-step reactions of $SiMe_2$ and $SiPh_2$ with camphor-L_2 (L = H, D) in hexanes at 25°C	48
Table 2.5.	Absolute rate constants (k_Q) for the reactions of $SiMe_2$ and $SiMes_2$ with acetone-L_6 and camphor-L_2 in hexanes solution at 25°C	50
Table 2.6.	Experimental UV-Vis absorption maxima (λ_{max} (nm)) of the silacarbonyl ylides from the reactions of $SiMe_2$ and $SiPh_2$ with enolizable ketones in hexanes at 25°C	58
Table 2.7.	Equilibrium constants (K_1) and H-migration rate coefficients (k_2) for the reactions of $SiMe_2$ and $SiPh_2$ with carbonyl compounds in hexanes at 25°C	59
Table 2.8.	Absolute rate constants (k_Q) for the reactions of $SiMe_2$, $SiPh_2$, and $SiMes_2$ with ketones in hexanes solution at 25°C	61

Table S2.1.	Decay rate coefficients for the H-migration step in the reaction of $SiMe_2$ containing 4.72 mM camphor in deoxygenated hexanes in the temperature range of 9.0 – 43.0°C, recorded at 600 nm.	68
Table S2.2.	Decay rate coefficients of the $SiPh_2$-camphor silacarbonyl ylide, in the reaction of $SiPh_2$ containing 4.8 mM camphor in deoxygenated hexanes in the temperature range of 9.0 – 43.0°C, recorded at 600 nm.	68
Table S2.3.	^{1}H NMR chemical shift assignments for **6** (see pg. 37)	68
Table S2.4.	^{1}H NMR chemical shift assignments for **16** (see pg. 54)	69
Table 3.1.	Absolute rate constants (k_Q) for the reactions of $SiMe_2$, $SiPh_2$, and $SiMes_2$ with pivalaldehyde in hexanes solution at 25°C	73
Table 3.2.	Experimental UV-Vis absorption maxima (λ_{max} (nm)) of the silacarbonyl ylides from the reactions of $SiMe_2$, $SiPh_2$, and $SiMes_2$ with 2-adamantanone (**5**) in hexanes at 25°C	74
Table 3.3.	^{1}H NMR assignments for compound **12** in $CDCl_3$ (Figure 3.8), refer to Figure 3.9 for structural assignments	82
Table 3.4.	^{13}C NMR assignments for compound **12** in $CDCl_3$ (Figure 3.10), refer to Figure 3.9 for structural assignments	84
Table 3.5.	Crystal data and structure refinement for compound **12**	85
Table 3.6.	^{1}H NMR assignments for compound **13**, recorded from the spectrum of the crude photolysate in C_6D_{12} (Figure 3.13b), refer to Figure 3.15 for structural assignments	87
Table 3.7.	^{13}C NMR assignments for compound **13**, recorded from the spectrum of the crude photolysate in C_6D_{12} (Figure 3.14), refer to Figure 3.15 for structural assignments	88
Table 3.8.	^{1}H NMR chemical shift assignments for compound **9c**, recorded in $CDCl_3$ (Figure 3.18), refer to Figure 3.19 for structural assignments	92
Table 3.9.	^{13}C NMR assignments for compound **9c**, determined in $CDCl_3$ (Figure 3.20), refer to Figure 3.19 for structural assignments	93

Table 3.10. Experimental UV-Vis absorption maxima (λ_{max} (nm)) of the silacarbonyl ylides formed by reactions of $SiMe_2$, $SiPh_2$, and $SiMes_2$ with non-enolizable carbonyl compounds in hexanes at 25°C 118

Table 3.11. Absolute second order rate constants (k_Q) for the reactions of $SiMe_2$, $SiPh_2$, and $SiMes_2$ with non-enolizable ketones in hexanes solution at 25°C, where silacarbonyl ylides could not be detected 118

Table 3.12. Equilibrium (K_1) and the unimolecular ring-closure rates (k_2) for the reactions of $SiMe_2$, $SiPh_2$, and $SiMes_2$ with carbonyl compounds in hexanes at 25°C 120

Table 3.13. Rate coefficients of the [2+3]-cycloaddition (k_3) and unimolecular ring closure (k_2) for the reactions of $SiMe_2$, $SiPh_2$, and $SiMes_2$-derived silacarbonyl ylide with carbonyl compounds in hexanes at 25°C 122

Table S3.1. ^{1}H NMR assignments for compound **12**, recorded from the spectrum of the crude photolysate in C_6D_{12} (Figure 3.6), refer to Figure 3.9 for the proton assignments 138

Table S3.2. ^{13}C NMR assignments for compound **12**, recorded from the spectrum of the crude photolysate in C_6D_{12}, using Figure 3.9 for the carbon assignments 138

COMPOUND NUMBERS

Chapter 1

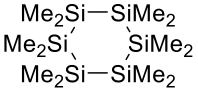

1

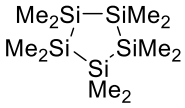

2

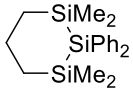

3

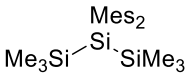

4

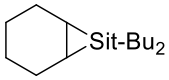

5

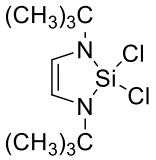

6

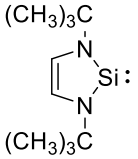

7

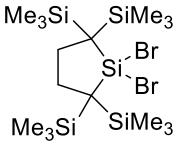

8

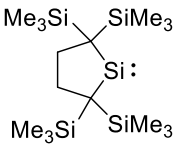

9

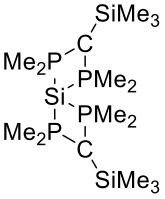

10

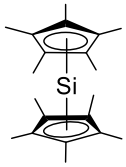

11

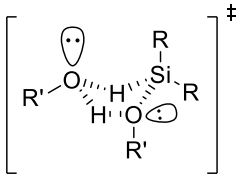

12

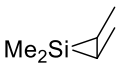

13

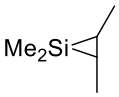

14

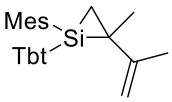

15

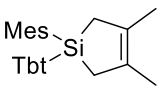

16

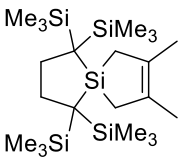

17

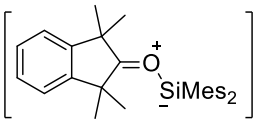

18

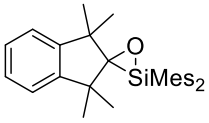

19

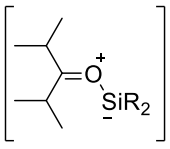

20

20a. R = Me
20b. R = Mes

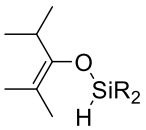

21

21a. R = Me
21b. R = Mes

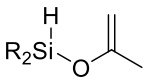

22

22a. R = Me
22b. R = Ph
22c. R = Mes

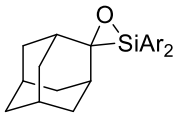

Ar = 2-(Me_2NCH_2)C_6H_4

23

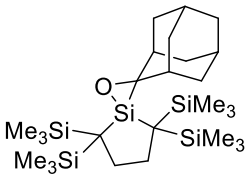

24

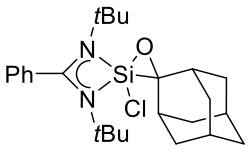

25

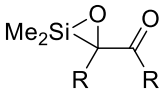

26

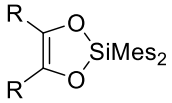

27

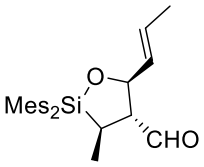

28

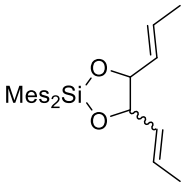

29

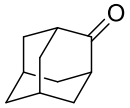

30

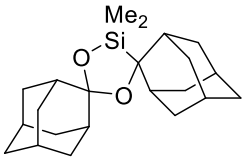

31

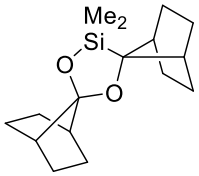

32

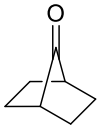

33

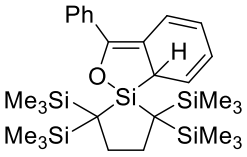

34

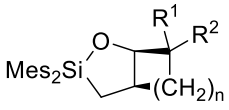

35

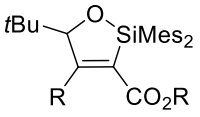

36

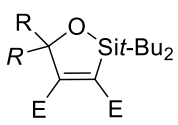

37

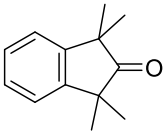

38

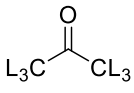

39a: L = H
39b: L = D

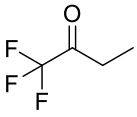

40

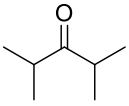

41

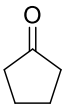

42

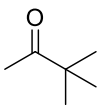

43

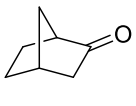

44

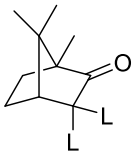

45a: L = H
45b: L = D

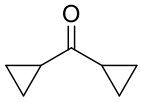

46

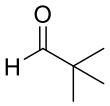

47

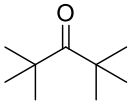

48

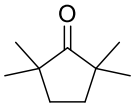

49

Chapter 2

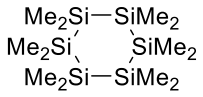

1

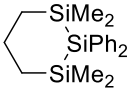

2

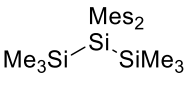

3

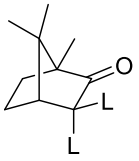

4a: L = H
4b: L = D

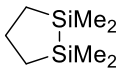

5

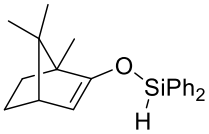

6

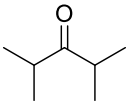

7

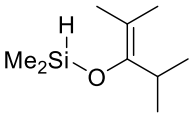

8

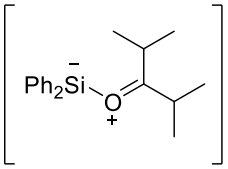

9

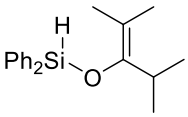

10

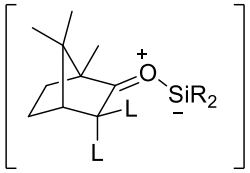

11a: L = H
11b: L = D

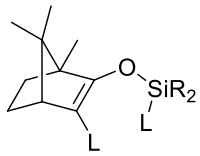

12a: L = H
12b: L = D

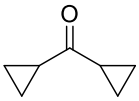

13

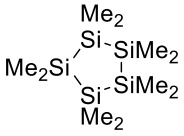

14

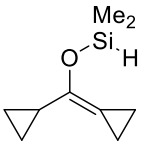

15

Chapter 3

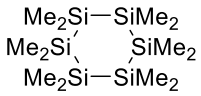

1

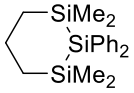

2

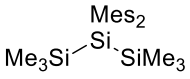

3

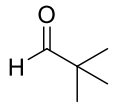

4

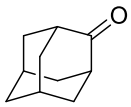

5

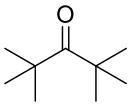

6

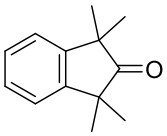

7

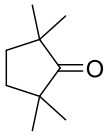

8

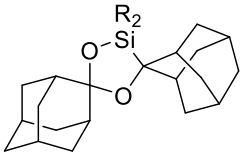

9a: R = Me
9b: R = Mes
9c: R = Ph

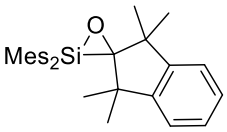

10

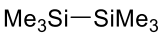

11

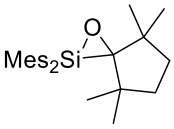

12

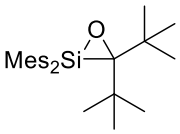

13

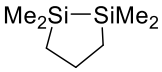

14

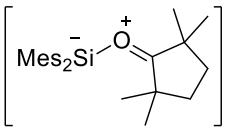

15

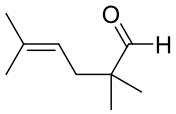

16

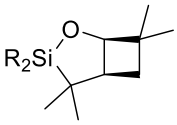

17a: R = Me
17b: R = Ph

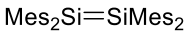

18

Chapter 5

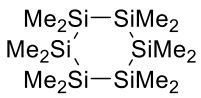

1

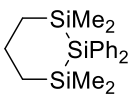

2

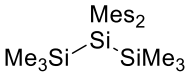

3

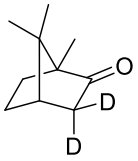

4

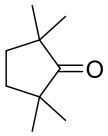

5

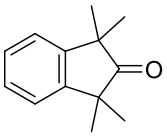

6

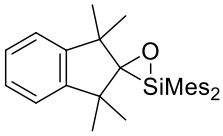

7

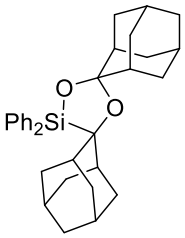

8

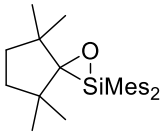

9

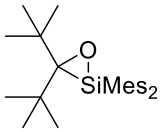

10

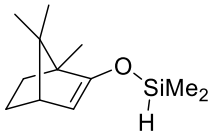

11

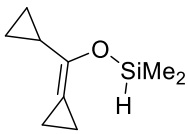

12

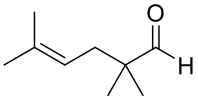

13

LIST OF ABBREVIATIONS AND SYMBOLS

Me	methyl, -CH_3
Ph	phenyl, -C_6H_5
i-Pr	iso-propyl, -$CH(CH_3)_2$
t-Bu	tert-butyl, -$C(CH_3)_3$
Mes	2,4,6-trimethylphenyl
Tbt	2,4,6-tris[bis(trimethylsilyl)methyl]phenyl
Ad	adamantyl
THF	tetrahydrofuran
TMS	trimethylsilyl, -$SiMe_3$
Et_2O	diethyl ether
NHSi	N-heterocyclic silylene
$\Delta H^{\ddagger}$	Enthalpy of activation
$\Delta S^{\ddagger}$	Entropy of activation
E_a	Activation energy
NMR	nuclear magnetic resonance
COSY	Correlation spectroscopy
HSQC	Heteronuclear Single Quantum Coherence Spectroscopy
HMBC	Heteronuclear Multiple Bond Correlation
DFT	Density Functional Theory
ppm	Parts per million

HPLC High Performance Liquid Chromatography

GCMS Gas Chromatography Mass Spectroscopy

FMO Frontier Molecular Orbital

HRMS High Resolution Mass Spectrometry

CONTRIBUTIONS TO THE WORK

This work could not have been completed without the large contributions made by undergraduate summer students Claire Browne and Alex Sever.

The contributions by Claire Browne are the laser flash photolysis experiments (spectrum and quenching plots) of the following systems: $SiMe_2$, $SiPh_2$, and $SiMes_2$ with 1,1,1-trifluoro-2-butanone, 2,4-dimethyl-3-pentanone, 3,3-dimethyl-2-butanone, camphor, and pivalaldehyde, $SiMe_2$ with acetone, $SiMe_2$ and $SiMes_2$ with cyclopentanone, and $SiPh_2$ and $SiMes_2$ with norcamphor. Furthermore, preliminary laser flash photolysis experiments were done on the three silylenes with 2-adamantanone. In addition, variable temperature experiments were done on the reactions of $SiMe_2$ and $SiPh_2$ with camphor, as well as a steady-state photolysis experiment studying the reaction of $SiPh_2$ with camphor.

The contributions by Alex Sever are the steady-state photolysis experiment of $SiPh_2$ with 2-adamantonone, as well as the isolation and characterization of the corresponding product from this system, 3,5-diadamantyl-2,4-dioxa-1,1-diphenylsilacyclopentane.

My contributions to the work were to compile all the previous students work and complete any study in which deficiencies exist. The following systems were found to have deficiencies: $SiPh_2$ with cyclopentanone, $SiMe_2$ with norcamphor, and all three silylenes with 2-adamantanone. An investigation of kinetic isotope effects on the reactions with enolizable carbonyl compounds involved studying the kinetics of the three

silylenes with acetone-d_6 and camphor-d_2. The effects of ring and angle strain on the reaction kinetics were investigated through a study of the reactions of the three silylenes with dicyclopropyl ketone. Furthermore, the reactions of the three silylenes with 2,2,5,5-tetramethylcyclopentanone and di-*tert*-butyl ketone were investigated.

Chapter 1 - Introduction

1.1 Overview

Silylenes, the silicon homologues of carbenes, are key intermediates in many photochemical and thermal reactions of organosilicon compounds.[1-2] The fundamental aspects of many of their reactions have been extensively studied.[3-8] One class of silylene reactions is that with carbonyl compounds, which generates a variety of products depending on the substituents in the silylene and in the carbonyl compound. The study of these reactions is the subject of this thesis.

The main focus of this work is to study the kinetics and thermodynamics of the reactions of the simple transient silylene derivatives dimethyl-, diphenyl-, and dimesitylsilylene ($SiMe_2$, $SiPh_2$, and $SiMes_2$, respectively) with a selection of enolizable and non-enolizable carbonyl compounds in solution by laser flash and steady state photolysis methods, featuring the direct detection of the corresponding silacarbonyl ylides and characterization of their uni- and bimolecular reactivity. The results provide quantitative information on the reactivities of silylenes, and in some cases the silacarbonyl ylide intermediates, with a range of enolizable and non-enolizable aliphatic carbonyl compounds of varying electronic and steric effects.

1.2 Nomenclature

Compounds containing one of the Group 14 elements in the +2 oxidation state are collectively known as tetrylenes or (in the older literature) metallylenes.[9-10] Individually, they are referred to as carbenes (CR_2), silylenes (SiR_2), germylenes (GeR_2), stannylenes

(SnR_2), or plumbylenes (PbR_2), depending on the identity of the central Group 14 element. Compounds containing double bonds to one of the heavy group 14 elements are known generally as tetrelenes, while the prefix "di" indicates that the double bond is between two group 14 elements of the same identity. A list of common group 14 compounds is given in Table 1.1.

Table 1.1. Common nomenclature of group 14 compound derivatives

M	MR_4	MR_2	$R_2C{=}MR_2$	$R_2M{=}MR_2$
C	alkane	carbene	alkene	alkene
Si	silane	silylene	silene	disilene
Ge	germane	germylene	germene	digermene
Sn	stannane	stannylene	stannene	distannene
Pb	plumbane	plumbylene	plumbene	diplumbene

1.3. Structure and Properties of Silylenes

Tetrylenes have six valence electrons, with two substituents connected to the central group 14 atom and two non-bonding electrons. There are two possible group state electronic configurations: the singlet and the triplet state. In the lowest energy singlet state, the two non-bonding electrons are paired in an orbital with predominant s-character, leaving a vacant p-orbital. In the lowest energy triplet state, the electrons are unpaired and located in different orbitals. The structures of the singlet and triplet states of tetrylenes are depicted in Figure 1.1.

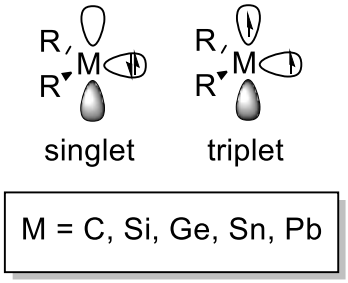

Figure 1.1. Electronic structures of the lowest energy singlet and triplet states of tetrylenes

Theoretical calculations reported methylene (CH_2) is a ground state triplet with the singlet state lying 9.0 kcal/mol higher in energy, while the parent heavier carbene analogues (SiH_2, GeH_2, SnH_2) are ground state singlets with the triplet state lying significantly higher in energy by 20, 26, and 26 kcal mol^{-1}, respectively.[11-13] In parallel to theoretical studies, experimental studies have shown the heavier carbene analogues exhibit reactivity consistent with a singlet ground state, where the central Group 14 element possess both an open coordination site and paired valence electrons, which can behave as both an electrophile and as a nucleophile. The triplet state should exhibit reactivity consistent with that of a biradical.

The stabilization of the tetrylenes in the +2 oxidation state relative to the +4 oxidation state in group 14 compounds can be quantified by the divalent state stabilization energy (DSSE). DSSE is defined as the difference between the BDEs of MX_4 and MX_3 bond dissociation reaction as seen in eq 1.1-1.4.[11, 14] The smaller the ΔH_r value for the latter reaction relative to the first, the larger the DSSE. The second dissociation energies were found to be lower than the first, which suggests a stabilizing

effect in the divalent MX_2 species. This stabilizing effect has been associated with the lone-pair orbital containing substantial s-character.[15]

$$MX_4 \rightarrow MX_3 + X \ \ (\Delta H_1) \qquad (1.1)$$

$$MX_3 \rightarrow MX_2 + X \ \ (\Delta H_2) \qquad (1.2)$$

$$\text{Net: } MX_4 \rightarrow MX_2 + 2X \ \ (\Delta H_r = \Delta H_1 + \Delta H_2) \qquad (1.3)$$

$$DSSE = BDE(MX_4) - BDE\ (MX_3) = \ \Delta H_1 - \Delta H_2 \qquad (1.4)$$

With increasing size of the Group 14 element, the DSSE increases. This is represented by the parent methylene, and its inorganic homologs, where the DSSEs of CH_2, SiH_2, GeH_2, and SnH_2 were predicted to be -6, +22, +28, and 26 $kcal^{-1}$ mol^{-1} respectively.[16-19]

1.4. Generation of Silylenes

Transient silylenes can be prepared from a variety of photochemical and thermal precursors.[20-22] The most common route to generate silylenes involves Si-Si bond cleavage, as the bond is weak.[23] Linear and cyclic trisilanes, tetrasilanes, oligo- and polysilanes all typically extrude an internal SiR_2 moiety upon photolysis.[24-28] For example, the photolysis of dodecamethylcyclohexasilane (**1**) yields $SiMe_2$ and decamethylsilacyclopentane (**2**) as the co-product (eq. 1.5).[29] Similarly, diphenylsilylene and dimesitylsilylene are formed in high yield by photolysis of the trisilanes **3**[30] and **4**[31], respectively (eq. 1.6 and 1.7).

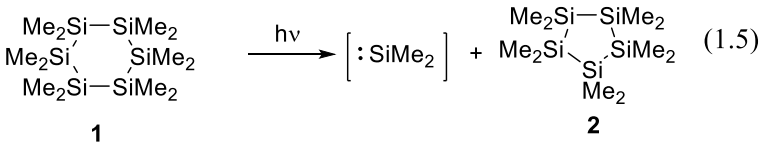

1 **2**

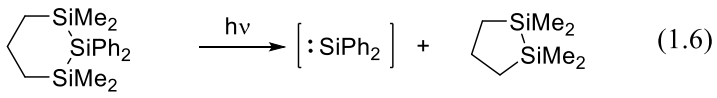

3

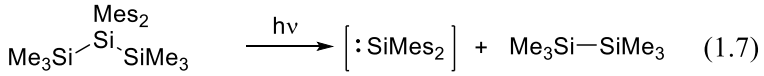

4

Another method for generating silylenes is the thermolysis or photolysis of silacyclopropanes (siliranes).[32-34] One example is the silirane **5**, which affords di-tert-butylsilylene and cyclohexene upon either thermolysis or photolysis (eq. 1.8).[35]

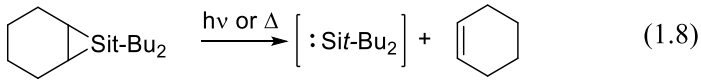

5

Similarly, hydridosilacyclobutanes and -silacyclobutenes are also sources of silylenes.[20, 36] These compounds undergo thermal or photochemical [2+2]-cycloreversion to afford the corresponding hydridosilenes and alkene or alkyne as the primary products; the formation of silylene proceeds by rapid (1,2) H-migration from Si to the silenic carbon (eq. 1.9).[37]

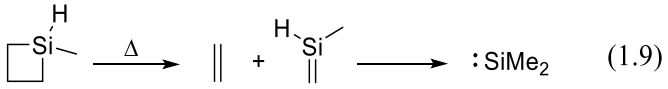

Silylenes can also be generated from dihalosilanes under strong reducing conditions. This method has been extensively used to generate numerous stabilized

silylenes.[38] For example, West and coworkers reported the synthesis of a stable N-heterocyclic silylene, **7**, which was obtained by reducing **6** with potassium (eq. 1.10).[39] Similarly, Kira and coworkers prepared the kinetically stable dialkylsilylene **9** by reducing **8** with potassium graphite (eq. 1.11).[40]

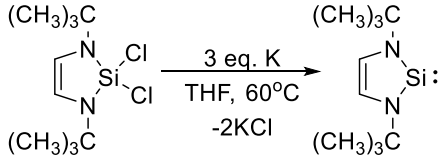

6 **7** (1.10)

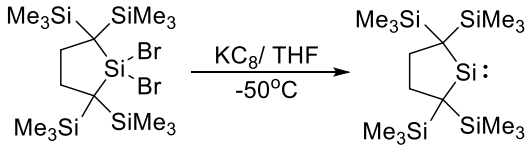

8 **9** (1.11)

1.5. Stability of Silylenes

Before the introduction of N-heterocyclic silylenes (NHSi's), there were only two known examples of stable divalent silicon compounds, the tetracoordinate phosphorus complex Si[CH(PMe_2)$_2$] (**10**)[41] and the π-complex decamethylsilicocene (**11**).[42] However, due to their coordination numbers being greater than 2, the reactivities of these compounds differ from silylenes. Di-coordinate silylenes at this point had only been studied in low temperature matrixes or in trapping experiments.

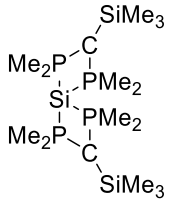

10

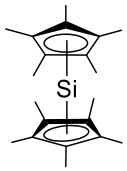

11

However, a series of stable di-coordinate silylenes have emerged with the introduction of NHSis, the first by West and co-workers describing an NHSi (**7**) stable at ambient temperature.[39] The t-butyl groups provide some kinetic stabilization to the silylene but electronic factors arising from the pseudoaromaticity of the silylene are primarily responsible for the stability. NHSis are stabilized by a strong resonance interaction between the vacant p-orbital at the divalent silicon atom and the π-type lone pair orbitals of the nitrogen atoms.

Kira and co-workers reported the first stable dialkylsilylene (2,2,5,5-tetrakis(trimethylsilyl)silacyclopentane-1,1-diyl) (**9**), which is protected sterically from dimerization and is minimally perturbed electronically.[40] Since then, there have been numerous examples of different and unique stable silylenes developed by taking advantage of kinetic and/or electronic stabilization.[43-47] Chart 1 illustrates many of the stable silylenes that have been reported, including base-stabilized silylenes,[48-54] dialkylsilylenes,[40, 55-57] acyclic silylenes,[8, 58-60] and silylenes bearing π and/or σ-coordination.[61]

Chart 1. Stable Silylenes

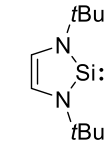

West, **1994**[39]

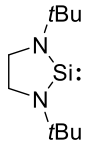

West, **1994**[39]

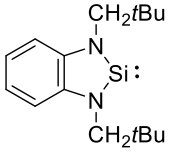

Gehrhus, **1995**[52]

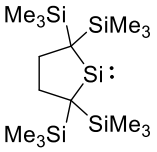

Kira, **1999**[40]

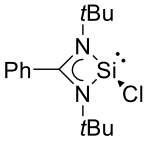

Roesky, **2006**[44]

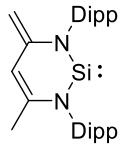

Driess, **2006**[43]

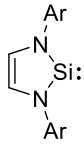

Ar = 2,4,6-Me_3-C_6H_2
Ar = 2,6-iPr_2-C_6H_3

Cui, **2009**[45]

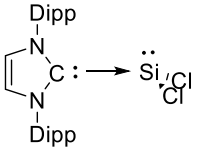

Roesky, **2009**[49]

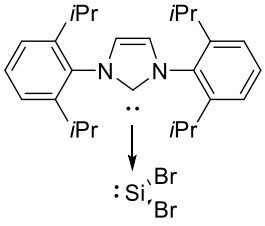

Filippou, **2009**[48]

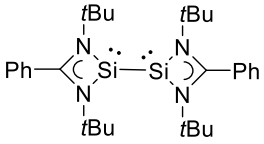

Roesky, **2009**[47]

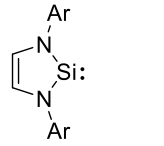

Ar = 2,6-Me_2-C_6H_3

Müller, **2010**[46]

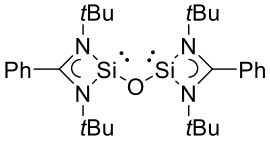

Driess, **2010**[53]

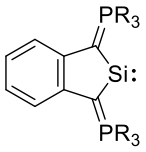

R = Ph
R = *m*-tol

Driess, **2011**[54]

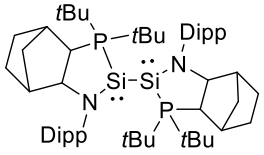

Baceiredo, **2011**[51]

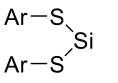

Ar = C_6H_3-2,6-(C_6H_2-2,4,6-Me_3)$_2$

Power, **2012**[57]

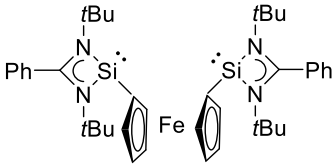

Driess, **2012**[50]

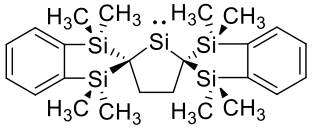

Iwamoto, **2012**[56]

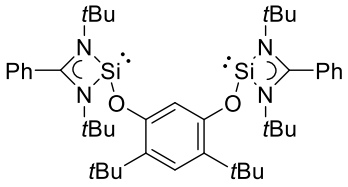

Driess, **2012**[54]

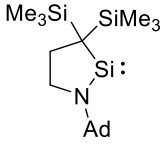

Iwamoto, **2016**[60]

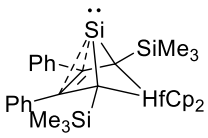

Müller, **2017**[61]

1.6. Reactions of Silylenes

The reactions of transient silylenes with various substrates have been investigated extensively.[5, 28, 62-70] The more common reactions of silylenes include dimerization, insertion into σ-bonds such as L-H (L = O, N, S, B, Si, halogens) and Si-X (X = Si, -OR, halogens), and addition to π-bonds (C=C, C≡C, C=O, C=N) to form the corresponding silacycles and their derivatives, and atom-abstraction reactions.

1.6.1. Dimerization

In the absence of a substrate, silylenes undergo dimerization to generate the corresponding disilene, which features a trans-bent geometry (eq. 1.12).[71-74]

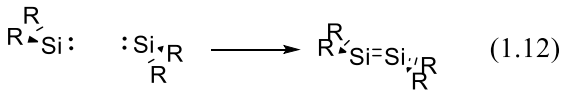

(1.12)

Dimerization can be prevented by introducing electronic stabilization and/or sterically bulky substituents.[38]

1.6.2. Bond Insertion Reactions

Insertion reactions of silylenes into various σ-bonds such as O-H, N-H, Si-H, Si-halogen, and Si-O bonds (Scheme 1) has been extensively studied theoretically[75-76] and experimentally.[1, 16, 27, 77-83]

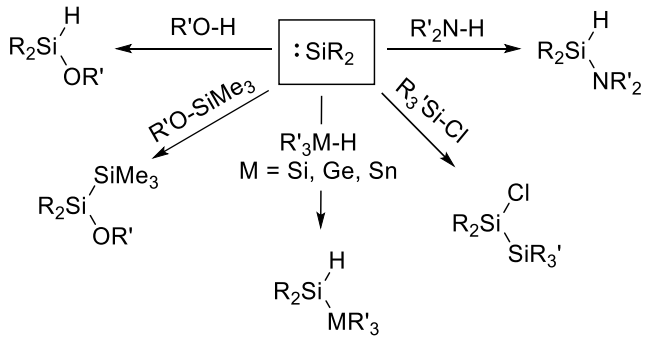

Scheme 1. Insertion reactions of silylenes with various substrates

These reactions are thought to proceed via the initial formation of a Lewis acid-base complex between the silylene and a basic site in the substrate, followed by migration of a substituent on the basic site to silicon to form the insertion product (eq.1.13).

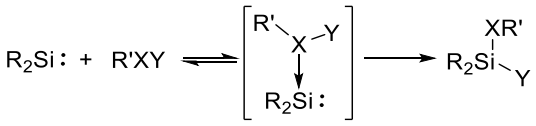

(1.13)

The insertion of silylenes into the O-H bonds of alcohols has been studied both experimentally and theoretically, and is known to afford an alkoxysilane.[77-78, 84-85] The experimental evidence for the intermediacy of Lewis acid-base complexes in these reactions was obtained through their direct detection in low temperature matrixes and in solution.[77-78, 84]

Leigh and coworkers investigated the reaction of silylenes with methanol and *t*-BuOH to elucidate a reaction mechanism for the O-H insertion process in solution.[84] The reaction proceeds via the initial reversible formation of the silylene-alcohol donor-acceptor complex, which has been detected at low concentrations of substrate. Interestingly, the second step was shown to involve catalytic proton transfer by a second molecule of alcohol, via a five-membered transition state, **12**, to generate the

corresponding alkoxysilane (eq. 1.14). Experimental and theoretical evidence for this mechanism has also been reported for the reactions of SiH_2 with water and methanol in the gas phase.[75, 86] The absolute rate constants for the initial complexation step in the reactions of silylenes with methanol and *t*-BuOH in solution were found to be close to the diffusional limit ($k_{diff} \approx 2 \times 10^{10}$ $M^{-1}s^{-1}$), as seen in Table 1.2.[84, 87] As shown in the table, there is a systematic decrease in the reactivity with increasing steric bulk in either the silylene or the alcohol.

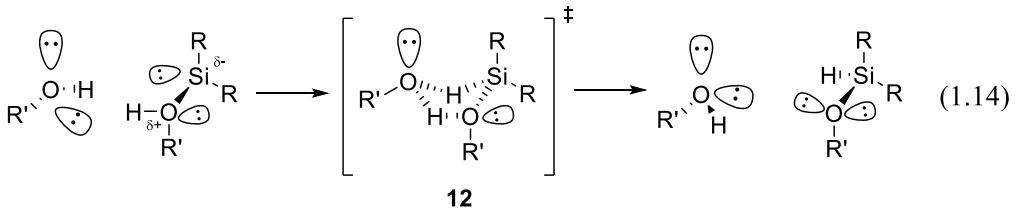

12 (1.14)

Table 1.2. Absolute rate constants (in units of 10^9 $M^{-1}s^{-1}$) for the reactions of transient silylenes with alcohols in hexanes or cyclohexane solution at 25°C

Substrate	k_Q (10^9 $M^{-1}s^{-1}$)		
	$SiMe_2$	$SiPh_2$	$SiMes_2$
MeOH	21 ± 3 [a]	18 ± 2 [a]	1.01 ± 0.09 [a]
t-BuOH [a]	14 ± 2 [a]	14 ± 1 [a]	0.136 ± 0.005 [a]

a. Data from ref 84.

1.6.3. Addition to Unsaturated C-C Bonds

The reactions of silylenes with alkenes and alkynes form three-membered ring compounds, the corresponding siliranes and silirenes, respectively (eq. 1.15 and 1.16).

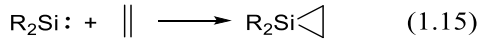

(1.15)

(1.16)

The reaction is thought to proceed in a concerted manner via [1+2] cycloaddition, with retention of the stereochemistry in the alkene component.[88-90] For example, the

addition of *cis* and *trans*-2-butene to $SiMe_2$ afford the corresponding siliranes **13** and **14**, respectively, with their stereochemistry maintained (eq.1.17 and 1.18).

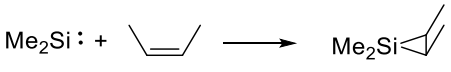

(1.17)

13

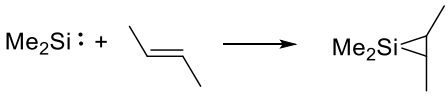

(1.18)

14

The reaction of silylenes with conjugated dienes affords the corresponding vinylsilirane and silacyclopent-3-ene derivatives. For example, Okazaki and coworkers have demonstrated that the sterically hindered silylenes, $SiMes_2$ and SiMes(Tbt) react with 2,3-dimethyl-1,3-butadiene to afford a mixture of [1+2] and [1+4] cycloadducts (**15** and **16**) (eq. 1.19).[90]

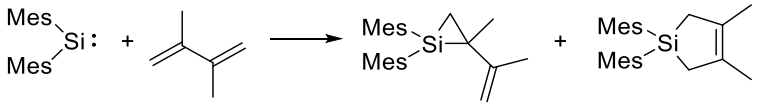

(1.19)

15 (55%) **16** (45%)

It has been proposed that the [1+2] and [1+4] cycloaddition pathways are parallel, competing processes, with [1+2] cycloaddition being faster but more sensitive to steric hindrance.[91] For example, the reaction of the bulkier silylene, **9**, with 2,3-dimethyl-1,3-butadiene led to the formation of the silacyclopentene, **17** (eq.1.20), with no evidence of the corresponding vinylsilirane, which would be expected to be thermally stable and observable if it was generated.[90] This example thus supports the view that steric hindrance has a proportionally greater inhibitory effect on [1+2]-cycloaddition than on [1+4]-cycloaddition.[92]

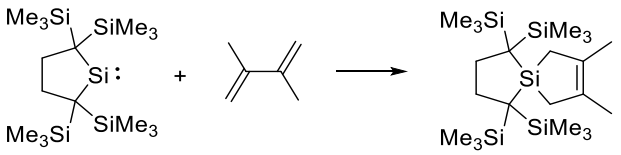

(1.20)

17

1.6.4. Complexation with Lewis Bases

Another reaction that silylenes undergo is complexation with Lewis bases such as amines, phosphines, ethers, and sulfides, where the electrons are donated towards the electrophilic silicon center, affording donor-stabilized silylene derivatives. The resulting complexes are typically less reactive than the uncoordinated silylenes.

The direct detection of silylene-donor complexes was reported by the groups of Ando and West in low temperature matrixes by UV-vis spectroscopy.[77, 93] This was followed by a theoretical study of the involvement of complexes in the X-H insertion reactions of SiH_2 with the parent hydride donors (H_2O, H_2S, NH_3, and PH_3) by Gordon and coworkers.[94] The complexes exhibit low energy absorption bands that are blue-shifted relative to the *n* – *p* absorption band of the free silylene.[95] The blue shift is caused by the change in the nature of the lowest energy excited state on complexation, from *n*, *p* in the free silylene to *n*, σ^* in the complex.

Our group has investigated the complexation reactions of silylenes with O-donors in solution.[30, 96] The rate and equilibrium constants for complexation of $SiMe_2$, $SiPh_2$, and $SiMes_2$ with Et_2O, THF, and 1,4-dioxane are shown in Table 1.3, where measurable equilibrium constants correlate with the Lewis acidity of the silylene and decrease in the order $SiPh_2$> $SiMe_2$>> $SiMes_2$. This trend reflects the σ- and π-electron withdrawing

effects of the phenyl substituent relative to methyl, which enhances the Lewis acidity of the silylene. In the case of the mesityl substituent, steric hindrance causes a destabilizing effect on complexation which diminishes the Lewis acidity of the silylene.

Table 1.3. Equilibrium (K_C) and forward rate (k_C) constants for complexation of transient silylenes with O-donors in hexanes at 25°C

Substrate	$[K_C]$ (M^{-1}) | k_C (10^9 $M^{-1}s^{-1}$)		
	$SiMe_2$	$SiPh_2$	$SiMes_2$
Et_2O	[1260 ± 50] [a]	[7100 ± 600] [a] 15 ± 4[a]	[0.9 ± 0.1] [a]
THF	17.3 ± 1.5[a]	15 ± 1[a]	[2.4 ± 0.4] [a]
1,4-dioxane		18 ± 1[b]	

a. Data from ref 96; b. Data from ref 30.

1.6.5. Reactions with Carbonyl Compounds

The reactions of silylenes with aldehydes and ketones were extensively studied as one of the fundamental reactions of silylenes by several groups beginning in the late 1970s.[31, 97-105] These reactions afford a variety of different products, depending on the structures of the silylene and the carbonyl compound. Generally, the reactions of silylenes with enolizable ketones proceed via ene-addition to generate the corresponding silyl enol ether, while the reactions with non-enolizable carbonyl compounds yield 3-, 5-, and/or 6-membered rings via (1+2)-, (1+2+2)-, or (1+1+2+2)-cycloaddition pathways (Scheme 2).

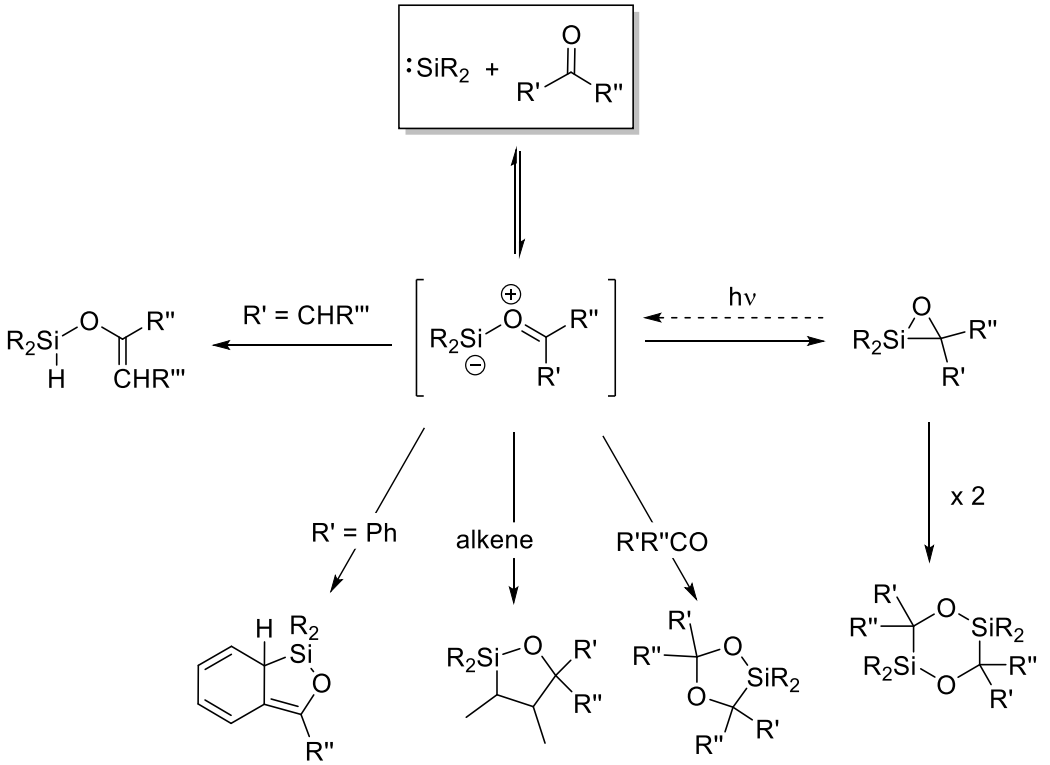

Scheme 2. Reactions of silylenes with carbonyl compounds.

The mechanisms of these reactions have been investigated and are thought to proceed via the initial formation of a silacarbonyl ylide intermediate. Ando and co-workers reported the first spectroscopic evidence for such intermediates in low temperature matrixes.[102] The reaction of dimesitylsilylene with 1,1,3,3-tetramethyl-2-indanone generates the corresponding silacarbonyl ylide (**18**) exhibiting a broad UV-vis absorption band at λ_{max} = 610 nm, which disappears upon photolysis or heating to generate the corresponding oxasilirane (**19**) (eq. 1.21). Interestingly, when **19** is photolyzed with 254 nm light, **18** is re-formed, indicating the photochemical conversion of **18** to **19** is reversible under matrix conditions. The silacarbonyl ylides (**20**) were also detected as intermediates in the reactions of dimethylsilylene and dimesitylsilylene with diisopropyl ketone and found to exhibit absorption bands centered at λ_{max} = 625 and 582

nm respectively, which immediately disappear upon photolysis or heating to generate the corresponding silyl enol ether (**21**) (eq. 1.22).

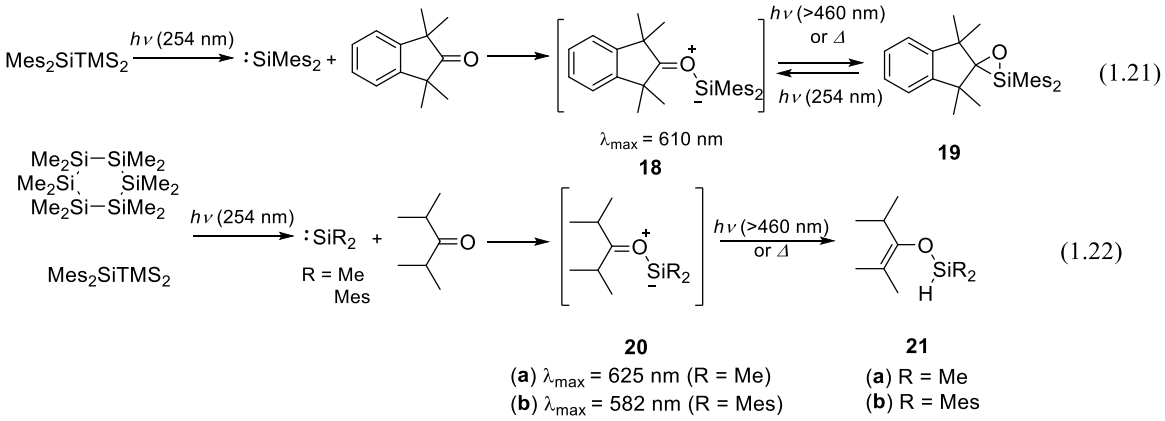

There are numerous examples of the formation of silyl enol ethers (**22**) from the reaction of silylenes with enolizable carbonyl compounds (eq. 1.23).[30, 82, 99, 106]

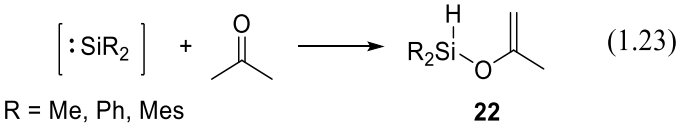

On the other hand, the reactions of silylenes with non-enolizable ketones are not as straightforward, as they can proceed to afford various cycloadducts. One possible cycloadduct that can be generated is a [1+2]-cycloadduct, or oxasilirane. There are only four known examples of stable oxasiliranes reported (**19** and **23**-**25**) all of them prepared by the reaction of silylenes with non-enolizable carbonyl compounds.[102, 107-109]

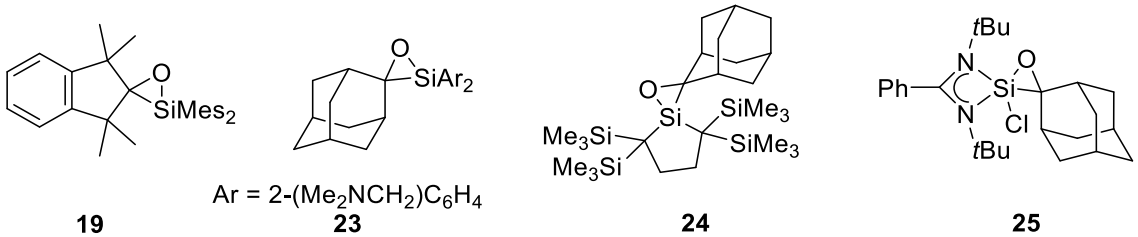

Other than these four examples, oxasiliranes are proposed to be reactive intermediates in the reactions of silylenes with carbonyl compounds. The reaction of $SiMe_2$ with a variety of dialkyl-substituted 1,2-diketones generates the corresponding dioxasilacyclopentene (eq. 1.24).[103] The mechanism for formation of the dioxasilacyclopentene was proposed to involve the initial formation of an acyl-substituted oxasilirane (**26**), which then undergoes ring expansion to afford dioxasilacyclopentene (**27**).[104]

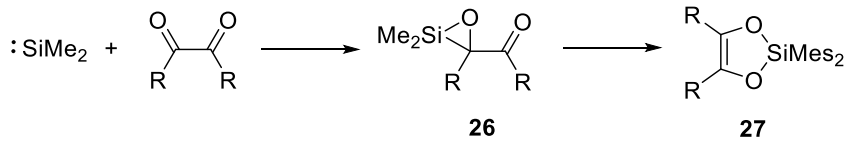

26 **27** (1.24)

The reaction of $SiMes_2$ with crotonaldehyde affords the 1:2 cycloadducts, **28** and **29**. These structures were proposed to be generated by 1,3-dipolar cycloaddition of the silacarbonyl ylide with the C=C or C=O double bond of a second molecule of aldehyde, respectively. (eq. 1.25).[110]

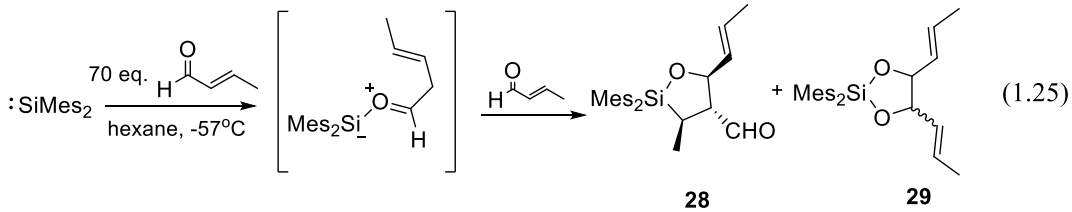

28 **29** (1.25)

Conversely, Ando and coworkers studied the reaction of $SiMe_2$ with 2-adamantanone (**30**) (eq. 1.26) and isolated the corresponding 1,4-dioxasilacyclopentane, **31**.[98] The analogous product (**32**) is formed upon generation of $SiMe_2$ in the presence of norbornone (**33**) under similar conditions (eq. 1.27).

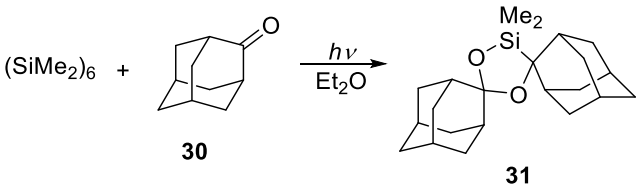

(1.26)

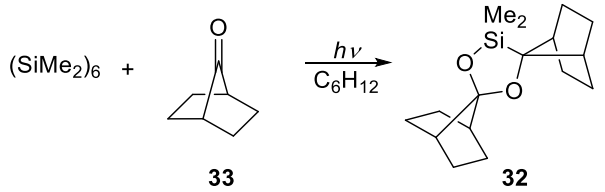

(1.27)

The regioselectivity of the cycloaddition of silacarbonyl ylides with C=O double bonds is dependent on the substituents surrounding the silacarbonyl ylide center and the structure of the carbonyl compound. 1,3-Dioxasilacyclopentenes and 1,3-dioxasilacyclopentanes are generated in the reactions of silylenes with α-diketones[103-104, 111] and α,β-unsaturated aldehydes[110], respectively, while 1,4-dioxasilacyclopentanes are typically formed from reactions with alkyl aldehydes[110] and dialkyl ketones.[98, 110] Theoretical calculations suggest that the regioselectivities of these cycloaddition reactions are dictated by the relative values of the orbital coefficients in the frontier molecular orbitals (FMOs) of the reaction partners.[110] The 1,4-dioxasilacyclopentane is obtained preferentially when the orbital coefficients on O and C are very different, while if the difference between the orbital coefficients on the oxygen and carbonyl carbon of the aldehyde is small, then the electrostatically controlled product, 1,3-dioxasilacyclopentane, tends to be favored.

Kira and co-workers have studied the reactions of the isolable dialkylsilylene **9** with a series of ketones, including 2-adamantanone, acetone, benzophenone, di(*tert*-butyl)- and diphenylcyclopropenone.[108] The reactions of **9** with 2-adamantanone and

acetone afforded the corresponding oxasilacyclopropane and silyl enol ether, respectively. In the case of benzophenone, the reaction proceeds to generate 2-oxa-silacyclopentene **34** (eq.1.28). The formation of **34** is thought to arise from intramolecular [2+3]-cycloaddition between an aromatic C=C bond and the carbonyl ylide as a 1,3-dipole. The reactions of other silylenes with benzophenone proceed similarly.[31, 104, 107]

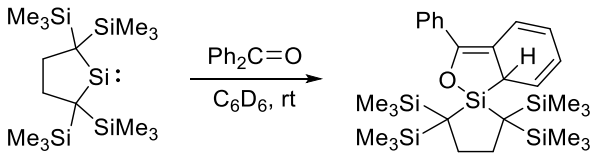

9 **34** (1.28)

The variation in the mode of cycloaddition of silylenes with non-enolizable carbonyl compounds can be traced back to the electronic structure of the silacarbonyl ylide intermediate, which has been investigated using DFT calculations.[108] It was found that the charge distribution in the initially formed silacarbonyl ylide, formally a 1,3-dipole, is dependent on the substituents on the silylene and carbonyl compound. The three resonance structures that contribute to the hybrid electronic structure of the silacarbonyl ylide are shown in eq. 1.29. Type I involves a nucleophilic silicon, Type II involves an electrophilic silicon, and Type III describes a 1,3-biradical moiety. The Type II structure is favored by electron withdrawing groups on the carbonyl carbon, while Type I is favored by electron donating groups.

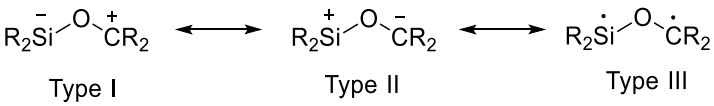

Type I Type II Type III (1.29)

The electronic nature of the silacarbonyl ylide was best exemplified in the experimental and theoretical calculations on the reactions of silylenes with

cyclopropenones and cyclopentadienones, by utilizing aromatic stability.[107-108] The reactions of **9** with di(*tert*-butyl)- and diphenylcyclopropenone afford products derived from the corresponding oxasilacyclopropane (eq. 1.30). The reactivity was explained by considering the electronic structure of the silacarbonyl ylide which has a strong contribution of Type I (eq. 1.30). On the other hand, the corresponding silacarbonyl ylide from the reactions with cyclopentadienones, has a strong contribution of Type II (eq. 1.31).[107]

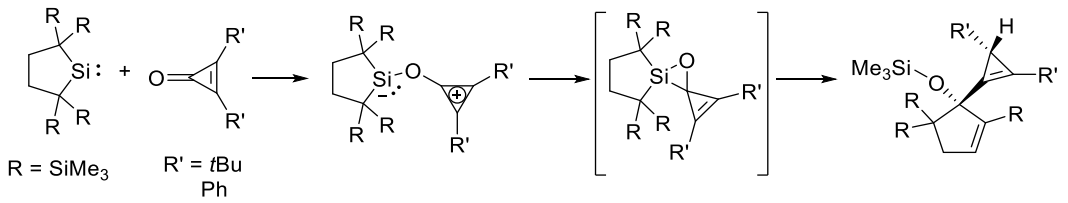

(1.30)

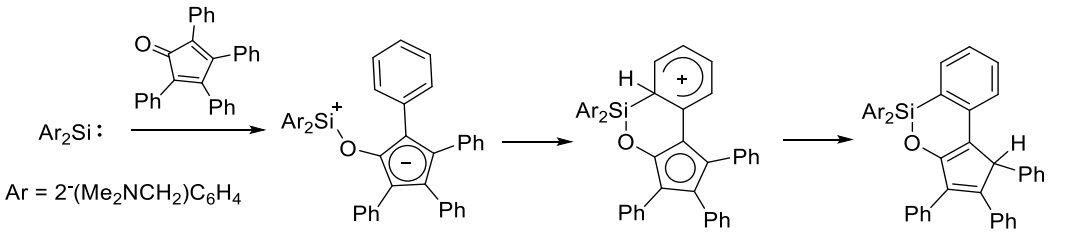

(1.31)

The reactions of silylenes with carbonyl compounds provide a versatile route for the preparation of various heterocyclic compounds. For example, Komatsu and co-workers demonstrated the intramolecular cycloaddition of silacarbonyl ylides tethered to unactivated dipolarophiles proceeds to afford bicyclic siloxanes (**35**) (eq. 1.32).[112] The reaction is thought to proceed via the initial formation of the silacarbonyl ylide, followed by ($2\pi + 4\pi$) intramolecular cycloaddition with the tethered dipolarophile.

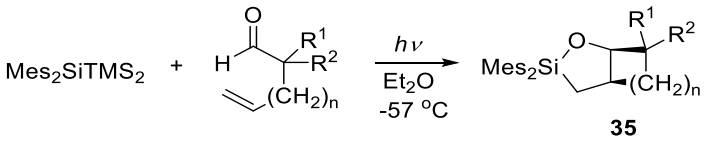

35 (1.32)

The same group also described an intermolecular cycloaddition of a silacarbonyl ylide, generated by the reaction of $SiMes_2$ with pivalaldehyde, with an acetylenic dipolarophile to generate oxasilacyclopentene (**36**) (eq. 1.33).[110]

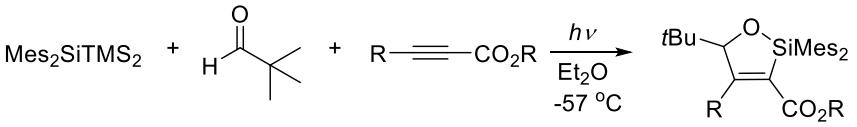

36 (1.33)

Woerpel and co-workers have obtained similar products from the metal-catalyzed silylene transfer to carbonyl compounds in the presence of an electron-deficient alkyne, which affords oxasilacyclopentane (**37**) (eq. 1.34).[113] It should be noted that the reaction does not involve the free silylene, but rather proceeds via a silylenoid mechanism.

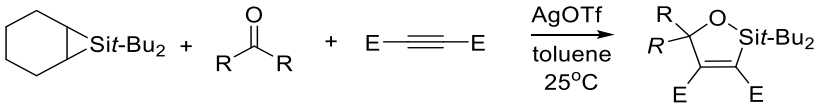

37 (1.34)

There have been a few kinetic studies reported on the reactions of silylenes with carbonyl compounds in solution. They are limited to the reactions of $SiMe_2$, $SiPh_2$, and $SiMes_2$ with acetone[30, 82, 114] and of $SiMes_2$ with 1,1,3,3-tetramethyl-2-indanone[82] in hydrocarbon solvents. Early fast kinetic studies of the reactions of $SiMes_2$ with acetone were reported by Conlin and co-workers, who reported an unusually fast rate constant for the reaction, $k_Q = 2.5 \times 10^{10}$ $M^{-1}s^{-1}$.[82] The plot of k_{decay} vs concentration displayed an upward curvature which would imply an unusual mechanistic behavior.[82] This was later re-evaluated by Leigh and coworkers, who found the decay rate coefficient to be linearly

dependent on acetone concentration, leading to a rate constant of $k_Q = (1.4 \pm 0.1) \times 10^{10}$ $M^{-1}s^{-}$.[30] The reaction of $SiMes_2$ with 1,1,3,3-tetramethyl-2-indananone was also reported to proceed rapidly, but unlike the situation in solid low temperature matrixes[102], showed no evidence for the build-up of the corresponding silacarbonyl ylide in detectable amounts.[82] The absolute rate constants reported are shown in Table 1.4.[30, 78, 82, 87] The rate constants measured for the reactions with acetone systematically decrease in the order $SiMe_2 \approx SiPh_2 > SiMes_2$. The apparent difference in the rate constants for the reaction of $SiMes_2$ with acetone and **38** is remarkably small, considering the difference in steric bulk between the two ketones (eq. 1.35).

Table 1.4. Rate constants (k_Q) for the reactions of transient silylenes with carbonyl compounds in hydrocarbon solutions

Substrate	k_Q (10^9 $M^{-1}s^{-1}$)		
	$SiMe_2$	$SiPh_2$	$SiMes_2$
acetone	14 ± 1 [a]	14 ± 2 [a]	8.3 ± 0.4 [a]
1,1,3,3-tetramethyl-2-indanone (**38**)			1.6 ± 0.2 [b]

a. Data from ref 30, in hexanes.; b. Data from ref 82, in cyclohexane.

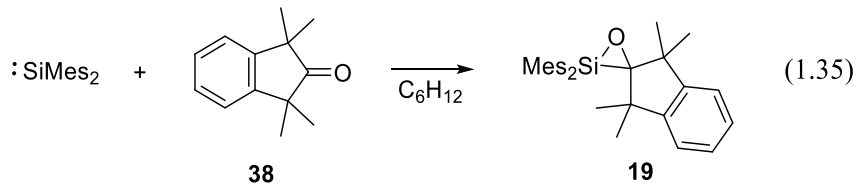

38 **19** (1.35)

1.7. Techniques Used for the Study of Transient Silylenes

The characterization of reactive intermediates in this thesis utilizes three main techniques: *steady state photolysis*, *laser flash* photolysis, and input from theoretical calculations. Steady state photolysis is used to identify primary products and determine

product yields, while laser flash photolysis is used to determine the reaction kinetics and thermodynamics by detecting directly and monitoring the reactive intermediates that are involved in the reaction.

1.8. Tools for Elucidation of Reaction Mechanisms

1.8.1. Kinetic Isotope Effect

The change in the rate constant caused by isotopic substitution in a reactant in a given reaction is referred as the kinetic isotope effect (KIE).[115] The KIE is expressed as the ratio of the rate constants observed with the natural abundance isotope (*e.g.* hydrogen) to one of its heavier isotopes (*e.g.* deuterium) (eq. 1.36). A primary isotope effect can arise when a bond to the isotope is formed or broken in the rate determining step and can be as large as $k_H/k_D \approx 7$. In principle, for a two-step reaction such as the ene-addition reaction of silylenes with enolizable ketones, the magnitude of k_H/k_D observed can in principle vary from $k_H/k_D \approx 1$ if formation of ylide is rate-determining to $k_H/k_D \approx 7$ if the H-migration step is rate-determining.

$$KIE = \frac{k_{natural\ abudance}}{k_{altered\ isotope}} = \frac{k_H}{k_D} \qquad (1.36)$$

The KIE originates from the difference in the frequencies of the various vibrational modes of a molecule that occurs when one isotope is switched with another.[116] The zero-point energy (ZPE) is the energy associated with the ground vibrational state of a molecule. The frequency is inversely proportional to mass so the stretching frequency of a bond to deuterium is lower than that of the corresponding bond to H, due to the heavier mass, which will result in a lower ZPE for the bond. The KIE is produced from the

difference of ZPE between the C-L (L = H, D) bonds in the transition state and the reactant (*Δ*ZPE). In exothermic and endothermic reactions, the structure of the transition state resembles the reactant and product respectively (Figure 1.2a and 1.2b). There is thus little difference in *Δ*ZPE between the reactant and transition state, which results in a small isotope effect. In the case of a thermoneutral reaction, the stretches centered around the isotope (H/D) at the transition state is symmetrical, which causes the frequency of the symmetric stretches to be independent of the isotope (Figure 1.2c). This results in the *Δ*ZPE at the transition state to be even smaller which causes a large KIE to be observed.

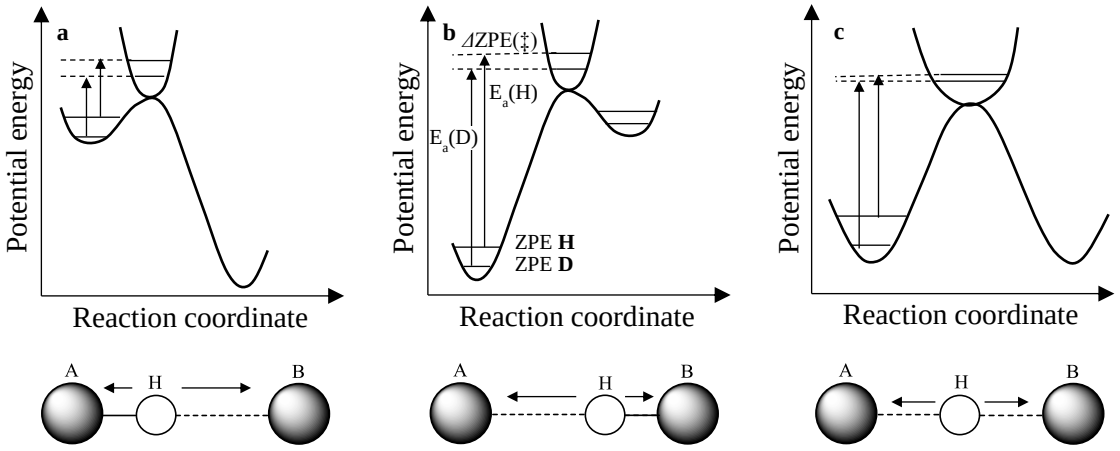

Figure 1.2. The zero-point energy difference between C-H and C-D bonds between the reactant and transition state changes as a function of the potential energy of the reaction and the corresponding transition state of the H-transfer (a) endothermic reaction (b) exothermic reaction (c) thermoneutral reaction. Figures were obtained from ref 116.

1.8.2. Variable Temperature and Determination of Activation Parameters

In general, most reactions show an increase in rate constant as the temperature increases because the higher temperature gives the reactants more thermal energy to overcome the activation barrier and proceed to the products.[117] The Arrhenius (eq.1.37) and Eyring (eq. 1.39) equations describes the temperature dependence of the reaction rate

constant. The Arrhenius equation (eq. 1.37), where A is the pre-exponential factor and E_a is the activation energy[115] , informs on the energy required to overcome the transition state barrier. The Arrhenius equation can be manipulated to give eq. 1.38 and can be determined from a plot of ln(k) vs. T^{-1}.

$$k = A\ exp(\frac{-E_a}{RT}) \qquad (1.37)$$

$$\ln(k) = -\frac{E_a}{RT} + \ln A \qquad (1.38)$$

The Eyring equation (eq. 1.39), where k_B is the Boltzmann constant and h is Planck's constant, provides the enthalpy of activation ($\Delta H^{\ddagger}$) and entropy of activation ($\Delta S^{\ddagger}$) from a plot of ln(k/T) vs. T^{-1} (eq. 1.40).[115] However, this equation requires the assumption that $\Delta S^{\ddagger}$ and $\Delta H^{\ddagger}$ do not vary with temperature, based on transition state theory.[115] The entropy of activation informs on the change in entropy that occurs as the reactants combine to form the transition state; a positive value indicates an increase in entropy at the transition state, or a dissociative reaction mechanism, while a negative value indicates a decrease in entropy, or an associative reaction mechanism. The enthalpy of activation represents the difference in enthalpy between the reactant(s) and the transition state.

$$k = \frac{kT}{h}\exp\left(\frac{\Delta S^{\ddagger}}{R}\right)\exp(\frac{-\Delta H^{\ddagger}}{RT}) \qquad (1.39)$$

$$\ln(k/T) = -\frac{\Delta H^{\ddagger}}{RT} + ln\frac{k_B}{h} + \frac{\Delta S^{\ddagger}}{R} \qquad (1.40)$$

The Arrhenius activation energy correlates with the Eyring enthalpy of activation as shown in eq. 1.41, while the pre-exponential factor (A) correlates with the Eyring entropy of activation as shown in eq. 1.42.

$$E_a = \Delta H^{\ddagger} + RT \qquad (1.41)$$

$$\Delta S^{\ddagger} = 4.576(lnA - 10.753 - lnT) \quad (1.42)$$

1.9. Goals and Outline of the Thesis

Over the past *ca.* five years, our group has studied the kinetics of the reactions of transient silylenes ($SiMe_2$, $SiPh_2$ and $SiMes_2$) with a variety of carbonyl compounds in solution by steady state and laser flash photolysis methods.[118]

The first goal of this thesis is to compile our group's studies of the reactions of $SiMe_2$, $SiPh_2$, and $SiMes_2$ with carbonyl compounds in solution and complete any study in which deficiencies exist. The carbonyl compounds that have been studied in complete detail so far are acetone, 1,1,1-trifluoro-2-butanone, pinacolone, 2,4-dimethyl-3-pentanone, pivalaldehyde, and camphor. The carbonyl compounds for which only transient spectra have been obtained, but the kinetic analysis is incomplete are acetone-d_6, 2-adamantanone, norcamphor, and cyclopentanone. The work has been extended to include the additional ketones camphor-3,3-d_2, dicyclopropyl ketone, 2,2,5,5-tetramethylcyclopentanone, and 2,2,4,4-tetramethyl-3-pentanone.

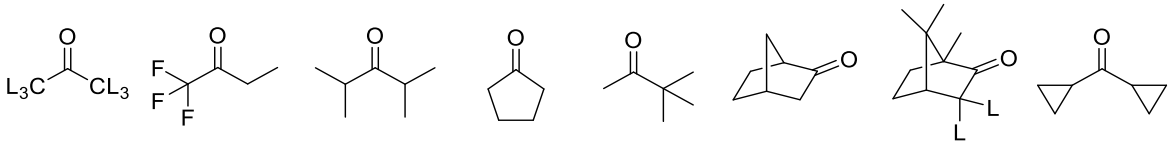

39a: L = H
39b: L = D

40 **41** **42** **43** **44**

45a: L = H
45b: L = D

46

The second goal of this thesis is to study the reactions of $SiMe_2$, $SiPh_2$, and $SiMes_2$ with a closely related system to 1,1,3,3-tetramethyl-2-indanone (**37**), previously reported by Ando and coworkers for the direct detection of the $SiMes_2$-**37** silacarbonyl ylide[92] and isolation and characterization of **19**,[97, 102] that is non-absorbing at 248 nm, using both kinetic and product studies. 2,2,5,5-Tetramethylcyclopentanone (**49**) has

similar structural parameters as **37** and the exclusion of the aromatic group meets our requirement for photolysis experiments.

The third goal was to isolate and identify the product of the reaction of $SiPh_2$ with 2-adamantanone, which is proposed to generate the corresponding 2,4-dioxa-1-silacyclopentane on the basis of the reported literature for its analogous silylene reactions $SiMe_2$ and $SiMes_2$.

Chapter 2 focuses on the reactions of $SiMe_2$, $SiPh_2$, and $SiMes_2$ with enolizable carbonyl compounds. Following a review of what has been accomplished so far by previous students in the group, the kinetic analyses of the reactions of the silylenes with acetone, 1,1,1-trifluoro-2-butanone, pinacolone, 2,4-dimethyl-3-pentanone, and camphor have been completed in great detail. Kinetic isotope effects were investigated for the reactions of the silylenes with camphor-d_2 (**45b)** and acetone-d_6 (**39b**). In addition, the reactions of the three silylenes with dicyclopropyl ketone (**46**) were studied for comparison to the results for diisopropyl ketone (**41**), to evaluate the effects of angle strain at the ketone α-carbon on the rate constant for H-migration in the ylide intermediate.

Chapter 3 reports a study of the reactions of the silylenes with the non-enolizable carbonyl compounds pivalaldehyde (**47**), 2-adamantanone (**30**), 2,2,4,4-tetramethyl-3-pentanone (**48**), and 2,2,5,5-tetramethylcyclopentanone (**49**). As mentioned earlier, **49** was studied as a non-absorbing 248 nm analogue to 1,1,3,3-tetramethyl-2-indanone. In addition, silacarbonyl ylide intermediates have been detected in the reactions of $SiMe_2$ and $SiPh_2$ with 2-adamantanone, 2,2,4,4-tetramethyl-3-pentanone, and 2,2,5,5-

tetramethylcyclopentanone, and of $SiMes_2$ with 2-adamantanone. The kinetic behavior of the ylides was found to differ fundamentally from what was observed with the ylides derived from enolizable carbonyl compounds, where in the presence of higher ketone concentrations (*ca.* > 5 mM), the lifetime of the ylides are dependent on the ketone concentration. This kinetic behavior suggests that the ylide might be undergoing a 1,3-dipolar cycloaddition with a second molecule of ketone. **48** was studied as the acyclic analogue of **49**, to examine the effects on the cycloaddition reaction. Silacarbonyl ylide intermediates have been detected in the reactions of $SiMe_2$ and $SiPh_2$ with **30**, **48**, and **49**, and $SiMes_2$ with **30**.

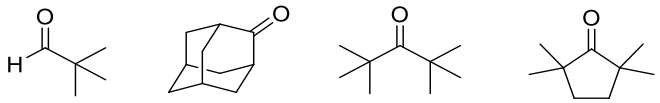

47 **30** **48** **49**

1.10. References:

1. Gaspar, P. P.; West, R., Silylenes. In *The chemistry of organic silicon compounds, Vol. 2*, Rappoport, Z.; Apeloig, Y., Eds. John Wiley and Sons: New York, 1998; Vol. 2, pp 2463-2568.
2. Tokitoh, N.; Ando, W., Silylenes (and Germylenes, Stannylenes, Plumbylenes). In *Reactive Intermediate Chemistry*, Moss, R. A.; Platz, M. S.; Jones, M., Jr., Eds. John Wiley & Sons: New York, 2004; pp 651-715.
3. Haaf, M.; Schmedake, T. A.; West, R., *Accounts of Chemical Research* **2000,** *33* (10), 704-714.
4. Haaf, M.; Schmiedl, A.; Schmedake, T. A.; Powell, D. R.; Millevolte, A. J.; Denk, M.; West, R., *J. Am. Chem. Soc.* **1998,** *120*, 12714-12719.
5. Kira, M., *J. Chem. Sci.* **2012,** *124*, 1205-1215.
6. Roesky, H. W., *J. Organomet. Chem.* **2013**.
7. Sen, S. S.; Khan, S.; Samuel, P. P.; Roesky, H. W., *Chem. Sci.* **2012,** *3* (3), 659-682.
8. Driess, M., *Nature Chem.* **2012,** *4* (7), 525-526.
9. Kira, M.; Ishida, S.; Iwamoto, T., *Chem. Record* **2004,** *4*, 243-253.
10. Mizuhata, Y.; Sasamori, T.; Tokitoh, N., *Chem. Rev.* **2009,** *109*, 3479-3511.
11. Apeloig, Y.; Pauncz, R.; Karni, M.; West, R.; Steiner, W.; Chapman, D., *Organometallics* **2003,** *22*, 3250-3256.
12. Bundhun, A.; Ramasami, P.; Gaspar, P. P.; Schaefer, H. F., *Inorg. Chem.* **2012,** *51*, 851-863.
13. Oláh, J.; De Proft, F.; Veszpr,émi, T.; Geerlings, P., *J. Phys. Chem. A* **2004,** *108*, 490-499.
14. Walsh, R.; Patai, S.; Rappoport, Z., Thermochemistry. In *The Chemistry of Organic Silicon Compounds*, John Wiley & Sons Ltd.: 1989; pp 371-391.
15. Walsh, R., *Acc. Chem. Res.* **1981,** *14*, 246-252.
16. Becerra, R.; Frey, H. M.; Mason, B. P.; Walsh, R.; Gordon, M. S., *J. Chem. Soc., Far. Trans.* **1995,** *91* (17), 2723-2732.
17. Horner, D. A.; Grev, R. S.; Schaefer, H. F., III, *J. Am. Chem. Soc.* **1992,** *114*, 2093-2098.
18. Becerra, R.; Boganov, S. E.; Egorov, M. P.; Faustov, V. I.; Nefedov, O. M.; Walsh, R., *J. Am. Chem. Soc.* **1998,** *120*, 12657-12665.
19. Allendorf, M. D.; Melius, C. F., *J. Phys. Chem. A* **2005,** *109* (22), 4939-4949.
20. Gaspar, P. P., Silylenes. In *Reactive Intermediates, Vol. 3*, Jones, M., Jr.; Moss, R. A., Eds. John Wiley & Sons: New York, 1985; Vol. 3, pp 333-427.
21. Gaspar, P. P., Silylenes. In *Reactive Intermediates, Vol. 2*, Jones, M., Jr.; Moss, R. A., Eds. John Wiley & Sons: New York, 1981; Vol. 2, pp 335-385.
22. Gaspar, P. P., Silylenes. In *Reactive Intermediates, Vol. 1*, Jones, M., Jr.; Moss, R. A., Eds. John Wiley & Sons: New York, 1978; Vol. 1, pp 229-277.
23. Miller, R. D.; Michl, J., *Chem. Rev.* **1989,** *89*, 1359-1410.
24. Braddock-Wilking, J.; Chiang, M. Y.; Gaspar, P. P., *Organometallics* **1993,** *12*, 197-209.

25. Masamune, S.; Murakami, S.; Tobita, H.; Williams, D. J., *J. Am. Chem. Soc.* **1983,** *105*, 7776-7778.
26. Helmer, B. J.; West, R., *Organometallics* **1982,** *1* (11), 1463-1466.
27. Ishikawa, M.; Kumada, M., *Adv. Organomet. Chem.* **1981,** *19*, 51-95.
28. Kira, M.; Miyazawa, T., Mechanistic aspects of the photochemistry of organosilicon compounds. In *The chemistry of organic silicon compounds, Vol. 2*, Rappoport, Z.; Apeloig, Y., Eds. John Wiley & Sons: New York, 1998; Vol. 2, pp 1311-1337.
29. Ishikawa, M.; Kumada, M., *Chem. Commun.* **1970,** *1970*, 612-612.
30. Moiseev, A. G.; Leigh, W. J., *Organometallics* **2007,** *26*, 6268-6276.
31. Ishikawa, M.; Nishimura, K.; Sugisawa, H.; Kumada, M., *J. Organomet. Chem.* **1980,** *194*, 147-158.
32. Lambert, R. L.; Seyferth, D., *J. Am. Chem. Soc.* **1972,** *94*, 9246-9248.
33. Palmer, W. S.; Woerpel, K. A., *Organometallics* **1997,** *16* (22), 4824-4827.
34. Ando, W.; Shiba, T.; Hidaka, T.; Morihashi, K.; Kikuchi, O., *J. Am. Chem. Soc.* **1997,** *119*, 3629-3630.
35. Boudjouk, P.; Black, E.; Kumarathasan, R., *Organometallics* **1991,** *10*, 2095-2096.
36. Barton, T. J.; Tillman, N., *J. Am. Chem. Soc.* **1987,** *109*, 6711-6716.
37. Arrington, C. A.; West, R.; Michl, J., *J. Am. Chem. Soc.* **1983,** *105* (19), 6176-6177.
38. Hill, N. J.; West, R., *J. Organomet. Chem.* **2004,** *689*, 4165-4183.
39. Denk, M.; Lennon, R.; Hayashi, R.; West, R.; Belyakov, A. V.; Verne, H. P.; Haaland, A.; Wagner, M.; Metzler, N., *J. Am. Chem. Soc.* **1994,** *116*, 2691-2692.
40. Kira, M.; Ishida, S.; Iwamoto, T.; Kabuto, C., *J. Am. Chem. Soc.* **1999,** *121*, 9722-9723.
41. Karsch, H. H.; Keller, U.; Gamper, S.; Müller, G., *Angewandte Chemie International Edition in English* **1990,** *29* (3), 295-296.
42. Jutzi, P.; Holtmann, U.; Kanne, D.; Krüger, C.; Blom, R.; Gleiter, R.; Hyla-Kryspin, I., *Chemische Berichte* **1989,** *122* (9), 1629-1639.
43. Driess, M.; Yao, S.; Brym, M.; van W√ºllen, C.; Lentz, D., *J. Am. Chem. Soc.* **2006,** *128* (30), 9628-9629.
44. So, C.-W.; Roesky, H. W.; Magull, J.; Oswald, R. B., *Angew. Chem. Int. Ed. Engl.* **2006,** *45* (24), 3948-3950.
45. Kong, L.; Zhang, J.; Song, H.; Cui, C., *Dalton Transactions* **2009,** (28), 5444-5446.
46. Zark, P.; Schäfer, A.; Mitra, A.; Haase, D.; Saak, W.; West, R.; Müller, T., *Journal of Organometallic Chemistry* **2010,** *695* (3), 398-408.
47. S., S. S.; Anukul, J.; W., R. H.; Carola, S., *Angewandte Chemie International Edition* **2009,** *48* (45), 8536-8538.
48. Filippou, A. C.; Chernov, O.; Schnakenburg, G., *Angew. Chem. Int. Ed. Engl.* **2009,** *48* (31), 5687-5690.
49. Ghadwal, R. S.; Roesky, H. W.; Merkel, S.; Henn, J.; Stalke, D., *Angew. Chem. Int. Ed. Engl.* **2009,** *48* (31), 5683-5686.

50. Wenyuan, W.; Shigeyoshi, I.; Stephan, E.; Matthias, D., *Angewandte Chemie International Edition* **2012,** *51* (25), 6167-6171.
51. Rodriguez, R.; Troadec, T.; Kato, T.; Saffon-Merceron, N.; Sotiropoulos, J.-M.; Baceiredo, A., *Angew. Chem. Int. Ed. Engl.* **2012,** *51* (29), 7158-7161.
52. Gehrhus, B.; Lappert, M. F.; Heinicke, J.; Boese, R.; Bläser, D., *Journal of the Chemical Society, Chemical Communications* **1995,** (19), 1931-1932.
53. Wang, W.; Inoue, S.; Yao, S.; Driess, M., *Journal of the American Chemical Society* **2010,** *132* (45), 15890-15892.
54. Wang, W.; Inoue, S.; Irran, E.; Driess, M., *Angewandte Chemie International Edition* **2012,** *51* (15), 3691-3694.
55. Asay, M.; Inoue, S.; Driess, M., *Angew. Chem. Int. Ed. Engl.* **2011,** *50*, 9589-9592.
56. Abe, T.; Tanaka, R.; Ishida, S.; Kira, M.; Iwamoto, T., *J. Am. Chem. Soc.* **2012,** *134*, 20029-20032.
57. Kira, M.; Iwamoto, T.; Ishida, S., *Bull. Chem. Soc. Jpn.* **2007,** *80*, 258-275.
58. Rekken, B. D.; Brown, T. M.; Fettinger, J. C.; Tuononen, H. M.; Power, P. P., *J. Am. Chem. Soc.* **2012,** *134* (15), 6504-6507.
59. Protchenko, A. V.; Birjkumar, K. H.; Dange, D.; Schwarz, A. D.; Vidovic, D.; Jones, C.; Kaltsoyannis, N.; Mountford, P.; Aldridge, S., *J. Am. Chem. Soc.* **2012,** *134* (15), 6500-6503.
60. Kosai, T.; Ishida, S.; Iwamoto, T., *Angewandte Chemie International Edition* **2016,** *55* (50), 15554-15558.
61. Dong, Z.; Reinhold, C. R. W.; Schmidtmann, M.; Müller, T., *J. Am. Chem. Soc.* **2017,** *139* (20), 7117-7123.
62. Leigh, W. J.; Moiseev, A. G.; Coulais, E.; Lollmahomed, F.; Askari, M. S., *Can. J. Chem.* **2008,** *86*, 1105-1117.
63. Moiseev, A. G.; Coulais, E.; Leigh, W. J., *Chem. Eur. J.* **2009,** *15*, 8485-8491.
64. Ishikawa, M.; Nakagawa, K. I.; Ishiguro, M.; Ohi, F.; Kumada, M., *J. Organomet. Chem.* **1978,** *152*, 155-174.
65. Miyazawa, T.; Koshihara, S. Y.; Liu, C.; Sakurai, H.; Kira, M., *J. Am. Chem. Soc.* **1999,** *121*, 3651-3656.
66. Gaspar, P. P.; Holten, D.; Konieczny, S.; Corey, J. Y., *Acc. Chem. Res.* **1987,** *20*, 329-336.
67. Gaspar, P. P.; Boo, B. H.; Chari, S.; Ghosh, A. K.; Holten, D.; Kirmaier, C.; Konieczny, S., *Chem. Phys. Lett.* **1984,** *105*, 153-157.
68. Becerra, R.; Cannady, J. P.; Walsh, R., *J. Phys. Chem. A* **2003,** *107*, 11049-11056.
69. Al-Rubaiey, N.; Becerra, R.; Walsh, R., *Phys. Chem. Chem. Phys.* **2002,** *4*, 5072-5078.
70. Goure, W. F.; Barton, T. J., *J. Organomet. Chem.* **1980,** *199*, 33-41.
71. Fink, M. J.; Michalczyk, M. J.; Haller, K. J.; West, R.; Michl, J., *Organometallics* **1984,** *3*, 793-800.
72. Malcolm, N. O. J.; Gillespie, R. J.; Popelier, P. L. A., *J. Chem. Soc., Dalton Trans.* **2002,** *2002*, 3333-3341.

73. Raabe, G.; Michl, J.; Patai, S.; Rappoport, Z., Multiple bonding to silicon. In *The chemistry of organic silicon compounds*, John Wiley & Sons: New York, 1989; pp 1015-1142.
74. Raabe, G.; Michl, J., *Chem. Rev.* **1985,** *85*, 419-509.
75. Becerra, R.; Goldberg, N.; Cannady, J. P.; Almond, M. J.; Ogden, J. S.; Walsh, R., *J. Am. Chem. Soc.* **2004,** *126*, 6816-6824.
76. Su, M. D., *Chem. Eur. J.* **2004,** *10*, 6073-6084.
77. Gillette, G. R.; Noren, G. H.; West, R., *Organometallics* **1989,** *8*, 487-491.
78. Moiseev, A. G.; Leigh, W. J., *Organometallics* **2007,** *26*, 6277-6289.
79. Levin, G.; Das, P. K.; Lee, C. L., *Organometallics* **1988,** *7*, 1231-1232.
80. Baggott, J. E.; Blitz, M. A.; Frey, H. M.; Lightfoot, P. D.; Walsh, R., *Internat. J. Chem. Kinet.* **1992,** *24*, 127-143.
81. Atwell, W. H.; Weyenberg, D. R., *Angew. Chem. Int. Ed. Engl.* **1969,** *8* (7), 469-477.
82. Conlin, R. T.; Netto-Ferreira, J. C.; Zhang, S.; Scaiano, J. C., *Organometallics* **1990,** *9*, 1332-1334.
83. Ishikawa, M.; Kumada, M., *J. Organomet. Chem.* **1972,** *42*, 325-332.
84. Leigh, W. J.; Kostina, S. S.; Bhattacharya, A.; Moiseev, A. G., *Organometallics* **2010,** *29*, 662-670.
85. Heaven, M. W.; Metha, G. F.; Buntine, M. A., *J. Phys. Chem. A* **2001,** *105*, 1185-1196.
86. Becerra, R.; Cannady, J. P.; Walsh, R., *J. Phys. Chem. A* **2011,** *115*, 4231-4240.
87. Murov, S. L.; Carmichael, I.; Hug, G. L., *Handbook of photochemistry*. 2nd ed.; Dekker: New York, 1993.
88. Ando, W.; Kabe, Y., Highly Reactive Small Ring Monosilacycles and Medium Ring Oligosilacycles. In *The Chemistry of Organic Silicon Compounds*, Rappoport, Z.; Apeloig, Y., Eds. Wiley: 1998; p 2401.
89. Driess, M.; Grutzmacher, H., *Angew. Chem. Int. Ed. Engl.* **1996,** *35*, 828-856.
90. Zhang, S.; Conlin, R. T., *J. Am. Chem. Soc.* **1991,** *113*, 4272-4278.
91. Takeda, N.; Tokitoh, N.; Okazaki, R., *Chem. Lett.* **2000,** *2000*, 622-623.
92. Ishida, S.; Iwamoto, T.; Kira, M., *Heteroatom Chem.* **2011,** *22*, 432-437.
93. Ando, W.; Sekiguchi, A.; Hagiwara, K.; Sakakibara, A.; Yoshida, H., *Organometallics* **1988,** *7*, 558-559.
94. Raghavachari, K.; Chandrasekhar, J.; Gordon, M. S.; Dykema, K. J., *J. Am. Chem. Soc.* **1984,** *106*, 5853-5859.
95. Lee, V. Y.; Sekiguchi, A., Heavy Analogs of Carbenes: Silylenes, Germylenes, Stannylenes and Plumbylenes. In *Organometallic Compounds of Low-Coordinate Si, Ge, Sn and Pb*, John Wiley & Sons, Ltd: Chichester, 2010; pp 139-197.
96. Kostina, S. S.; Singh, T.; Leigh, W. J., *Organometallics* **2012,** *31*, 3755-3767.
97. Ando, W.; Ikeno, M.; Sekiguchi, A., *J. Am. Chem. Soc.* **1977,** *99* (19), 6447-6449.
98. Ando, W.; Ikeno, M.; Sekiguchi, A., *J. Am. Chem. Soc.* **1978,** *100* (11), 3613-3615.
99. Ando, W.; Ikeno, M., *Chem. Lett.* **1978,** *7*, 609-610.

100. Ishikawa, M.; Nakagawa, K.; Kumada, M., *J. Organomet. Chem.* **1977,** *135*, C45-C49.
101. Schäfer, A.; Weidenbruch, M.; Pohl, S., *J. Organomet. Chem.* **1985,** *282* (3), 305-313.
102. Ando, W.; Hagiwara, K.; Sekiguchi, A., *Organometallics* **1987,** *6*, 2270-2271.
103. Ando, W.; Ikeno, M., *J. Chem. Soc., Chem. Commun.* **1979,** (15), 655-656.
104. Jutzi, P.; Eikenberg, D.; Bunte, E. A.; Mohrke, A.; Neumann, B.; Stammler, H. G., *Organometallics* **1996,** *15*, 1930-1934.
105. Gehrhus, B.; Hitchcock, P. B.; Lappert, M. F., *Organometallics* **1997,** *16* (22), 4861-4864.
106. Bobbitt, K. L.; Gaspar, P. P., *J. Organomet. Chem.* **1995,** *499*, 17-26.
107. Belzner, J.; Ihmels, H.; Pauletto, L.; Noltemeyer, M., *J. Org. Chem.* **1996,** *61* (10), 3315-3319.
108. Ishida, S.; Iwamoto, T.; Kira, M., *Organometallics* **2010,** *29*, 5526-5534.
109. Azhakar, R.; Ghadwal, R. S.; Roesky, H. W.; Hey, J.; Stalke, D., *Organometallics* **2011,** *30* (14), 3853-3858.
110. Sakai, S.; Fukushima, T.; Minakata, S.; Ryu, I.; Komatsu, M., *Chem. Commun.* **1999**, 1857-1858.
111. Ghadwal, R. S.; Sen, S. S.; Roesky, H. W.; Granitzka, M.; Kratzert, D.; Merkel, S.; Stalke, D., *Angew. Chem. Int. Ed. Engl.* **2010,** *49* (23), 3952-3955.
112. Sakai, N.; Fukushima, T.; Okada, A.; Ohashi, S.; Minakata, S.; Komatsu, M., *J. Organomet. Chem.* **2003,** *686* (1-2), 368-372.
113. Bourque, L. E.; Woerpel, K. A., *Org. Lett.* **2008,** *10*, 5257-5260.
114. Bhattacharya, A. Study of Steric and Electronic Effects on the Reactivities of Diarylsilylene in Solution by Laser Flash Photolysis Methods. M.Sc. Thesis, McMaster University, Hamilton, ON, 2010.
115. Anslyn, E. V.; Dougherty, D. A., *Modern Physical Organic Chemistry*. University Science Books: New York, 2005; p 259-296.
116. Anslyn, E. V.; Dougherty, D. A., *Modern Physical Organic Chemistry*. University Science Books: New York, 2005; p 421-488.
117. Wright, M. R., An introduction to chemical kinetics / Margaret Robson Wright. 2004; pp 1-2.
118. C. Browne, W. J. L., *unpublished results*.
119. Kostina, S. S.; Singh, T.; Leigh, W. J., *J. Phys. Org. Chem.* **2011,** *24*, 937-946.

Chapter 2 – Kinetic and Thermodynamic Studies of the Reactions of Silylenes with Enolizable Carbonyl Compounds

2.1. Overview

This chapter describes the results of detailed kinetic studies of the reactions of the transient silylenes $SiMe_2$, $SiPh_2$, and $SiMes_2$, generated by photolysis of **1** – **3** respectively, with a selection of enolizable carbonyl compounds in solution. The substrates that were studied include acetone, acetone-d_6, 3,3-dimethyl-2-butanone, 1,1,1-trifluoro-2-butanone, 2,4-dimethyl-3-pentanone, dicyclopropyl ketone, cyclopentanone, camphor, camphor-3,3-d_2, and norcamphor. Steady state photolysis studies of the reactions of $SiPh_2$ with camphor and of $SiMe_2$ with dicyclopropyl ketone were also carried out and were found to afford the corresponding silyl enol ether as the sole reaction products, in agreement with early reports of the reactions of these silylenes with other enolizable ketones (eq. 2.1).

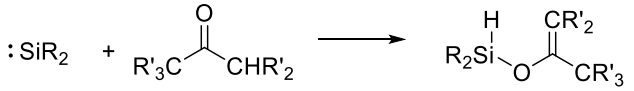

(2.1)

The reactions of $SiMe_2$ and $SiPh_2$ with acetone, 3,3-dimethyl-2-butanone, 1,1,1-trifluoro-2-butanone and cyclopentanone, $SiMe_2$ with 2,4-dimethyl-3-pentanone, and $SiMes_2$ with all ketones proceed with overall second order kinetics and absolute rate constants in the range of $10^7 – 10^{10}$ M^{-1} s^{-1} in hexanes at 25°C. No reaction intermediates could be detected for any of these systems by time-resolved UV-vis spectroscopy. On the other hand, the reactions of $SiMe_2$ and $SiPh_2$ with dicyclopropyl ketone, camphor, and

norcamphor, and $SiPh_2$ with 2,4-dimethyl-3-pentanone, showed more complex kinetic behavior. Flash photolysis of these systems led to the formation of new transient intermediates that exhibit broad absorption bands in the 500 – 650 nm range of the UV-visible spectrum, decay with first-order kinetics, and exhibit lifetimes in the 0.05 – 10 μs range depending on the silylene and carbonyl compound. The new species were assigned to the corresponding silacarbonyl ylides, formed by a bonding interaction between a carbonyl *n*-orbital and the vacant *p*-orbital on silicon. The ylides exhibit decay rate coefficients that vary with ketone concentration in a non-linear fashion, plateauing to a constant limiting value at high ketone concentration (10 – 50 mM) in each case. The limiting first-order rate constant for ylide decay is associated with that for the unimolecular H-migration pathway to afford the corresponding silyl enol ether. Primary kinetic isotope effects (k_H/k_D) in the range of 3 – 6 were measured for the reactions of $SiMe_2$, $SiPh_2$, and $SiMes_2$ with camphor and camphor-3,3-d_2. In addition, Arrhenius parameters were determined for the H-migration step in the reactions of $SiMe_2$ and $SiPh_2$ with camphor.

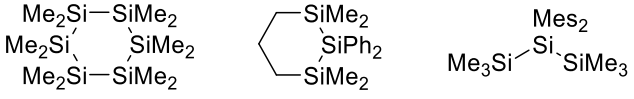

1 **2** **3**

2.2. Previous Studies in Our Group

Over the past *ca.* five years, our group has studied the reactions of $SiMe_2$, $SiPh_2$ and $SiMes_2$ with a variety of enolizable carbonyl compounds in solution by steady state and laser flash photolysis methods.[1] As was discussed in the previous chapter, many of

these reactions are known to generate the corresponding silyl enol ether as the major product.[2-14]

There are numerous known examples of $SiMe_2$- and $SiMes_2$- derived silyl enol ethers.[2, 10] However, there is only one example known of a $SiPh_2$-derived silyl enol ether, which is that from the reaction with acetone.[4] Our group studied the reaction of $SiPh_2$ with camphor, to confirm that the reaction does indeed proceed to yield the corresponding silyl enol ether in that case as well. Steady state photolysis of the $SiPh_2$ precursor **2** (0.05 M) in C_6D_{12} containing camphor (**4a**, 0.06 M) afforded the products shown in eq. 2.2.[1] Silyl enol ether **6** was identified in the crude photolysis mixture by ^{1}H NMR spectroscopy, as illustrated by the NMR spectra shown in Figure 2.1.[1] Particularly diagnostic of compounds of this type are the distinctive resonances due to the Si-H and vinylic protons at δ 5.51 and 4.62 respectively.[2, 4] The complete set of the ^{1}H assignments in the NMR spectrum of **6** are listed in Table S2.3.

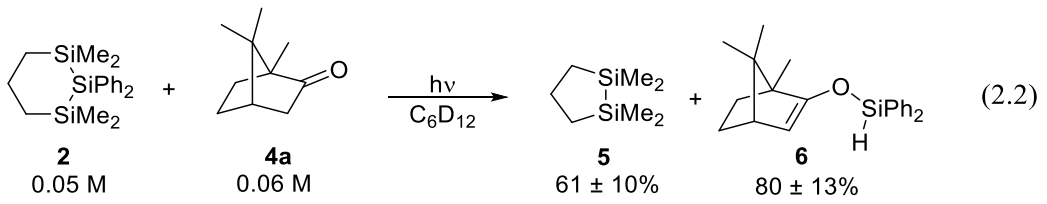

2 0.05 M + **4a** 0.06 M → **5** 61 ± 10% + **6** 80 ± 13% (2.2)

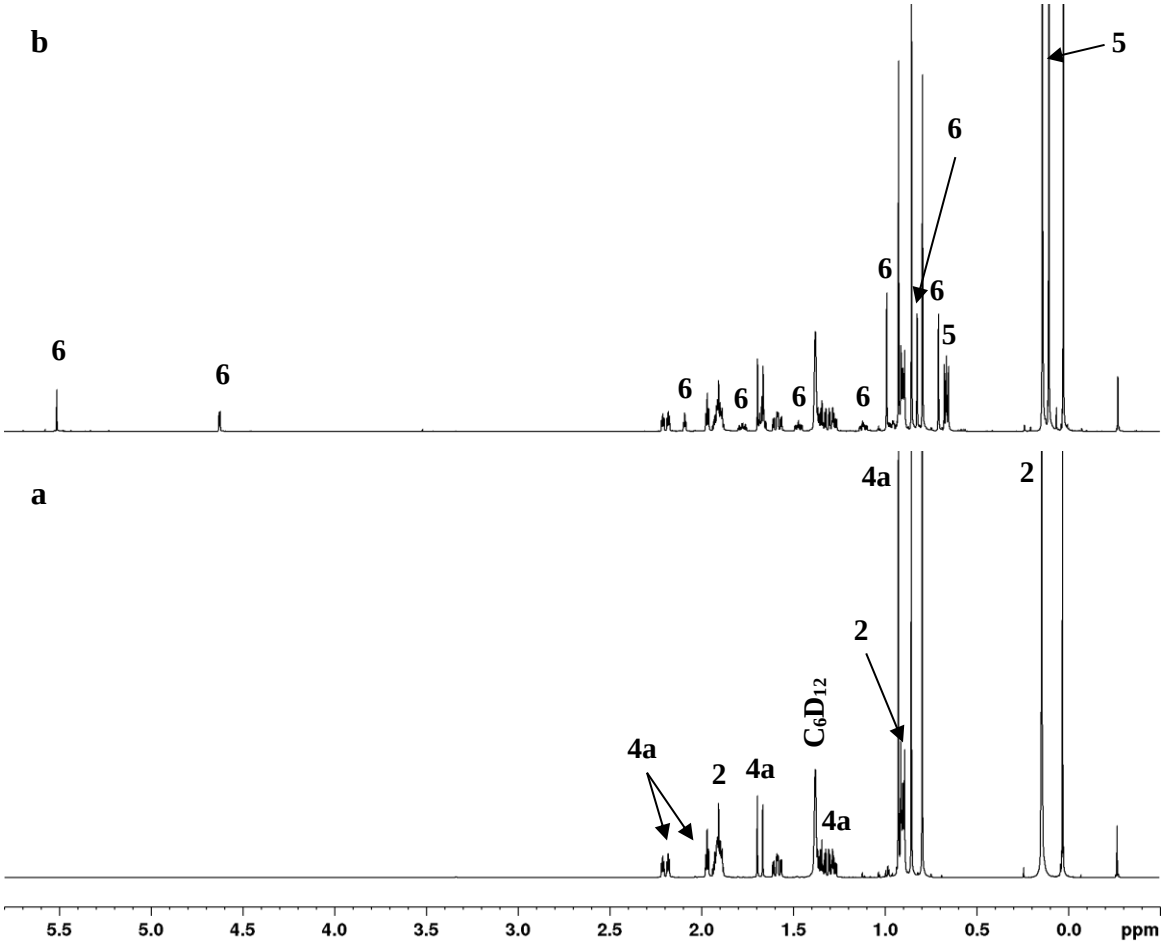

Figure 2.1. ^{1}H NMR spectra of a solution of **2** (0.05 M), camphor (**4a**) 0.05 M, and 0.01 M hexamethyldisilane in C_6D_{12} (a) before and (b) after 20 mins of photolysis. (*Data recorded by C. Browne*)

Flash photolysis studies focused initially on a broad survey of the kinetics of the reactions of the three silylenes with enolizable ketones of varying structure and substitution. In the absence of reactive substrates, 248 nm laser flash photolysis of **1** – **3** in deoxygenated, anhydrous hexanes affords the corresponding silylenes $SiMe_2$ (λ_{max} = 465 nm), $SiPh_2$ (λ_{max} = 300 and 515 nm), and $SiMes_2$ (λ_{max} = 290 and 580 nm), which decay to form the corresponding disilenes, Si_2Me_4 (λ_{max} = 360 nm), Si_2Ph_4 (λ_{max} = 290 and 460 nm), and Si_2Mes_4 (λ_{max} = 290 and 420 nm). The disilenes are significantly

longer-lived than the corresponding silylenes, as is evident from the transient absorbance-time profiles shown in Figure 2.2.[3, 15-16]

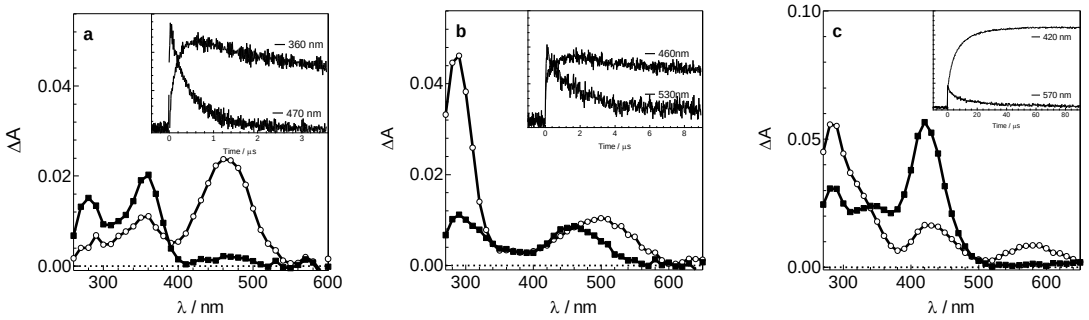

Figure 2.2. The open squares are the spectra of the silylenes (a) $SiMe_2$, (b) $SiPh_2$, and (c) $SiMes_2$, while the insets are the individual traces of the decay of the corresponding silylene and the growth of the corresponding disilene. (a) Transient absorption spectra recorded 0.09 - 0.12 μs (○) and 1.4 - 1.5 μs (■) after the laser pulse by laser flash photolysis of a hexanes solution of **1**. The inset shows transient decay traces recorded at 360 and 470. (b) Transient absorption spectra recorded 0.19 - 0.26 μs (○) and 4.2 - 4.3 μs (■) after the laser pulse by laser flash photolysis of a hexanes solution of **2**. The inset shows transient decay traces recorded at 460 and 530. (c) Transient absorption spectra recorded 0.0 - 1.3 μs (○) and 107 - 108 μs (■) after the laser pulse, from laser flash photolysis of a hexanes solution of **3**. The inset shows transient decay traces recorded at 420 and 570.

The addition of ketones such as acetone[3], 3,3-dimethyl-2-butanone, 1,1,1-trifluoro-2-butanone, 2,4-dimethyl-3-pentanone, or cyclopentanone to solutions of **1**, **2**, or **3** led to shortening of the silylene lifetimes and a change to pseudo-first order decay kinetics, and suppression of the formation of the corresponding disilene. No new products with absorption above *ca.* 300 nm were observed in any of these cases (*eg*. Figure 2.3a). These reactions are known to generate the corresponding silyl enol ethers.[10] Plots of the pseudo-first order decay coefficients (k_{decay}) of the silylenes versus carbonyl concentration were linear, as exemplified by the reaction of $SiMe_2$ with 2,4-dimethyl-3-pentanone (**7;**

Figure 2.3b) (eq. 2.3). The data were analyzed according to eq. 2.4, where Q denotes the substrate and k_Q is the bimolecular rate constant for its reaction with the free silylene. The absolute rate constants measured for these reactions are listed in Table 2.1.[1]

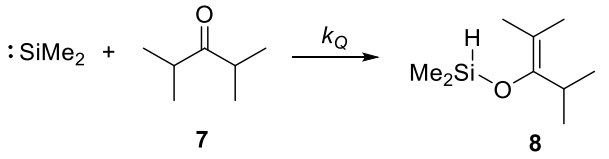

(2.3)

$$k_{decay} = k_Q[Q] + k_0 \qquad (2.4)$$

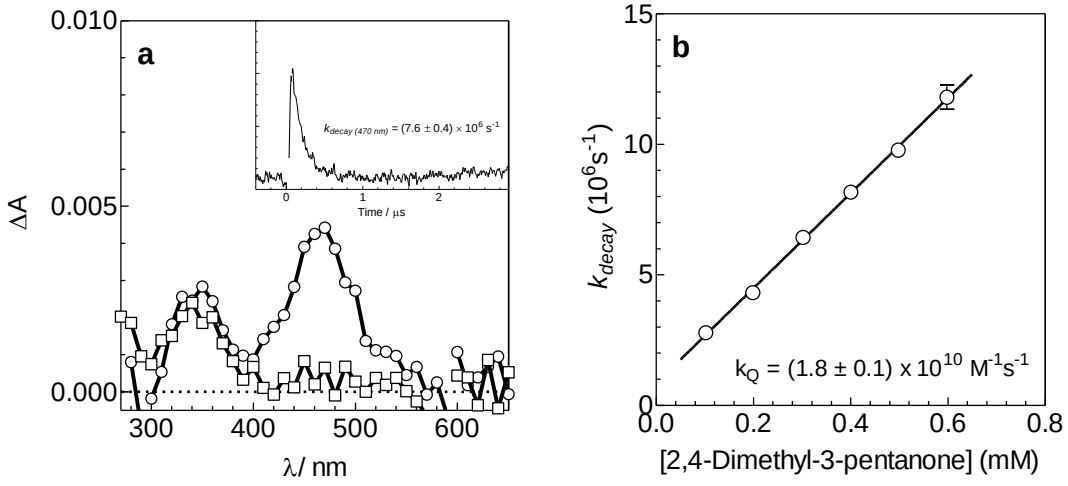

Figure 2.3. (a) Transient absorption spectra recorded 0.19 – 0.22 (○) and 0.56 – 0.59 μs (□) after the laser pulse by laser flash photolysis of **1** in the presence of 0.4 mM 2,4-dimethyl-3-pentanone (**7**) in deoxygenated hexanes at 25°C. The inset shows a transient decay trace recorded at 470 nm. (b) Plot of k_{decay} vs. ketone concentration for $SiMe_2$ monitored at 470 nm. The solid line is the linear least-squares fit of the data to eq. 2.4. (*Data recorded by C. Browne*)

Table 2.1. Absolute rate constants (k_Q) for the reactions of $SiMe_2$, $SiPh_2$, and $SiMes_2$ with ketones in hexanes solution at 25°C

Substrate	k_Q ($\times 10^{10}$ $M^{-1}s^{-1}$)		
	$SiMe_2$	$SiPh_2$	$SiMes_2$
acetone	2.0 ± 0.2[d]	1.3 ± 0.2[c]	0.83 ± 0.04[c]
acetone-d_6	1.8 ± 0.1[d]	-	-
1,1,1-trifluoro-2-butanone	1.7 ± 0.1[d]	0.63 ± 0.08[d]	0.039 ± 0.003[d]
2,4-dimethyl-3-pentanone	1.8 ± 0.1[d]	[b]	0.086 ± 0.01[d]
3,3-dimethyl-2-butanone	1.8 ± 0.1[d]	1.2 ± 0.1[d]	0.54 ± 0.06[d]
cyclopentanone	1.8 ± 0.1[d]	-	0.78 ± 0.1[d]
camphor	[b]	[b]	0.49 ± 0.04[d]
norcamphor	[b]	[b]	0.67 ± 0.1[d]

a. Errors in k_Q values are reported as twice the standard error from the linear least-square analysis of the plots of silylene k_{decay} values vs. [Q] according to eq. 2.4; b. Plot of k_{decay} vs. [Q] is non-linear.; c. Data from ref 15.; d. (*Data recorded by C. Browne*)

On the other hand, the reactions of $SiMe_2$ and $SiPh_2$ with camphor and norcamphor and $SiPh_2$ with 2,4-dimethyl-3-pentanone led to transient spectroscopic behavior that differed greatly from what was observed with the substrates described above.[1] For example, flash photolysis of $SiPh_2$ precursor **2** in the presence of 2,4-dimethyl-3-pentanone (**7**) led to the formation of a new transient intermediate that exhibited a broad UV-vis absorption band in the 500 – 650 nm range (Figure 2.4a), obscuring the transient absorptions due to the free silylene. The species decayed with first order kinetics and lifetime τ = 270 ns (k_{decay} = (3.7 ± 0.3) × 10^6 s^{-1}) in the presence of 10 mM ketone.

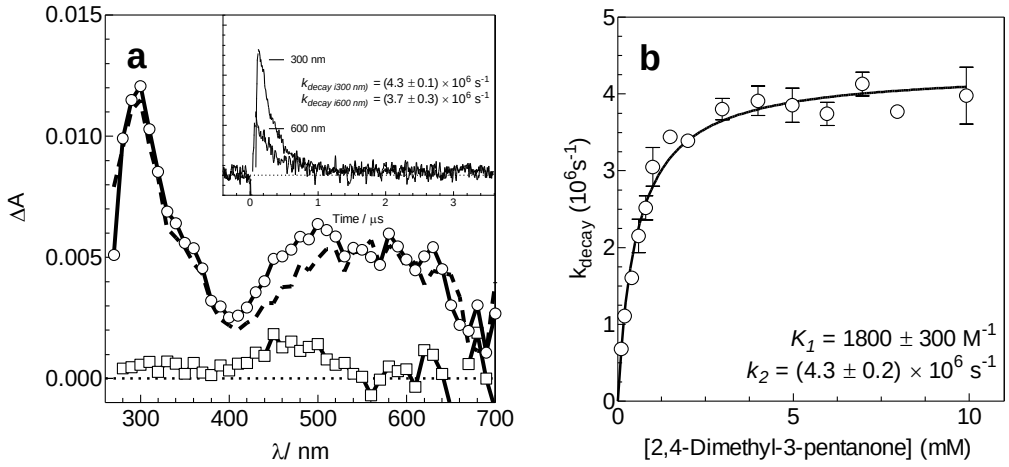

Figure 2.4. (a) Transient absorption spectra recorded 0.11 – 0.12 μs (○) and 1.2 – 1.3 μs (□) after the laser pulse by laser flash photolysis of **2** in the presence of 10 mM 2,4-dimethyl-3-pentanone (**7**) in deoxygenated hexanes at 25ºC. The dashed line spectrum (-) shows the difference between the spectra recorded at 0.11 – 0.12 μs and 1.2 – 1.3 μs after the laser pulse. The inset shows transient decay traces recorded at 300 and 600 nm. (b) Plot of k_{decay} vs. ketone concentration for the $SiPh_2$-**7** silacarbonyl ylide monitored at 600 nm. The solid line is the non-linear least-squares analysis of the data according to eq. 2.6. (*Data recorded by C. Browne*)

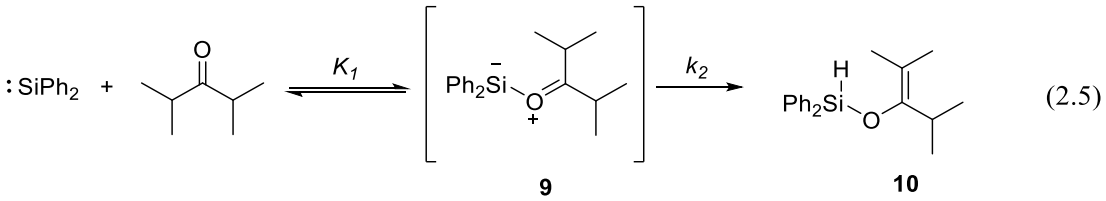

9 **10** (2.5)

The new transient is assigned to the silacarbonyl ylide intermediate (**9**; eq. 2.5), which is consistent with the reported UV-vis absorption spectra obtained from generation of $SiMe_2$ and $SiMes_2$ in the presence of **7** in low temperature matrixes.[10] Since the ylide exhibits a broad UV-vis absorption band that overlaps with the spectrum of the silylene, the kinetic analysis was done by monitoring the ylide at longer wavelengths where the silylene does not absorb. The decay coefficient of the ylide k_{decays} (monitored at 600 nm) varies with ketone concentration in a manner consistent with saturation kinetics, as

expressed in eq. 2.6 where Q denotes the substrate, K_1 is the equilibrium constant and k_2 is the rate constant for the H-migration reaction of the silacarbonyl ylide intermediate. At low substrate concentrations, k_{decay} varies approximately linearly with ketone concentration (eq. 2.7), while at high substrate concentrations, it is independent of ketone concentration (eq. 2.8).

Similar transient spectroscopic behaviors were observed in laser photolysis experiments with $SiMe_2$ and $SiPh_2$ in the presence of camphor and norcamphor, where the corresponding silacarbonyl ylides can be detected and the decay coefficient of the ylides varies with ketone concentration in a manner consistent with saturation kinetics (eq. 2.6). Table 2.2 lists the equilibrium constants and product forming rate constants for these reactions.[1]

$$k_{decay} = \frac{k_2 K_1 [Q]}{1 + K_1 [Q]} \qquad (2.6)$$

$$k_{decay} = K_1 k_2 [Q] \qquad (K_1[\mathrm{Q}] < 1) \qquad (2.7)$$

$$k_{decay} = k_2 \qquad (K_1[\mathrm{Q}] > 1) \qquad (2.8)$$

Table 2.2. Equilibrium (K_1) and H-migration rate constants (k_2) for the reactions of $SiMe_2$ and $SiPh_2$ with carbonyl compounds in hexanes at 25°C

Substrate	[K_1 ($\times 10^4$ M^{-1})] | k_2 ($\times 10^6$ s^{-1})	
	$SiMe_2$	$SiPh_2$
2,4-dimethyl-3-pentanone (**7**)	[b]	[0.28 ± 0.08] 4.5 ± 1
camphor (**4a**)	[0.15 ± 0.02] 19 ± 1	[1.2 ± 0.2] 0.55 ± 0.02
norcamphor	[c]	[1.3 ± 0.3] 0.65 ± 0.02

a. Errors in K_1 and k_2 values are reported as twice the standard error from non-linear least-square analysis of plots of silylene k_{decay} values vs. [Q] according to eq. 2.6.; b. No detectable silacarbonyl ylide; (Data recorded by C. Browne.); c. Not determined

As mentioned earlier, the reactions of $SiMe_2$ and $SiPh_2$ with camphor also afforded the corresponding silacarbonyl ylides as detectable reaction intermediates. Accordingly, the plots of k_{decay} vs. ketone concentration are also non-linear, as shown in Figure 2.5. At the standard temperature of our kinetic experiments (25°C), the H-migration rate constants measured for the $SiMe_2$- and $SiPh_2$-**4a** silacarbonyl ylides are k_2 = (19 ± 1) and (0.55 ± 0.02) × 10^6 s^{-1}, respectively.

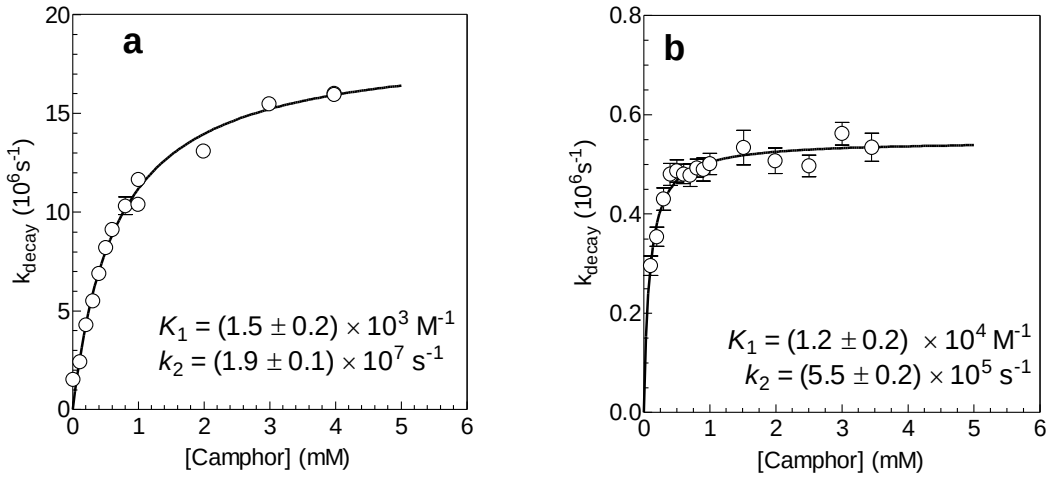

Figure 2.5. Plots of k_{decay} vs. ketone concentration for (a) $SiMe_2$ monitored at 470 nm and (b) $SiPh_2$-**4a** silacarbonyl ylide monitored at 600 nm at 25°C. The solid line is the non-linear least-squares analysis of the data according to eq. 2.6. (*Data recorded by C. Browne*)

The decay kinetics of the $SiMe_2$- and $SiPh_2$-camphor ylides were measured at several temperatures over the 9 – 57°C temperature range in hexanes containing 4.7 mM camphor, a concentration at which k_{decay} of the ylide is either at or within *ca.* 15% of its high concentration limiting value. Decay rate coefficients of the silacarbonyl ylides from reactions of $SiMe_2$ and $SiPh_2$ with (5 mM) camphor (**4a**) were measured at several

temperatures over the 0 – 50°C range. As the data of Figure 2.5. show, the decay of the ylide is rate determining at 5 mM ketone.

Table S2.1 and S2.2 lists the decay rate coefficients obtained in these variable temperature experiments of a solution of **1** or **2** in the presence of *ca.* 5 mM camphor, while Figure 2.6 shows the corresponding Eyring plots. The activation parameters obtained from least-square analysis of the data, according to the Arrhenius (eq. 2.9) and Eyring equations (eq. 2.10), are listed in Table 2.3.

$$\ln(k) = -\frac{E_a}{RT} + \ln A \qquad (2.9)$$

$$\ln(k/T) = -\frac{\Delta H^{\ddagger}}{RT} + ln\frac{k_B}{h} + \frac{\Delta S^{\ddagger}}{R} \quad (2.10)$$

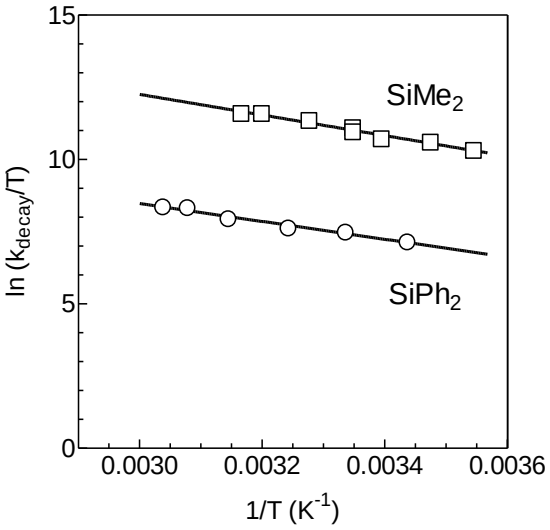

Figure 2.6. Eyring plots associated with the H-migration step from the silacarbonyl ylide in the reaction of $SiMe_2$ (□) and $SiPh_2$ (○) containing 5 mM camphor (**4a**), monitored at 600 nm, at temperatures of 0.0 – 50.0°C. The slopes and intercepts are as follows: (□): slope = (-3.57 ± 0.5) × 10^3 K^{-1} and intercept = (2.30 ± 0.1) × 10^1 and (○): slope = (-3.09 ± 0.2) × 10^3 K^{-1} and intercept = (1.77 ± 0.1) × 10^1.

Table 2.3. Activation parameters of the H-migration pathway for the $SiMe_2$- and $SiPh_2$-derived silacarbonyl ylide with camphor

Activation Parameters	$SiMe_2$	$SiPh_2$
k_{decay} (25°C) (× 10^6 s^{-1})	19 ± 1	0.55 ± 0.02
E_a (kcal mol^{-1})	7.7 ± 0.5	6.8 ± 0.5
log A	13 ± 0.7	11 ± 0.7
$\Delta H^{\ddagger}$ (kcal mol^{-1})	7.1 ± 0.5	6.1 ± 0.9
$\Delta S^{\ddagger}$ (cal mol^{-1} K^{-1})	-1.5 ± 0.1	-12 ± 2
$\Delta G^{\ddagger}$ (25°C) (kcal mol^{-1})	7.6 ± 1	9.7 ± 2

a. Errors are reported as twice the standard error from linear least-square analysis of Arrhenius and Eyring plots of the log (k_{decay}) vs. *1/T* and ln (k_{decay}/T) vs. *1/T* according to eq. 2.9 and 2.10, respectively. (*Data recorded by C. Browne*)

The enthalpy of activation of the H-migration pathway for both reactions were found to be positive which indicates an energetic barrier to the transition state, while the entropy of activation is found to be negative which is consistent with the transition state being more ordered compared to the ylide. Comparing the two silylenes, the results indicate that $\Delta G^{\ddagger}$ is larger for the $SiPh_2$-ylide than for the $SiMe_2$-ylide. The $\Delta H^{\ddagger}$ is the same within experimental error for both ylides, so the effect on $\Delta G^{\ddagger}$ is almost entirely due to the difference in $\Delta S^{\ddagger}$, which is quite large. For the $SiMe_2$-ylide, the $\Delta S^{\ddagger}$ is -1.5 ± 0.1 eu, which indicates there is very little difference in order between the favored geometry of the ylide and that at the transition state. On the other hand, the $\Delta S^{\ddagger}$ for the $SiPh_2$-ylide is *ca.* -12 eu. The $\Delta H^{\ddagger}$ are the same within error for $SiPh_2$ but the transition state is considerably more ordered than that for the corresponding reaction with $SiMe_2$, indicating the phenyl groups have to orient in a much more specific way to allow the transition geometry to be achieved, than is the case in the $SiMe_2$-derived ylide (*ie.* it is essentially a steric effect).

2.3. Scope of the Study

Previous workers in our group have studied the reactions of $SiMe_2$, $SiPh_2$, and $SiMes_2$ with acetone, 1,1,1-trifluoro-2-butanone, pinacolone, 2,4-dimethyl-3-pentanone, and camphor in complete detail. However, while the transient spectra were obtained for the reactions with cyclopentanone and norcamphor, their kinetic analyses are incomplete. This section will provide the kinetic analyses that were not done in the previous work.

The work has been extended to include camphor-d_2 and dicyclopropyl ketone. The kinetic isotope effect on the H-migration step of the reaction was investigated with camphor-d_2 and acetone-d_6. In addition, the reactions of $SiMe_2$, $SiPh_2$, and $SiMes_2$ with dicyclopropyl ketone were explored to evaluate the effects of ring strain in comparison to diisopropyl ketone as well as determine the product from this reaction as it has not been reported before. The following discussion will describe my efforts to complete the kinetic and product studies of all the enolizable carbonyl compounds studied to date in our group.

2.4. Kinetic Isotope Effects

2.4.1. Reactions of Silylenes with Camphor-3,3-d_2

The kinetic isotope effect was investigated for the reactions of the silylenes with camphor (**4a**) and camphor-3,3-d_2 (**4b**) (eq. 2.11). The reactions of $SiMe_2$ and $SiPh_2$ with **4b** led to detectable silacarbonyl ylides, whose first order decay rate coefficients varied non-linearly with ketone concentration – plateauing to maximum values of $k_{decay} = 3.1 \times 10^6\ s^{-1}$ and $1.0 \times 10^5\ s^{-1}$, respectively. No ylide could be detected with $SiMes_2$, and a plot of k_{decay} vs. [camphor-d_2] was linear with slope of $k_Q = (1.6 \pm 0.3) \times 10^9\ M^{-1}s^{-1}$. The

results for the three silylenes are qualitatively similar to what was observed with **4a** in each case. The reactions of $SiMe_2$ and $SiPh_2$ with **4a** led to first order decay rate coefficients plateauing to maximum values of $k_{decay} = 1.9 \times 10^7$ s^{-1} and 5.5×10^5 s^{-1} respectively, at higher ketone concentration, while the reaction with $SiMes_2$ afford an absolute rate constant of $k_Q = 4.9 \times 10^9$ $M^{-1}s^{-1}$. Figure 2.7 shows the plots of k_{decay} vs. [camphor-L_2] for $SiMe_2$ and $SiPh_2$, while the derived kinetic parameters are summarized in Table 2.4.

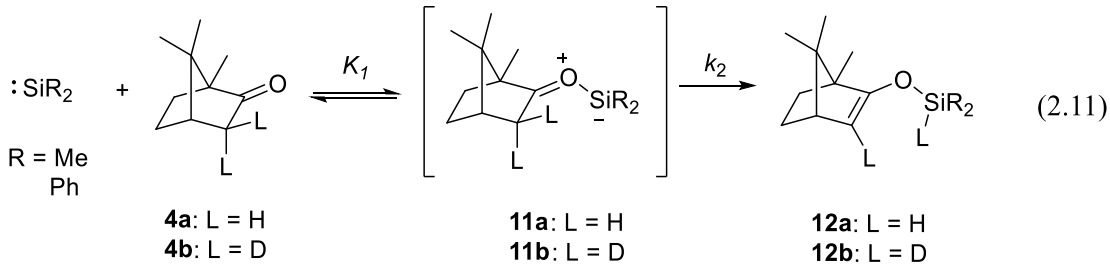

(2.11)

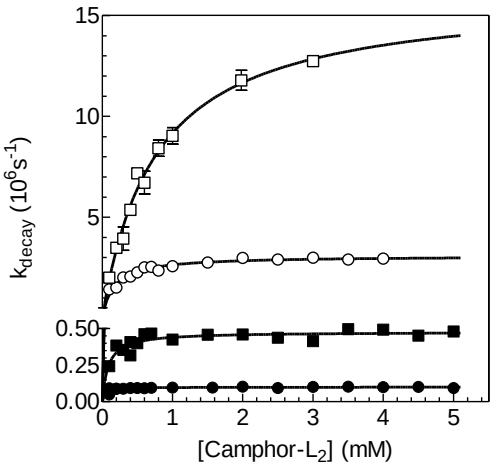

Figure 2.7. Plot of k_{decay} vs. [camphor-L_2] (L = H or D) for the $SiMe_2$-(□ and ■) and $SiPh_2$- (❍ and ●) camphor-L_2-derived silacarbonyl ylide monitored at 600 nm. The solid line is the non-linear least-squares analysis of the data according to equation 2.6.

Table 2.4. Kinetic parameters for the two-step reactions of $SiMe_2$ and $SiPh_2$ with camphor-L_2 (L = H, D) in hexanes at 25ºC

Substrate	K_1 (× 10^4 M^{-1}) | k_2 (× 10^6 s^{-1})	
	$SiMe_2$	$SiPh_2$
camphor	[0.15 ± 0.02][c]	[1.2 ± 0.2][c]
	19 ± 1[c]	0.55 ± 0.02[c]
camphor-3,3-d_2	-[b]	-[b]
	3.1 ± 0.1	0.10 ± 0.01

a. Errors in k_2 values are reported as twice the standard error from non-linear least-square analysis of plots of the silacarbonyl ylide k_{decay} values vs. [Q] according to eq. 2.6.; b. K_1 is indeterminable.; c. (*Data recorded by C. Browne*).

The k_{2H}/k_{2D} values calculated from the k_2-values (shown in Table 2.4) are 6.1 ± 0.4 and 5.5 ± 2 for the reactions of camphor-3-L_2 with $SiMe_2$ and $SiPh_2$ respectively. Similarly, the isotope effect on the overall second-order rate constant for reaction of $SiMes_2$ with camphor-L_2 was measured to be k_H/k_D = 3.1 ± 0.5, calculated from the k_2-values from Table 2.5. These values provide evidence that a normal primary isotope effect is present, which is consistent with the rate-determining step in the decay of the ylide involving migration of the carbonyl α-H to Si to generate the corresponding silyl enol ether. The results indicate that under the condition of our kinetic experiments, the rate-determining step is the H-migration step while the formation of the ylide is very fast. Continued addition of camphor-d_2, up to 0.1 M, to a solution of the $SiMe_2$ precursor (Figure 2.8) showed that the limiting k_{decay} value remains constant over the 2 – 100 mM concentration range at k_{decay} = (2.8 ± 0.2) × 10^6 s^{-1}.

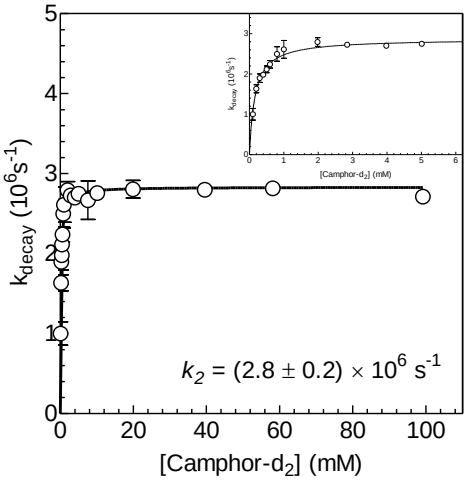

Figure 2.8. Plot of k_{decay} vs. [camphor-d_2] for the $SiMe_2$-camphor-d_2 silacarbonyl ylide, monitored at 600 nm. The solid line is the non-linear least-squares fit of the data to eq. 2.6. The inset shows the plot of k_{decay} vs. [camphor-d_2] from 0 – 100 mM.

Similar experiments were performed for the reactions of $SiMe_2$, $SiPh_2$, and $SiMes_2$ with acetone and acetone-d_6. The absolute rate constants are listed in Table 2.5. The reactions of $SiMe_2$ and $SiPh_2$ with acetone and acetone-d_6 are close to diffusional controlled ($k_{diff} \approx 2 \times 10^{10}$ M^{-1} s^{-1}),[16] which suggests that the initial diffusive encounter is rate determining and H-migration is therefore fast. This is reflective of the isotope effect measured, as they were quite small (k_H/k_D = 1.1 ± 0.1, 1.2 ± 0.2, and 1.2 ± 0.1 for $SiMe_2$, $SiPh_2$, and $SiMes_2$, respectively).

Table 2.5. Absolute rate constants (k_Q) for the reactions of $SiMe_2$ and $SiMes_2$ with acetone-L_6 and camphor-L_2 in hexanes solution at 25°C

Substrate	k_Q ($\times 10^{10}$ $M^{-1}s^{-1}$)		
	$SiMe_2$	$SiPh_2$	$SiMes_2$
acetone	2.0 ± 0.2[d]	1.3 ± 0.2[c]	0.83 ± 0.04[c]
acetone-d_6	1.8 ± 0.1[d]	1.1 ± 0.2	0.69 ± 0.05
camphor	[b]	[b]	0.49 ± 0.04[d]
camphor-3,3-d_2	[b]	[b]	0.16 ± 0.03

a. Errors in k_Q values are reported as twice the standard error from linear least-square analysis of plots of silylene k_{decay} values vs. [Q] according to eq. 2.4; b. Plot of k_{decay} vs. [Q] is non-linear.; c. Data from ref 15.; d. The value reported revises the earlier reported value[3] (*Data recorded by C. Browne*).

2.5. Reactions of Silylenes with Other Enolizable Carbonyl Compounds

2.5.1. Reaction of $SiPh_2$ with Cyclopentanone

The addition of cyclopentanone to a hexanes solution of **2** led to shortening of the silylene lifetime and quenching of the formation of the corresponding disilene. A plot of k_{decay} vs. ketone concentration is linear (Figure 2.9b) with a slope of $k_Q = (1.1 \pm 0.2) \times 10^{10}$ $M^{-1}s^{-1}$. A transient UV-vis spectrum recorded in hexanes solution containing 1.0 mM of ketone showed only absorptions attributable to $SiPh_2$ (Figure 2.9a), its lifetime (τ) reduced to *ca.* 85 ns compared to that in the absence of the ketone (typically 0.6 – 1.2 μs).[3]

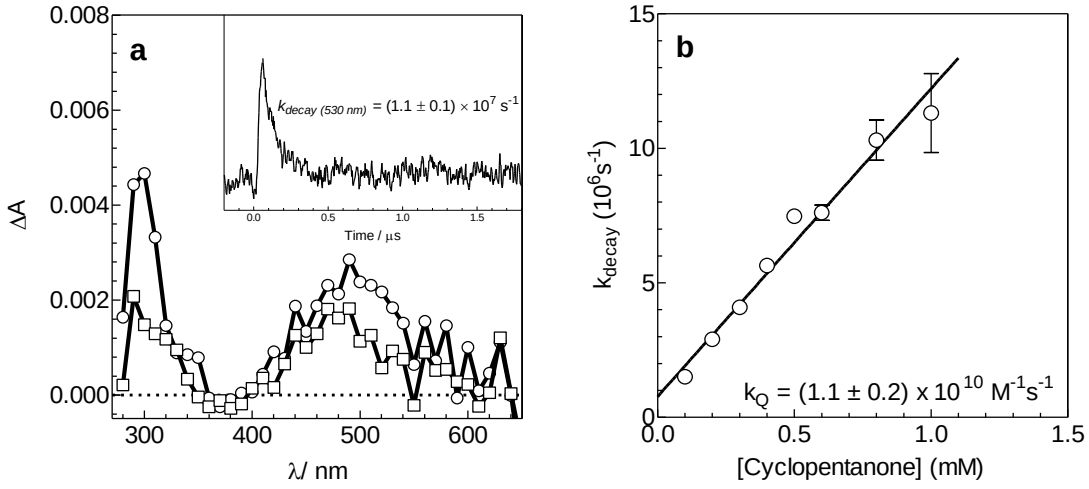

Figure 2.9. (a) Transient absorption spectra recorded 0.15 – 0.16 (○) and 0.28 – 0.30 μs (□) after the laser pulse by laser flash photolysis of **2** in the presence of 1 mM cyclopentanone in deoxygenated hexanes at 25°C. The inset shows transient decay traces recorded at 530 nm. (b) Plot of k_{decay} vs. ketone concentration for $SiPh_2$ monitored at 530 nm. The solid line is the result of linear least-squares analysis of the data according to eq. 2.4.

2.5.2. Reaction of $SiMe_2$ with Norcamphor

Addition of norcamphor (**13**) to hexanes solutions of **1** led to the appearance of a new transient species exhibiting broad UV-vis absorption bands to the red of the 470 nm absorption band of the silylene, which is assigned to the corresponding silacarbonyl ylide. Figure 2.10a shows a transient spectrum recorded in hexanes containing 1 mM of ketone, which is interpreted as the sum of the spectra of both the silylene and the ylide, in equilibrium with each other. The absorptions due to the ylide were monitored at 600 nm as a function of ketone concentration and found to decay with first order kinetics. A plot of k_{decay} vs. ketone concentration exhibited curvature consistent with saturation kinetics; analysis of the data according to eq. 2.6 afforded the coefficients $K_1 = (1.5 \pm 0.3) \times 10^3$ M^{-1} and $k_2 = (1.8 \pm 0.1) \times 10^7$ s^{-1} (Figure 2.10b).

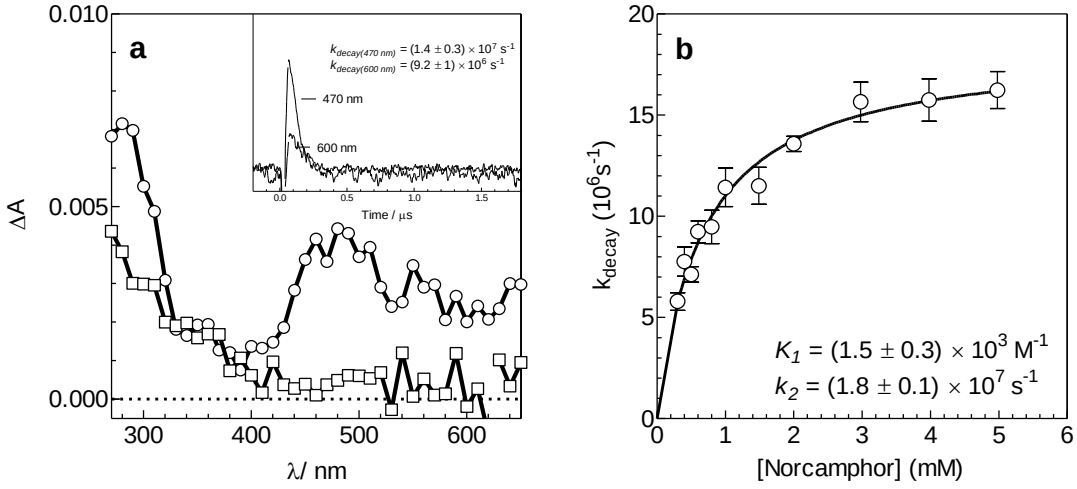

Figure 2.10. (a) Transient absorption spectra recorded 0.15 – 0.16 (○) and 0.28 – 0.29 μs (□) after the laser pulse by laser flash photolysis of **1** in the presence of 1 mM norcamphor in deoxygenated hexanes at 25ºC. The inset shows transient decay traces recorded at 470 and 600 nm. (*Data recorded by C. Browne*) (b) Plot of k_{decay} vs. ketone concentration for the $SiMe_2$-norcamphor silacarbonyl ylide monitored at 600 nm. The solid line is the non-linear least-squares fit of the data to eq. 2.6.

2.5.3. Reactions of Silylenes with Dicyclopropyl Ketone

As mentioned earlier, the reactions of the three silylenes with dicyclopropyl ketone (**14**) were studied for comparison to the results for diisopropyl ketone (**7**), in order to evaluate the effects of angle strain at the ketone α-carbon on the rate constant for H-migration in the ylide intermediate. As these reactions have not been studied previously, to our knowledge, we carried out a product study of the reaction of **14** with $SiMe_2$, in addition to studying the reactivity of the ketone with all three silylenes by laser flash photolysis.

Photolysis of a deoxygenated solution of **1** (0.023 M) in cyclohexane-d_{12} containing **14** (0.05 M) and hexamethyldisilane (0.01 M, internal standard) afforded decamethylcyclopentasilane (**15**) (67 ± 15 %) and a product identified tentatively as silyl

enol ether **16** (54 ± 6 %; eq. 2.12) in the ^{1}H NMR spectrum on the basis of its characteristic Si-H resonance at δ 4.87 ppm (septet).[2] The ^{1}H NMR spectrum of the photolysis mixture after *ca.* 67% conversion of **1** is shown in Figure 2.12, while the concentration versus time plots for the identified products are shown in Figure 2.11. The ^{1}H NMR assignments of **16** are listed in Table S2.4.

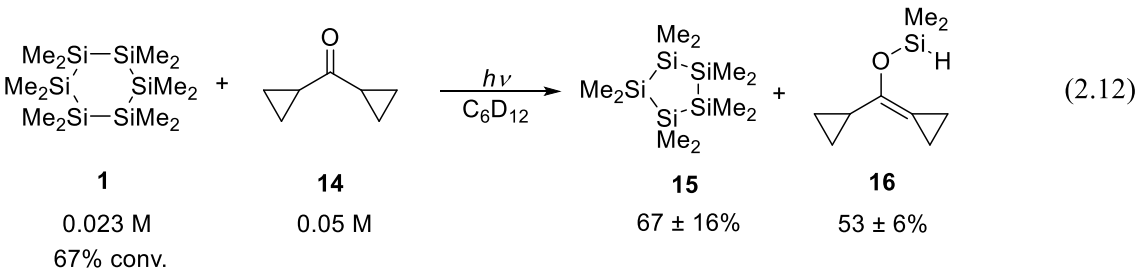

(2.12)

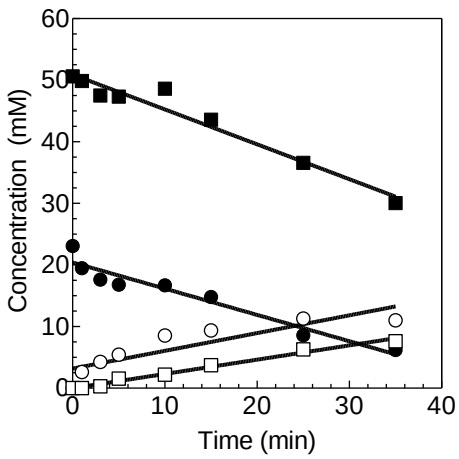

Figure 2.11: Concentration vs. time plots for the photolysis (254 nm) of **1** (23 mM) in the presence of **14** (50 mM) in cyclohexane-d_{12}. Shown is the depletion of **1** (●) and **14** (■) with time irradiated and the formation of **15** (○) and the silyl enol ether **16** (□). The slopes are as follows: (**1**; ●): (-0.43± 0.05) mM/min, (**14**; ■) :(-0.57 ± 0.05) mM/min, (**15**; ○):(0.29 ± 0.06) mM/min, (**16**; □): (0.23 ± 0.01) mM/min.

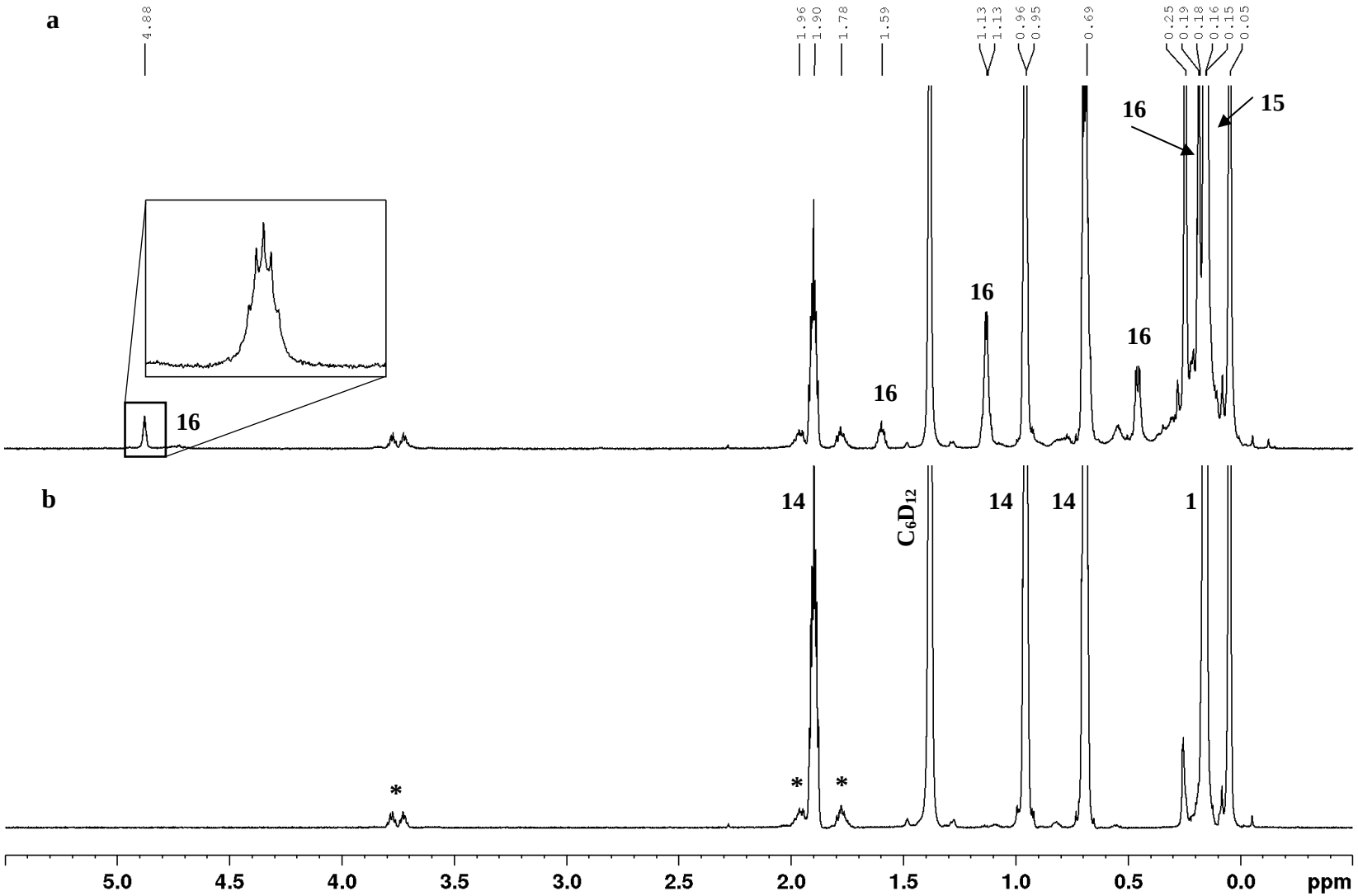

Figure 2.12: ^{1}H NMR spectra of a solution of **1** (0.023 M), 0.05 M dicyclopropyl ketone (**14**), and 0.01 M hexamethyldisilane in C_6D_{12} (a) before and (b) after 35 mins of photolysis (* unreactive impurity).

Flash photolysis of hexanes solutions of $SiMe_2$ precursor **1** in the presence of **14** resulted in a new transient species exhibiting a broad UV-vis absorption band over the 400 – 700 nm range (Figure 2.13a), which is assigned to the corresponding silacarbonyl ylide. A plot of k_{decay} at 600 nm vs. [Q] exhibits curvature consistent with saturation kinetics (Figure 2.13b), and analysis of the data according to eq. 2.6 affords the coefficients $K_1 = (1.3 \pm 0.5) \times 10^4$ M^{-1} and $k_2 = (1.2 \pm 0.1) \times 10^6$ s^{-1}.

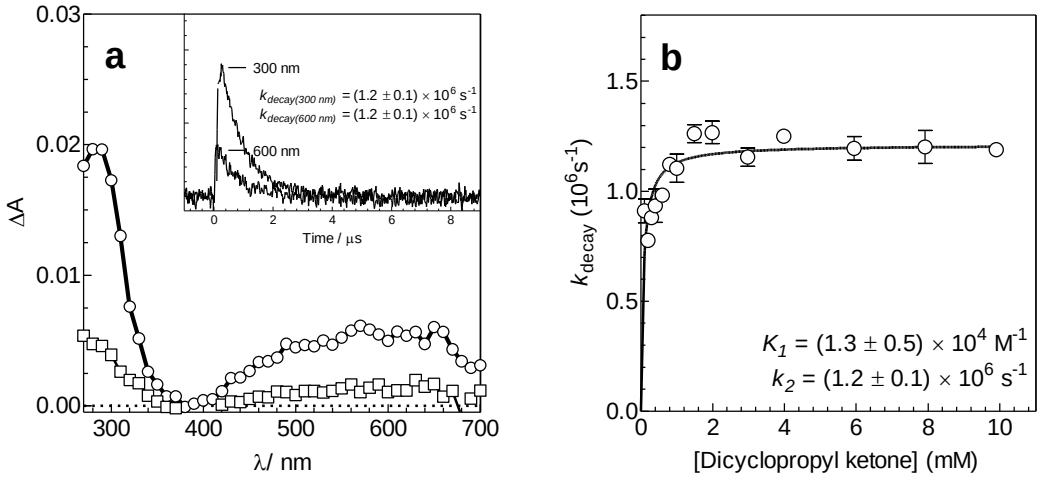

Figure 2.13. (a) Transient absorption spectra recorded 272 – 336 ns (○) and 1.39 – 1.47 μs (□) after the laser pulse by laser flash photolysis of **1** in the presence of 6 mM dicyclopropyl ketone (**14**) in deoxygenated hexanes at 25°C. The inset shows transient decay traces recorded at 300 and 600 nm. (b) Plot of k_{decay} vs. ketone concentration of the $SiMe_2$-**14** silacarbonyl ylide monitored at 600 nm. The solid line is the non-linear least-squares fit of the data to eq. 2.6.

Flash photolysis of hexanes solutions of $SiPh_2$ precursor **2** in the presence of **14** (1 mM) shows a mixture of both $SiPh_2$ and a transient absorption extending over the 400 – 700 nm range, consistent with a mixture of $SiPh_2$ in addition to a stronger band centred at ~300 nm and the corresponding transient silacarbonyl ylide (eq. 2.13). Figure 2.14a shows transient UV-vis spectra, recorded immediately and 4.3 – 5.3 μs after the laser

pulse. The ylide could be detected at 600 nm in solution of concentration ≥ 0.2 mM, the initial ΔA_0 value increasing with ketone concentration over the 0.2 – 2.0 mM range but the lifetime remaining approximately constant (see Figure 2.14b).

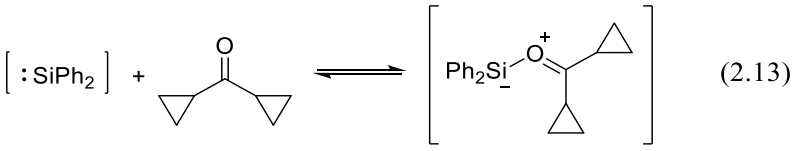

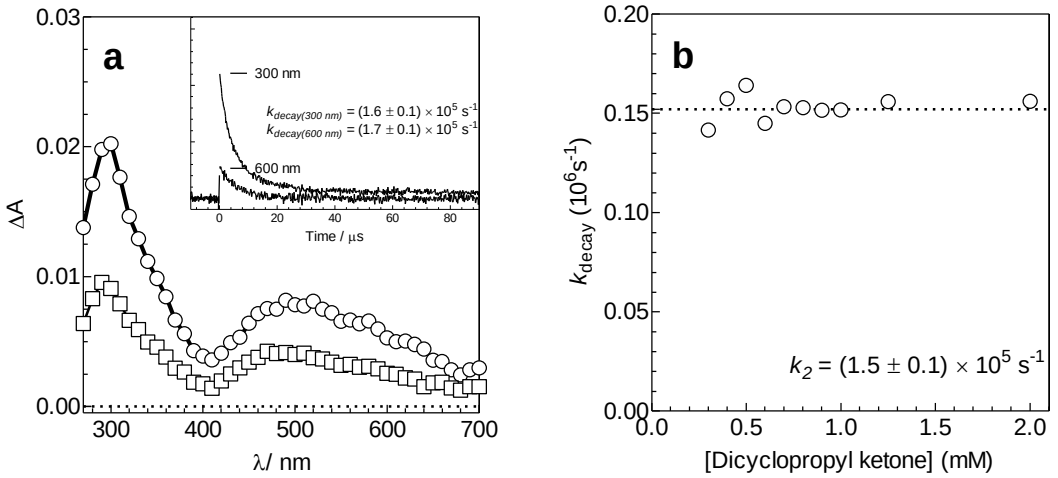

Figure 2.14. (a) Transient absorption spectra recorded 0.16 – 0.80 ns (○) and 4.32 – 5.28 μs (□) after the laser pulse by laser flash photolysis of **2** in the presence of 1 mM dicyclopropyl ketone in deoxygenated hexanes at 25°C. The inset shows transient decay traces recorded at 300 and 600 nm. (b) Plot of k_{decay} vs. ketone concentration for the $SiPh_2$-**14** silacarbonyl ylide monitored at 600 nm. The dashed line is the average k_2 value.

The addition of **14** to a hexanes solution of $SiMes_2$ precursor **3** resulted in acceleration of the silylene decay, a change to pseudo-first order decay kinetics, and suppression of the formation of the corresponding disilene. No new transient absorptions above *ca.* 300 nm could be detected in the presence of 0.01 M ketone (Figure 2.15a), analogous to what was observed with diisopropyl ketone (**7**). There is a linear dependence of the silylene decay rate coefficient (k_{decay}) on ketone concentration, and analysis of the

data according to eq. 2.4 afforded an absolute rate constant of $k_Q = (4.1 \pm 0.2) \times 10^8$ $M^{-1}s^{-1}$ (Figure 2.15b).

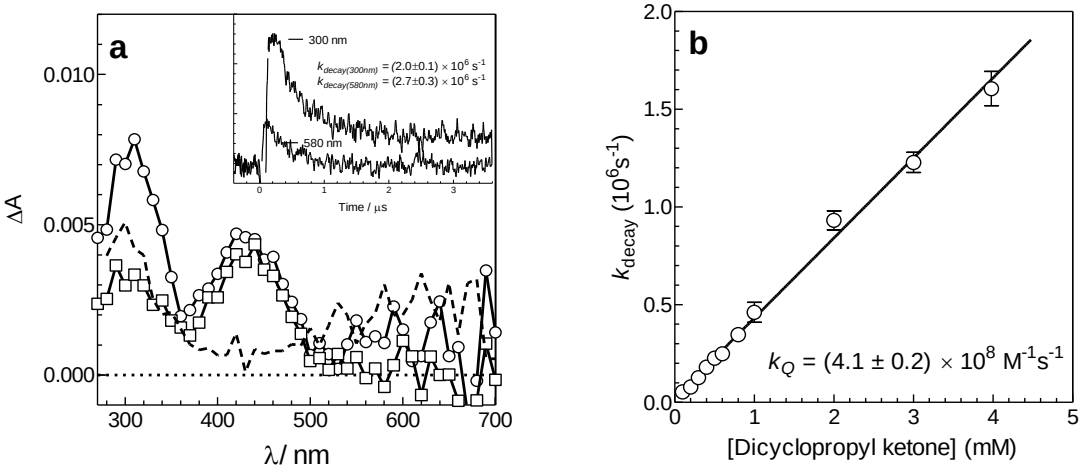

Figure 2.15. (a) Transient absorption spectra recorded 0.14 – 0.15 (○) and 0.56 – 0.59 μs (□) after the laser pulse by laser flash photolysis of **3** in the presence of 10 mM dicyclopropyl ketone (**14**) in deoxygenated hexanes at 25°C. The dashed line spectrum (-) shows the difference between the two spectra. The inset shows transient decay traces recorded at 300 and 580 nm. (b) Plot of k_{decay} vs. ketone concentration for $SiMes_2$, monitored at 580 nm. The solid line is the linear least-squares analysis of the data according to eq. 2.4.

2.6. Discussion

The results presented in this work confirm that the reactions of silylenes with enolizable carbonyl compounds proceed via the initial formation of the corresponding silacarbonyl ylide, which reacts by unimolecular H-migration to afford the silyl enol ether.[10] In some systems, the corresponding silacarbonyl ylide intermediates are detectable under ambient conditions; the UV-vis absorption maxima of these species are listed in Table 2.6.

Table 2.6. Experimental UV-Vis absorption maxima (λ_{max} (nm)) of the silacarbonyl ylides from the reactions of $SiMe_2$ and $SiPh_2$ with enolizable ketones in hexanes at 25°C

Substrate	λ_{max} (nm)	
	$SiMe_2$	$SiPh_2$
2,4-dimethyl-3-pentanone (**7**)	-[a]	560[b]
camphor (**4a**)	550[b]	510
camphor-3,3-d_2 (**4b**)	550	510
norcamphor (**13**)	580[b]	520
dicyclopropyl ketone (**14**)	570	540

a. No detectable silacarbonyl ylide.; b. UV-Vis absorption maximum of the ylide was determined by the difference of two spectra recorded at two different time windows.

The first (reversible) step in the sequence can be viewed as a Lewis acid/base complexation, for which the equilibrium constant (K_1) should depend primarily on the Lewis acidity and basicity of the silylene and the carbonyl compound, respectively. This conclusion is supported by a comparison of the apparent K_1 values for the reactions of $SiMe_2$ and $SiPh_2$ with diisopropyl ketone, camphor-L_2, norcamphor, and dicyclopropyl ketone, to the equilibrium constants for complexation of $SiMe_2$ and $SiPh_2$ with Et_2O.[17] The equilibrium constants measured for these systems are shown in Table 2.7.

Table 2.7. Equilibrium constants (K_1) and H-migration rate coefficients (k_2) for the reactions of $SiMe_2$ and $SiPh_2$ with carbonyl compounds in hexanes at 25°C

Substrate	$SiMe_2$		$SiPh_2$	
	K_1 ($\times 10^4$ M^{-1})	k_2 ($\times 10^6$ s^{-1})	K_1 ($\times 10^4$ M^{-1})	k_2 ($\times 10^6$ s^{-1})
2,4-dimethyl-3-pentanone (**7**)	[b]	[b]	0.28 ± 0.08[d]	4.5 ± 1[d]
camphor (**4a**)	0.15 ± 0.02[d]	19 ± 1[d]	1.2 ± 0.2[d]	0.55 ± 0.02[d]
camphor-3,3-d_2 (**4b**)	0.60 ± 0.1	3.1 ± 0.1	[c]	0.10 ± 0.04
norcamphor (**13**)	0.14 ± 0.03	18 ± 1	1.3 ± 0.3[d]	0.65 ± 0.02[d]
dicyclopropyl ketone (**14**)	0.12 ± 0.04	1.4 ± 0.1	[c]	0.16 ± 0.01

a. Errors in K_1 and k_2 values are reported as twice the standard error from non-linear least-square analysis of plots of silylene k_{decay} values vs. [Q] according to eq. 2.7.; b. Silacarbonyl ylide not detectable; c. K_1 is indeterminable.; d. Data recorded by C. Browne.

The equilibrium constants for silacarbonyl ylide formation in these systems are similar to those for the simple Lewis acid-base complexation with Et_2O, which have been reported to be 1.3×10^3 and 7.1×10^3 for $SiMe_2$ and $SiPh_2$, respectively.[17] On the other hand, none of the ketones of Table 2.7 form detectable ylides with $SiMes_2$, which is consistent with its much lower acidity compared to the other silylenes (K_{Et2O} = 0.9 ± 0.1 M^{-1}; hexanes, 25°C).[17]

In addition to the Lewis acidity of the silylene, the structural parameters of the silylene and carbonyl compound also affect the rate of the H-migration step (k_2). Bulky substituents on the ketone and/or the generation of ring- and/or angle strain in the silyl enol ether raises the kinetic barrier to the product, lowering the rate constant for H-migration. The reactions of $SiMe_2$ and $SiPh_2$ with dicyclopropyl ketone (**14**), camphor

(**4a**), and norcamphor (**13**) led to a detectable ylide because of the slowed k_2 step due to the α-H is constrained geometrically or is attached to a strain ring.

In all the reactions of $SiMe_2$ and $SiPh_2$ where the silacarbonyl ylide is detectable, only the reactions of $SiMe_2$ with camphor and norcamphor and $SiPh_2$ with 2,4-dimethyl-3-pentanone show a mixture of both the silylene and the corresponding ylide in their transient absorption spectra. These reactions show a mix of both the silylene and ylide because the H-migration step is relatively fast, which prevents the ylide from building up to as high a concentration relative to the free silylene as it would when the H-migration step is slower. The completed table of the UV-Vis absorption maxima, equilibrium constant and H-migration rate constants are shown in Tables 2.6 and 2.7, respectively. Overall, the detectability of the silacarbonyl ylide depends on a balance of both structural and electronic factors of the silylene and carbonyl compound and is enhanced by a favorable pre-equilibrium coupled with a relatively slow H-migration step.

For both $SiMe_2$ and $SiPh_2$, the kinetic parameters for reaction with camphor and norcamphor are the same within experimental error, indicating that the addition of methyl substitution in the former has no effect on either step in the reaction sequence.

The reaction of $SiPh_2$ with dicyclopropyl ketone (**14**) shows a 30-fold decrease in the H-migration rate coefficient relative to its acyclic analogue diisopropyl ketone (**7**). This significant decrease is most likely caused by the constrained bond angles at the α-carbons, which inhibits the hybridization change at C_α in going from the ylide to the enol ether.

Table 2.8. Absolute rate constants (k_Q) for the reactions of $SiMe_2$, $SiPh_2$, and $SiMes_2$ with ketones in hexanes solution at 25°C

Substrate	k_Q ($\times 10^{10}$ $M^{-1}s^{-1}$)		
	$SiMe_2$	$SiPh_2$	$SiMes_2$
acetone	2.0 ± 0.2[d]	1.3 ± 0.2[c]	0.83 ± 0.04[c]
acetone-d_6	1.8 ± 0.1[d]	1.1 ± 0.2[c]	0.69 ± 0.05
1,1,1-trifluoro-2-butanone	1.7 ± 0.1[d]	0.63 ± 0.08[d]	0.039 ± 0.003[d]
2,4-dimethyl-3-pentanone	1.8 ± 0.1[d]	[b]	0.086 ± 0.01[d]
3,3-dimethyl-2-butanone	1.8 ± 0.1[d]	1.2 ± 0.1[d]	0.54 ± 0.06[d]
cyclopentanone	1.8 ± 0.1[d]	1.3 ± 0.1	0.78 ± 0.1[d]
camphor	[b]	[b]	0.49 ± 0.04[d]
camphor-3,3-d_2	[b]	[b]	0.16 ± 0.03
norcamphor	[b]	[b]	0.67 ± 0.1[d]
dicyclopropyl ketone	[b]	[b]	0.041 ± 0.002

a. Errors in k_Q values are reported as twice the standard error from linear least-square analysis of plots of silylene k_{decay} values vs. [Q] according to eq. 2.4; b. System exhibits saturation kinetics; k_Q is indeterminable; c. Data from ref 15; d. (*Data recorded by C. Browne*)

The absolute rate constants measured for the reactions of $SiMe_2$, $SiPh_2$, and $SiMes_2$ with enolizable carbonyl compounds studied in this work are shown in Table 2.8. The rate constants for the reactions of $SiMe_2$ with the first six of the ketones in Table 2.8 show no variation with substrate structure as the k_Q-values are all close to the diffusional limit ($k_{diff} \approx 2.2 \times 10^{10}$ M^{-1} s^{-1}), consistent with the initial (complexation) step being rate determining in these cases.[16] $SiPh_2$ exhibits similar behavior in most cases, though the rate constants are *ca*. 30% smaller than those for $SiMe_2$; this difference in reactivity between $SiMe_2$ and $SiPh_2$ is a general one.[17-19]

Rate constants for the reaction of $SiPh_2$ with acetone, pinacolone, and cyclopentanone are all $(1.2 – 1.3) \times 10^{10}$ $M^{-1}s^{-1}$ consistent with diffusion-controlled reaction. There is thus no variation in rate constant with the number of α-hydrogens or upon incorporating them in a C_5 ring. There is a factor of *ca.* 2 reduction in reactivity with trifluorobutanone compared to pinacolone, indicating that inductive electron-withdrawal from the acyl carbon reduces reactivity, most likely by reducing the equilibrium constant for the initial complexation (ylide-forming) step of the reaction.

The rate constants for the $SiMes_2$ reactions vary modestly but systematically with substitution on the carbonyl compound. The rate constants vary with steric effects, which includes bulky substituents and the degree of ring- or angle-strain generated in the reaction. The rate constants for the reactions of $SiMes_2$ with camphor and norcamphor are quite similar, again indicating that the increased alkyl substitution in camphor has no effect on overall reactivity. Similarly, increasing the ring size of the ketone between 5 (cyclopentanone) and 6 (norcamphor) also does not have a large effect. In contrast, the rate constant measured for reaction with 2,4-dimethyl-3-pentanone (**7**) is twice that for reaction with dicyclopropyl ketone (**14**). The silyl enol ether from dicyclopropyl ketone is destabilized relative to that from diisopropyl ketone because of the angle strain at the sp^2 carbon that results from constraining it in the ring. The factor of only ~2 reduction in k_Q for $SiMes_2$ can be compared to the corresponding reduction in k_2 measurements for $SiPh_2$-derived silacarbonyl ylide. The much smaller effect observed with $SiMes_2$ may indicate an earlier transition state for H-migration in the ylide compared to that in the $SiPh_2$-systems.

Comparison of the data for the reaction of the three silylenes show the overall rate constants to decrease from $SiMe_2 > SiPh_2 > SiMes_2$, which is consistent with what is generally seen with other reactions of these silylenes considering the variation in steric and electronic effects.

There is a larger variation in the rate constants for the reactions of $SiMes_2$ with the series of ketone than is the case with $SiPh_2$. This can be attributed to $SiPh_2$ being much more reactive intrinsically than $SiMes_2$, which results in a lower sensitivity to steric and electronic effects in the ketone (*e.g.* $k_{acetone} \approx k_{pinacolone} \approx 2 \times k_{trifluorobutanone}$). On the other hand, the reduced intrinsic reactivity of $SiMes_2$ results in larger variations in rate constant with ketone structure (*e.g.* $k_{acetone} \approx 2\ k_{pinacolone} \approx 12 \times k_{trifluorobutanone}$). As mentioned earlier, the reduced reactivity of trifluorobutanone compared to acetone can be attributed to the electron withdrawing group ($-CF_3$ group) reducing the basicity of the ketone, lowering the equilibrium constant for the first step. The effect may be enhanced further with $SiMes_2$ by the much reduced Lewis acidity of the silylene relative to that of $SiPh_2$.

2.7. Conclusion

The reactions of the transient silylenes $SiMe_2$, $SiPh_2$, and $SiMes_2$, with enolizable carbonyl compounds have been investigated and their reactivities characterized quantitatively in hexanes solution under ambient conditions. The silylenes were found to react rapidly with unhindered ketones (acetone, 1,1,1-trifluoro-2-butanone, 2,4-dimethyl-3-pentanone, 3,3-dimethyl-2-butanone, cyclopentanone) and without the formation of detectable intermediates. In contrast, the reactions of $SiMe_2$ and $SiPh_2$ in the presence of

more hindered ketones (camphor, norcamphor, and dicyclopropyl ketone) and $SiPh_2$ with 2,4-dimethyl-3-pentanone proceed via detectable intermediates, which were identified as the corresponding silacarbonyl ylides on the basis of their broad absorption bands in the visible region ($\lambda_{max} \approx 500 – 650$ nm) and kinetic behavior. The species decay with 1st-order kinetics, with their decay rate coefficients responding to ketone concentration in a manner consistent with saturation kinetics, where a fast pre-equilibrium is followed by a relatively slow product forming step that becomes the rate-determining step for both silylene and ylide decay in the limit of high substrate concentration. The overall absolute rate constants and the individual pre-equilibrium and product-forming rate constants are systematically influenced by steric effects and ring strain in the carbonyl compounds, as well as the Lewis acidity and steric effects of the silylene. $SiMe_2$ reacts with these carbonyl compounds with absolute rate constants close to the diffusion-controlled rate ($k_{diff} \approx 2.2 \times 10^{10}\ M^{-1}\ s^{-1}$) in hexanes at 25 °C while $SiPh_2$ and $SiMes_2$ behave analogously with absolute rate constants in the range of $10^8 – 10^{10}\ M^{-1}\ s^{-1}$. The equilibrium constants for $SiMe_2$ and $SiPh_2$ were found to be in the ranges of 10^3 - $10^4\ M^{-1}$, while the product forming rates were 10^5 - $10^7\ s^{-1}$. The kinetic analysis, detection of the silacarbonyl ylide and steady-state experiments support a reaction mechanism involving the initial formation of a silacarbonyl ylide intermediate, followed by H-migration to afford the corresponding silyl enol ether.

2.8. Supporting Information

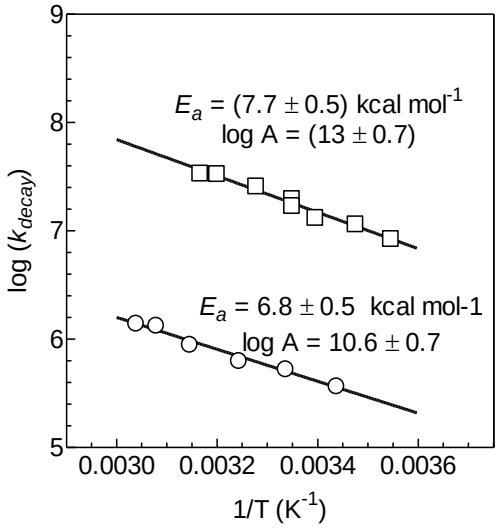

Figure S2.1. Arrhenius plots associated with the product-forming step from the silacarbonyl ylide in the reactions of $SiMe_2$ (□) and $SiPh_2$ (○) with 5 mM camphor (**4a**), monitored at 600 nm, at temperatures of 0.0 – 50.0°C. The slopes of the lines are as follows:(□): $-E_a/R = (-1.68 \pm 0.11) \times 10^3$ K^{-1} and (○): $-E_a/R = (-1.48 \pm 0.11) \times 10^3$ K^{-1}

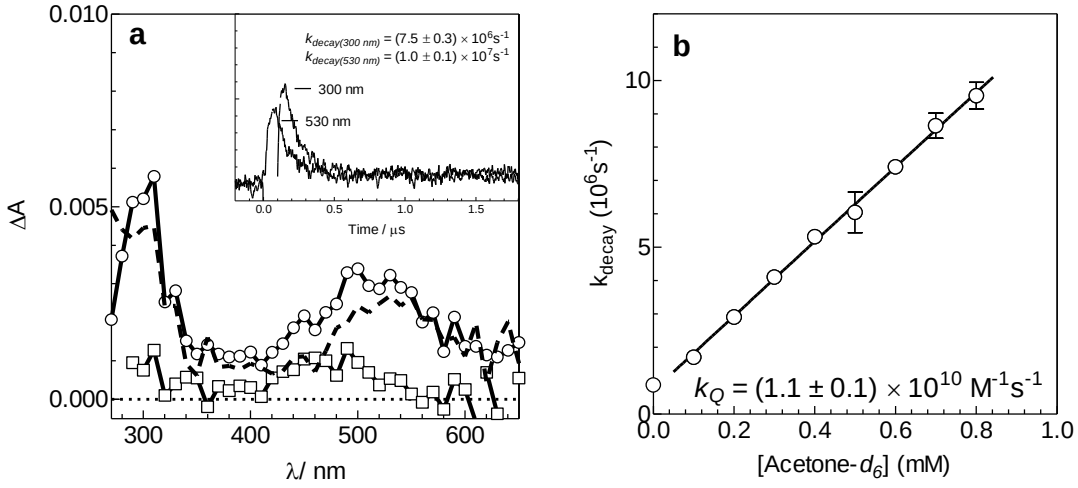

Figure S2.2. (a) Transient absorption spectra recorded 0.12 – 0.13 (○) and 0.44 – 0.45 μs (□) after the laser pulse by laser flash photolysis of **2** in the presence of 0.8 mM acetone-d_6 in deoxygenated hexanes at 25°C. The inset shows transient decay traces recorded at 300 and 530 nm. (b) Plot of k_{decay} vs. ketone concentration for $SiPh_2$ monitored at 530 nm. The solid line is the linear least-squares fit of the data to eq. 2.4.

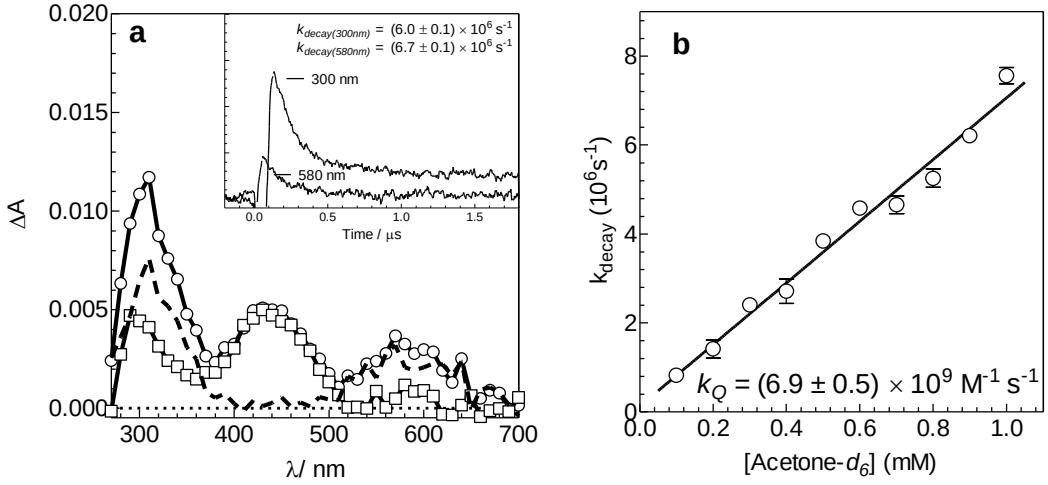

Figure S2.3. (a) Transient absorption spectra recorded 0.10 – 0.12 (○) and 0.44 – 0.45 μs (□) after the laser pulse by laser flash photolysis of **3** in the presence of 1 mM acetone-d_6 in deoxygenated hexanes at 25°C. The inset shows transient decay traces recorded at 300 and 580 nm. (b) Plot of k_{decay} vs. ketone concentration for $SiMes_2$ monitored at 580 nm. The solid line is the linear least-squares fit of the data to eq. 2.4.

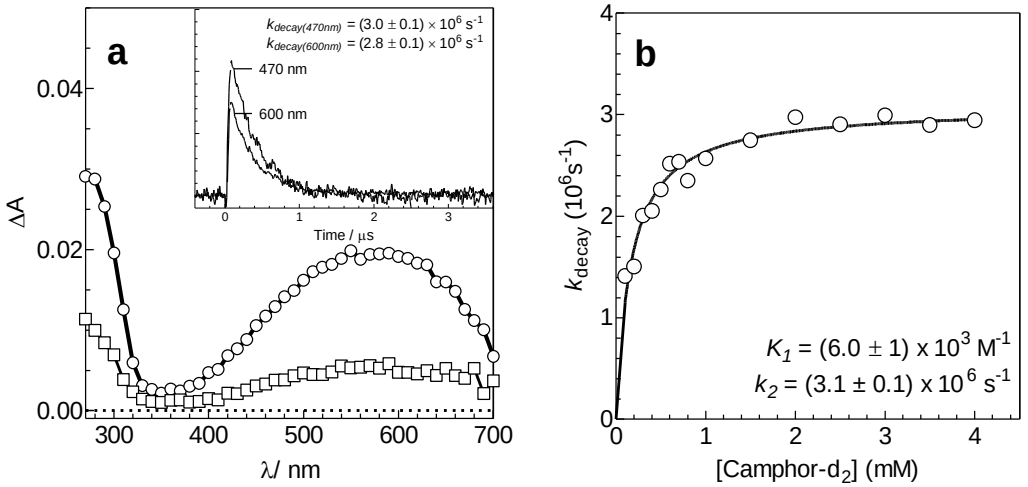

Figure S2.4. (a) Transient absorption spectra recorded 0.12 – 0.15 (○) and 0.56 – 0.59 μs (□) after laser pulse by laser flash photolysis of **1** in the presence of 5 mM camphor-d_2 in deoxygenated hexanes at 25°C. The inset shows transient decay traces recorded at 470 and 600 nm. (b) Plot of k_{decay} vs. ketone concentration for the $SiMe_2$-**4b** silacarbonyl ylide monitored at 600 nm. The solid line is the non-linear least-squares fit of the data to eq. 2.6.

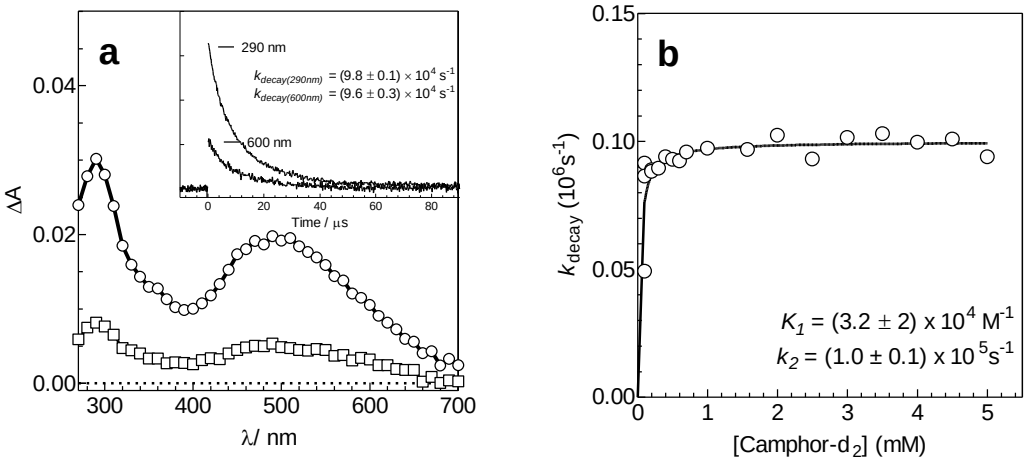

Figure S2.5. (a) Transient absorption spectra recorded 0.00 – 0.80 (○) and 13.92 – 14.72 μs (□) after laser pulse by laser flash photolysis of **2** in the presence of 4 mM camphor-d_2 in deoxygenated hexanes at 25°C. The inset shows transient decay traces recorded at 290 and 600 nm. (b) Plot of k_{decay} vs. ketone concentration for the $SiPh_2$-**4b** silacarbonyl ylide monitored at 600 nm. The solid line is the non-linear least-squares fit of the data to eq. 2.6.

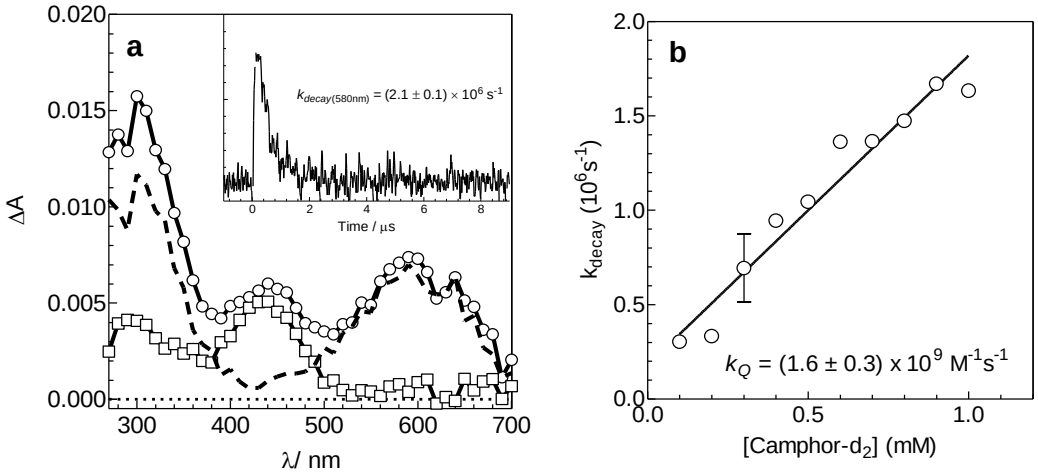

Figure S2.6. (a) Transient absorption spectra recorded 0.11 – 0.13 (○) and 2.80 – 2.83 μs (□) after laser pulse by laser flash photolysis of **3** in the presence of 3.90 mM camphor-d_2 in deoxygenated hexanes at 25°C. The dashed line spectrum (-) shows the difference between the two spectra. The inset shows transient decay trace recorded at 580 nm. (b) Plot of k_{decay} vs. ketone concentration for $SiMes_2$ monitored at 580 nm. The solid line is the linear least-squares fit of the data to eq. 2.4.

Table S2.1. Decay rate coefficients for the H-migration step in the reaction of $SiMe_2$ containing 4.72 mM camphor in deoxygenated hexanes in the temperature range of 9.0 – 43.0°C, recorded at 600 nm.

T (°C)	k_{decay} (× 10^6 s^{-1})	T (°C)	k_{decay} (× 10^6 s^{-1})
9.0	8.50 ± 0.25	32.1	26.1 ± 2.7
14.7	11.6 ± 0.40	39.5	33.8 ± 4.9
21.6	13.3 ± 0.85	42.8	34.2 ± 8.5
25.6	19.9 ± 0.99		

a. Errors are reported as the standard error

Table S2.2. Decay rate coefficients of the $SiPh_2$-camphor silacarbonyl ylide, in the reaction of $SiPh_2$ containing 4.8 mM camphor in deoxygenated hexanes in the temperature range of 9.0 – 43.0°C, recorded at 600 nm.

T (°C)	k_{decay} (× 10^6 s^{-1})	T (°C)	k_{decay} (× 10^6 s^{-1})
17.9	0.371 ± 0.011	44.3	0.901 ± 0.037
26.7	0.534 ± 0.017	51.1	1.35 ± 0.051
35.3	0.637 ± 0.042	56.4	1.41 ± 0.12

a. Errors are reported as the standard error

Table S2.3. ^{1}H NMR chemical shift assignments for **6** (see pg. 37)

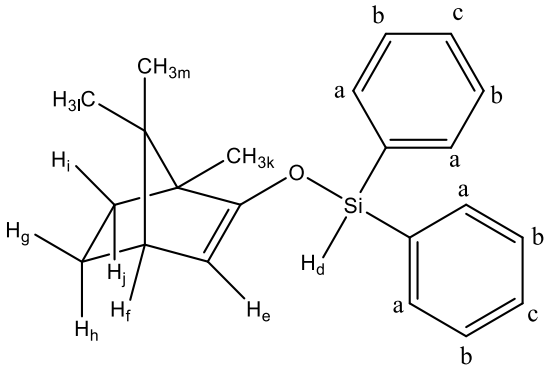

6

Proton	**^{1}H chemical shift (ppm)**
a	7.57 (m, 4 H)
b	7.30 (m, 4 H)
c	7.26 (m, 2 H)
d	5.51 (s, 1 H)
e	4.62 (d, 1 H, ^{3}J = 3.54)
f	2.09 (t, 1 H)
g	1.77 (m, 1 H)
h	1.47 (m, 1 H)
i	1.11 (m, 1 H)
j	0.95 (m, 1 H)
k	0.83 (s, 3 H)
l	0.99 (s, 3 H)
m	0.71 (s, 3 H)

Table S2.4. ^{1}H NMR chemical shift assignments for **16** (see pg. 54)

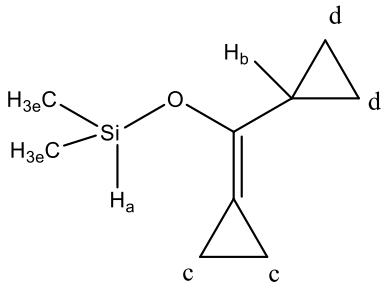

15

Proton	^{1}H chemical shift (ppm)
a	4.87 (septet, 1 H, ^{3}J = 2.75)
b	1.60 (m,1 H)
c	1.00 (m, 4 H)
d	0.45 (m, 4H)
e	0.18 (m, 6H, ^{3}J = 2.75)

2.9. References

1. C. Browne, W. J. L., *unpublished results*.
2. Ando, W.; Ikeno, M., *Chem. Lett.* **1978,** *7*, 609-610.
3. Moiseev, A. G.; Leigh, W. J., *Organometallics* **2007,** *26*, 6268-6276.
4. Bobbitt, K. L.; Gaspar, P. P., *J. Organomet. Chem.* **1995,** *499*, 17-26.
5. Conlin, R. T.; Netto-Ferreira, J. C.; Zhang, S.; Scaiano, J. C., *Organometallics* **1990,** *9*, 1332-1334.
6. Ando, W.; Ikeno, M.; Sekiguchi, A., *J. Am. Chem. Soc.* **1977,** *99* (19), 6447-6449.
7. Ando, W.; Ikeno, M.; Sekiguchi, A., *J. Am. Chem. Soc.* **1978,** *100* (11), 3613-3615.
8. Ishikawa, M.; Nakagawa, K.; Kumada, M., *J. Organomet. Chem.* **1977,** *135*, C45-C49.
9. Schäfer, A.; Weidenbruch, M.; Pohl, S., *J. Organomet. Chem.* **1985,** *282* (3), 305-313.
10. Ando, W.; Hagiwara, K.; Sekiguchi, A., *Organometallics* **1987,** *6*, 2270-2271.
11. Ando, W.; Ikeno, M., *J. Chem. Soc., Chem. Commun.* **1979,** (15), 655-656.
12. Ishikawa, M.; Nishimura, K.; Sugisawa, H.; Kumada, M., *J. Organomet. Chem.* **1980,** *194*, 147-158.
13. Jutzi, P.; Eikenberg, D.; Bunte, E. A.; Mohrke, A.; Neumann, B.; Stammler, H. G., *Organometallics* **1996,** *15*, 1930-1934.
14. Gehrhus, B.; Hitchcock, P. B.; Lappert, M. F., *Organometallics* **1997,** *16* (22), 4861-4864.
15. Moiseev, A. G.; Leigh, W. J., *Organometallics* **2007,** *26*, 6277-6289.
16. Murov, S. L.; Carmichael, I.; Hug, G. L., *Handbook of photochemistry*. 2nd ed.; Dekker: New York, 1993.
17. Kostina, S. S.; Singh, T.; Leigh, W. J., *Organometallics* **2012,** *31*, 3755-3767.
18. Kostina, S. S.; Singh, T.; Leigh, W. J., *J. Phys. Org. Chem.* **2011,** *24*, 937-946.
19. Leigh, W. J.; Kostina, S. S.; Bhattacharya, A.; Moiseev, A. G., *Organometallics* **2010,** *29*, 662-670.

Chapter 3 – Kinetic and Thermodynamic Studies of the Reactions of Silylenes with Non-Enolizable Carbonyl Compounds

3.1. Overview

This chapter describes the results of a detailed study of the kinetics and thermodynamics of the reactions of silylenes ($SiMe_2$, $SiPh_2$, and $SiMes_2$), generated photochemically from the corresponding precursors **1** – **3**, respectively, with a selection of non-enolizable carbonyl compounds: pivalaldehyde (**4**), 2-adamantanone (**5**), di-*tert*-butyl ketone (**6**), and 2,2,5,5-tetramethylcyclopentanone (**8**). Product and kinetic studies of the reaction with $SiMes_2$ with 1,1,3,3-tetramethyl-2-indanone (**7**) were also carried out in an attempt to reproduce some of the originally reported data for this system.[1-2]

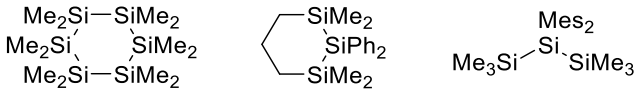

1 **2** **3**

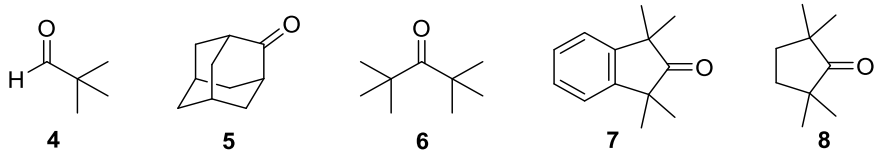

4 **5** **6** **7** **8**

3.2. Previous Studies in Our Group

In conjunction with the work on enolizable carbonyl compounds that was described in Chapter 2, our group also studied the reactions of the three silylenes with the non-enolizable carbonyl compounds pivalaldehyde and 2-adamantanone. Two different types of kinetic behavior were again observed, similar to what was observed in the previous chapter.

The addition of pivalaldehyde to hexanes solutions of **1**, **2**, or **3** led to shortening of the silylene lifetime and suppression of the formation of the corresponding disilene, as was observed in the previous chapter for ketones such as acetone, pinacolone, and cyclopentanone. There is a linear dependence of the silylene decay rate coefficient with ketone concentration (Figure 3.1b), which was analyzed according to eq. 3.1, where Q denotes the substrate, and k_Q is the bimolecular rate constant for its reaction with the free silylene. For the case of $SiMe_2$ with pivalaldehyde, the absolute rate constant was determined to be $k_Q = (1.5 \pm 0.1) \times 10^{10}$ M^{-1} s^{-1}, from the slope of the plot of k_{decay} vs. [Q] (Figure 3.1b). The absolute rate constants measured for this and the other two silylenes studied are shown in Table 3.1.[3]

No new transient intermediates could be detected for any of the three systems at aldehyde concentrations up to 5 – 10 mM. For example, Figure 3.1a shows the transient absorption spectra exhibited by **1** in the presence of 4.57 mM pivalaldehyde; the spectrum recorded over the first *ca.* 100 ns after the laser pulse shows only the absorption at $\lambda_{max} \approx$ 470 nm due to $SiMe_2$.

$$k_{decay} = k_Q[Q] + k_0 \qquad (3.1)$$

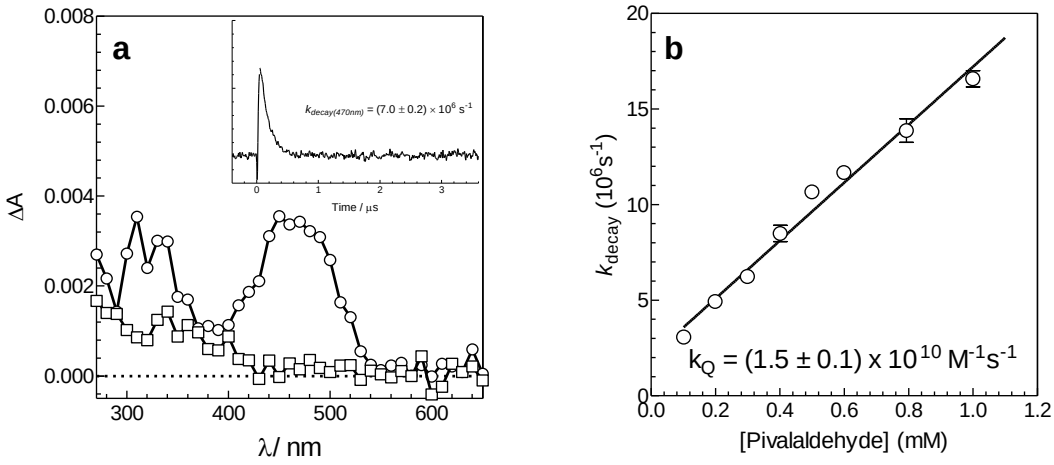

Figure 3.1. (a) Transient absorption spectra recorded 0.14 – 0.17 μs (○) and 0.56 – 0.59 μs (□) after the laser pulse by laser flash photolysis of **1** in the presence of 0.6 mM pivalaldehyde in deoxygenated hexanes at 25°C. The inset shows transient decay trace recorded at 470 nm. (b) Plot of k_{decay} vs ketone concentration for $SiMe_2$ monitored at 470 nm. The solid line is the linear least-squares regression of the data according to eq. 3.1.

Table 3.1. Absolute rate constants (k_Q) for the reactions of $SiMe_2$, $SiPh_2$, and $SiMes_2$ with pivalaldehyde in hexanes solution at 25°C[3]

Substrate	k_Q (x 10^{10} $M^{-1}s^{-1}$)		
	$SiMe_2$	$SiPh_2$	$SiMes_2$
pivalaldehyde	1.5 ± 0.1	1.1 ± 0.1	0.46 ± 0.03

(*Data recorded by C. Browne*)

In contrast, laser flash photolysis of the $SiMe_2$, $SiPh_2$, and $SiMes_2$ precursors (**1** – **3**) in the presence of 2-adamantanone (**5**) leads to the formation of transient products exhibiting broad UV-vis absorption bands centred in the range λ_{max} = 500 – 700 nm. For example, Figure 3.2 shows the transient spectra obtained from flash photolysis of **1** in hexanes containing 10 mM 2-adamantanone. These transients are assigned to the corresponding silacarbonyl ylides, on the basis of what was observed in Chapter 2, as well as the early low temperature spectroscopic studies of Ando *et al*.[1] The absorption

band maxima of the ylides formed by reaction of $SiMe_2$, $SiPh_2$, and $SiMes_2$ with **5** are listed in Table 3.2.[3]

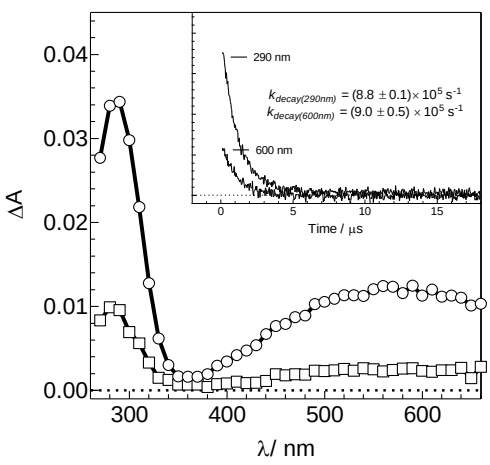

Figure 3.2. Transient absorption spectra recorded 0.13 – 0.26 μs (○) and 1.66 – 1.86 μs (□) after laser pulse by laser flash photolysis of **1** in the presence of 10 mM 2-adamantanone in deoxygenated hexanes at 25°C. The inset shows transient decay traces recorded at 290 and 600 nm. (*Data recorded by C. Browne*)

Table 3.2. Experimental UV-Vis absorption maxima (λ_{max} (nm)) of the silacarbonyl ylides from the reactions of $SiMe_2$, $SiPh_2$, and $SiMes_2$ with 2-adamantanone (**5**) in hexanes at 25°C[3]

Substrate	λ_{max} (nm)		
	$SiMe_2$	$SiPh_2$	$SiMes_2$
2-adamantanone	620	530	640

(*Data recorded by C. Browne*)

Preliminary kinetic studies have been done on these systems, but they were not completed fully. The kinetic analysis of the reaction of $SiMe_2$ with 2-adamantanone was done by monitoring at both 470 nm and 600 nm, where the silylene and silacarbonyl ylide individually absorb, but the kinetic analyses of the reactions with $SiPh_2$ and $SiMes_2$ were done by monitoring the transient absorptions only at wavelengths corresponding to λ_{max} of the respective silylene, which are difficult to interpret unambiguously because of interference from the overlapping absorptions from the silacarbonyl ylide.

The plots of k_{decay} at 470 and 570 nm vs. ketone concentration for the reaction of $SiMe_2$ with **5** are shown in Figure 3.3a. It can be seen that there is a linear dependence of k_{decay} (570 nm) on ketone concentration and analysis of the data according to eq. 3.1 afforded a rate constant of $k_Q = (1.9 \pm 0.1) \times 10^7\ M^{-1}\ s^{-1}$. On the other hand, there is a negative dependence of the k_{decay} (470 nm) values on ketone concentration, indicative of more complex behavior. However, reviewing the kinetic decay of the 470 nm decay traces, this behavior is due to overlap of a mixed 1st and 2nd order decay of $SiMe_2$ and 1st order decay of the ylide, and thus the k_{decay} values obtained from a simple 1st order exponential analysis are dominated by the 2nd-order component (due to silylene dimerization), which is much faster than the pseudo-first order reaction with the substrate. It should be possible to reduce the contribution from the 2nd-order component by working at lower laser intensities.

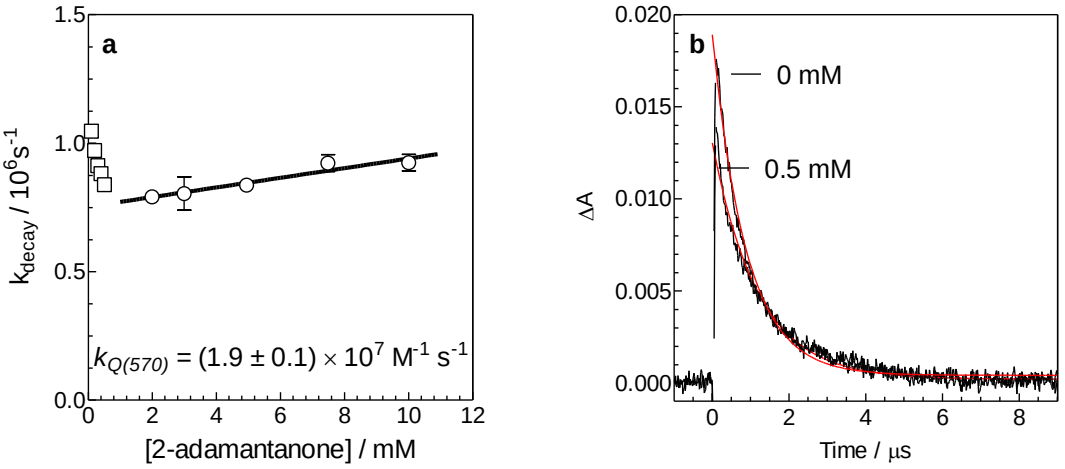

Figure 3.3. (a) Plot of k_{decay} vs ketone concentration for $SiMe_2$ and the $SiMe_2$-**5** silacarbonyl ylide monitored at 470 (□) and 570 (○) nm. The solid line is the linear least-squares fit of the data to eq. 3.1. (b) Decay trace of the silylene (monitored at 470 nm) in the presence of 0 and 0.5 mM 2-adamantnone. The red solid line is the non-linear regression of the one-phase decay. (*Data recorded by C. Browne*).

Preliminary kinetic analysis of the reaction of $SiPh_2$ with **5** was done by evaluating the apparent first-order decay of the transient absorbance at 520 nm over the 0 – 2 mM concentration range in added **5** (Figure 3.4a). It can be seen that k_{decay} is approximately independent of ketone concentration and equal to $k_{decay} \approx 2 \times 10^5\ s^{-1}$. This suggests that the second step in the mechanism (*ie.* product formation from the ylide) is the rate determining step in the reaction, with the ylide and silylene being in mobile equilibrium with each other at all concentrations.

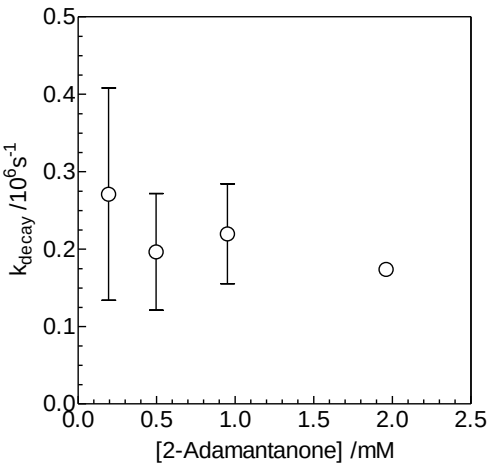

Figure 3.4. Plot of k_{decay} vs ketone concentration from laser flash photolysis of **2** in the presence of **5**, monitoring transient absorption at 520 nm.

A plot of k_{decay} vs. ketone concentration for $SiMes_2$ monitored at 580 nm is shown in Figure 3.5. It can be seen that the k_{decay} varies approximately linearly with ketone concentration at lower concentrations (0 – 2 mM) but deviates from linear behavior at higher ketone concentrations (*ca.* 10 mM), in a manner suggesting saturation kinetics as observed in the previous chapter. This has been reevaluated in this chapter.

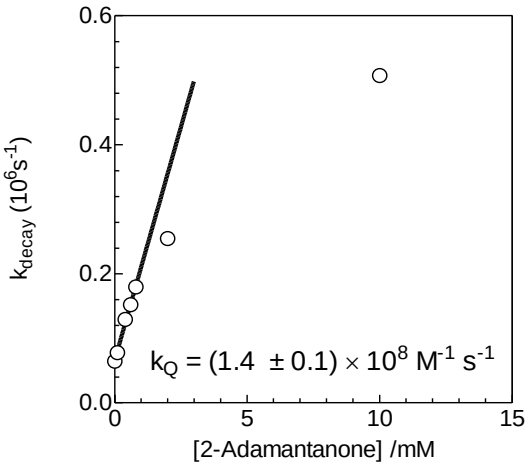

Figure 3.5. Plot of k_{decay} vs ketone concentration for $SiMes_2$ monitored at 580 nm. The solid line is the linear least-square fit to eq. 3.1.

3.3. Scope of the Study

The selection of ketones studied was chosen on the basis of the reported literature for the reactions of $SiMe_2$ and $SiMes_2$ with various ketones.[4-5] The reactions of $SiMe_2$ and $SiMes_2$ with 2-adamantanone have been reported to afford the corresponding dioxasilacyclopentane derivatives (**9a** and **9b**) (eq. 3.2).[4-5] However there is limited information known on these compounds, as ^1H and ^{13}C, IR, and MS spectral data have been reported only for the $SiMe_2$ derivative. In addition, the course of the reaction of $SiPh_2$ with 2-adamantanone is not known. Therefore, our goal was to complete the kinetic analyses previously initiated in our group, and also synthesize and characterize the product of reaction of $SiPh_2$ with 2-adamantanone. Based on the reported behavior of $SiMe_2$ and $SiMes_2$ with this ketone, we expected the reaction to yield the corresponding dioxasilacyclopentane, **9c** (eq. 3.2).

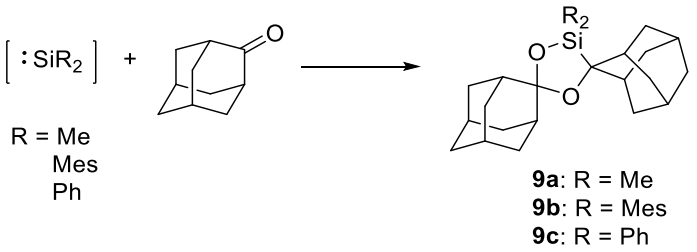

(3.2)

In addition to completing the steady state and flash photolysis studies of the reactions of the three silylenes with 2-adamantanone, we were also interested in studying a closely related system to 1,1,3,3-tetramethyl-2-indanone (**7**). Ando and co-workers reported the detection of a silacarbonyl ylide at 77 K and isolated the corresponding oxasilirane (**10**) from the reaction of $SiMes_2$ with **7** (eq. 3.3).[1] The aryl group in **7** leads to strong UV absorption at 248 nm that can be expected to interfere in the LFP studies, making it difficult to study the kinetics of the reactions of **7** with $SiMe_2$, $SiPh_2$, and $SiMes_2$ reliably. We thus needed to identify a closely-related analogue with more appropriate light-absorption properties.

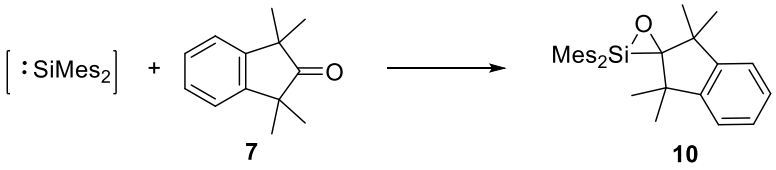

(3.3)

2,2,5,5-Tetramethylcyclopentanone (**8**) has similar structural characteristics to **7**, and the exclusion of the aryl group will reduce the ketone's absorptivity below 300 nm and reduce the extent to which competes with the silylene precursor for light. It was therefore chosen for detecting and studying the kinetic behavior of the corresponding silacarbonyl ylides in solution at ambient temperature, as well as for the isolation and characterization of the corresponding oxasiliranes. Furthermore, we were interested in

learning how the course of the reaction and its kinetics are affected by the structural rigidity inherent in **8**, so we have also examined the reactions of the three silylenes with the acyclic analogue di-*tert*-butyl ketone (**6**).

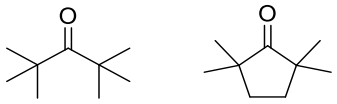

6 **8**

3.4. Product Studies

3.4.1 Reaction of $SiMes_2$ with 2,2,5,5-Tetramethylcyclopentanone (**8**)

Photolysis of **3** (0.025 M) in the presence of 2,2,5,5-tetramethylcyclopentanone (**8**) (0.05 M) in C_6D_{12} in a quartz NMR tube, with periodic monitoring by ^1H NMR spectroscopy, led to the formation of hexamethyldisilane (**11**) (71 ± 5%) and the corresponding oxasilirane (**12**) (36 ± 6%) (eq. 3.4). Compound **12** was initially identified in the crude photolysate by comparing its ^1H, ^{13}C, and ^{29}Si NMR spectra to those reported for **10**.[6] The ^1H NMR spectra of the crude photolysate before and after photolysis for 35 mins shows a *ca.* 70% conversion of **3**, as shown in Figure 3.6. Product yields were determined from the relative slopes of the concentration vs time plots shown in Figure 3.7 for the reactants and products. The ^1H and ^{13}C NMR assignments of compound **12** in C_6D_{12} are listed in the Supporting Information in Tables S3.1 and S3.2 respectively.

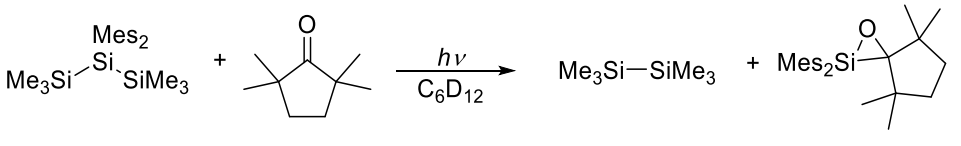

3 0.025 M + **8** 0.045 M → $h\nu$, C_6D_{12} → $Me_3Si—SiMe_3$ (**11**) 71 ± 5% + Mes_2Si (**12**) 36 ± 6% (3.4)

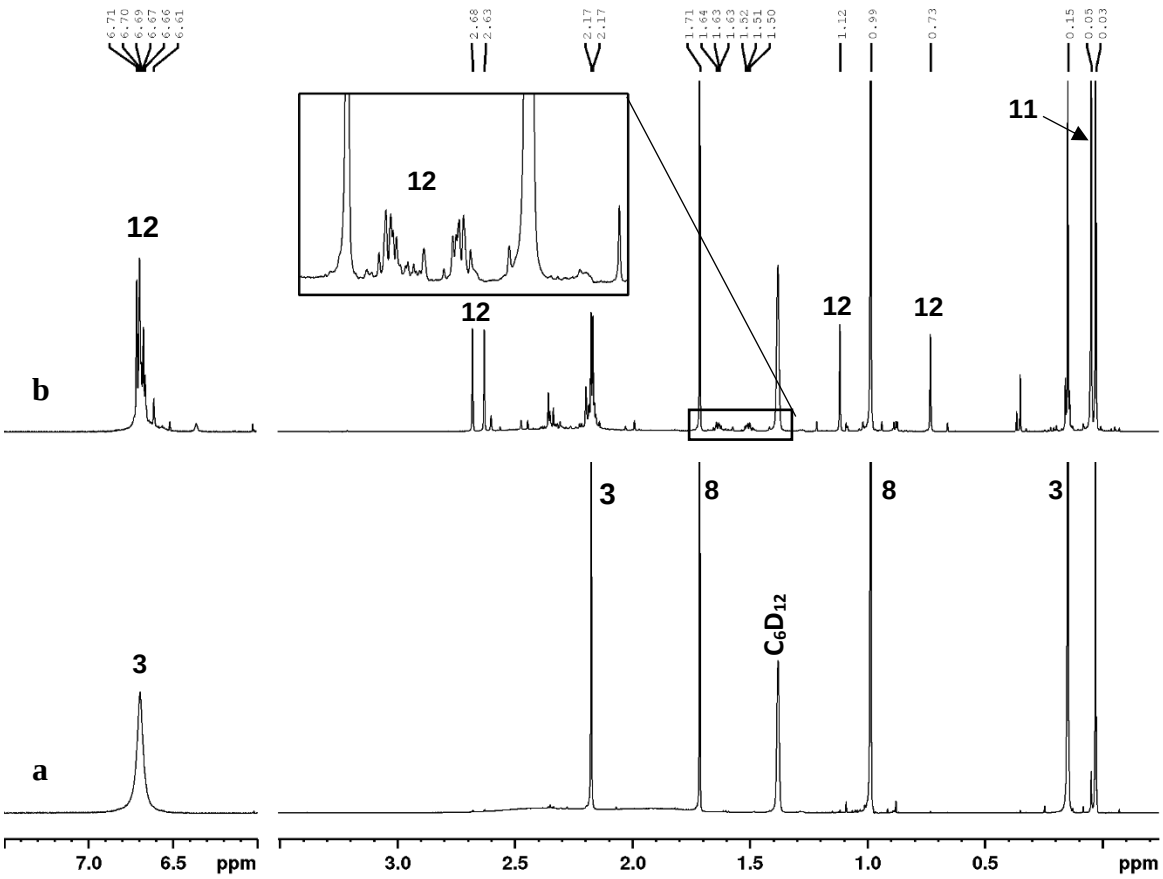

Figure 3.6. ^{1}H NMR spectra of a solution of 0.025 M **3**, 0.05 M **8**, and 0.01 M bis(trimethylsilyl)methane in C_6D_{12} (a) before and (b) after 35 mins of photolysis. The inset shows the region of the ^{1}H NMR spectrum between 1.20 – 1.80 ppm.

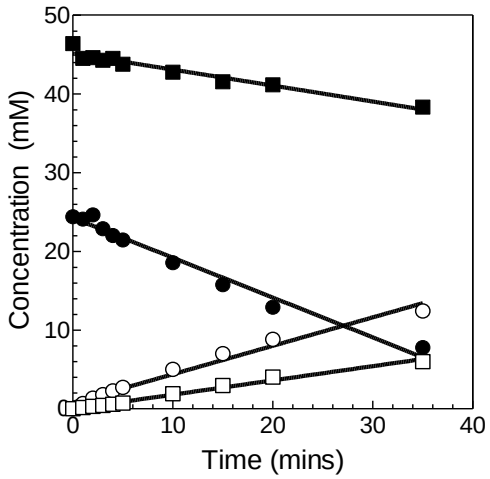

Figure 3.7. Concentration vs. time plots for the photolysis of **3** in the presence of 2,2,5,5-tetramethylcyclopentanone (**8**) in cyclohexane-d_{12}. Shown is the depletion of **3** (●) and **8** (■) over irradiation time, along with the formation of **11** (○) and oxasilirane **12** (□). Slopes are as follows: (**3**; ●): (-0.51± 0.05) mM/min, (**8**; ■): (-0.20 ± 0.03) mM/min, (**11**; ○): (0.36 ± 0.04) mM/min, **(12**; □): (0.18 ± 0.01) mM/min.

A preparative scale synthesis of **12** was performed, in order to isolate the cycloadduct.[6] A solution of 2,2-dimesityl-1,1,1,3,3,3-hexamethyltrisilane (**3**: 250.0 mg, 0.61 mmol) and 2,2,5,5-tetramethylcyclopentanone (**8**: 135.2 mg, 0.97 mmol) was prepared in dry cyclohexane, argon-purged, and irradiated with 2 × 254 nm lamps for 4 hrs. Compound **12** was isolated by radial thick-layer chromatography, using a 1 mm thick basic alumina chromatotron plate, with 100% hexanes as the eluent. Following chromatography, the product was recrystallized twice from MeOH to yield a white solid (14.3 mg, 6%; m.p. 142 – 145^{o}C).

The 600 MHz ^{1}H NMR spectrum of purified **12** in $CDCl_3$ is shown in Figure 3.8. The ^{1}H NMR chemical shift assignments are listed in Table 3.3, with the labelled protons in Figure 3.9. The spectrum shows singlets at δ1.14 (6H) and 0.75 (6H) assignable to the aliphatic -CH_3 protons (H_a and H_b respectively), while the multiplets at δ 1.65 (2H) and 1.54 (2H) can be assigned to the -CH_2 protons (H_c and H_d). The next sets of singlets are the two *o*-Me (δ2.70, 6H, H_e and δ2.65, 6H, H_f) and the *p*-Me protons (δ2.23, 6H, H_g) of the mesityl substituents. The *m*-protons on the phenyl ring appear at δ6.79 (4H, H_h). This is consistent with the published spectrum of **10** in CCl_4, in which the aromatic protons appear at δ 7.04 and 6.79, the ortho and para methyl protons of the mesityl groups at δ 2.70 and 2.25, respectively, and the aliphatic methyl protons at δ 1.31 and 0.97.[6]

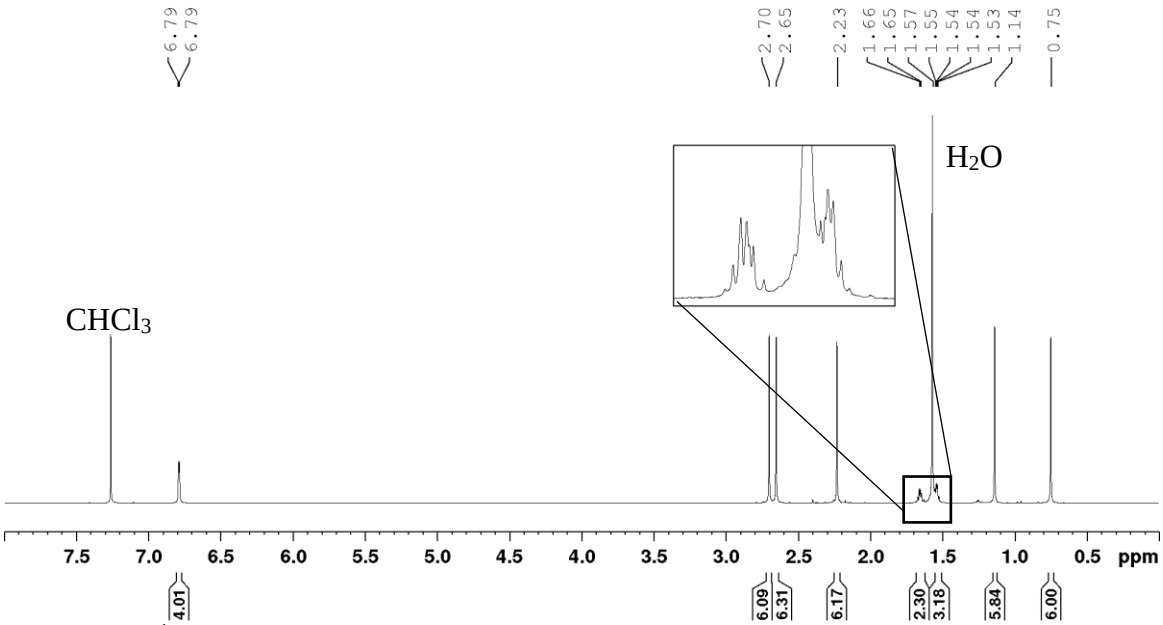

Figure 3.8. ^{1}H NMR spectrum of **12** in $CDCl_3$.

Table 3.3. ^{1}H NMR assignments for compound **12** in $CDCl_3$ (Figure 3.8), refer to Figure 3.9 for structural assignments

Chemical Shift (ppm)	Assignment	Chemical Shift (ppm)	Assignment
1.14 (s)	H_a	2.70 (s)	H_e
0.75 (s)	H_b	2.65 (s)	H_f
1.65 (m)	H_c	2.23 (s)	H_g
1.54 (m)	H_d	6.79 (s)	H_h

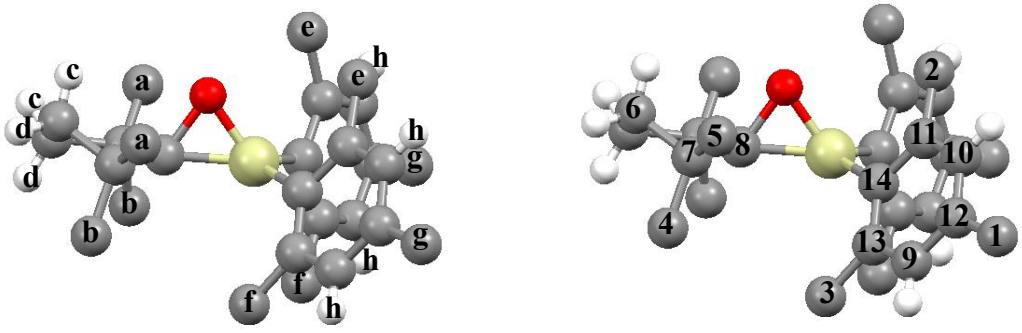

Figure 3.9. The proton (left) and carbon (right) assignments, used for Tables 3.3 and 3.4, for compound **12**

The ^{13}C NMR assignments were done with the aid of 2D ^{1}H-^{13}C HMBC and HSQC NMR experiments, given the assigned protons from above (see Figures S3.2 and S3.3). The ^{13}C NMR chemical shift assignments are listed in Table 3.4, with the labelled carbons shown in Figure 3.9. The ^{13}C DEPTQ spectrum ($CDCl_3$, see Figure 3.10) of **12** shows negatively phased peaks at δ21.3, 23.4, and 27.0, which are assigned to the *p*- and *o*-methyl carbons (C-1, C-2, and C-3) respectively. The next set of peaks with negatively phased peaks at δ26.7 and 29.4 are assigned to the methyl carbons on the C_5 ring (C-4 and C5). The positively phased peak at δ40.7 is assigned to the -CH_2 carbons (C-6), while that at δ46.0 is assigned to the two quaternary carbons on the C_5 ring bearing the methyl groups (*ie.* C-7). The relative weak peak at δ89.4 is assigned to the quaternary carbon of the oxasilacyclopropane moiety (C-8). The next set of peaks at δ128.3 (C-9) and 129.3 (C-10) are assigned to the carbons on the *m*-position of the aromatic ring, while the peaks at δ129.3 (C-11), 140.1 (C-12), 143.1 (C-13), and 145.4 (C-14) are assigned to the carbons in the *ipso*-, *p*-, and *o*-positions of the aromatic ring, respectively.

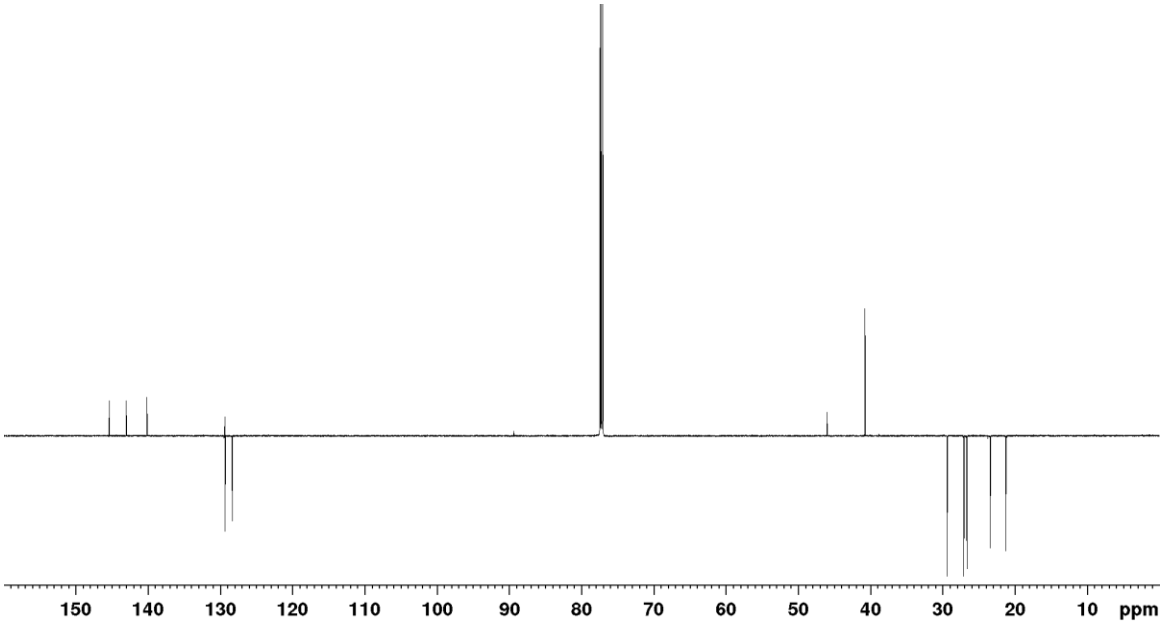

Figure 3.10. DEPTQ ^{13}C NMR spectrum of **12** in $CDCl_3$ (-CH and -CH_3 groups are negatively phased and -C and -CH_2 groups are positively phased).

Table 3.4. ^{13}C NMR assignments for compound **12** in $CDCl_3$ (Figure 3.10), refer to Figure 3.9 for structural assignments

Chemical Shift (ppm)	Assignment	Chemical Shift (ppm)	Assignment
21.3	C-1	89.4	C-8
23.4	C-2	128.3	C-9
27.0	C-3	129.3	C-10
26.7	C-4	129.3	C-11
29.4	C-5	140.1	C-12
40.7	C-6	143.1	C-13
46.0	C-7	145.4	C-14

The ^{29}Si chemical shift in **12** is δ -50.0, which corresponds reasonably closely to the ^{29}Si chemical shift reported for **10** of δ -53.6 in CCl_4 (see Figure S3.4).[6]

The structure of **12** was further confirmed by X-ray crystallography (see Figure 3.11 for ORTEP drawing and Table 3.5 for crystal data and structure refinements).

Table 3.5. Crystal data and structure refinement for compound **12**

	12
Empirical formula	$C_{27}H_{38}OSi$
FW, g/mol	406.27
Temp, K	100.0 (1)
Cryst. syst.	Monoclinic
Space group	$P2_1/c$
Unit cell dimens.	
a (Å)	14.6595(11)
b (Å)	17.9072(13)
c (Å)	19.2722(15)
β	105.620(5)°
Volume, Å^3	4872.3(6)
Z	8
μ(MoKα), mm^{-1}	0.111 mm
Dcalc, g/cm^3	1.109
Reflections collected	158648, 12097 unique (R_{int} = 0.0629, R_{sigma} = 0.0357)
Final R indice [I >2σ(I)]	R_1 = 0.0545, wR_2 = 0.1408

The average bond angles in the siloxirane ring of **12** are 58.28º (Si-C-O), 70.32º (C-O-Si), and 51.12º (O-Si-C), while the average bond lengths are 1.862 Å(Si-C), 1.541 Å(C-O), and 1.677 Å(Si-O). The bond angles and distances in **12** are similar to those in **10:** 58.5º (Si-C-O), 71.0º (C-O-Si), and 50.4º (O-Si-C), 1.849 Å(Si-C), 1.507 Å(C-O), and 1.668 Å(Si-O), respectively.[6]

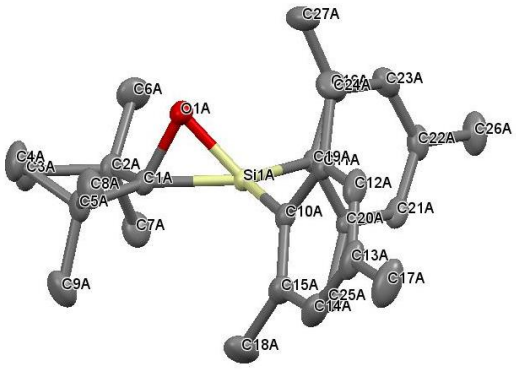

Figure 3.11. ORTEP drawing and labeling scheme of **12**. Hydrogen atoms are omitted for clarity.

*3.4.2. Steady State Photolysis of **3** in the Presence of Di-tert-butyl Ketone (**6**)*

Steady-state photolysis of **3** (0.05 M) in C_6D_{12} containing di-*tert*-butyl ketone (**6**: 0.05 M) affords **11** (57 ± 6%) and a product identified as the corresponding oxasilirane (**13**, 35 ± 7%) (eq. 3.5), where the product yields are given by the relative consumption of **3**. Compound **13** was identified from the NMR spectra of the crude photolysate, on the basis of its ^{1}H, ^{13}C, and ^{29}Si chemical shifts compared to those in the spectra of **12** and **10**. The concentration vs. time plots are shown in Figure 3.13, while he ^{1}H and ^{13}C NMR spectra are shown in Figures 3.12 and 3.14 respectively. The ^{1}H and ^{13}C NMR assignments, made with the aid of 2D ^{1}H-^{13}C HMBC and HSQC NMR spectroscopy (see Figures S3.5 and S3.6), are listed in Table 3.6 and 3.7 respectively, with the assigned protons and carbons shown in Figure 3.14. The ^{1}H-^{29}Si HMBC NMR spectrum showed a ^{29}Si resonance at δ -47.6, assignable to **13** (see Figure S3.7).

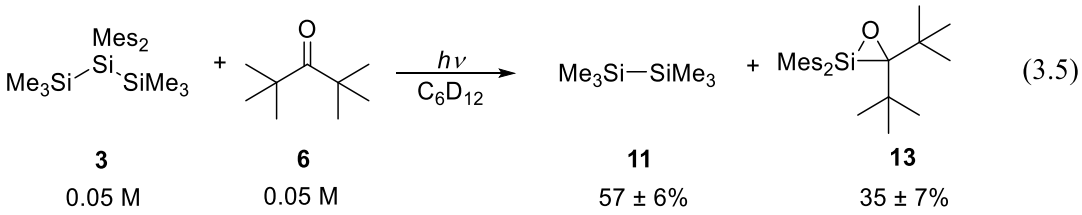

(3.5)

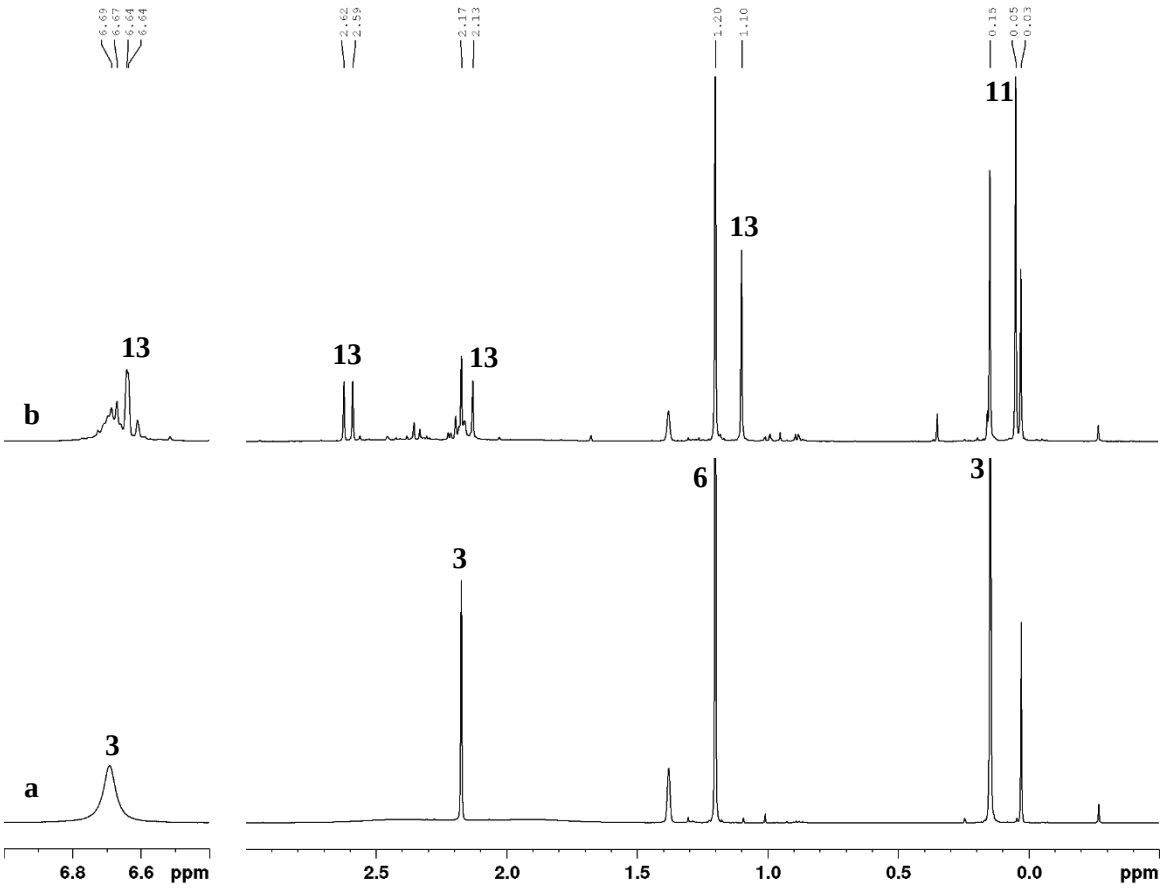

Figure 3.12. ^{1}H NMR spectra of a solution of 0.05 M **3**, 0.05 M **6**, and 0.01 M bis(trimethylsilyl)methane in C_6D_{12} (a) before and (b) after 60 mins of photolysis (*ca.* 70% conversion of **3**).

Table 3.6. ^{1}H NMR assignments for compound **13**, recorded from the spectrum of the crude photolysate in C_6D_{12} (Figure 3.13b), refer to Figure 3.15 for structural assignments

Chemical Shift (ppm)	Assignment	Chemical Shift (ppm)	Assignment
1.10 (s)	H_a	2.62 (s)	H_d
2.13 (s)	H_b	6.64 (m)	H_e
2.59 (s)	H_c		

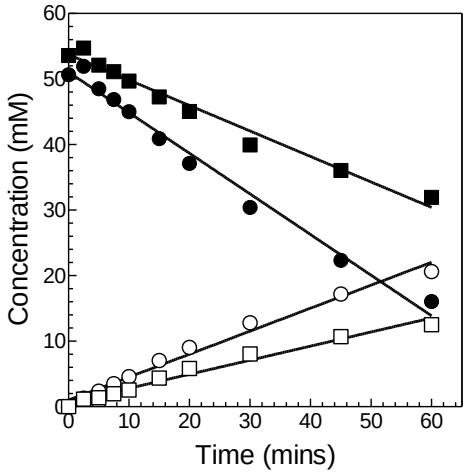

Figure 3.13. Concentration vs. time plots for the photolysis of **3** in the presence of di-*tert*-butyl ketone (**6**) in cyclohexane-d_{12}. Shown is the depletion of **3** (●) and **6** (■) over irradiation time, along with the formation of **11** (○) and oxasilirane **13** (□). Slopes are as follows: (**3**; ●): (-0.62± 0.03) mM/min, (**6**; ■): (-0.39 ± 0.02) mM/min, (**11**; ○): (0.35 ± 0.02) mM/min, (**13**; □): (0.21 ± 0.01) mM/min.

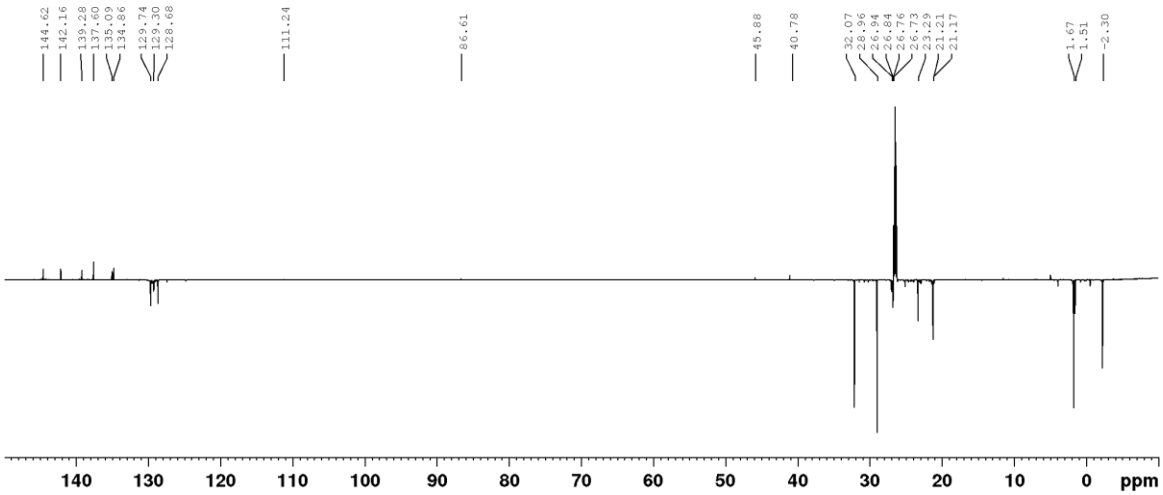

Figure 3.14. DEPTQ ^{13}C NMR spectrum of a solution of 0.05 M **3**, 0.05 M **6**, and 0.01 M bis(trimethylsilyl)methane in C_6D_{12} after 60 mins of photolysis.

Table 3.7. ^{13}C NMR assignments for compound **13**, recorded from the spectrum of the crude photolysate in C_6D_{12} (Figure 3.14), refer to Figure 3.15 for structural assignments.

Chemical Shift (ppm)	Assignment	Chemical Shift (ppm)	Assignment
21.2	C-1	128.7	C-8
23.3	C-2	129.7	C-9
26.8	C-3	135.1	C-10
32.0	C-4	139.3	C-11
40.8	C-5	142.2	C-12
86.6	C-6	144.6	C-13

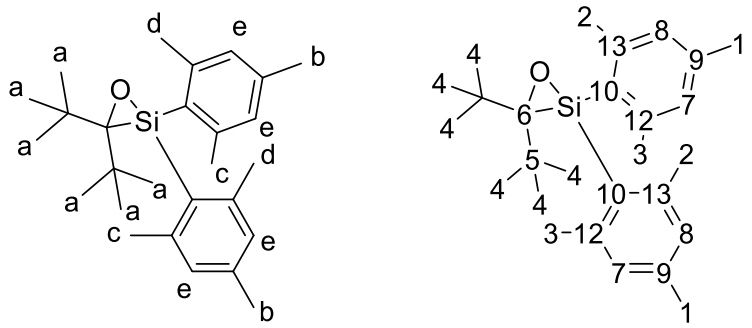

Figure 3.15. The proton (left) and carbon (right) assignments, used for Tables 3.5 and 3.6, for compound **13**.

3.4.3. Reaction of $SiPh_2$ with 2-Adamantanone (**5**)*

Steady state photolysis of **2** (0.05 M) in the presence of 2-adamantanone (**5**) (0.11 M) in C_6D_{12} afforded 1,1,2,2-tetramethyl-1,2-disilacyclopentane (**14**) (103 ± 3%) and a product identified as the corresponding dioxasilacyclopentane (**9c**) (86 ± 5%) (eq. 3.6).

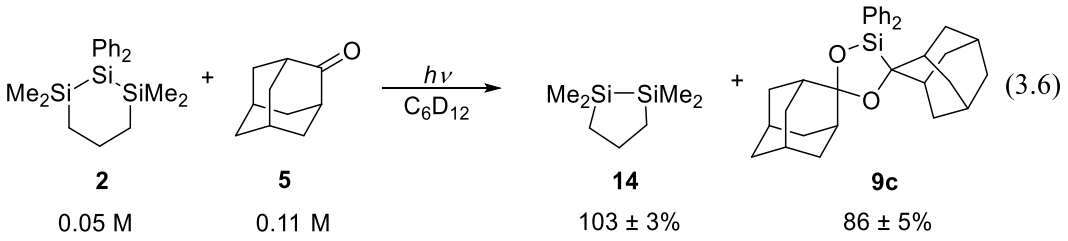

The ^{1}H NMR spectra of the crude photolysis mixture are shown in Figure 3.16, while the concentration versus time plots for the reactants and identified products are shown in Figure 3.17. The product yields were determined relative to the consumption of **2** from the slopes of the concentration vs time plots. The plots show that roughly two molecule of **5** are consumed for every molecule of **2**, which is consistent with the proposed stoichiometry in **9c**.

* I thank A. Sever for carrying out these experiments.

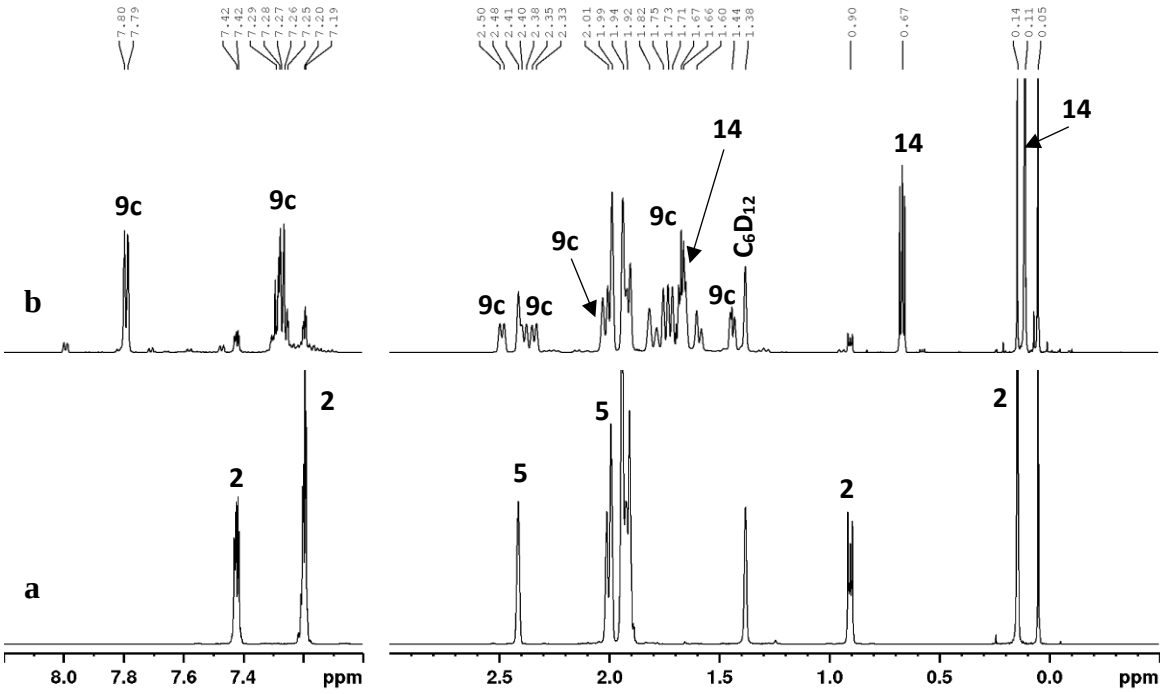

Figure 3.16. ^{1}H NMR spectra of a C_6D_{12} solution of 0.053 M **2** containing 0.11 M of **5**, and 0.01 M hexamethyldisilane (a) before and (b) after 45 mins of photolysis (*ca.* 40% conversion of **2**). (*Data recorded by A. Sever*)

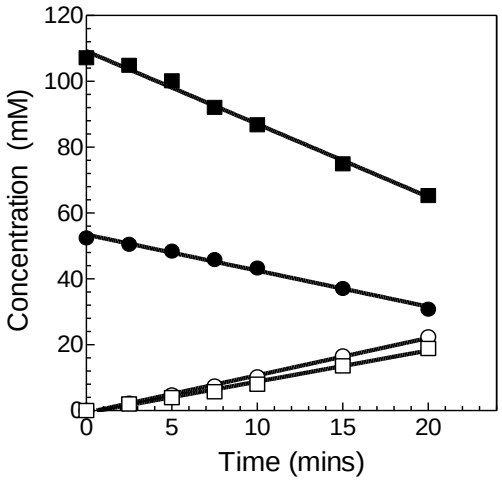

Figure 3.17. Concentration vs. time plots for the photolysis of **2** in the presence of 2-adamantanone (**5**) in cyclohexane-d_{12}. Shown is the depletion of **2** (●) and **5** (■) with irradiation time and the formation of **14** (○) and dioxasilacyclopentane (**9c**) (□). Slopes are as follows: (**2**; ●): (-0.11± 0.01) mM/min, (**5**; ■): (-0.22 ± 0.01) mM/min, (**14**; ○): (0.11 ± 0.01) mM/min, (**9c**; □): (0.95 ± 0.01) x 10^{-1} mM/min. (*Data recorded by A. Sever*)

The identification of **9c** was carried out by ^{1}H, ^{13}C, and ^{29}Si NMR spectroscopy after isolation of the compound from the photolysate by silica gel column

chromatography, using 100% hexanes as the eluent, followed by recrystallization from MeOH/$CHCl_3$.

The 600 MHz ^{1}H NMR spectrum of **9c** in $CDCl_3$ (Figure 3.18) integrates to a total of 10 H in the aromatic region and 28 H in the aliphatic region, which is also consistent with its proposed stoichiometry. The ^{1}H NMR chemical shift assignments, made with the aid of ^{1}H-^{13}C HSQC (see Figure S3.9), ^{1}H-^{13}C HMBC (see Figure S3.10), and homonuclear COSY NMR experiments, are listed in Table 3.8. ^{1}H-^{29}Si HMBC NMR spectrum was used to identify the proximate α-proton (H_f) of the adamantyl group to the Si atom at δ1.99 (see Figures S3.11). In addition to identifying the two quaternary carbons in the core 5-membered ring, ^{1}H-^{13}C HMBC was used to identify and distinguish the α-protons of the two adamantyl groups. The identification of the other protons was done using COSY NMR (see Figure S3.8).

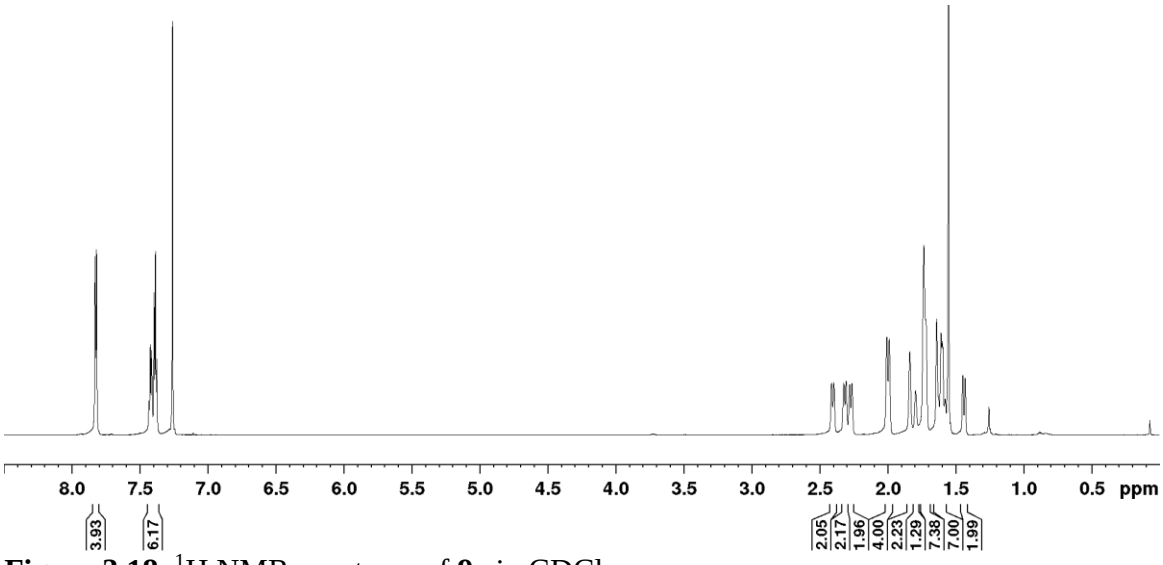

Figure 3.18. ^{1}H NMR spectrum of **9c** in $CDCl_3$.

Table 3.8. ^{1}H NMR chemical shift assignments for compound **9c**, recorded in $CDCl_3$ (Figure 3.18), refer to Figure 3.19 for structural assignments

Chemical Shift (ppm)	Assignment	Chemical Shift (ppm)	Assignment
1.43 (d)	H_a	2.26 (d)	H_g
1.59 (m)	H_b	2.31 (d)	H_h
1.72 (br)	H_c	2.40 (d)	H_i
1.79 (br)	H_d	7.40 (m)	H_j
1.84 (br)	H_e	7.81 (d)	H_k
1.99 (d)	H_f		

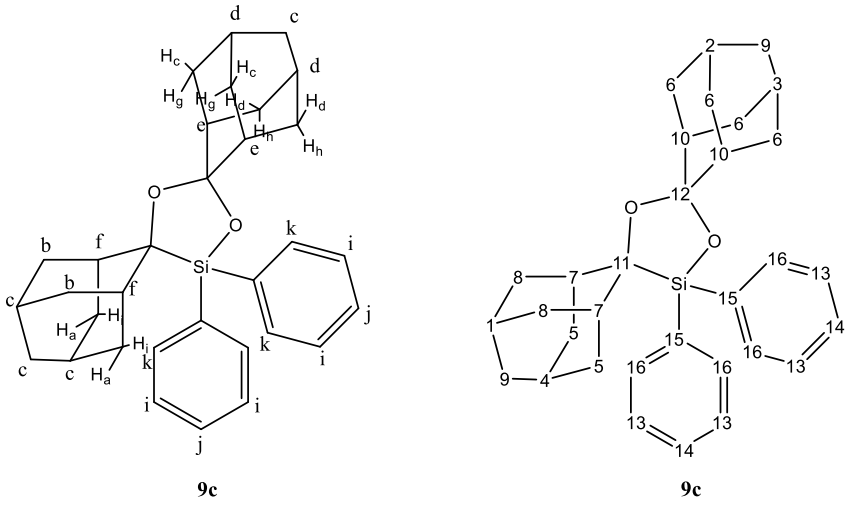

Figure 3.19. The proton (left) and carbon (right) assignments, used for Tables 3.7 and 3.8, for compound **9c**

The ^{13}C NMR assignments were made with the aid of 2D NMR experiments (^{1}H-^{13}C HSQC and HMBC). The DEPTQ ^{13}C NMR spectrum ($CDCl_3$, see Figure 3.20) of **9c** shows peaks from δ27.0 – 41.7 due to the secondary and tertiary carbons of the adamantyl substituents. The weak peaks at δ80.5 and 110.0 are assigned to the quaternary carbons within the core 5-membered ring C-11 and C-12, respectively. The four peaks in the δ128.0 – 135.4 region correspond to the carbons of the two equivalent phenyl substituents.

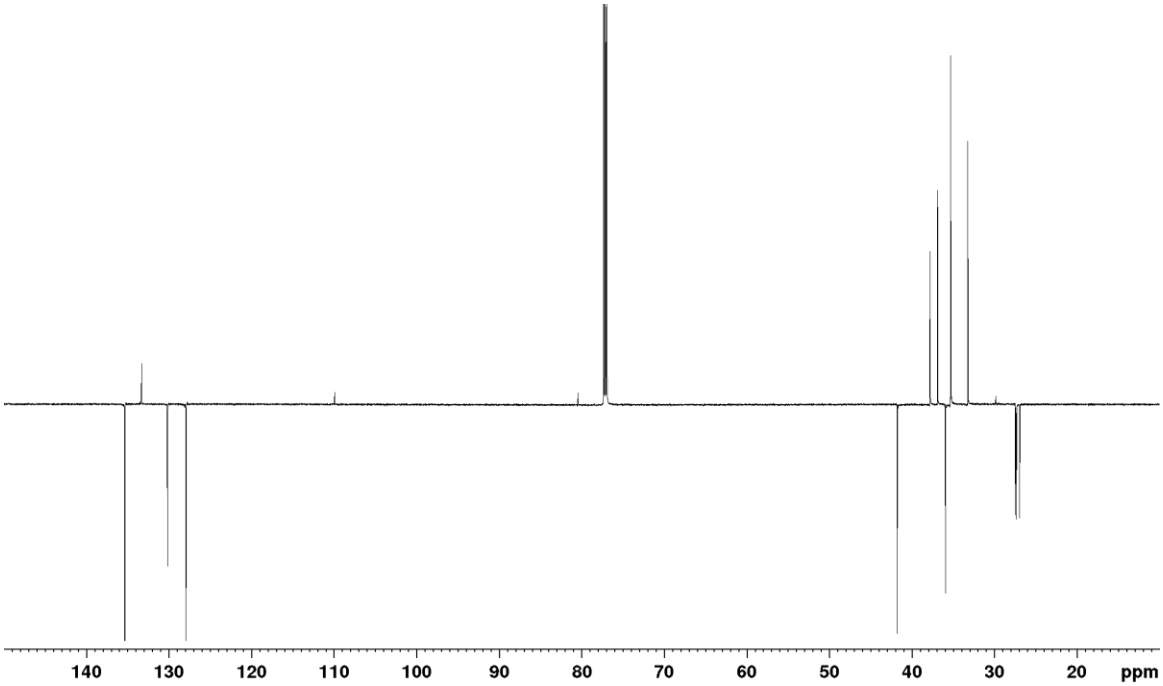

Figure 3.20. DEPTQ ^{13}C NMR spectrum of **9c** in $CDCl_3$ (-CH and -CH_3 groups are negatively phased and -C and -CH_2 groups are positively phased).

Table 3.9. ^{13}C NMR assignments for compound **9c**, determined in $CDCl_3$ (Figure 3.20), refer to Figure 3.19 for structural assignments

Chemical Shift (ppm)	Assignment	Chemical Shift (ppm)	Assignment
27.0	C-1	37.8	C-9
27.3	C-2	41.7	C-10
27.4	C-3	80.5	C-11
27.5	C-4	110.0	C-12
33.2	C-5	128.0	C-13
35.3	C-6	130.2	C-14
35.9	C-7	133.3	C-15
36.9	C-8	135.4	C-16

The complete assignment of the ^{13}C NMR spectrum of the molecule is shown in Table 3.9. The ^{29}Si chemical shift in **9c** was found to be δ 0.17 ppm (see Figure S3.11), which is consistent with compounds with alkoxy diphenyl-alkyl substitution at Si; for

example, the ^{29}Si chemical shift in bis(methyldiphenylsilyl)acetal (**15**) is at δ: -2.74 ppm in C_6D_6.[7]

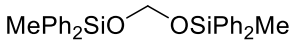

15

3.4.4. Reaction of $SiPh_2$ with 2,2,5,5-Tetramethylcyclopentanone (**8**)

Steady state photolysis of **2** (0.05 M) in the presence of **8** (0.12 M) in C_6D_{12} led to the formation of **14** (106 ± 5%) (eq. 3.7) and a collection of weak resonances in the alkyl and aryl regions of the NMR spectrum (Figure 3.21), that could not be assigned definitively. Figure 3.22 shows the concentration vs. time plots for **2**, **8**, and **14** in the experiment. The ketone was found to be consumed at only *ca.* 1/3rd the rate of **2** over an hour of irradiation. There is no evidence for the formation of resonances consistent with the formation of the corresponding oxasilirane.

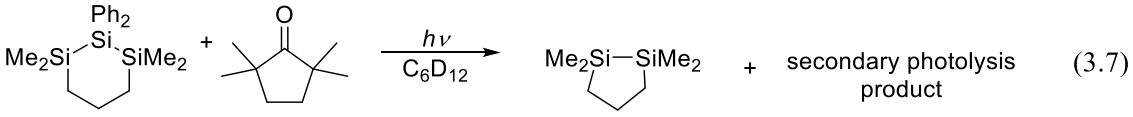

(3.7)

2 0.05 M

8 0.12 M

14 106 ± 5%

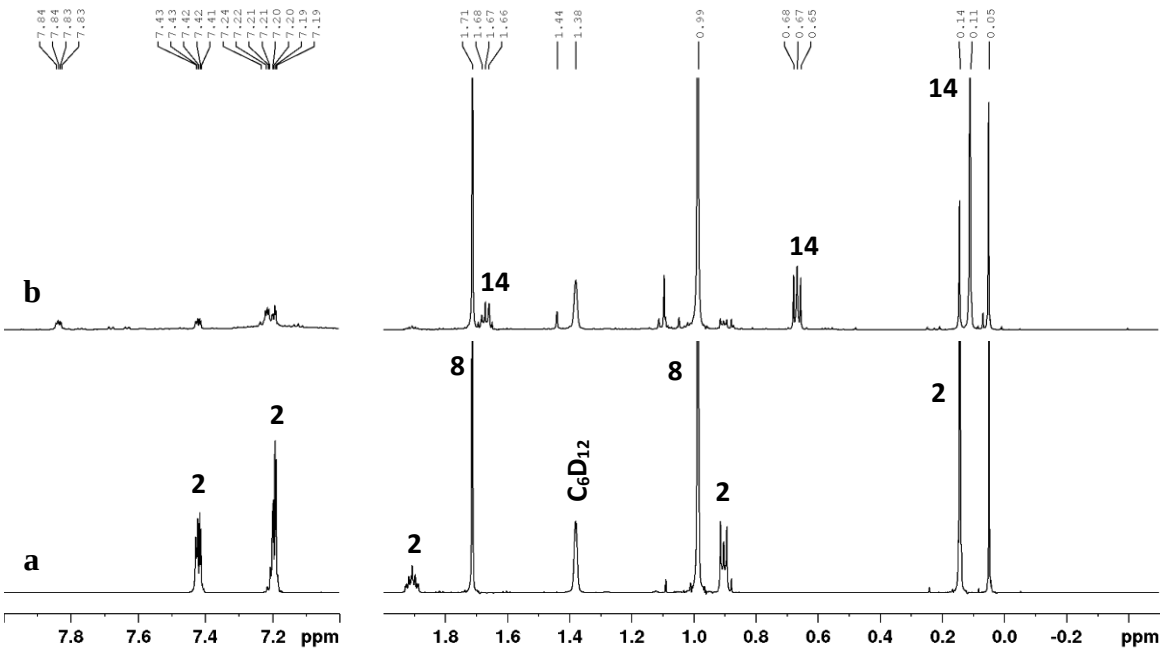

Figure 3.21. ^{1}H NMR spectra of a C_6D_{12} solution of 0.05 M **1**, 0.12 M of **8**, and 0.01 M hexamethyldisilane (a) before and (b) after 60 mins of photolysis (*ca.* 40% conversion of **1**).

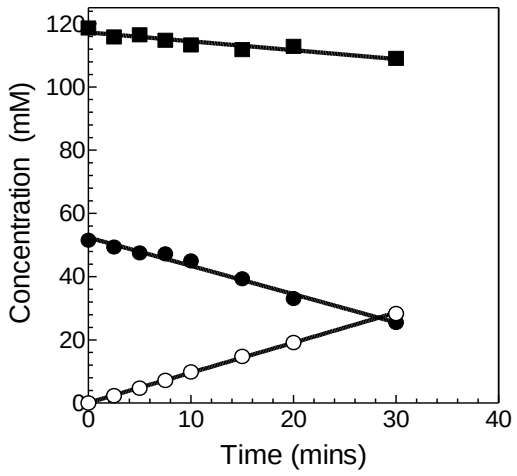

Figure 3.22. Concentration vs. time plots for the photolysis of **2** in the presence of 2,2,5,5-tetramethylcyclopentanone (**8**) in cyclohexane-d_{12}. Shown is the depletion of **2** (●) and **8** (■) and the formation of **14** (○) over time irradiated. Slopes are as follows: (**2**; ●): (-0.90 ± 0.01) mM/min, (**8**; ■): (-0.28 ± 0.01) mM/min, (**14**;○): (0.95 ± 0.01) mM/min.

Analogous results were obtained from photolysis of a 0.04 M solution of **2** in C_6D_{12} containing 0.10 M di-*tert*-butyl ketone (**6**); the ^{1}H NMR spectra of the photolyzed mixture showed the ketone to be consumed at *ca.* 10% to the rate of consumption of **2** and

showed no new resonances that could be assigned to the corresponding oxasilirane. Generation of $SiMe_2$ in the presence of **6** has also been reported not to lead to identifiable Si-containing products, which was proposed to be due to steric factors.[4]

3.5. Laser Flash Photolysis

Laser flash photolysis studies were performed on continuously flowing anhydrous deoxygenated hexanes solutions of **1** (*ca.* 4×10^{-4} M), **2** (*ca.* 6×10^{-5} M), or **3** (*ca.* 6×10^{-5} M) at 25°C using excitation from a 248 nm KrF excimer laser, as described in the previous chapter.

3.5.1. Reactions of Silylenes with 2-Adamantanone (**5**)

In the preliminary work, the addition of 2-adamantanone (**5**) to a hexanes solution of **1** led to the formation of a new transient intermediate that exhibited a broad UV-vis absorption band centered at $\lambda_{max} \approx 570$ nm (Figure 3.23a). This transient has been assigned to the $SiMe_2$-**5** silacarbonyl ylide, based on the similarity of the spectrum to those observed in the previous chapter for $SiMe_2$ in the presence of ketones such as camphor, norcamphor, and dicyclopropyl ketone.

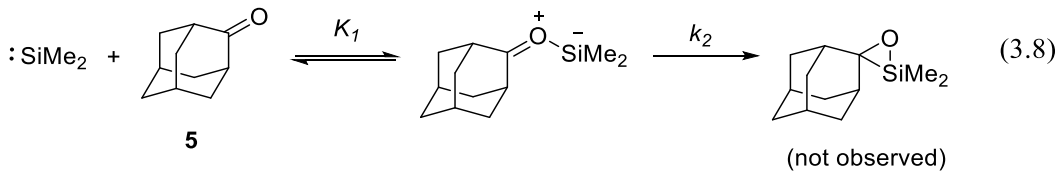

(3.8)

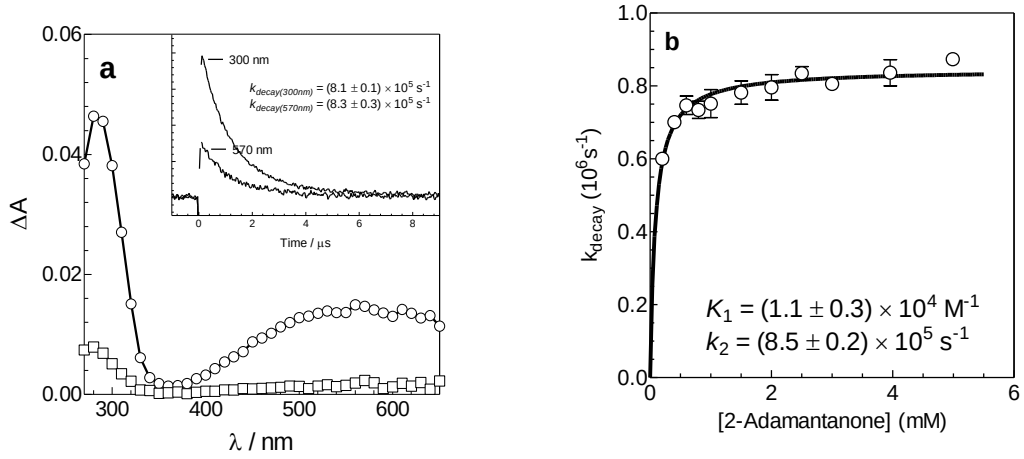

Figure 3.23. (a) Transient absorption spectra recorded 0.13 – 0.26 μs (○) and 1.66 – 1.86 μs (□) after the laser pulse by laser flash photolysis of **1** in the presence of 10 mM 2-adamantanone in deoxygenated hexanes at 25°C. The inset shows transient decay traces recorded at 300 and 570 nm. (b) Plot of k_{decay} vs ketone concentration (0 – 5mM) for the $SiMe_2$-**5** silacarbonyl ylide monitored at 600 nm. The solid line is the non-linear least-squares fit of the data to eq. 3.9.

Since the ylide exhibits a broad UV-vis absorption band that overlaps with the spectrum of the silylene, the kinetic analysis was done by monitoring the ylide at longer wavelengths where the silylene does not absorb. A plot of k_{decay} of the ylide (monitored at 600 nm) vs. ketone concentration is non-linear (Figure 3.23b), showing behavior similar to saturation kinetics over the 0 – 6 mM range in added ketone. The data were thus fit to eq. 3.9, where Q denotes the substrate, K_1 is the equilibrium constant for formation of the ylide, and k_2 is the first-order rate coefficient for the product formation from the silacarbonyl ylide (eq. 3.8). The non-linear least squares fit afforded values of K_1 = (1.1 ± 0.3) × 10^4 M^{-1} and k_2 = (8.5 ± 0.2) × 10^5 s^{-1} (R^2 = 0.865).

$$k_{decay} = \frac{k_2 K_1 [Q]}{1 + K_1 [Q]} \qquad (3.9)$$

However, reviewing the kinetic plot, it can be noted that k_{decay} may not in fact plateau at high concentrations, but rather increase gently with increasing concentration above 1 mM. Such behavior was not observed in the reactions with enolizable carbonyl compounds (see Chapter 2). The kinetic analysis was therefore extended to higher concentrations in order to investigate this possibility further.

Addition of higher concentrations of **5** to a solution of **1** led to systematic shortening of the silacarbonyl ylide lifetime. A plot of k_{decay} at 600nm vs. ketone concentration exhibited a linear correlation at higher concentrations (*ca.* 10 – 60 mM; see Figure 3.24). A potential interpretation of this behavior is that the silacarbonyl ylide reacts with a second molecule of ketone to afford the corresponding dioxasilacyclopentane, the reported product of the reaction of $SiMe_2$ with **5** (eq. 3.10).[4] The dependence of k_{decay} of the ylide on [**5**] can potentially be expressed as in eq. 3.11, where k_3 is the rate constant for the [2+3] cycloaddition of the ylide with a second molecule of ketone and k_2 is the rate coefficient of the unimolecular ring closure. Linear least-square analysis of the data of Figure 3.24 according to eq. 3.11 afforded the rate coefficients $k_3 = (1.5 \pm 0.1) \times 10^7\ M^{-1}s^{-1}$ and $k_2 = (6.3 \pm 0.4) \times 10^5\ s^{-1}$.

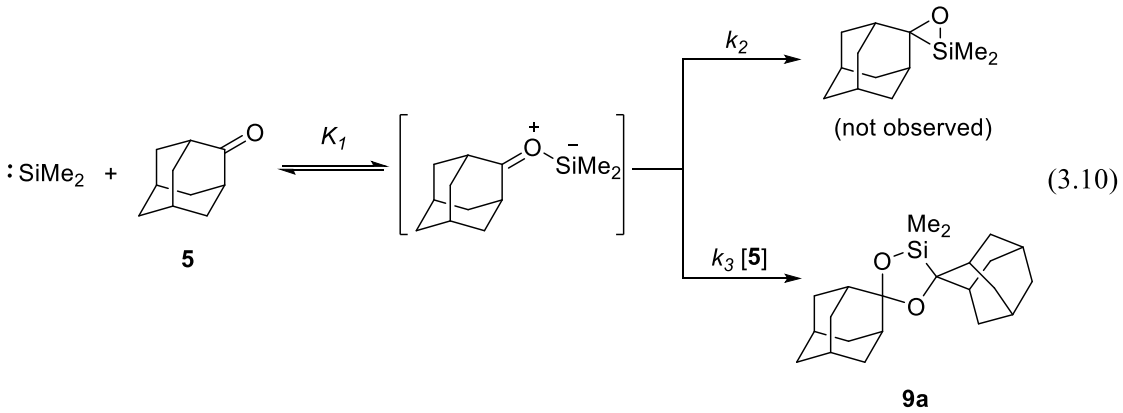

(3.10)

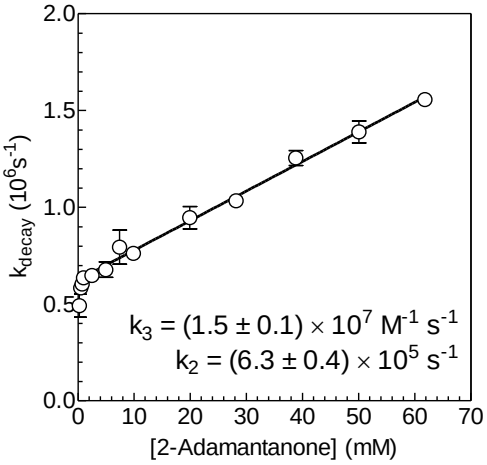

Figure 3.24. Plot of k_{decay} vs ketone concentration for the $SiMe_2$-**5** silacarbonyl ylide monitored at 600 nm. The solid line is the linear least-squares regression of the data according to eq. 3.11.

$$k_{decay} = k_3[Q] + k_2 \qquad (3.11)$$

Addition of **5** to a hexanes solution of **2** led to the formation of a new transient intermediate that exhibited a broad UV-vis absorption band centered at λ_{max} = 530 nm, which can be assigned to the corresponding silacarbonyl ylide (Figure 3.25a). The plot of k_{decay} (monitored at 600 nm) vs. ketone concentration over the 0 – 5 mM range in added **5** was force-fit to the saturation kinetics expression of eq. 3.9, as shown in Figure 3.25b. However, as observed for $SiMe_2$ in the presence of **5**, there appears to be a gentle increase in k_{decay} with increasing ketone concentration, which might be attributed to the silacarbonyl ylide reacting with a second molecule of **5** to afford the corresponding dioxasilacyclopentane (**9c**), the product that was actually observed upon lamp photolysis of **2** in the presence of 0.11 M **5** (Section 3.4.3).

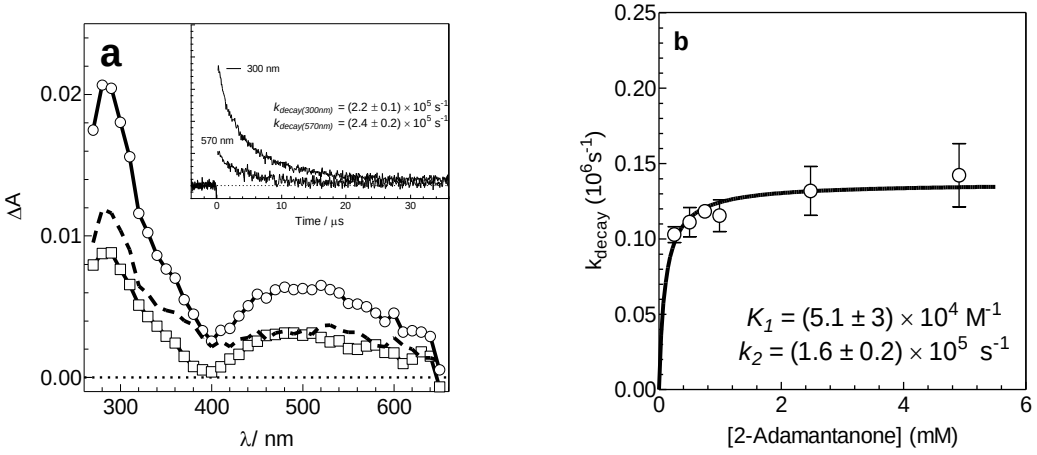

Figure 3.25. (a) Transient absorption spectra recorded 0.19 – 0.32 μs (○) and 3.65 – 4.03 μs (□) after the laser pulse by laser flash photolysis of **2** in the presence of 5 mM 2-adamantanone in deoxygenated hexanes at 25°C. The dashed line spectrum (-) shows the difference between the two spectra. The inset shows transient decay traces recorded at 300 and 570 nm. (b) Plot of k_{decay} vs ketone concentration (0 – 5mM) for the $SiPh_2$-**5** silacarbonyl ylide monitored at 600 nm. The solid line is the non-linear least-squares fit of the data to eq. 3.9.

Further addition of up to *ca.* 60 mM **5** led to further shortening of the silacarbonyl ylide lifetime. The plot of k_{decay} vs. [**5**] over the full range of ketone concentration is linear, as shown in Figure 3.26. Least squares analysis according to eq. 3.11 afforded the rate coefficients $k_3 = (7.9 \pm 0.3) \times 10^6$ $M^{-1}s^{-1}$ and $k_2 = (1.1 \pm 0.1) \times 10^5$ s^{-1}.

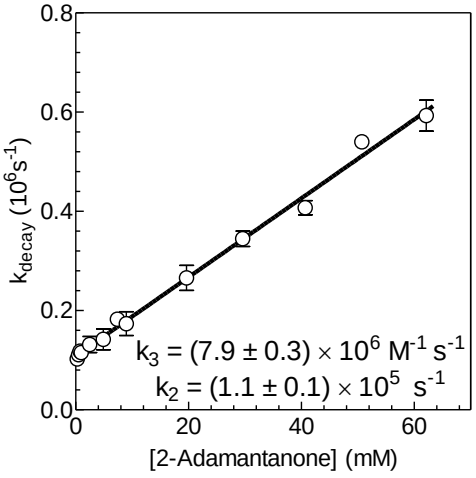

Figure 3.26. Plot of k_{decay} vs ketone concentration for the $SiPh_2$-**5** silacarbonyl ylide monitored at 600 nm. The solid line is the linear least-squares regression of the data according to eq. 3.11.

Addition of **5** to a hexanes solution of **3** also led to the formation of a new transient intermediate, which exhibited a broad UV-vis absorption band centered at λ_{max} = 640 nm (Figure 3.27a) that can be assigned to the corresponding silacarbonyl ylide. Interestingly, this is the only example of a detectable $SiMes_2$-derived silacarbonyl ylide that we have been able to observe. At low concentrations (0 – 5 mM), the plot of k_{decay} at 650 nm vs. ketone concentration is non-linear, and analysis according to eq. 3.9 afforded $K_1 = (1.0 \pm 0.2) \times 10^3$ M^{-1} and $k_2 = (3.5 \pm 0.3) \times 10^5$ s^{-1} (Figure 3.27b). Continued addition of **5** up to *ca.* 80 mM again revealed a linear dependence of k_{decay} on concentration, as shown in Figure 3.28. Linear least squares analysis of the data over the 10 – 80 mM concentration range according to eq. 3.11 afforded the rate coefficients $k_3 = (1.4 \pm 0.1) \times 10^7$ $M^{-1}s^{-1}$ and $k_2 = (3.9 \pm 0.4) \times 10^5$ s^{-1}.

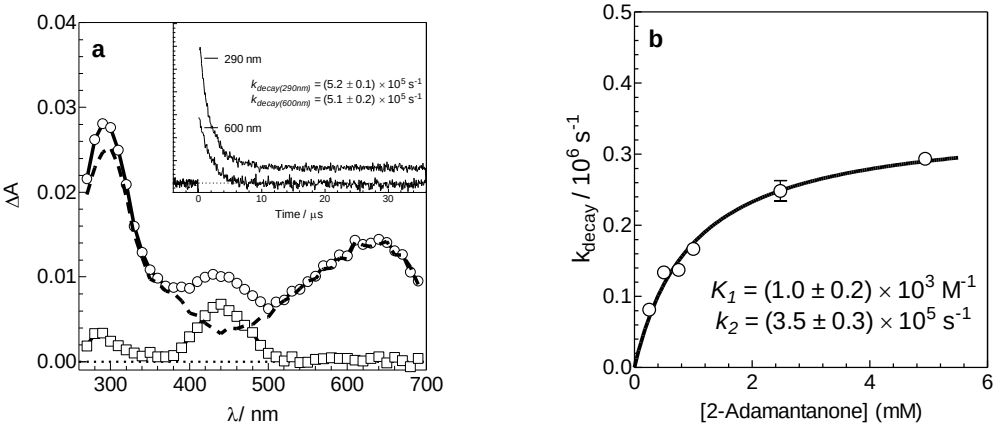

Figure 3.27. (a) Transient absorption spectra recorded 0.26 – 0.51 μs (○) and 28.0 – 28.3 μs (□) after the laser pulse by laser flash photolysis of **3** in the presence of 5 mM 2-adamantanone in deoxygenated hexanes at 25°C. The dashed line spectrum (-) shows the difference between the two spectra. The inset shows transient decay traces recorded at 290 and 600 nm. (b) Plot of k_{decay} vs ketone concentration (0 – 5 mM) for the $SiMes_2$-**5** silacarbonyl ylide monitored at 650 nm. The solid line is the linear least-squares analysis of the data according to eq. 3.9.

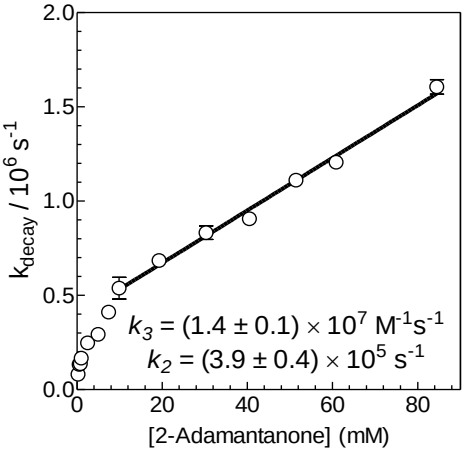

Figure 3.28. Plot of k_{decay} vs ketone concentration (10 – 80 mM) for the $SiMes_2$-**5** silacarbonyl ylide monitored at 650 nm. The solid line is the linear least-squares analysis of the data according to eq. 3.11.

3.5.2. Reactions of Silylenes with 2,2,5,5-Tetramethylcyclopentanone (**8**)

Addition of 2,2,5,5-tetramethylcyclopentanone (**8**) to a hexanes solution of **3** led to a shortening of the silylene lifetime and change to pseudo-first order decay kinetics, and suppression of the formation of the corresponding disilene. A plot of k_{decay} (monitored at 580 nm) vs. ketone concentration is linear with a slope of k_Q = (3.1 ± 0.2) × 10^7 $M^{-1}s^{-1}$ (Figure 3.29b). A transient UV-vis spectrum recorded in hexanes solution containing 10 mM of ketone showed only absorptions attributable to $SiMes_2$ (Figure 3.29a). The reaction proceeds to generate **12**, as shown by the results of steady state photolysis of **3** in the presence of **8** (Sect. 3.4.1. eq. 3.12). The fact that the ylide is undetectable suggests that the ylide is a steady state intermediate in this case, and therefore the absolute second order rate constant is approximately equal to the product of the pre-equilibrium and forward rate constants for the two steps in the mechanism, $k_Q \approx K_1 k_2$).

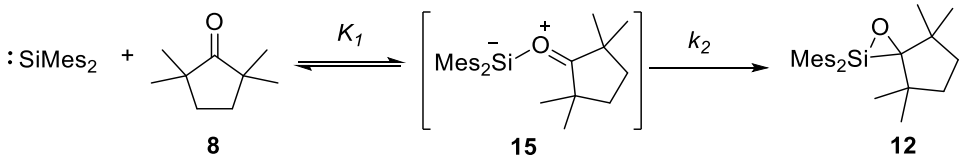

(3.12)

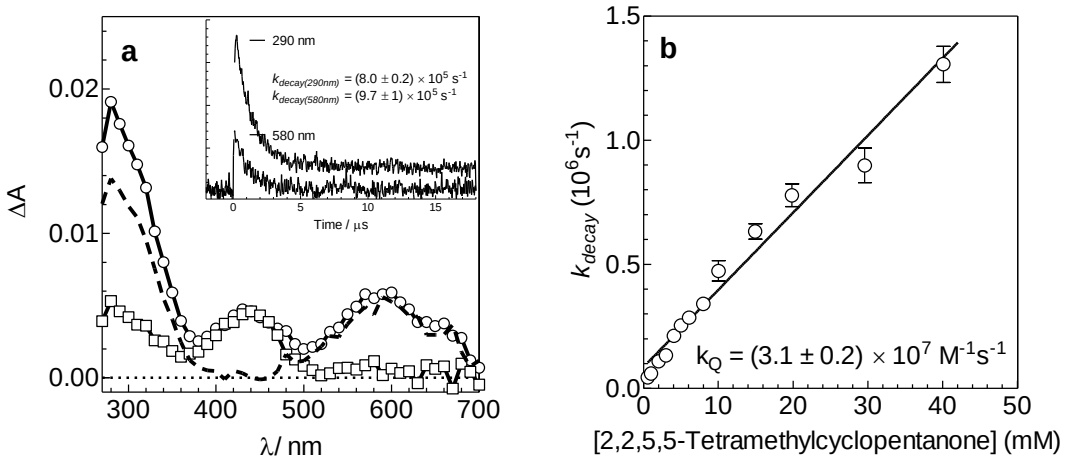

Figure 3.29. (a) Transient absorption spectra recorded 0.22 - 0.35 μs (○) and 2.8 - 2.9 μs (□) after the laser pulse from laser flash photolysis of **3** in the presence of 10 mM 2,2,5,5-tetramethylcyclopentanone in deoxygenated hexanes at 25°C. The dashed line spectrum (-) shows the difference between the spectra recorded at 0.22 – 0.35 and 2.8–2.9 μs after the laser pulse; the inset shows transient decay traces at 290 and 580 nm. (b) Plot of k_{decay} vs ketone concentration for $SiMes_2$, monitored at 580nm. The solid line is the linear least-squares fit of the data to eq. 3.1.

In contrast to the behavior of $SiMes_2$ in the presence of **8**, laser flash photolysis of hexanes solutions of $SiMe_2$ precursor **1** in the presence of this ketone led to the appearance of a new transient species exhibiting a broad UV-vis absorption band centred at $\lambda_{max} \approx 640$ nm, which could be detected at ketone concentrations as low as 0.2 mM. Figure 3.30a shows a transient spectrum recorded in a hexanes solution of **1** containing 10 mM ketone.

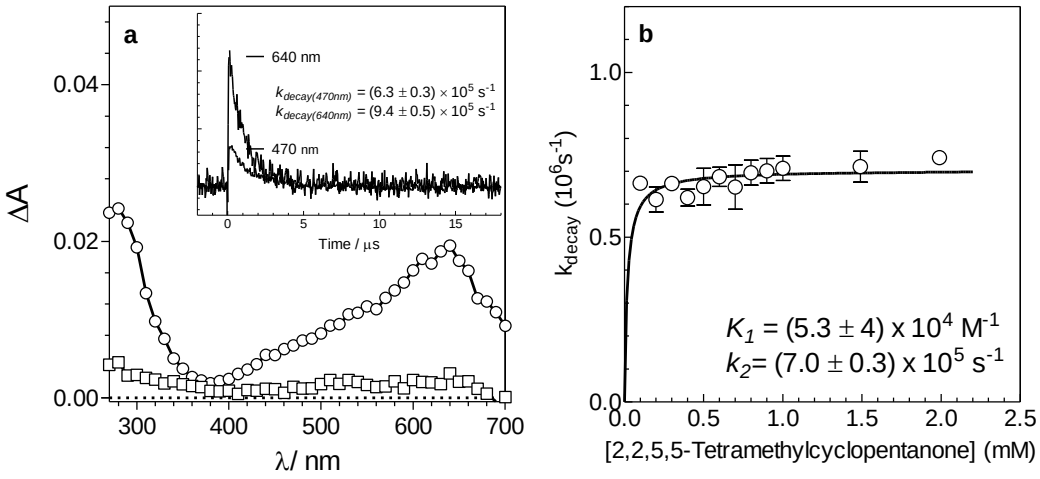

Figure 3.30. (a) Transient absorption spectra recorded 0.22 - 0.35 μs (○) and 2.8 - 2.9 μs (□) after the laser pulse by laser flash photolysis of $SiMe_2$ precursor **1** in the presence of 10 mM 2,2,5,5-tetramethylcyclopentanone in deoxygenated hexanes at 25°C. The inset shows transient decay traces at 470 and 640 nm. (b) Plot of the average first-order decay rate coefficient of the 470 and 640 nm transient absorptions vs. ketone concentration (0 – 2mM). The solid line is the non-linear least-squares fit of the data to eq. 3.9.

Transient decays recorded at 470 and 600 nm in the presence of **8** were approximated equal to each other and appeared to be independent of concentration. A plot of the decay rate coefficients (monitored at 470 and 600 nm) vs. ketone concentration over the 0 – 2 mM range in added **8** is shown in Figure 3.30b. The non-linear least squares fit of the averages of the k_{decay} values at 470 and 600 nm to the saturation expression of eq. 3.9 affords the equilibrium and rate constants $K_1 = (5.3 \pm 4) \times 10^4$ M^{-1} and $k_2 = (7.0 \pm 0.3) \times 10^5$ s^{-1}.

The experiment was repeated in order to monitor the lifetime of the $SiMe_2$-**8** silacarbonyl ylide (λ_{max} = 600 nm) at higher ketone concentrations, using the same sample of **8** as used in the previous experiment. A plot of k_{decay} for the silacarbonyl ylide vs. ketone concentration exhibited a linear correlation at higher concentration (*ca.* 10 – 60

mM). The linear least-square analysis of the data according to eq. 3.11 afforded the average rate coefficients, monitored at 470 and 600 nm, $k_3 = (4.1 \pm 0.2) \times 10^7$ $M^{-1}s^{-1}$ and $k_2 = (8.5 \pm 0.5) \times 10^5$ s^{-1} (Figure 3.31), as defined in eq. 3.13.

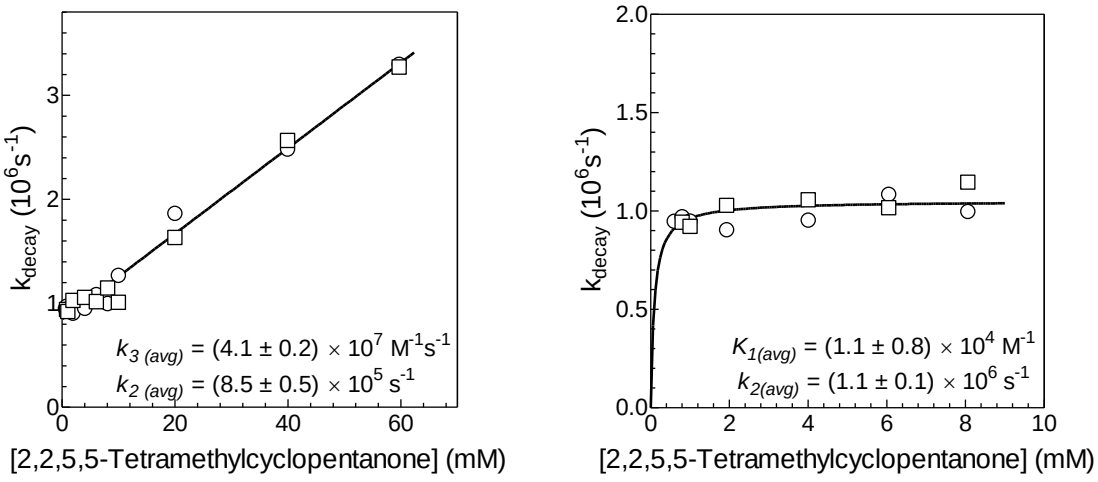

Figure 3.31. (a) Plot of k_{decay} vs ketone concentration of $SiMe_2$ and $SiMe_2$-**8** ylide monitored at 470 (○) and 600 (□) nm over the 10 – 60 mM concentration range. The solid line is the linear least-squares analysis of the data, by analyzing the 470 and 600 nm data sets as a single data set, to eq. 3.11. (b) Expanded plot of the data of (a) over the 0 – 10 mM concentration range. The solid line is the non-linear least squares regression of the data, by analyzing the 470 and 600 nm data sets as a single data set, to eq. 3.9.

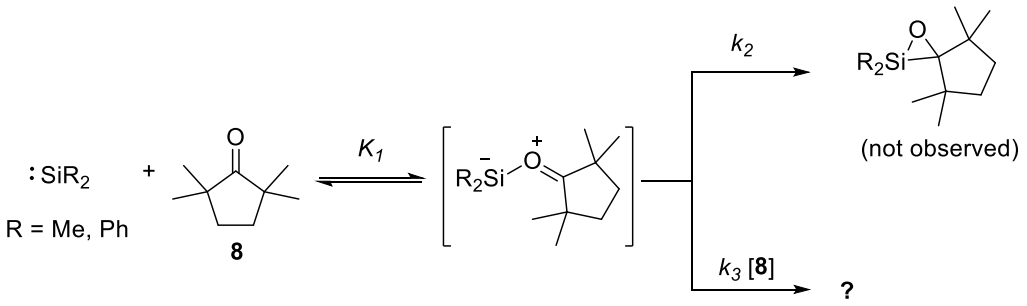

(3.13)

Addition of 2,2,5,5-tetramethylcyclopentanone (**8**) to a hexanes solution of **2** also led to the formation of a new transient intermediate, which exhibited a broad UV-vis absorption band centered at λ_{max} = 520 nm (Figure 3.32a), assignable to the corresponding

silacarbonyl ylide. A plot of k_{decay} (monitored at 600 nm) vs. ketone concentration over the 0 – 2 mM concentration range fit to the saturation kinetics expression of eq. 3.9, affording the equilibrium and rate coefficients $K_1 = (2 \pm 1) \times 10^4$ M^{-1} and $k_2 = (1.3 \pm 0.1) \times 10^5$ s^{-1}, respectively (Figure 3.32b).

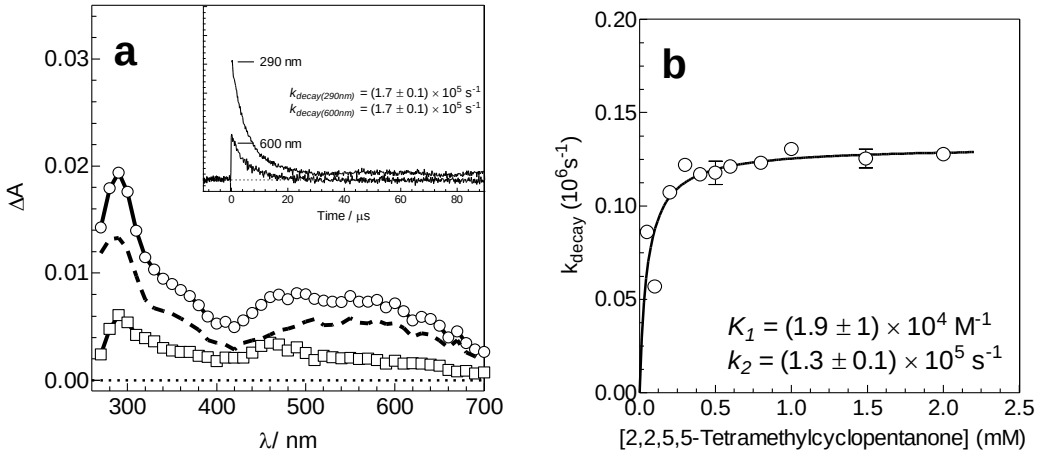

Figure 3.32. (a) Transient absorption spectra recorded 0.16 – 0.80 μs (○) and 2.78 – 2.94 μs (□) after laser pulse by laser flash photolysis of **2** in the presence of 10 mM 2,2,5,5-tetramethylcyclopentanone in deoxygenated hexanes at 25°C. The dashed line spectrum (-) shows the difference between the two spectra. The inset shows transient decay traces recorded at 290 and 600 nm. (b) Plot of k_{decay} vs ketone concentration for the $SiPh_2$-**8** silacarbonyl ylide monitored at 600 nm. The solid line is the non-linear least-squares fit of the data to eq. 3.9.

As observed earlier with the other systems, addition of higher concentrations of **8** revealed a gentle linear dependence of k_{decay} on ketone concentration. The plot of k_{decay} for the silacarbonyl ylide vs. ketone concentration (Figure 3.33) over the 10 – 60 mM range was linear and linear least squares regression according to eq. 3.11 afforded the rate coefficients $k_3 = (2.5 \pm 0.2) \times 10^7$ $M^{-1}s^{-1}$ and $k_2 = (3.2 \pm 0.1) \times 10^5$ s^{-1} (Figure 3.33).

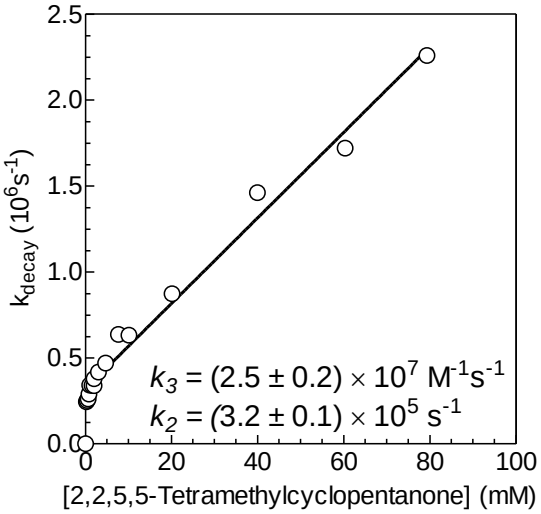

Figure 3.33. Plot of k_{decay} vs ketone concentration for the $SiPh_2$-**8** silacarbonyl ylide monitored at 600 nm. The solid line is the linear least-squares regression of the data to eq. 3.11.

Both the $SiMe_2$ and $SiPh_2$-**8** systems thus exhibit concentration dependent decay kinetics similar to that observed with 2-adamantanone (**5**), where the final isolated products were the corresponding dioxasilacyclopentane derivatives (**9a-c**), in spite of the fact that no stable silylene-ketone adducts could be detected in steady state photolysis experiments in either case. Therefore, it is not really clear how the kinetic results for these systems should be interpreted.

Flash photolysis experiments in which $SiMe_2$ and $SiMes_2$ were generated in the presence of di-*tert*-butyl ketone (**6**) gave results similar to those obtained with **8** and are shown in the Supporting Information (see Figures S3.12-S3.14).

On the other hand, the behavior of $SiPh_2$ in the presence of **6** was different than that observed in the presence of **8**, in that in this case new transient absorptions assignable to the corresponding ylide were detected. Figure 3.34a shows a transient spectrum recorded in hexanes containing 5 mM of ketone, which is interpreted as the sum of the spectra of both the silylene and the ylide in equilibrium with each other. The absorption

due to the ylide was monitored at 600 nm as a function of ketone concentration and found to decay with first order kinetics over the 0.1 – 60 mM range. A plot of k_{decay} vs. ketone concentration (Figure 3.34b) exhibited curvature consistent with saturation kinetics. Analysis of the data according to eq. 3.11 afforded the equilibrium and rate constants K_1 = (3.2 ± 0.6) × 10^2 M^{-1} and k_2 = (2.6 ± 0.1) × 10^6 s^{-1} (Figure 3.34b). The kinetic behavior of the ylide observed at higher ketone concentration is unusual as the other $SiPh_2$ systems displayed a linear dependence of the ylide k_{decay} values with ketone concentration.

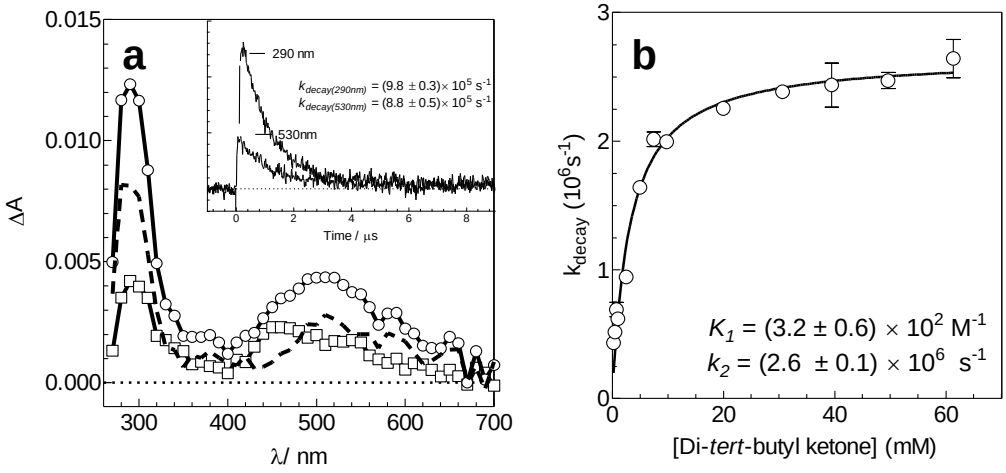

Figure 3.34. (a) Transient absorption spectra recorded 0.16 – 0.22 μs (○) and 1.39 – 1.47 μs (□) after laser pulse by laser flash photolysis of **2** in the presence of 5 mM di-*tert*-butyl ketone in deoxygenated hexanes at 25°C. The dashed line spectrum (-) shows the difference between the two spectra. The inset shows transient decay traces recorded at 290 and 530 nm with k_{decay} values of (9.8 ± 0.2) × 10^5 and (8.8 ± 0.5) × 10^5 s^{-1}, respectively. (b) Plot of k_{decay} vs ketone concentration for the $SiPh_2$-**6** silacarbonyl ylide monitored at 600 nm. The solid line is the linear least-squares fit of the data to eq. 3.11.

The preceding experiment thus lead to plots of ylide k_{decay} values vs. ketone concentration are linear at higher concentration in all cases except for the $SiPh_2$-**6** system. Our initial interpretation of this linear dependence was that it was likely due to [2+3]

cycloaddition of the silacarbonyl ylide with a second molecule of ketone to afford the corresponding dioxasilacyclopentane, on the basis of what is known for the reactions of $SiMe_2$, $SiPh_2$, and $SiMes_2$ with 2-adamantanone. However, generation of $SiMe_2$ and $SiPh_2$ in the presence of **8** and **6** does not lead to the formation of identifiable products of any sort, while with $SiMes_2$, the corresponding oxasilirane appears to be formed exclusively, although in low yield. This raises questions as to whether the kinetic analysis we used is really appropriate. One possible complication of the results is that ketones such as **6** and **8** are themselves quite reactive photochemically, and yield products derived from alkyl radicals or biradicals.[8] For example, photolysis of 2,2,5,5-tetramethylcyclopentanone (**8**) using 300 nm light is known to lead to Norrish Type I cleavage, affording 2,2,5-trimethyl-4-hexenal (**16**) as the major product (eq. 3.14).[8] We thus decided to characterize the photochemistry of **6** and **8** under conditions close to those employed in our experiments.

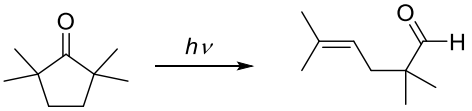

16 (3.14)

Steady state photolysis (254 nm) of a 0.045 M solution of **8** in C_6D_{12} solution led to *ca.* 10% consumption of the ketone over a time period of 60 mins. There are new resonances formed, which have been tentatively assigned to 2,2,5-trimethyl-4-hexenal (**16**) based on the characteristic resonances at δ 5.06 and 9.38 due to the vinylic and aldehyde protons, respectively (Figure 3.35). The concentration vs. time plots are shown in the Supporting Information (Figure S3.16) and afford a chemical yield of **16** is 64 ± 10%.

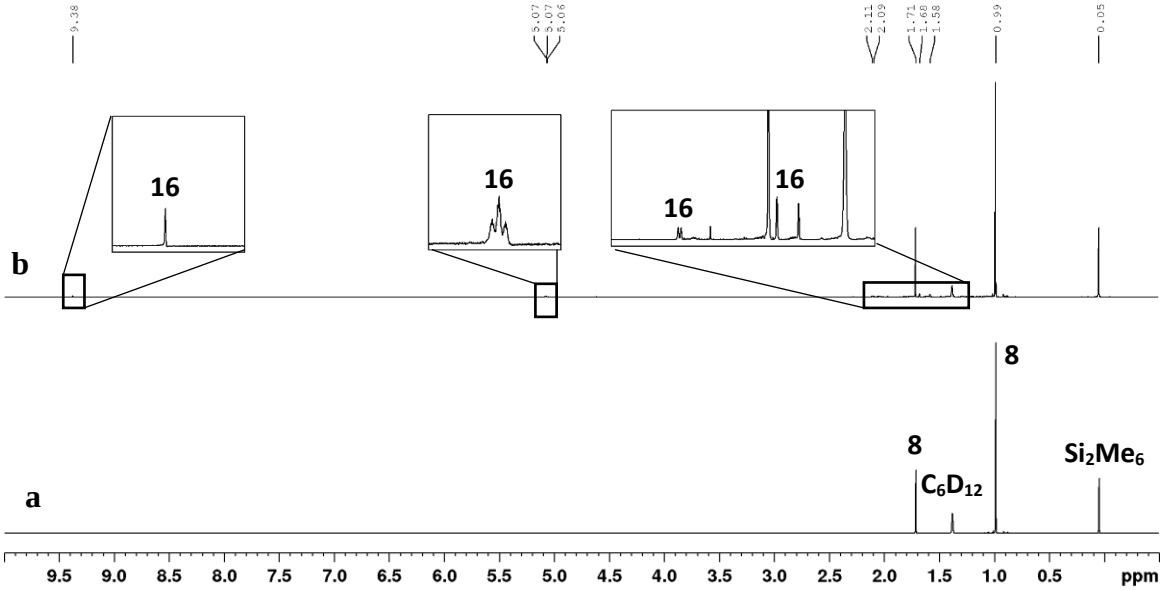

Figure 3.35. ^{1}H NMR spectra of a C_6D_{12} solution containing 0.045 M 2,2,5,5-tetramethylcyclopentanone (**8**) and 0.01 M hexamethyldisilane (a) before and (b) after 60 mins of photolysis.

In the steady state experiments of $SiMe_2$ and $SiPh_2$ with 2,2,5,5-tetramethylcyclopentanone, there is no evidence for the formation of **16** in yields greater than 1% as there is a lack of the vinylic and aldehyde proton. Alternatively, the lack of formation of **16** could be that it is readily reacting with the silylene, forming the corresponding silacarbonyl ylide, followed by a 1,3-dipolar cycloaddition[9], which would generate the corresponding bicyclo[3.2.0]oxasilacycloheptane (**17**, eq. 3.15), but the integrations of the new resonances in the aliphatic region, in particular the alkyl groups (-CH, -CH_2, and -CH_3), do not support the formation of such species.

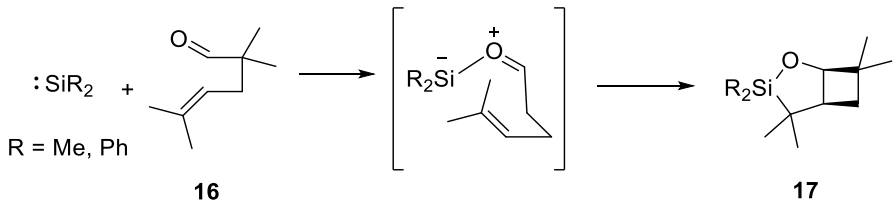

(3.15)

Furthermore, the extinction coefficients of the silylene precursors **1** ($\varepsilon_{254} \approx 1500$ cm^{-1} M^{-1}) and **2** ($\varepsilon_{254} \approx 15{,}000$ cm^{-1} M^{-1}) are at least three order of magnitudes larger than the extinction coefficient of the ketone ($\varepsilon_{254} \approx 5$ cm^{-1} M^{-1}). In terms of the steady state experiments, the relative absorbances of **1** and **2** (*ca.* 0.05 M) with ketone (*ca.* 0.10 M) are *ca.* 150 and 1500, respectively. On the other hand, in the laser experiments, the relative absorbances of **1** (*ca.* 4×10^{-4} M) and **2** (*ca.* 6×10^{-5} M) with ketone (up to *ca.* 0.60 M) are *ca.* 2 and 3, respectively, which the ketone will likely compete for the light.

Flash photolysis of a flowed, deoxygenated hexanes solution containing 0.04 M of 2,2,5,5-tetramethylcyclopentanone ($A_{248} = 0.6142$) exhibits a very weak transient absorption band below *ca.* 300 nm in the 2 μs timescale, as shown in Figure 3.36. A definite assignment could not be made for this transient. This transient could affect the kinetic results obtained from the kinetic studies, as it is short-lived and could react with the ylide. Overall, the co-photolysis of the ketone cannot be ruled out as a cause to the linear dependence of the ylide k_{decay} values on ketone concentration.

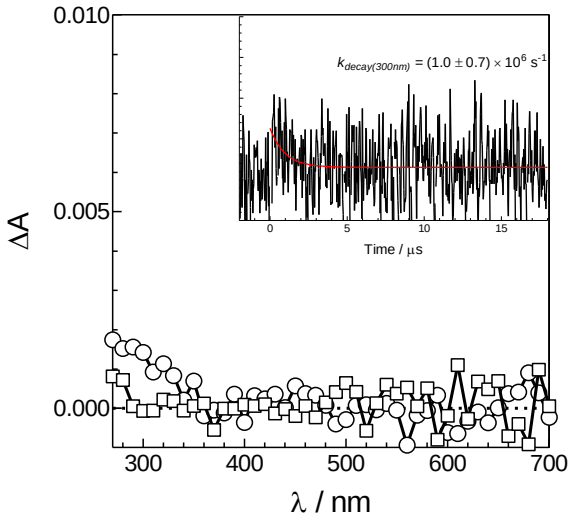

Figure 3.36. Transient absorption spectra recorded 0.22 – 0.35 μs (○) and 2.78 – 2.94 μs (□) after laser pulse by laser flash photolysis of 40 mM 2,2,5,5-tetramethylcyclopentanone in deoxygenated hexanes at 25°C. The inset shows transient decay traces at 300 nm.

Another possible reason for the linear dependence of the ylide decay coefficients (k_{decay}) on ketone concentration is quenching of the ylide by impurities in the sample of ketone. If the impurity reacts with the silylene or the ylide at close to the diffusion-controlled rate ($k_{diff} \approx 2 \times 10^{10}$ $M^{-1}s^{-1}$), then a concentration of only 1 mM could lead to k_{decay} values in the range of 10^6 s^{-1}. This corresponds to a relative concentration of 2% in the sample of ketone, used in the experiments. The difficulty with working with the synthesized ketone is that a large quantity of material is required (*ca.* 1g per flash photolysis experiment). As a result, the ketone **8** was purified further to resolve the possibility of impurity quenching found in the kinetic studies.

The ketone was synthesized and purified by the same procedure as before and was then further purified by column chromatography followed by vacuum distillation. The static UV-vis absorption and ^{1}H NMR spectra of the more extensively purified sample of the ketone are shown in Figure 3.37 and Figure S3.15, respectively. The spectra show that while the purification procedure was successful in removing some impurities that were present in the initial sample, a new impurity absorbing at 248 nm has evidently been introduced. The measured extinction coefficient of the purified ketone sample is $\varepsilon_{248} = 15$ cm^{-1} M^{-1}, while that of the ketone sample used in the previous experiments was $\varepsilon_{248} = 3$ cm^{-1} M^{-1}.

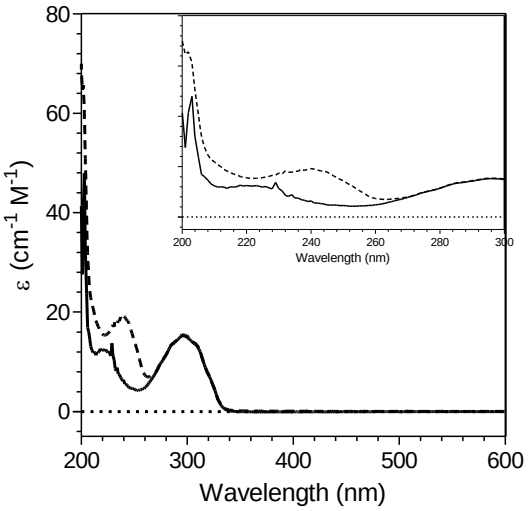

Figure 3.37. Plot of extinction coefficients vs. wavelength of the synthesized 2,2,5,5-tetramethylcyclopentanone. The solid line (—) is the synthesized ketone used for the experiments mentioned above (Figures 3.29 – 3.33), while the dashed line (---) is the ketone used for the experiment below (Figure 3.38). The inset shows the same plot zoomed in the 200 – 300 nm range.

Flash photolysis of **1** in the presence of the additionally purified sample of **8** in hexanes solution led to the prompt formation of the corresponding silacarbonyl ylide as observed in the earlier experiments and similar results to those obtained with the original sample. As before, the plot of k_{decay} vs. ketone concentration of the silylene and silacarbonyl ylide (monitored at 470 and 640 nm) exhibited a linear correlation at higher concentration (*ca.* 10 – 60 mM), linear least-squares regression of which according to eq. 3.11 afforded the coefficients $k_3 = (2.1 \pm 0.3) \times 10^7$ $M^{-1}s^{-1}$ and $k_2 = (1.1 \pm 0.1) \times 10^6$ s^{-1} (obtained from the average of the 470 and 640 decay traces) (Figure 3.38a). The results indicate that additional "purification" of the ketone had little effect on the kinetic results above 10 mM **8** (Figure 3.31). Similarly, there is little effect at lower concentrations (<10 mM), which the plot has been fitted to saturation kinetic behavior expressed to eq. 3.9 affording $K_1 = (4.6 \pm 0.2) \times 10^4$ M^{-1} and $k_2 = (1.2 \pm 0.1) \times 10^6$ s^{-1} (Figure 3.38b). As a

result, it cannot be concluded whether impurity quenching was involved in these kinetic analyses.

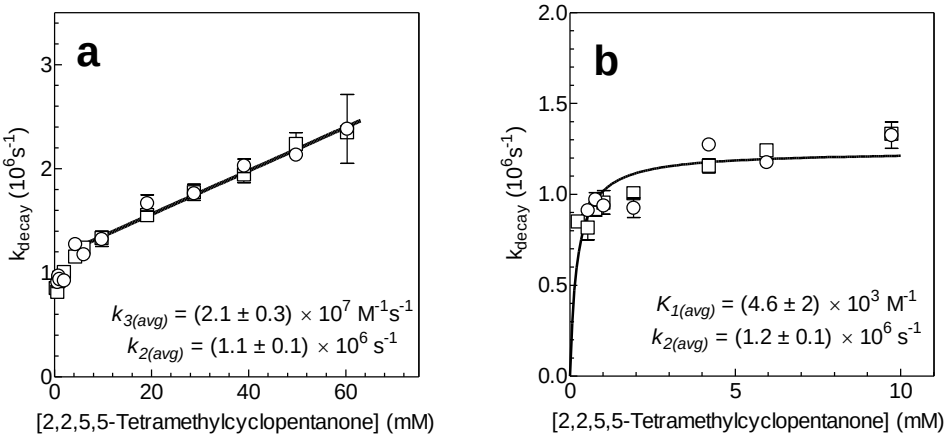

Figure 3.38. Plots of k_{decay} vs ketone concentration of $SiMe_2$ and $SiMe_2$-**8** ylide monitored at 470 (○) and 640 (□) nm. (a) The solid line is the average linear least-squares fit of the data to eq. 3.11 over the 0 – 60 mM ketone concentration range. (b) The same plot zoomed in the 0 – 10 mM ketone concentration range. The solid line is the non-linear least-squares analysis of the data, by analyzing the 470 and 600 nm data sets as a single data set, to eq. 3.9.

3.6. Laser Flash Photolysis of Oxasilirane (10)

3.6.1. Laser Flash Photolysis of Oxasilirane (**10**)

The reaction of $SiMes_2$ with 1,1,3,3-tetramethyl-2-indanone (**7**) in low temperature matrixes has been shown to afford the corresponding silacarbonyl ylide, the decay of which is thought to yield oxasilacyclopropane **10**.[6] It was also shown that photolysis of **10** in the matrix regenerate the corresponding ylide (eq. 3.16).[1] We were interested in characterizing the photolysis of **10** in solution, to determine whether we can detect the silacarbonyl ylide under ambient conditions.

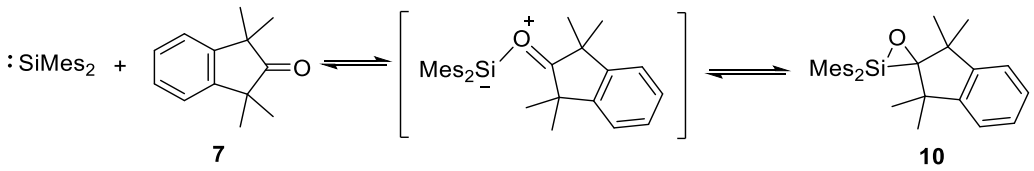

(3.16)

Flash photolysis of **10** (1.3×10^{-5} M^{-1}) in flowed deoxygenated hexanes led to the formation of two UV-vis absorption bands centered at 420 and 580 nm. As time progresses, the absorption band at 580 nm decays, with 2nd-order kinetics, with the concurrent growth of the 420 nm absorption; see Figure 3.39. The spectra are consistent with the formation of $SiMes_2$ (λ_{max} = 580 nm) and its subsequent dimerization to form tetramesityldisilene (**18**; λ_{max} = 420 nm) (eq. 3.17). This compound provides another photochemical source to generating silylene. In addition, the generation of the silylene from **10** is cleaner relative to photolysis of **3**, as it does not contain the non-reactive byproduct whose UV-vis spectrum overlaps with that of **18** (see Fig. 2.2c).

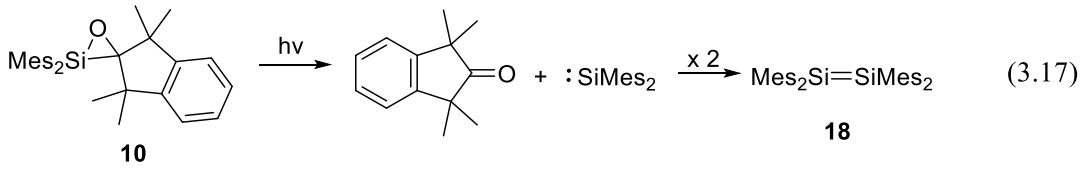

(3.17)

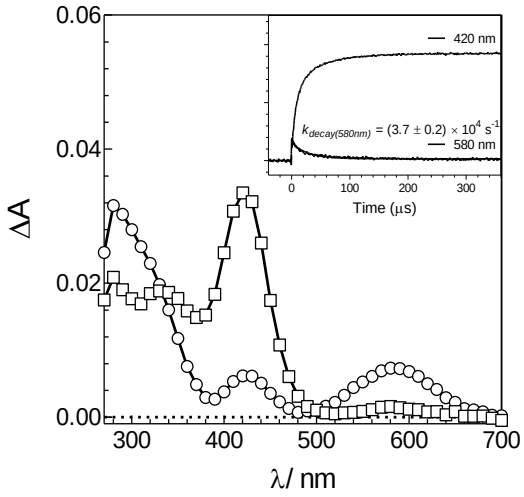

Figure 3.39. Transient absorption spectra recorded 0.00 – 2.56 μs (○) and 55.68 – 58.88 μs (□) after the laser pulse by laser flash photolysis of **7** in deoxygenated hexanes at 25°C. The inset shows transient decay traces at 420 and 580 nm.

It is to be noted that the exact extrusion mechanism of this reaction is not known. Specifically, it is not known whether a step-wise pathway is involved in which **10** generates the corresponding silacarbonyl ylide, preceding cleavage to form $SiMes_2$ and carbonyl compound, or if the extrusion of $SiMes_2$ occurs concertedly.

*3.6.2. Reaction of $SiMes_2$ with 1,1,3,3-Tetramethyl-2-indanone (**7**)*

The reaction of $SiMes_2$ with 1,1,3,3-tetramethyl-2-indanone (**7**) has been reported to proceed with a rate constant of $k_Q = 1.6 \times 10^9$ $M^{-1}s^{-1}$, based on measurements of the $SiMes_2$ lifetime by 266 nm laser photolysis of **3** in the presence of 0 – 0.27 mM ketone.[2] The value is *ca.* 10^2 times larger than the rate constant measured in this work for the reaction of $SiMes_2$ with **8**, and thus does not seem reasonable. As a result, the kinetics of the reaction of $SiMes_2$ with **7** was re-evaluated in this work. The kinetic studies on **7** were limited to the 0.2 – 0.8 mM range in ketone concentration, as the lather competes with **3** for the excitation light quite effectively (248 nm, $\varepsilon_{248} = 162$ cm^{-1} M^{-1}). The resulting plot

of k_{decay} of the silylene vs. ketone concentration (Figure 3.40) is linear, and regression analysis according to eq. 3.1 affords the rate constant $k_Q = (7.2 \pm 1) \times 10^7$ $M^{-1}s^{-1}$. This new rate constant is more consistent than the original value with what was measured with the reactions of $SiMes_2$ with di-*tert*-butyl ketone ($k_Q = (2.1 \pm 0.2) \times 10^7$ $M^{-1}s^{-1}$) and 2,2,5,5-tetramethylcyclopentanone in the present work ($k_Q = (3.1 \pm 0.2) \times 10^7$ 10^7 $M^{-1}s^{-1}$: *vide supra*). No transient absorptions other than those assignable to $SIMes_2$ could be detected in the experiment.

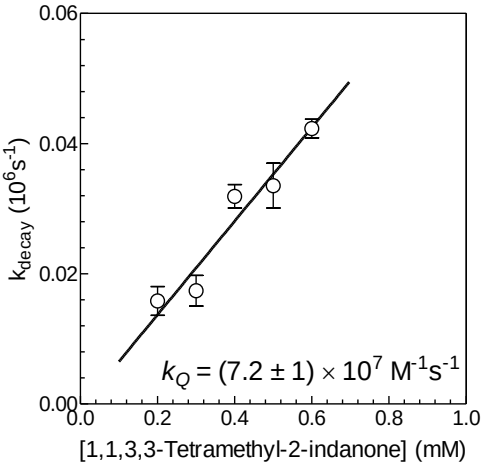

Figure 3.40. Plot of k_{decay} vs ketone concentration for $SiMes_2$ monitored at 580 nm. The solid line is the linear least-squares fit of the data to eq. 3.1.

3.7 Discussion

The results presented above are broadly analogous to what was observed in Chapter 2 for the reactions of $SiMe_2$, $SiPh_2$, and $SiMes_2$ with enolizable carbonyl compounds, which have been shown to proceed via the initial formation of the corresponding silacarbonyl ylide. The corresponding transient silacarbonyl ylides were successfully detected in the reactions of $SiMe_2$ and $SiPh_2$ with 2-adamantanone, di-*tert*-

butyl ketone, and 2,2,5,5-tetramethylcyclopentanone, and of $SiMes_2$ with 2-adamantanone. The UV-vis absorption maxima of the silacarbonyl ylides detected in this work are listed in Table 3.10. The UV-vis absorption maxima of the ylides are in the same range as those derived from the enolizable carbonyl compounds studied in Chapter 2 ($\lambda_{max} \approx 510 – 580$ nm), as well as those detected under matrix conditions in the older literature.[1]

Table 3.10. Experimental UV-Vis absorption maxima (λ_{max} (nm)) of the silacarbonyl ylides formed by reactions of $SiMe_2$, $SiPh_2$, and $SiMes_2$ with non-enolizable carbonyl compounds in hexanes at 25°C

Substrate	λ_{max} (nm)		
	$SiMe_2$	$SiPh_2$	$SiMes_2$
2-adamantanone (**5**)	640	530	640
di-*tert*-butyl ketone (**6**)	640[b]	550[b]	-[a]
2,2,5,5-tetramethylcyclopentanone (**8**)	615[b]	520[b]	-[a]

a. No detectable silacarbonyl ylide b. UV-Vis absorption maximum of the ylide was determined by the difference of two spectra recorded at two different time windows.

Table 3.11. Absolute second order rate constants (k_Q) for the reactions of $SiMe_2$, $SiPh_2$, and $SiMes_2$ with non-enolizable ketones in hexanes solution at 25°C, where silacarbonyl ylides could not be detected

Substrate	k_Q (x 10^{10} $M^{-1}s^{-1}$)		
	$SiMe_2$	$SiPh_2$	$SiMes_2$
pivalaldehyde	1.5 ± 0.1[c]	1.1 ± 0.1[c]	0.61 ± 0.1[c]
2-adamantanone (**5**)	[b]	[b]	[b]
di-*tert*-butyl ketone (**6**)	[b]	[b]	0.0021 ± 0.0002
2,2,5,5-tetramethylcyclopentanone (**8**)	[b]	[b]	0.0031± 0.0002
1,1,3,3-tetramethyl-2-indanone (**7**)	-	-	0.0072± 0.001

a. Errors in k_Q values are reported as twice the standard error from the linear least-square analysis of the plots of silylene k_{decay} values vs [Q] according to eq. 3.1; b. Silacarbonyl ylide detected.; c. (*Data recorded by C. Browne*)

The absolute second order rate constants that could be determined for the reactions of $SiMe_2$, $SiPh_2$, and $SiMes_2$ with the four non-enolizable carbonyl compounds studied in this work are listed in Table 3.11. The rate constants for reaction of the three silylene with pivalaldehyde are within a factor of 2 – 3 of the diffusional rate constant in hexanes at 25°C ($k_{diff} \approx 2 \times 10^{10}$ $M^{-1}s^{-1}$),[10] and no intermediate could be detected. This suggests the initial association step is the rate determining step, and if any intermediate is involved it is at steady state throughout the entire concentration range studied.

In the $SiMes_2$ series, there is a 100 – 300 fold decrease in the rate constant for reaction with the bulkier substituted ketones, di-*tert*-butyl ketone (**6**) and 2,2,5,5-tetramethylcyclopentanone (**8**), relative to that with pivaldehyde. This is presumably due to the more severe steric factors about the carbonyl group in the ketone compared to the aldehyde. Comparison of the rate constants for reaction of $SiMes_2$ with **6** and **8** shows that all else being equal, incorporating the C=O in a C_5 ring accelerates the reaction but only very modestly.

Comparing the absolute rate constants measured for the reactions of $SiMes_2$ with **6** - **8** to its enolizable analogue, di-*iso*-propyl ketone ($k_Q = (9 \pm 1) \times 10^8$ M^{-1} s^{-1}) indicates 12 – 45 × lower than the reactivity with the non-enolizable ketones., they afford similar rate constants. This suggests that the pre-equilibrium is affected the most due to the substituents on the ketone structure (*ie*. steric effects slow down the pre-equilibrium step). On the other hand, the reactivity of $SiMes_2$ with pivalaldehyde and pinacolone ($k_Q = (6 \pm 1) \times 10^9$ M^{-1} s^{-1}) are similar, as they both are close to the diffusional control rate. This suggests the initial complexation of the silylene and ketone is the rate determining step.

The estimated equilibrium (K_1) and forward unimolecular rate (k_2) constants for the reactions of the three silylenes with the four non-enolizable carbonyl compounds, determined by the saturation kinetic expression (eq. 3.9), are listed in Table 3.12. The equilibrium constants measured are similar to those measured for the reactions of the silylenes ($10^3 – 10^4$ M^{-1}) with enolizable carbonyl compounds (see Chapter 2) and as well as those for Lewis acid-base complexation of the silylenes with ethers.[11] For example, the equilibrium constants for the complexation of $SiMe_2$, $SiPh_2$, and $SiMes_2$ with Et_2O are 1.3 $\times 10^3$, 7.1 $\times 10^3$, and 1 M^{-1}, respectively[11], which can be compared to the values measured for ylide formation with **5**. The trend in the equilibrium constants for the silylenes is $SiPh_2 > SiMe_2 >> SiMes_2$, which reflects the variation in Lewis acidity of the three silylenes, as measured by their K_{Et2O} values.

Table 3.12. Equilibrium (K_1) and the unimolecular ring-closure rates (k_2) for the reactions of $SiMe_2$, $SiPh_2$, and $SiMes_2$ with carbonyl compounds in hexanes at 25°C

Substrate	[K_1 ($\times 10^4$ M^{-1})] | k_2 ($\times 10^6$ s^{-1})		
	$SiMe_2$	$SiPh_2$	$SiMes_2$
2-adamantanone (**5**)	[1.1 ± 0.3][b] 0.85 ± 0.02	[5.1 ± 3][b] 0.16 ± 0.02	[0.10 ± 0.02][b] 0.35 ± 0.03
di-*tert*-butyl ketone (**6**)	[0.62 ± 0.2][b] 1.1 ± 0.1	-	[c]
2,2,5,5-tetramethylcyclopentanone (**8**)	[2.1 ± 2][b] 0.71 ± 0.04	[2 ± 1] 0.32 ± 0.01	[c]

a. Errors in K_1 and k_2 values are reported as twice the standard error from the non-linear least-square fit of the plots of the silacarbonyl ylide k_{decay} values vs. ketone concentration according to eq. 3.9, respectively.; b. K_1 was estimated by the non-linear least-square fit of the plot to eq 3.9; c. Silacarbonyl ylide not detected.

The first-order rate coefficients k_2 is tentatively associated with the electrocyclic ring-closure reactions of the $SiMe_2$- and $SiPh_2$-derived silacarbonyl ylide. With the $SiMe_2$-ylide series, k_2 is similar for all three ketones. In addition, the $SiPh_2$-ylide series also have similar k_2 for both ketones. It can be seen that the $SiPh_2$-**5** and $SiPh_2$-**8** ylides are systematically less reactive than the corresponding $SiMe_2$-ylides toward ring closure.[12]

On the other hand, the k_2 value determined for the $SiMes_2$-**5** ylide is markedly larger than that of the $SiPh_2$-**5** ylide. This effect could be caused by electronic effects from the substituents on the silylene. The phenyl groups are more electron withdrawing, relative to mesityl groups, which could slow down the ring closure process by reducing electron density at silicon.[11] In addition, there may be steric acceleration involved in the reaction, where the mesityl groups lock the silacarbonyl ylide into a favorable conformation for cycloaddition to occur, compared to the Me and Ph substituents.[13] The possible combination of these effects would lower the barrier for the reaction of $SiMes_2$ with 2-adamantanone.

It is to be noted that the putative first order rate coefficient k_2 is tentatively assigned above to that for electrocyclic ring closure of the ylide. However, there is no evidence of these systems affording the corresponding 3-membered ring product, as shown in the steady state experiments. It can be concluded that if k_2 really is associated with ring closure, the resulting products must be unstable (on a timescale of minutes). Their decomposition presumably leads to the formation of oligomeric compounds.

Table 3.13. Rate coefficients of the [2+3]-cycloaddition (k_3) and unimolecular ring closure (k_2) for the reactions of $SiMe_2$, $SiPh_2$, and $SiMes_2$-derived silacarbonyl ylide with carbonyl compounds in hexanes at 25°C

Substrate	k_3 (× 10^7 M^{-1} s^{-1}) | k_2 (× 10^6 s^{-1})		
	$SiMe_2$	$SiPh_2$	$SiMes_2$
2-adamantanone (**5**)	1.5 ± 0.1 0.63 ± 0.04	0.79 ± 0.03 0.11 ± 0.01	1.4 ± 0.1 0.39 ± 0.04
di-*tert*-butyl ketone (**6**)	3.5 ± 0.2 0.99 ± 0.09	-	[b]
2,2,5,5-tetramethylcyclopentanone (**8**)	4.1 ± 0.4 0.84 ± 0.08	2.5 ± 0.2 0.32 ± 0.01	[b]

a. Errors in k_3 and k_2 values are reported as twice the standard error from linear least-square analysis of plots of silacarbonyl ylide k_{decay} values vs. ketone concentration according to eq. 3.11; b. Silacarbonyl ylide not detected.; c. k_3 is indeterminable.

The rate coefficients for the putative [2+3] cycloaddition of the ylide with a second molecule of ketone (k_3) and the tentatively assigned ring closure (k_2), determined from the linear expression (eq. 3.11), are listed in Table 3.13. Comparing the k_2 values measured from the two kinetic expressions, they are the same within error. This suggests the k_2 values measured are independent of ketone concentration.

There is a systematic decrease from $SiMe_2$ to $SiPh_2$, followed by an increase with $SiMes_2$, for the case of 2-adamantanone. It is to be noted that the dioxasilacyclopentane, derived from the [2+3] cycloaddition pathway, was only observed in the reactions of the silylenes with 2-adamantanone, and thus the linear dependence of the silacarbonyl ylide decay rate coefficient on ketone concentration is to some extent consistent with the [2+3] cycloaddition reaction.[4-5] However, it is difficult to understand the *ca.* 2-fold higher reactivity of the $SiMes_2$-**5** ylide toward reaction with a second molecule of ketone, compared to that of the $SiPh_2$-**5** ylide. On the other hand, the reactions of silylenes with

di-*tert*-butyl ketone and 2,2,5,5-tetramethylcyclopentanone were not observed, yet it shows the same prevalence as the reactions of 2-adamantanone. If the k_3 values, measured for the reactions of the silylenes with **6** and **8**, really are associated with [2+3] cycloaddition, then there are no steric effects associated with these reactions, relative to **5**. Furthermore, ring and angle strain do not pose any influence as we compare **6** and **8**.

It is to be noted that impurity quenching cannot be ruled out from these measurements and may be the cause for the silacarbonyl ylide decay rate coefficients being dependent on ketone concentration. As a result, fully definitive conclusions are difficult to make.

3.8. Conclusion

The cycloaddition reactions of $SiMe_2$, $SiPh_2$, and $SiMes_2$ with non-enolizable carbonyl compounds, pivalaldehyde (**4**), 2-adamantanone (**5**), di-*tert*-butyl ketone (**6**), and 2,2,5,5-tetramethylcyclopentanone (**8**) have been investigated by a combination of steady state and laser flash photolysis experiments. The reaction mechanism has been shown to involve the initial formation of the corresponding silacarbonyl ylide intermediate, which decays by competing first- and second-order processes where the latter involves a second molecule of ketone. The reactions of $SiMe_2$ and $SiPh_2$ with 2-adamantanone, di-*tert*-butyl ketone, and 2,2,5,5-tetramethylcyclopentanone, and $SiMes_2$ with 2-adamantanone, have been shown to afford the corresponding silacarbonyl ylides, which exhibit broad UV-vis absorption bands in the visible region ($\lambda_{max} \approx 500 – 650$ nm). Unfortunately, the data do not allow us to necessarily associate these decay processes with the formation of the

specific products that have been shown to be formed in these reactions: the corresponding oxasiliranes in the reactions of $SiMes_2$ with di-*tert*-butyl ketone and 2,2,5,5-tetramethylcyclopentanone, or the corresponding dioxasilacyclopentane derivatives in the reactions of all three silylenes with 2-adamantanone.

3.9. Supporting Information

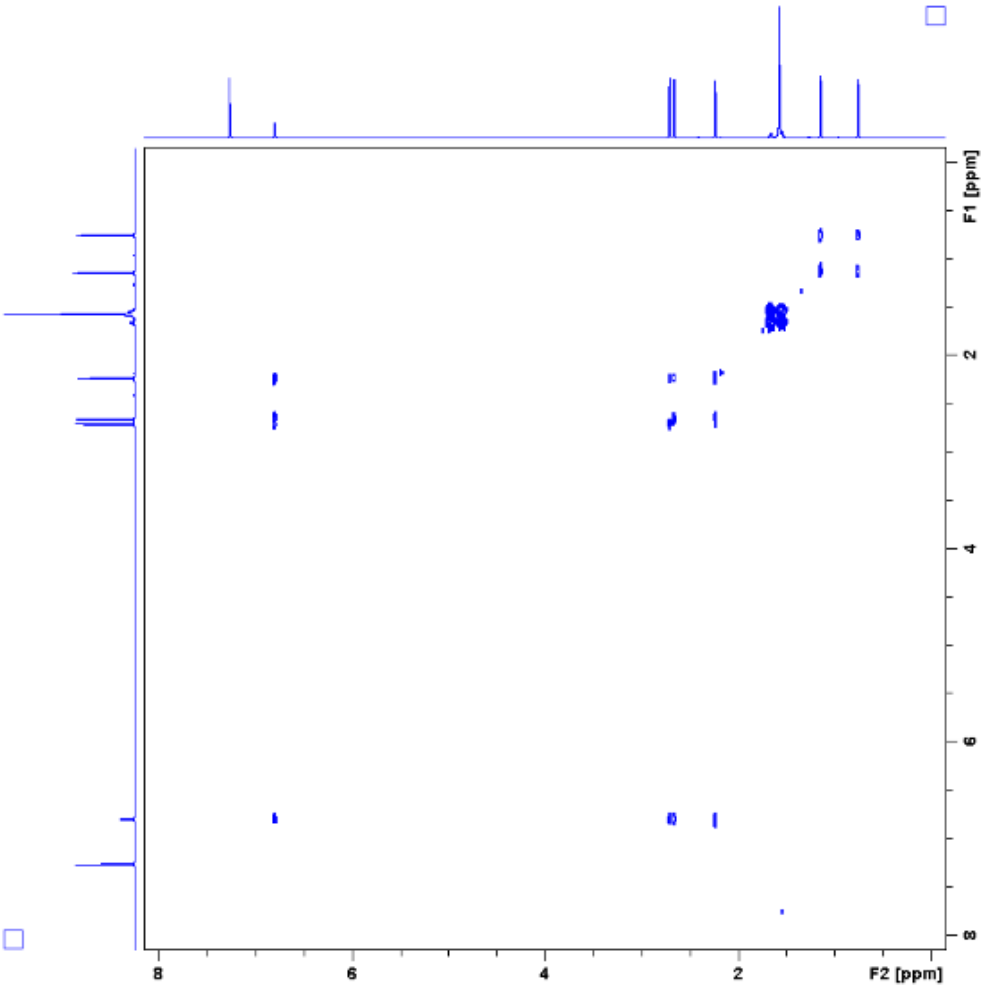

Figure S3.1. ^{1}H-^{1}H COSY spectrum of the solution of **12** in $CDCl_3$, with the ^{1}H NMR spectrum from Figure 3.8 used as a projection for both axes.

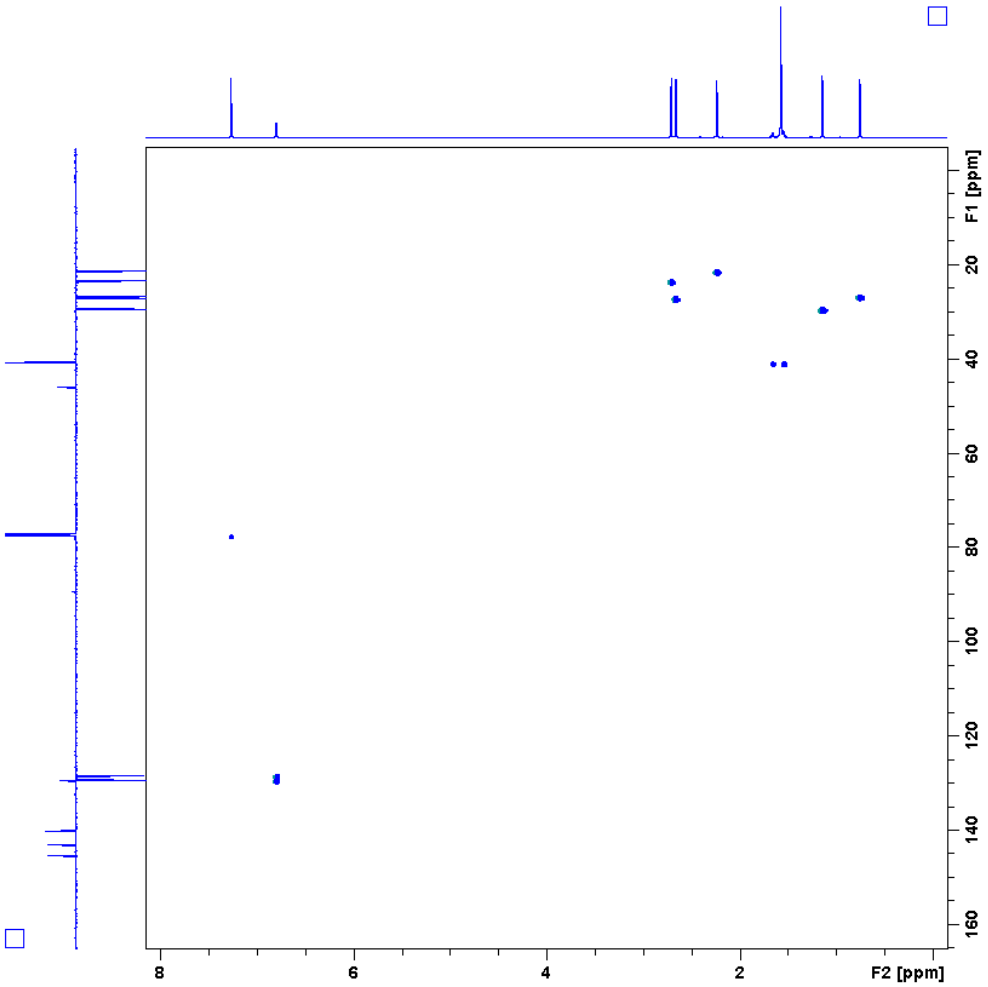

Figure S3.2. ^{1}H-^{13}C HSQC spectrum of the solution of **12** in $CDCl_3$, with the ^{1}H NMR and ^{13}C NMR spectra from Figures 3.8 and 3.10, used as a projection for the axes.

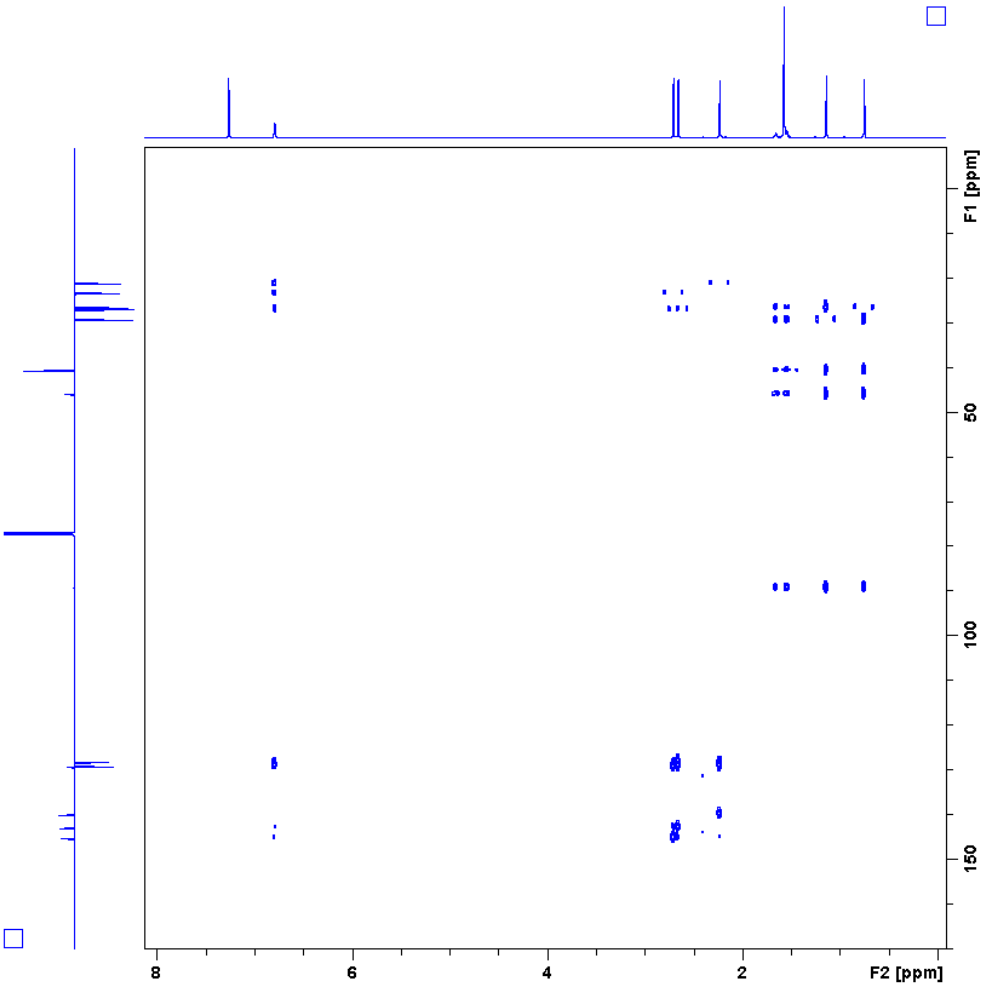

Figure S3.3. ^{1}H-^{13}C HMBC spectrum of the solution of **12** in $CDCl_3$, with the ^{1}H NMR and ^{13}C NMR spectra from Figures 3.8 and 3.10, used as a projection for the axes, respectively.

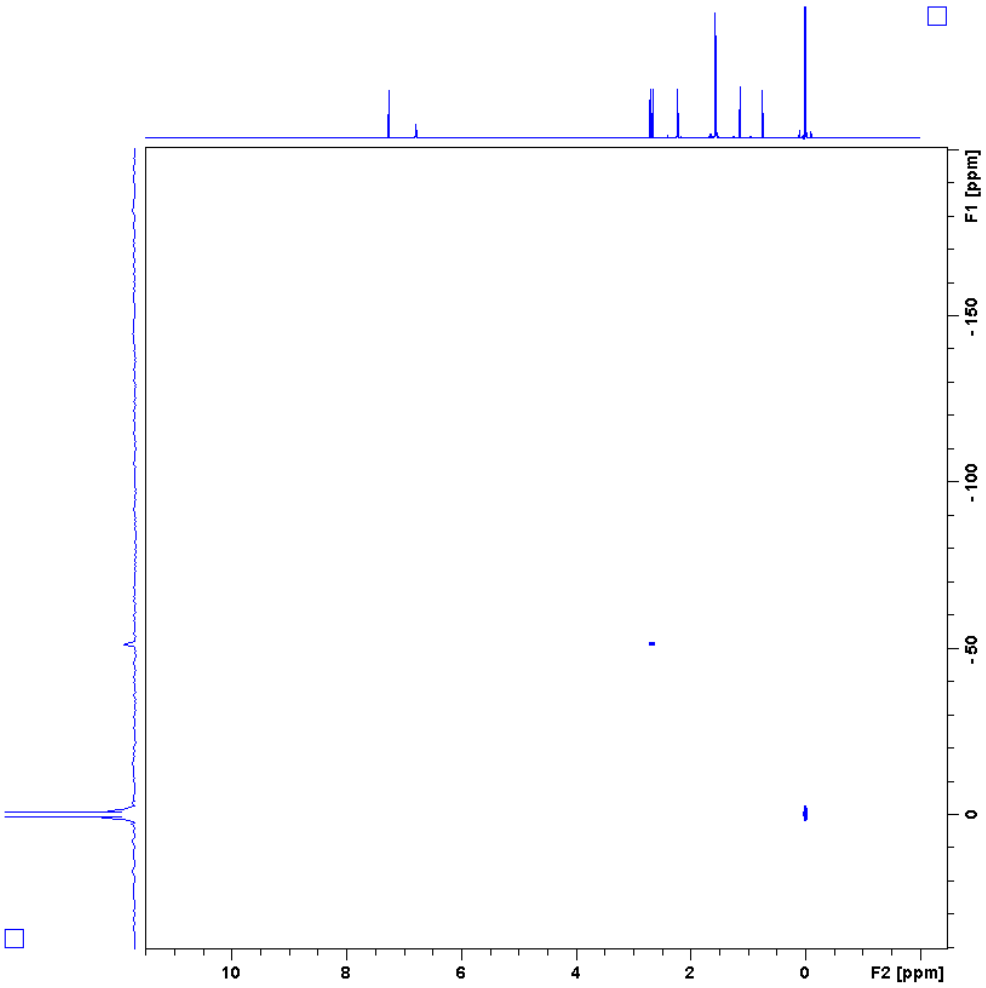

Figure S3.4. ^{1}H-^{29}Si HMBC spectrum of the solution of **12**, containing TMS, in $CDCl_3$.

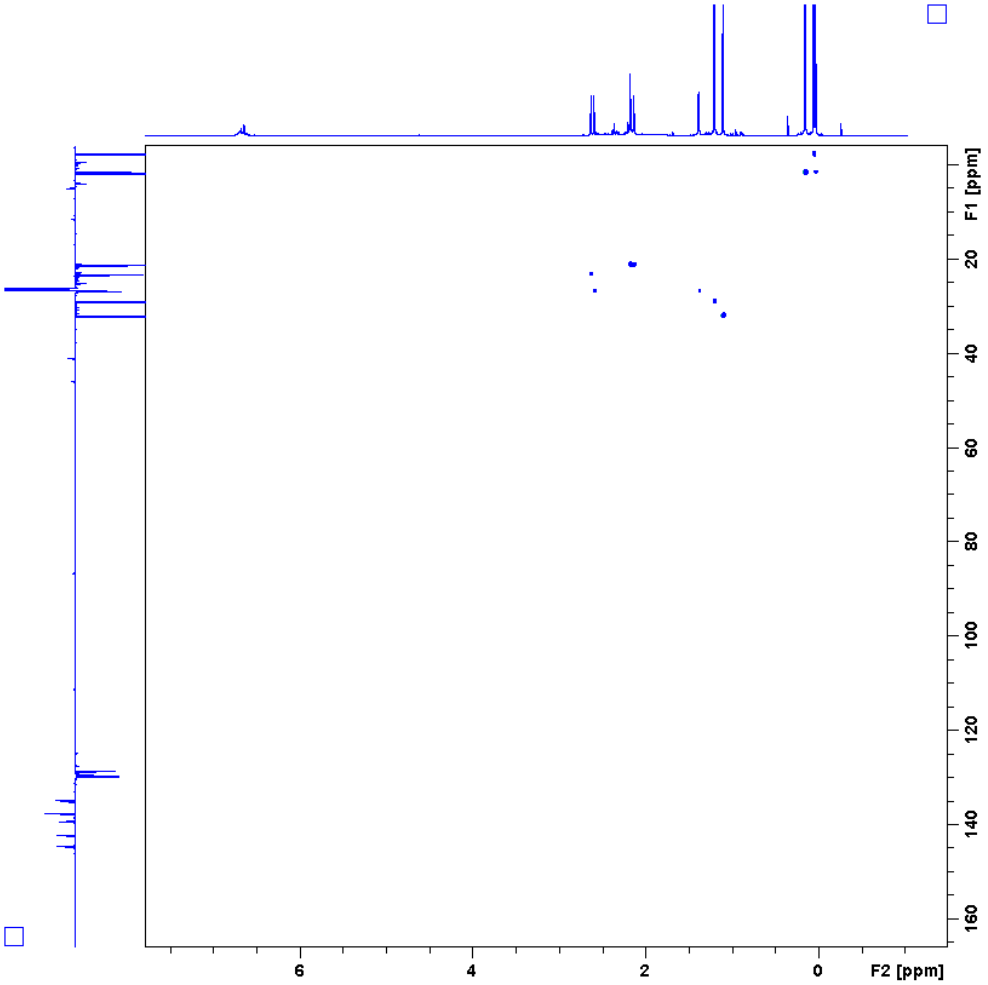

Figure S3.5. ^{1}H-^{13}C HSQC spectrum of the crude photolysate solution of 0.05 M **3**, 0.05 M **6**, and 0.01 M bis(trimethylsilyl)methane in C_6D_{12} photolyzed for 60 mins, with the ^{1}H NMR and ^{13}C NMR spectra from Figures 312 and 3.13, used as a projection for the axes.

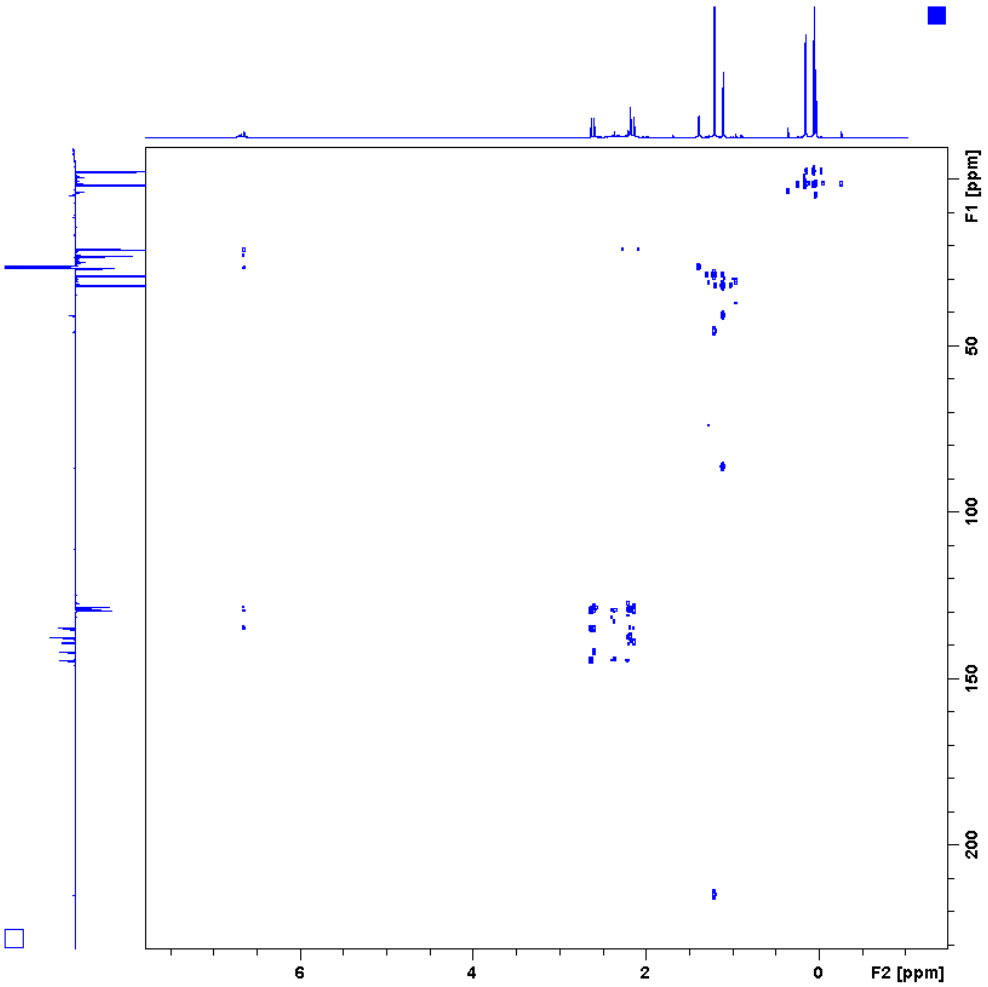

Figure S3.6. ^{1}H-^{13}C HMBC spectrum of the crude photolysate solution of 0.05 M **3**, 0.05 M **6**, and 0.01 M bis(trimethylsilyl)methane in C_6D_{12} photolyzed for 60 mins, with the ^{1}H NMR and ^{13}C NMR spectra from Figures 3.12 and 3.13, used as a projection for the axes.

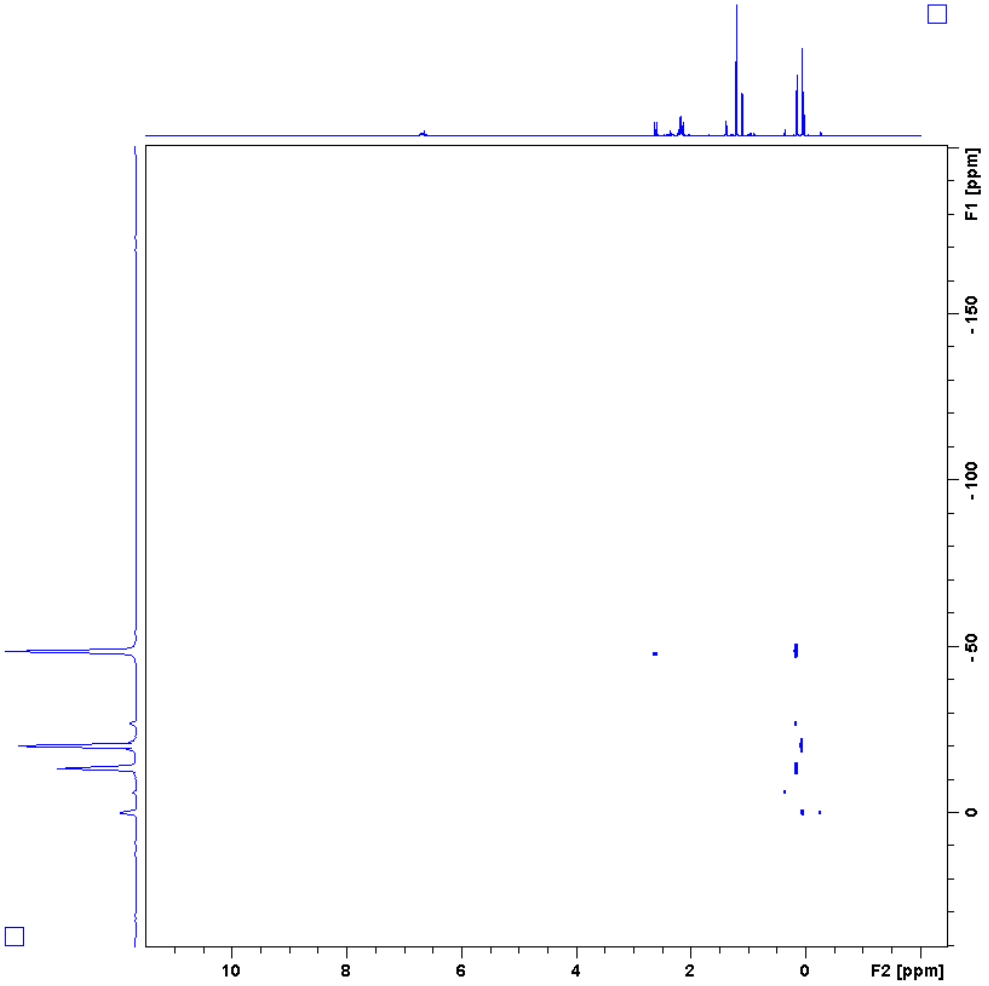

Figure S3.7. ^{1}H-^{29}Si HMBC spectrum of the crude photolysate solution of 0.05 M **3**, 0.05 M **6**, and 0.01 M bis(trimethylsilyl)methane in C_6D_{12} photolyzed for 60 mins.

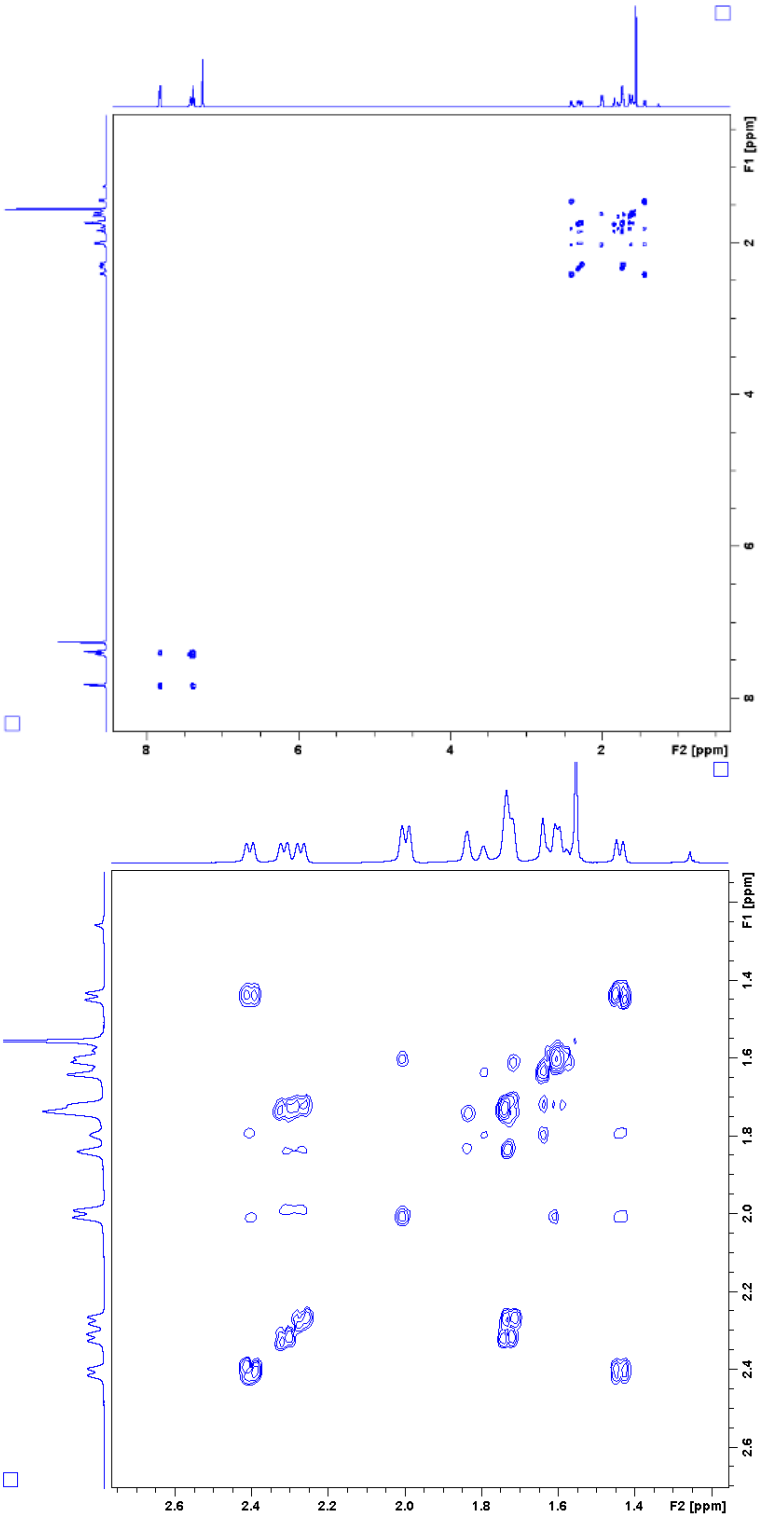

Figure S3.8. ^{1}H-^{1}H COSY spectrum of the solution of **9c** in $CDCl_3$, with the ^{1}H NMR spectrum from Figure 3.18, used as the projection for the axes. The figure on the bottom is zoomed in the 1.1 – 2.7 ppm range on both axes.

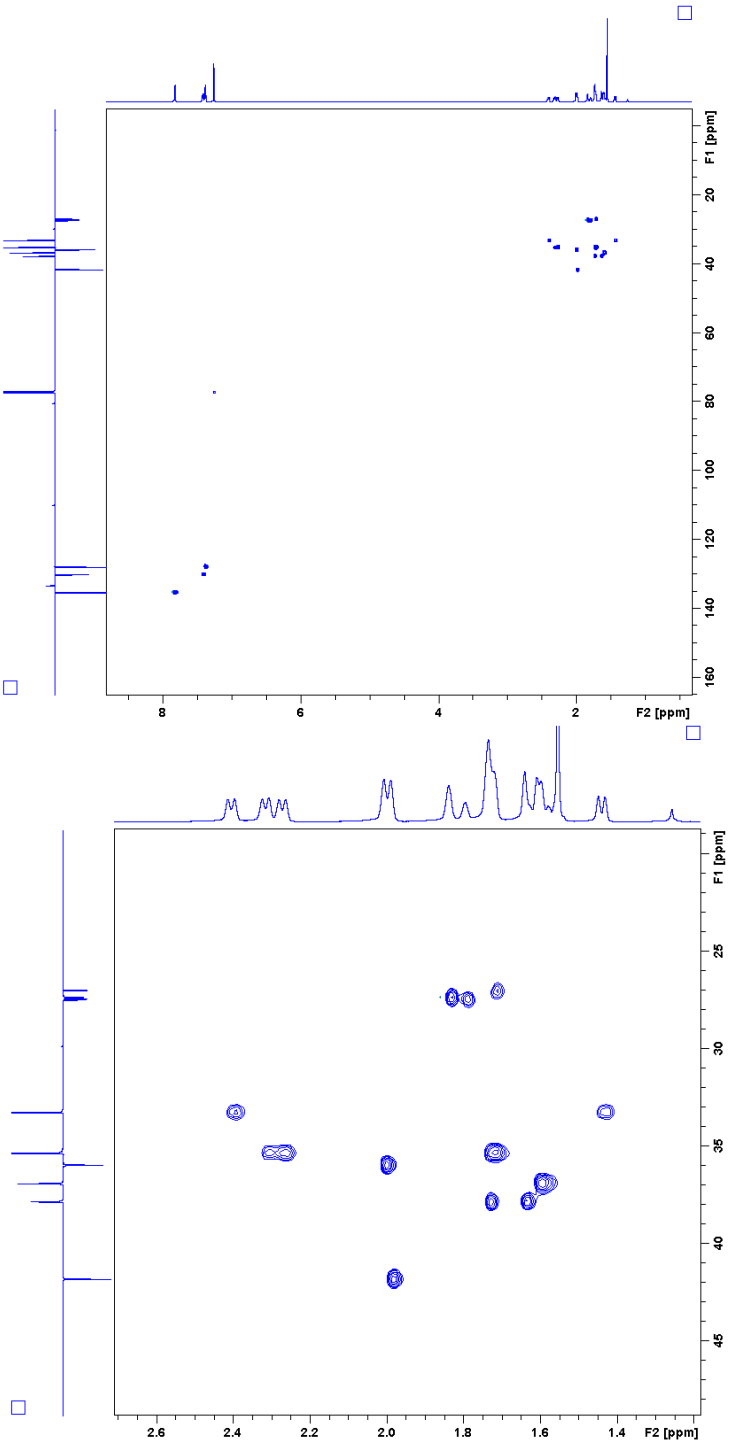

Figure S3.9. ^{1}H-^{13}C HSQC spectrum of the solution of **9c** in $CDCl_3$, with the ^{1}H NMR and ^{13}C NMR spectra from Figures 3.18 and 3.20, used as the projection for the axes. The figure on the bottom is zoomed in the 1.1 – 2.7 ppm (^{1}H NMR) and 18 – 48 ppm (^{13}C NMR) range.

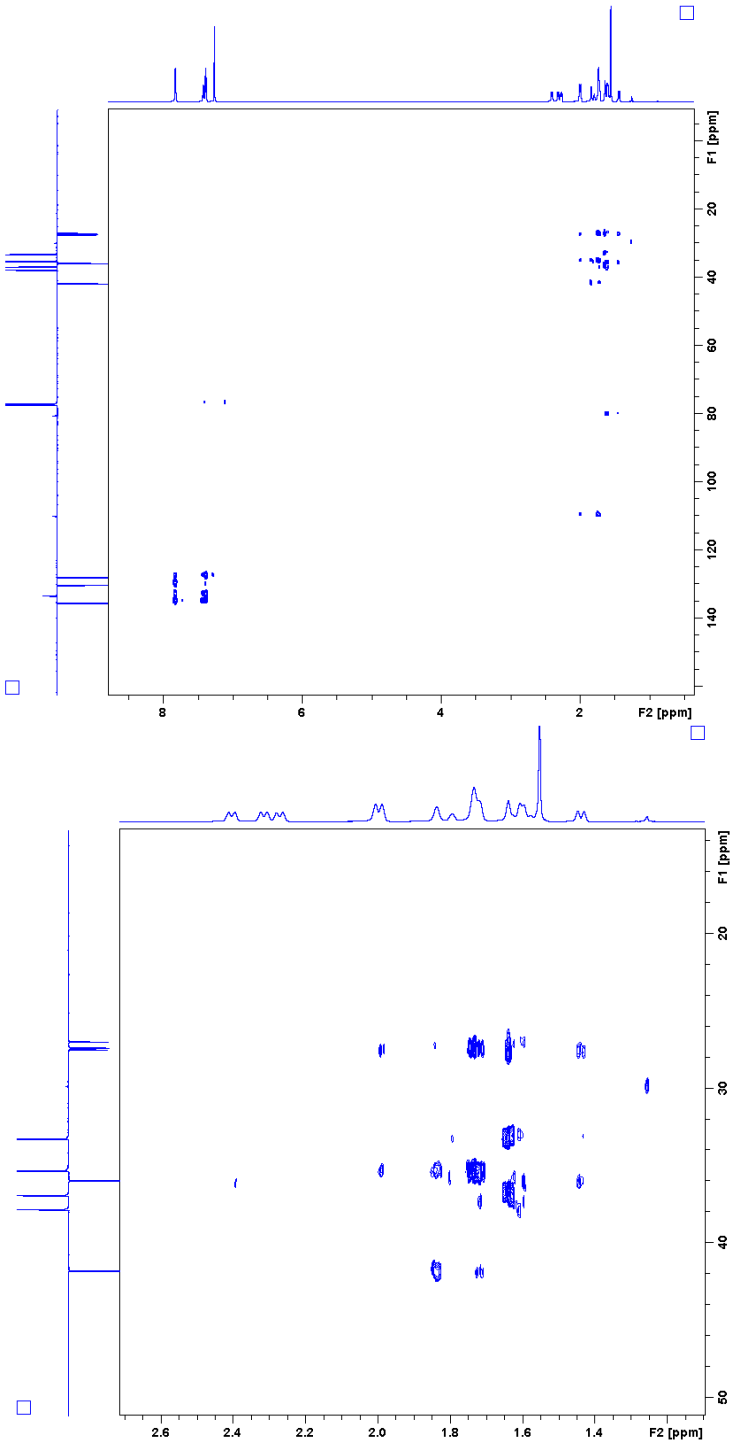

Figure S3.10. ^{1}H-^{13}C HMBC spectrum of the solution of **9c** in $CDCl_3$, with the ^{1}H NMR and ^{13}C NMR spectra from Figures 3.18 and 3.20, used as the projection for the axes. The figure on the right is zoomed in the 1.1 – 2.7 ppm (^{1}H NMR) and 13 – 50 ppm (^{13}C NMR) range.

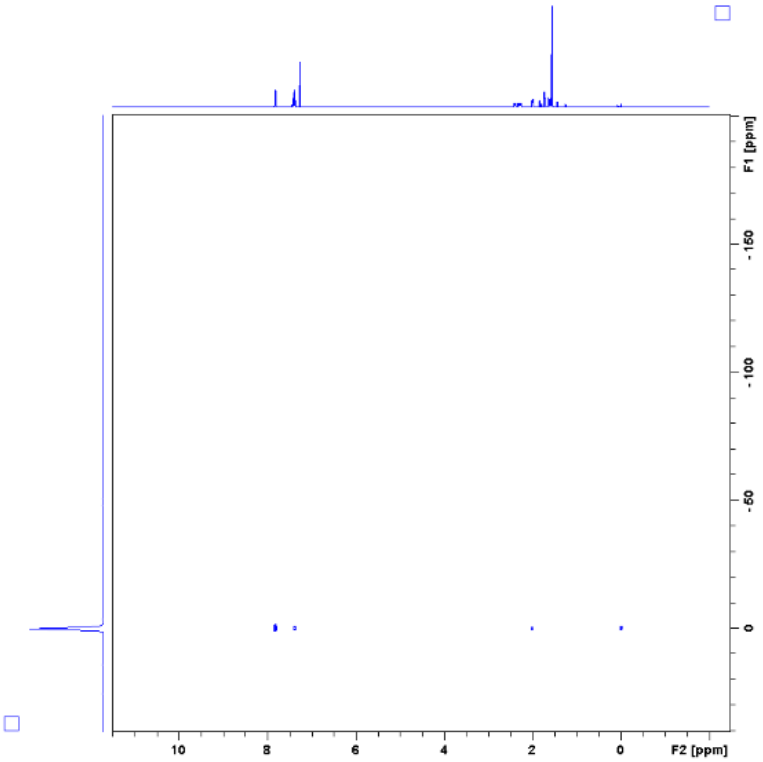

Figure S3.11. ^{1}H-^{29}Si HMBC spectrum of the solution of **9c**, containing TMS, in $CDCl_3$.

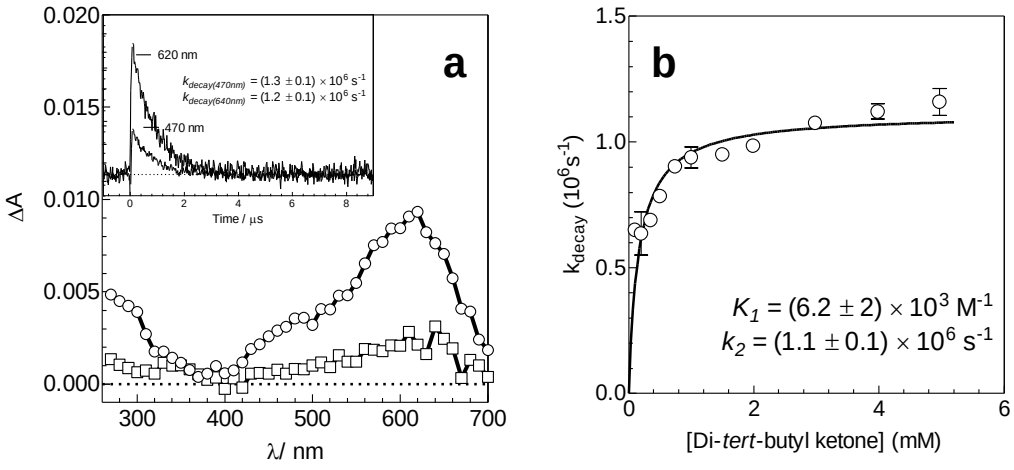

Figure S3.12. (a) Transient absorption spectra recorded 0.27 – 0.34 µs (○) and 1.39 – 1.47 µs (□) after the laser pulse by laser flash photolysis of **1** in the presence of 5 mM di-*tert*-butyl ketone (**6**) in deoxygenated hexanes at 25°C. The inset shows transient decay traces recorded at 470 and 620 nm with k_{decay} = (1.2 ± 0.1) × 10^6 and (1.3 ± 0.1) × 10^6 s^{-1}, respectively. (b) Plot of k_{decay} vs ketone for the $SiMe_2$-**6** silacarbonyl ylide monitored at 620 nm. The solid line is the non-linear least-squares fit of the data to eq. 3.9

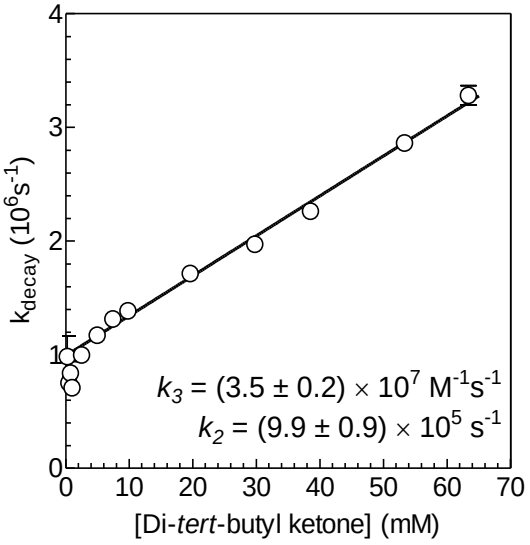

Figure S3.13. Plot of k_{decay} vs ketone for the $SiMe_2$-**6** silacarbonyl ylide monitored at 620 nm. The solid line is the linear least-squares fit of the data to eq. 3.11.

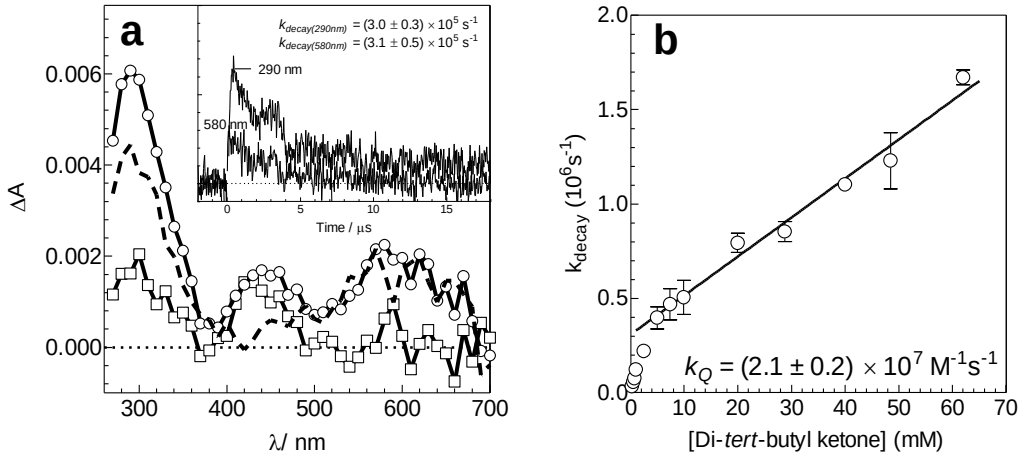

Figure S3.14. (a) Transient absorption spectra recorded 0.51 – 0.67 μs (○) and 4.06 – 4.22 μs (□) after laser pulse by laser flash photolysis of **3** in the presence of 5 mM di-*tert*-butyl ketone (**6**) in deoxygenated hexanes at 25°C. The dashed line spectrum (-) shows the difference between the two spectra. The inset shows transient decay traces recorded at 290 and 580 nm. (b) Plot of k_{decay} vs ketone concentration for $SiMes_2$ monitored at 580 nm. The solid line is the linear least-squares fit of the data to eq. 3.1.

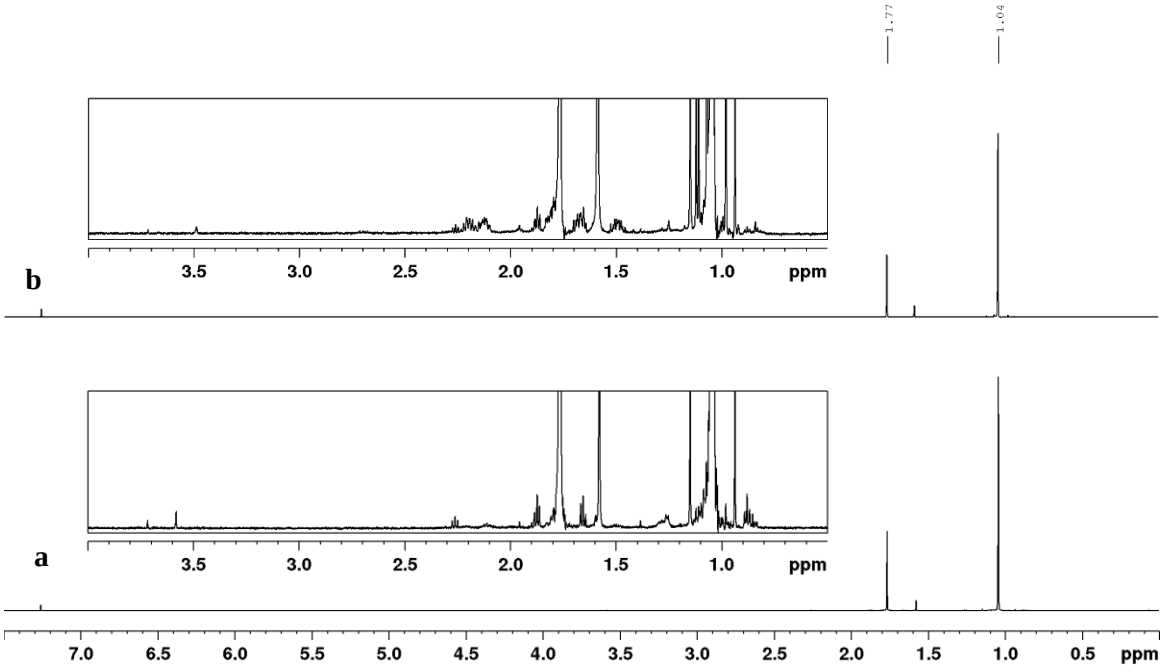

Figure S3.15. ^{1}H NMR spectra of 2,2,5,5-tetramethycyclopentanone in $CDCl_3$. (a) Sample used in the initial studies. (b) Synthesis and attempted further purification of ketone.

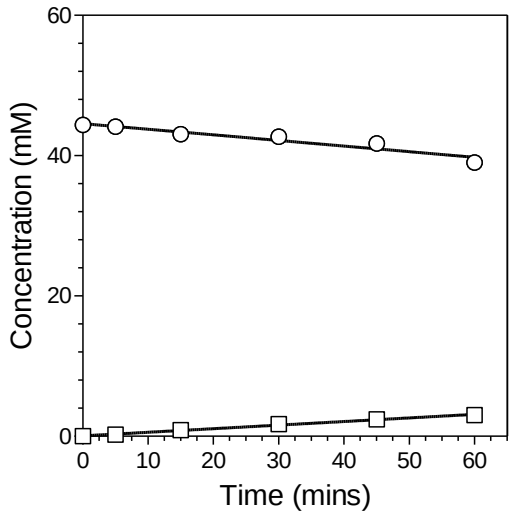

Figure S3.16. Concentration vs. time plots for the photolysis of 0.045 M 2,2,5,5-tetramethylcyclopentanone (**7**) in cyclohexane-d_{12}. Shown is the depletion of **7** (○) and the formation of 2,2,5-trimethyl-4-hexenal (**15**, □). The slope of the consumption of ketone is are as follows: (○):(-8.0 ± 0.2) × 10^{-2} mM/min. (□): (5.1 ± 0.4) × 10^{-2} mM/min.

Table S3.1. ^{1}H NMR assignments for compound **12**, recorded from the spectrum of the crude photolysate in C_6D_{12} (Figure 3.6), refer to Figure 3.9 for the proton assignments.

Chemical Shift (ppm)	Assignment	Chemical Shift (ppm)	Assignment
1.12 (s)	H_a	2.68 (s)	H_e
0.74 (s)	H_b	2.63 (s)	H_f
1.63 (m)	H_c	2.16 (s)	H_g
1.51 (m)	H_d	6.69 (s)	H_h

Table S3.2. ^{13}C NMR assignments for compound **12**, recorded from the spectrum of the crude photolysate in C_6D_{12}, refer to Figure 3.9 for the carbon assignments

Chemical Shift (ppm)	Assignment	Chemical Shift (ppm)	Assignment
21.3	C-1	89.1	C-8
23.4	C-2	128.7	C-9
27.3	C-3	129.9	C-10
26.9	C-4	130.3	C-11
29.8	C-5	140.1	C-12
41.3	C-6	143.4	C-13
46.6	C-7	146.1	C-14

3.10. References

1. Ando, W.; Hagiwara, K.; Sekiguchi, A., *Organometallics* **1987,** *6*, 2270-2271.
2. Conlin, R. T.; Netto-Ferreira, J. C.; Zhang, S.; Scaiano, J. C., *Organometallics* **1990,** *9*, 1332-1334.
3. C. Browne, W. J. L., *unpublished results*.
4. Ando, W.; Ikeno, M.; Sekiguchi, A., *J. Am. Chem. Soc.* **1978,** *100* (11), 3613-3615.
5. Ando, W.; Hamada, Y.; Sekiguchi, A., *J. Chem. Soc., Chem. Commun.* **1983,** (17), 952-954.
6. Ando, W.; Hamada, Y.; Sekiguchi, A.; Ueno, K., *Tet. Lett.* **1982,** *23* (50), 5323-5326.
7. Metsänen, T. T.; Oestreich, M., *Organometallics* **2015,** *34* (3), 543-546.
8. Dalton, J. C.; Dawes, K.; Turro, N. J.; Weiss, D. S.; Barltrop, J. A.; Coyle, J. D., *Journal of the American Chemical Society* **1971,** *93* (26), 7213-7221.
9. Sakai, N.; Fukushima, T.; Okada, A.; Ohashi, S.; Minakata, S.; Komatsu, M., *J. Organomet. Chem.* **2003,** *686* (1-2), 368-372.
10. Murov, S. L.; Carmichael, I.; Hug, G. L., *Handbook of photochemistry*. 2nd ed.; Dekker: New York, 1993.
11. Kostina, S. S.; Singh, T.; Leigh, W. J., *Organometallics* **2012,** *31*, 3755-3767.
12. Moiseev, A. G.; Leigh, W. J., *Organometallics* **2007,** *26*, 6277-6289.
13. Jung, M. E.; Piizzi, G., *Chemical Reviews* **2005,** *105* (5), 1735-1766.

Chapter 4 – Conclusions and Future Work

4.1. Conclusion

The reactions of the transient silylenes $SiMe_2$, $SiPh_2$ and $SiMes_2$, with a variety of carbonyl compounds in solution have been studied in this thesis by steady state and laser flash photolysis methods. The reactions afford various products, the identities of which are determined by structural parameters in the ketone and the silylene. All three silylenes react with enolizable carbonyl compounds via ene-addition to afford the corresponding silyl enol ethers. On the other hand, reaction with non-enolizable carbonyl compounds proceeds to yield 3-membered or 5-membered cycloadducts, derived from cycloaddition of the silylene with one or two molecules of the substrate.

The three silylenes were found to react rapidly with relatively unhindered carbonyl compounds (acetone, 1,1,1-trifluoro-2-butanone, 2,4-dimethyl-3-pentanone, 3,3-dimethyl-2-butanone, cyclopentanone, and pivalaldehyde) and without the formation of detectable intermediates. $SiMe_2$ reacts with these carbonyl compounds with absolute rate constants close to the diffusion-controlled rate ($k_{diff} \approx 2.0 \times 10^{10}\ M^{-1}\ s^{-1}$) in hexanes at 25°C while $SiPh_2$ and $SiMes_2$ behave analogously with absolute rate constants in the range of $10^8 – 10^{10}\ M^{-1}\ s^{-1}$.

In contrast, the reactions of $SiMe_2$ and $SiPh_2$ in the presence of more hindered or structurally constrained ketones (camphor, norcamphor, dicyclopropyl ketone, 2-adamantanone, 2,2,5,5-tetramethylcyclopentanone, and 2,2,4,4-tetramethyl-3-pentanone) and $SiPh_2$ with 2,4-dimethyl-3-pentanone, proceed via detectable intermediates, that were

identified as the corresponding silacarbonyl ylides on the basis of their broad absorption bands in the visible region ($\lambda_{max} \approx 500 - 650$ nm) and kinetic behavior. The species decay with 1st-order kinetics, with their decay rate constants responding to ketone concentration in two different manners.

In the case of enolizable carbonyl compounds, the plots of the ylides k_{decay} values with ketone concentration are consistent with saturation kinetics, where a fast pre-equilibrium is followed by a relatively slow product forming step that becomes the rate-determining step for both the silylene and ylide in the limit of high substrate concentration. The absolute rate, equilibrium, and product-forming rate constants are systematically influenced by steric effects and ring strain of the carbonyl compounds, as well as the Lewis acidity and steric effects of the silylene. The equilibrium constants for ylide formation from $SiMe_2$ and $SiPh_2$ were found to be in the ranges of 10^3 - 10^4 M^{-1}, while the product forming (H-migration) rate constants are in the range of 10^5 - 10^7 s^{-1}. The kinetic analysis, detection of the silacarbonyl ylide and steady-state experiments support a reaction mechanism involving the initial formation of a silacarbonyl ylide intermediate, followed by H-migration to afford the corresponding silyl enol ether.

The cycloaddition reactions of $SiMe_2$ and $SiPh_2$ with non-enolizable carbonyl compounds (2-adamantanone, 2,2,4,4-tetramethyl-3-pentanone, and 2,2,5,5-tetramethylcyclopentanone) also proceed via the initial formation of the corresponding silacarbonyl ylide intermediates, which exhibit similar UV-vis absorption spectra to those formed from enolizable ketones, as might we expect. The silacarbonyl ylides were found to decay by a combination of first- and second-order processes, where the latter involves

a second molecule of ketone. The reactions of the three silylenes with 2-adamantanone yields the corresponding 2,4-dioxasilacyclopentanes (one of which has been isolated), while the reactions of $SiMes_2$ with 2,2,5,5-tetramethylcyclopentanone and di-*tert*-butyl ketone generate the corresponding stable oxasiliranes. The adduct of $SiMes_2$ and 2,2,5,5-tetramethylcyclopentanone has been isolated and characterized spectroscopically and its structure proven by X-ray crystallography. The kinetic behavior of the corresponding silacarbonyl ylides, in the case of the 2-adamantanone series, and of $SiMes_2$ in the cases of 2,2,5,5-tetramethylcyclopentanone and di-*tert*-butyl ketone are consistent with their proposed reaction mechanisms. On the other hand, stable cycloadducts could not be detected in the reactions of $SiMe_2$ and $SiPh_2$ with 2,2,4,4-tetramethyl-3-pentanone and 2,2,5,5-tetramethylcyclopentanone. As a result, the kinetic data obtained for these reactions do not allow us to associate their corresponding observed decay traces of the silacarbonyl ylide to a specific cycloaddition mechanism.

4.2. Future Work

The reactions of the three silylenes with enolizable carbonyl compounds have been extensively studied and are known to afford the corresponding silyl enol ethers. Laser flash and steady-state photolysis results support the ene-addition reaction mechanism and have provided quantitative information about the reactivity of the silylene and in some cases, the silacarbonyl ylide. An additional experiment that can be done in these series is to quantitively measure the equilibrium constants, from the silylene and ylide. It is assumed that the equilibrium constant measured are under a pre-equilibrium

assumption, where the silylene and silacarbonyl ylide is already in equilibrium. This can be analyzed by monitoring and comparing the decay rates of the silylene and the corresponding silacarbonyl ylide at lower ketone concentration, where the equilibrium constant is well defined in the kinetic plots, such as the reactions of $SiMe_2$ with camphor and norcamphor.

On the other hand, the kinetic studies on the reactions of the three silylenes with the non-enolizable carbonyl compounds were found to be inconclusive. As discussed in Chapter 3, the kinetic behavior of the silacarbonyl ylides observed cannot be associated with a reaction mechanism, as there is a lack of specific products obtained from the reactions of $SiMe_2$ and $SiPh_2$ with 2,2,5,5-tetramethylcyclopentanone and 2,2,4,4-tetramethyl-3-pentanone. Further efforts should focus on identifying the kinetic and mechanistic differences on the reactions of silylenes with non-enolizable carbonyl compounds (2-adamantanone, 2,2,4,4-tetramethyl-3-pentanone, and 2,2,5,5-tetramethylcyclopentanone) studied in this thesis. The reactions of $SiMe_2$, $SiPh_2$, and $SiMes_2$ with 2-adamantanone have shown to afford the [1+2+2] cycloadduct, dioxasilacyclopentane. The kinetic analyses of these reactions have shown the decay rate coefficients of the silacarbonyl ylide to be linearly dependent on ketone concentration, which supports this reaction mechanism. On the other hand, the reactions of $SiMe_2$ and $SiPh_2$ with 2,2,5,5-tetramethylcyclopentanone do not show any evidence for the formation of the [1+2+2] cycloadduct but nevertheless exhibit similar kinetic behavior to that observed for the reactions with 2-adamantanone. This also raises questions. Our working hypothesis is that the kinetic results obtained for the two latter ketones are due to

impurity quenching. As a result, further work should focus on purifying the ketones to validate whether impurity quenching is the cause for the unusual kinetic behaviors observed from the corresponding silacarbonyl ylides.

Chapter 5 – Experimental

5.1 General

^{1}H and ^{13}C NMR spectra were recorded on Bruker AV200, AV600, or AV700 spectrometers in deuterated chloroform-*d*, benzene-d_6, or cyclohexane-d_{12} and were referenced to the solvent residual proton and ^{13}C signals, respectively. ^{29}Si NMR spectra were recorded on the AV600 spectrometer using the standard 2D-HMBC pulse sequence and were referenced to an external standard of tetramethylsilane or internal standard of bis(trimethylsilyl)methane (^{29}Si δ 0.16, ^{1}H δ -0.27 (s, 2H), 0.03 (s, 18H)). High-resolution electrospray ionization and exact masses were determined on an Agilent G1969A TOF mass spectrometer using electrospray ionization and nitrogen desolvation and nebulizer gas. GC/MS analyses were performed on a Varian Saturn 2200 GC/MS/MS system equipped with a VF-5 ms capillary column (30 m × 0.25 mm; 0.25 μm; Agilent Technologies). Melting points were measured using a Mettler FP82 Hot Stage mounted on an Olympus BH-2 microscope and controlled by a Mettler FP80 Central Processor and are uncorrected. Static UV-visible absorption spectra were recorded using a Cary 50 UV-Vis spectrophotometer. Column chromatography employed SiliaFlash P60 40-63 μm silica gel (Silicycle, 230-400 mesh) or neutral Brockmann Activity I alumina (Fisher Scientific, 60 – 325 mesh). A chromatotron (Harrison Research, Inc.), equipped with 1 mm plates fabricated from Alumina w/Gypsum and UV254 for TLC (Sorbtech, 5 – 25 μm) was employed for radial thick-layer chromatographic separations. Basic alumina

plates were prepared by using a 10% slurry of neutral alumina suspended in NaOH solution (pH = 10 - 11) for 24 hrs, followed by washing with aqueous NaOH (pH = 10).

Single crystal X-ray crystallography was performed as described below. A suitable crystal was selected, cut, and mounted on a Bruker APEX-II CCD' diffractometer using n-paratone oil and a MiTeGen loop. The crystal was kept at 100.0(1) K during data collection. Using Olex2[1], the structure was solved with the XT[2] structure solution program using Intrinsic Phasing and refined with the XL[3] refinement package using Least Squares minimization.

Dodecamethylcyclohexasilane (**1**), 1,1,3,3-tetramethyl-2-2-diphenyl-1,2,3-trisilacyclohexane (**2**) and 2,2-dimesityl-1,1,1,3,3,3-hexamethyltrisilane (**3**) were synthesized as reported previously.[4-5] They were purified by column chromatography on silica gel with hexanes as eluent, followed by recrystallization from methanol. Purities were determined by GC/MS analysis and ^{1}H NMR spectroscopy and were found to be >97% in each case.

5.2. Solvents

Hexanes (Caledon) for laser flash photolysis experiments were dried by passage through activated alumina under nitrogen using a Solv-Tek solvent purification system (Solv-Tek Inc.). Hexanes (Caledon) for synthesis/purification was distilled under nitrogen. Tetrahydrofuran (THF, Caledon) for synthesis was distilled under nitrogen from sodium/benzophenone. Cyclohexane for synthesis was refluxed with sodium and distilled under nitrogen. Pentane (Caledon), dichloromethane (DCM, Caledon), dimethyl sulfoxide

(DMSO, Caledon), chloroform-*d* (Sigma-Aldrich), benzene-d_6 (Cambridge Isotope), deuterium oxide (Cambridge Isotope), and cyclohexane-d_{12} (Cambridge Isotope) were used as received from the suppliers.

5.3. Commercial Reagents

All commercially-available materials were used as received from the suppliers or further purified prior to use as described below; solvents were all reagent grade or better. Acetone (Caledon), pivalaldehyde (Aldrich, 96%), 2,4-dimethyl-3-pentanone (Aldrich, 98%), 2,2,4,4-tetramethyl-3-pentanone (Sigma-Aldrich, 98%), pinacolone (Aldrich, 98%), and dicyclopropyl ketone (Aldrich, 98%) were distilled from calcium sulfate ($CaSO_4$). Cyclopentanone (Aldrich, 99%) was distilled from magnesium sulfate ($MgSO_4$). Camphor (Sigma-Aldrich, 96%), norcamphor (Lancaster, 98%), and 2-adamantanone (Sigma-Aldrich, 99%) were purified by sublimation. Lithium wire (Sigma-Aldrich, 98%) and potassium (J. T. Baker) were freshly cut and washed with dry hexanes prior to use. Potassium hydroxide (Caledon), sodium chloride (Caledon), iodomethane (Sigma-Aldrich, 99%), cyclopentanone (Aldrich, 99%), 2-indanone (Aldrich, 98%), and acetone-d_6 (Cambridge Isotope) were used as received from the suppliers. Dichlorodimesitylsilane and chlorotrimethylsilane were used as received from Gelest, Inc.

5.4. Laser Flash Photolysis

Laser flash photolysis experiments were carried out using a Lambda Physik Compex 120 excimer laser filled with F_2/Kr/Ne (248 nm, 20 ns, 40 – 100 mJ) and a Luzchem Research mLFP-111 laser flash photolysis system, modified as described previously.[6] Solutions of silylene precursors were prepared in deoxygenated anhydrous hexanes such that the absorbance at the excitation wavelength (248 nm) was between 0.4 and 0.7. The solutions were flowed through a 7 × 7 mm Suprasil flow cell connected to calibrated 100 mL or 250 mL reservoirs, which contain a glass frit to allow bubbling of argon gas through the solution for 30 mins prior to and throughout the experiment. The flow cell was connected to a Masterflex^{TM} 77390 peristaltic pump fitted with Teflon tubing (Cole-Parmer Instrument Co.) which pulls the solution through the cell at a constant rate of 2 - 3 mL/min. The reservoirs were flame-dried under an atmosphere of nitrogen, while the sample cell and transfer lines were dried in a vacuum oven (55 – 75^{o}C) and vented with dry nitrogen before use. For experiments at 25^{o}C, solution temperatures were measured with a Teflon-coated copper/constantan thermocouple inserted into the thermostated sample compartment in close proximity to the sample cell. Variable temperature experiments were carried out using a modified flow cell that allowed insertion of the Teflon-coated copper/constantan thermocouple directly into the sample solution. Substrates were added directly to the reservoir by microliter syringe as aliquots of standard solutions.

Transient absorbance-time profiles were recorded by signal-averaging of data obtained from 10 – 20 individual laser shots. Decay rate coefficients were calculated by

nonlinear least-square analysis of the transient absorbance-time profiles using the Prism 7.0 software package (GraphPad Software, Inc.) and the appropriate user-defined fitting equations, after importing the raw data from the Luzchem mLFP software. Rate constants were calculated by linear or non-linear least-squares analysis of transient absorbance data that spanned as large a range in transient decay rate coefficient or initial signal intensity as possible. Errors are reported as twice the standard error obtained from the least-square analysis.

5.5. Steady State Photolysis

Steady-state photolysis experiments were carried out using a Rayonet photochemical reactor (Southern New England Ultraviolet Co.) equipped with two RPR-2537 lamps (254 nm) and a merry-go-round apparatus and were monitored periodically at selected time intervals by 600 MHz ^{1}H NMR spectroscopy. Cyclohexane-d_{12} solutions containing the desired combinations of silylene precursor, substrate, and bis(trimethylsilyl)methane (*ca.* 0.01 M; internal integration standard) were prepared in 1 mL volumetric flasks. Portions of the solutions were transferred to quartz NMR tubes, deoxygenated with a slow stream of dry argon gas for *ca*. 10 mins, and the tubes were sealed with an NMR tube cap. Irradiation were carried out over a total time period of *ca.* 30 – 60 mins, with regular monitoring of the photolysates by ^{1}H NMR spectroscopy. Product yields were calculated from the relative initial slopes of the concentration versus time plots for the products relative to the silylene precursor.

5.6. Synthesis

5.6.1. Synthesis of 2,2-Dimesityl-1,1,1,3,3,3-hexamethyltrisilane

2,2-Dimesityl-1,1,1,3,3,3-hexamethyltrisilane (**3**) was synthesized as reported previously, by coupling dichlorodimesitylsilane with chlorotrimethylsilane using lithium metal in dry THF.[5] A flame-dried three-neck round bottom flask was fitted with a stir bar, condenser, addition funnel, and gas inlet and placed under an argon atmosphere. The flask was charged with dry THF (15 mL) and lithium wire, cut into small pieces directly into the reaction vessel. The solution was cooled with an ice bath and chlorotrimethylsilane (1.4 mL, 11.03 mmol) was added into the reaction mixture via a gas-tight syringe. A solution of dichlorodimesitylsilane (1.49 g, 4.42 mmol) in 15 mL of dry THF was added through the addition funnel over 1 hr. The ice bath was removed, and the mixture was stirred for an additional 2 hrs. The progress of the reaction was evidenced by the discoloration of the metal surface. The THF solution was decanted from the unreacted lithium metal, and the solvent was removed on the rotary evaporator, leaving behind a white solid. Hexanes (100 mL) was added to the flask, resulting in a white suspension, followed by the addition of water (50 mL). The solution was transferred to a separatory funnel and the organic and aqueous layers were separated. The aqueous layer was washed twice with hexanes, followed by washing the combined organic extracts with water (2 × 15 mL) and brine (15 mL), resulting in a clear yellow solution. The solution was dried over sodium sulfate, filtered, and the solvent was removed on the rotary evaporator to afford **3** as a white solid (3.29 g, 75%). Further purification was done by column chromatography on silica gel

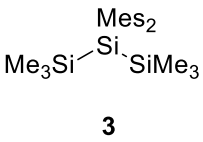

3

using hexanes as the eluent, followed by recrystallization from hexanes to yield colourless plates. ^{1}H NMR (C_6D_6): δ 2.03 (s, 6 H), 2.08 (s, 6 H), 2.31 (s, 12 H), 2.53 (s, 12 H), 6.55 (s, 4 H), 6.55 (s, 4 H), 6.70 – 6.90 (m, 6 H), 7.50 – 7.70 (m, 4 H). m.p. 170 – 172°C. lit. m.p. 174 - 176°C.[5]

5.6.2. Synthesis of Camphor-3,3-d_2

Camphor-3,3-d_2 (**4**) was synthesized according to the reported procedure.[7] A solution of dioxane (30 mL) and D_2O (50 mL, 2.77 mol) was prepared under an argon atmosphere. Na metal (1.08 g, 46.9 mmol), cut into small pieces, was added into the reaction vessel. After the Na had reacted, camphor (5.94 g, 39.02 mmol) was added to the solution, which was then stirred at 50°C for 144 hrs and then cooled to ambient temperature. Brine (30 mL) and ether (30 mL) were added to the resulting solution and the aqueous layer was separated and extracted with ether (3 × 30 mL). The combined organic extracts were washed with brine (30 mL) and dried over $MgSO_4$. The solvent was removed on the rotary evaporator to afford a white solid, which was recrystallized from 50% ethanol/water. The resulting crystals were sublimed at 50°C (0.5 mm Hg) to afford pure camphor-3,3-d_2. ^{1}H NMR ($CDCl_3$): δ 0.83 (s, 3 H), 0.91 (s, 3 H), 0.96 (s, 3 H), 1.38 (m, 2 H), 1.68 (m, 1 H), 1.95 (m, 1 H), 2.07 (d, 1 H).

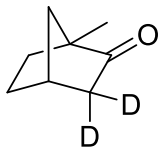

4

5.6.3. Synthesis of 2,2,5,5-Tetramethylcyclopentanone

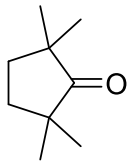

5

2,2,5,5-Tetramethylcyclopentanone (**5**) was synthesized following the reported procedure.[8] A 250 mL two-neck round bottom flask was fitted with a stir bar, condenser, gas inlet, and an addition funnel. KOH pellets (28.23 g, 0.50 mol) and DMSO (50 mL) were added to the reaction vessel, which was then heated to 50 – 60ºC in an oil bath. A mixture of cyclopentanone (1.90 g, 0.023 mol) and iodomethane (27.4 g, 0.19 mol) was added into the reaction vessel through the addition funnel, and the resulting mixture was then stirred at 50 – 60ºC for *ca.* 2 hrs. The colour of the solution gradually turned dark red upon addition of the cyclopentanone and iodomethane, and then slowly faded to a pale orange colour. The reaction was monitored by GC/MS, using *ca. 0.5* mL aliquots of the reaction mixture which were worked up by adding water (*ca.* 2 mL) and hexanes (*ca.* 2 mL), separation of the organic layer followed by drying over $MgSO_4$, and filtering prior to injection. Upon completion of the reaction, the mixture was transferred to an Erlenmeyer flask containing ice water (50 mL), which was then extracted with pentane (3 × 50 mL). The combined organic extracts were washed with water (2 × 50 mL), and then dried over $MgSO_4$. The solvent was removed on the rotary evaporator to afford a pale-yellow oil (4.02 g). The product was purified by column chromatography on silica gel using a gradient of hexanes to 50% DCM in hexanes, followed by vacuum distillation using a water aspirator, and obtained as a colourless oil (2.59 g, 0.018 mol, 80%). ^1H NMR ($CDCl_3$): δ 1.04 (s, 12 H), 1.77 (s, 4 H); b.p. 60 – 62ºC (48 Torr), lit. b.p. 38 – 39ºC (12 Torr).[8]

5.6.4. Synthesis of 1,1,3,3-Tetramethyl-2-indanone

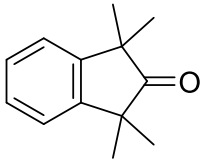

6

1,1,3,3-Tetramethyl-2-indanone (**6**) was synthesized according to the reported procedure.[8] A 100 mL two-neck round bottom flask was fitted with a stir bar, condenser, gas inlet, and an addition funnel. KOH pellets (10.10 g, 180 mmol) and DMSO (30 mL) were added to the reaction vessel, which was then heated to 50 – 60°C. 2-Indanone (1.00 g, 7.57 mmol) and iodomethane (9.12 g, 64.3 mmol) were added dropwise over *ca.* 30 mins, resulting in a dark red mixture which was stirred at 50 – 60°C for an additional 2 hrs. The reaction was monitored by GC/MS, using a similar workup procedure to that derived above for **5**. The pale orange solution was cooled and then transferred to an Erlenmeyer flask containing ice water (20 mL), which was then extracted with pentane (3 × 20 mL). The combined organic extracts were washed with water (2 × 20 mL) and then dried over $MgSO_4$. The solvent was removed on the rotary evaporator to afford a yellow solid (0.82 g). The product was isolated by column chromatography on silica gel using a gradient of hexanes to 50% DCM in hexanes, and further purified by recrystallization from hexanes to yield white crystalline plates (0.44 g, 31%). ^{1}H NMR ($CDCl_3$): δ 1.34 (s, 12 H), 1.55 (s, 4 H), 7.26 – 7.31 (m, 4 H); m.p. 60 – 62°C, lit. m.p. 60 – 62°C.[8]

5.6.5. Synthesis of 2',2'-Dimesityl-1,1,3,3-tetramethyl-1,3-dihydrospiro[indene-2,3'-[1,2]oxasilirane (**7**)

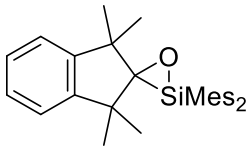

7

Compound **7** was prepared by using a modified version of the reported procedure.[9] A solution of 2,2-dimesityl-1,1,1,3,3,3-hexamethyltrisilane (**3**: 100 mg, 0.24 mmol) and 1,1,3,3-tetramethyl-2-indanone (**6**: 66 mg, 0.35 mmol) in cyclohexane-d_{12}, was prepared in a 2 mL volumetric flask. The solution was divided between two quartz NMR tubes, which were then purged with a slow stream of dry argon gas for *ca.* 10 mins. The solution was photolyzed in the photochemical reactor, equipped with 2 × 254 nm lamps and a merry-go-round apparatus, for *ca.* 5 hrs. The solvent was removed by vacuum distillation and the resulting solid was recrystallized twice from distilled hexanes, affording colourless crystalline plates (40.3 mg, 0.089 mmol, 36%). ^{1}H NMR ($CDCl_3$): δ 1.03 (s, 6 H), 1.41 (s, 6 H), 2.27 (s, 6 H), 2.75 (s, 12 H), 6.85 (s, 4 H), 7.09 (m, 2 H), 7.17 (m, 2H); ^{29}Si NMR ($CDCl_3$): δ -51.0.; m.p. 200 – 203ºC, lit. m.p. 202.5 – 203.5ºC.

5.6.6. Synthesis of 3,5-Diadamantyl-2,4-dioxa-1,1-diphenylsilacyclopentane (**8**)

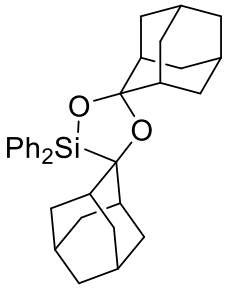

8

The synthesis of **8** was prepared by a modification of the reported procedure.[10] A solution of 1,1,3,3-tetramethyl-2-2-diphenyl-1,2,3-trisilacyclohexane (**2**, 40.8 mg, 0.12 mmol) and 2-adamantanone (44.5 mg, 0.30 mmol) in cyclohexane was prepared in a 1 mL volumetric flask. The solution was transferred to a quartz tube and purged with a slow stream of dry argon for 10 mins. The solution was irradiated in the photochemical reactor, equipped with 2 × 254 nm lamps

and a merry-go-round apparatus, for *ca.* 60 mins. The progress of the reaction was monitored by TLC. The product was isolated by silica gel column chromatography using 100% distilled hexanes as the eluent, and then recrystallized from methanol to yield colourless crystalline plates (23.9 mg, 0.050 mmol, 44%). m.p. 115 – 121ºC. Compound **6** was identified on the basis of its ^{1}H, ^{13}C, ^{29}Si, and mass spectra. ^{1}H NMR ($CDCl_3$): δ 1.43 (d, 2, ^{3}J = 12.2 Hz), 1.59 – 1.83 (m, 16H), 1.99 (d, 4, ^{3}J = 12.6 Hz), 2.26 (d, 2, ^{3}J = 12.0 Hz), 2.31 (d, 2, ^{3}J = 12.6 Hz), 2.40 (d, 2, ^{3}J = 12.0 Hz), 7.40 (m, 6), 7.82 (d, 2); ^{13}C NMR ($CDCl_3$): δ 26.9 (s, CH), 27.3 (s, CH), 27.4 (s, CH), 27.5 (s, CH), 35.3 (s, CH_2), 35.9 (s, CH), 36.9 (s, CH_2), 37.7 (s, CH_2), 37.8 (s, CH_2), 41.8 (s, CH) , 80.5 (s, Si-C-O), 101.0 (s, O-C-O), 127.9 (s, aromatic C), 130.2 (s, aromatic C), 133.3 (s, aromatic C), 135.4 (s, aromatic C). ^{29}Si NMR ($CDCl_3$): δ 0.17. m.p. 80.4 – 89.2ºC. ESI-MS, m/z (relative intensity): 483.27 (100, M^+), 333.17 (11), 199.06 (37), 123.09 (13). HRMS: ($C_{32}H_{38}O_2Si$): calc.: 483.2714, found: 483.2709.

5.6.7. Synthesis of 2,2-Dimesityl-4,4,7,7-tetramethyl-1-oxa-2silaspiro[2.4]heptane (**9**)

A solution of 2,2-dimesityl-1,1,1,3,3,3-hexamethyltrisilane (**3**: 250.0 mg, 0.61 mmol) and 2,2,5,5-tetramethylcyclopentanone (**5**: 135.2 mg, 0.97 mmol) in dry cyclohexane (5 mL) was prepared in a 5 mL volumetric flask. The solution was transferred to a quartz tube, which was then purged with dry argon for 10 mins. The solution was irradiated in the photochemical reactor, equipped with 2 × 254 nm lamps and a merry-go-round apparatus, for 4 hrs monitoring by TLC. The product was isolated by radial thick-layer

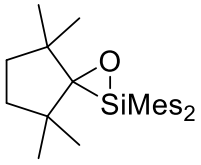

9

chromatography, using the chromatotron with a 1 mm basic alumina plate, and distilled hexanes as the eluent. The product was recrystallized from methanol to yield a colourless crystalline needles (14.3 mg, 0.035 mmol, 6%). m.p. 142 – 145ºC. Compound **9** was identified on the basis of its ^{1}H, ^{13}C, ^{29}Si, mass spectra, and by X-ray crystallography. ^{1}H NMR ($CDCl_3$): δ 0.75 (s, 12H), 1.14 (s, 12H), 1.54 (m, 4H), 1.65 (m, 4H), 2.23 (s, 12H), 2.65 (s, 12H), 2.70 (s, 12H), 6.79 (d, 8H); ^{13}C NMR 14.3/100($CDCl_3$): δ 21.3 (s, *p*-CH_3), 23.4 (s, *o*-CH_3), 26.7 (s, CH_3), 27.0 (s, *o*-CH_3), 29.4 (s, CH_3), 40.7 (s, CH_2), 46.0 (s, $\underline{C}(CH_2)C(CH_3)_2$), 89.4 (s, Si-$\underline{C}$-O), 128.3 (s, *m*-$CH_2$), 129.3 (s, *m*-$CH_2$), 129.3 (s, Si-$\underline{C}$-$C_2$), 140.1 (s, *p*-$\underline{C}(CH_3)C_2$), 143.1 (*o*-$\underline{C}(CH_3)C_2$), 145.4 (*o*-$\underline{C}(CH_3)C_2$). ^{29}Si NMR ($CDCl_3$): δ -51.1ºC. EI-MS, m/z (relative intensity): 406.27 (M+, 15), 391.25 (30), 283.15 (60), 251.1 (75), 146.05 (100). (HRMS: ($C_{27}H_{38}OSi$): calc.: 406.2692, found: 406.2683.

Crystal Data for $C_{27}H_{38}OSi$ (M = 406.66 g/mol): monoclinic, space group $P2_1/c$ (no. 14), a = 14.6595(11) Å, b = 17.9072(13) Å, c = 19.2722(15) Å, β = 105.620(5)°, V = 4872.3(6) $Å^3$, Z = 8, T = 100.0(1) K, μ(MoKα) = 0.111 mm^{-1}, *Dcalc* = 1.109 g/cm^3, 158648 reflections measured (2.884° ≤ 2Θ ≤ 56.564°), 12097 unique (R_{int} = 0.0629, R_{sigma} = 0.0357) which were used in all calculations. The final R_1 was 0.0545 (I > 2σ(I)) and wR_2 was 0.1408 (all data).

5.7. Compounds Identified *in-situ*

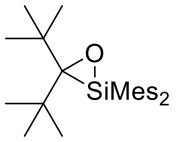

10

3,3-Di-*tert*-butyl-2,2-dimesityl-1,2-oxasilirane (**10**): ^{1}H NMR (C_6D_{12}): δ 1.10 (s, 18H), 2.13 (s, 6H), 2.59 (s, 6H), 2.62 (s, 6H). The protons on the *meta*-position of the mesityl ring could not be resolved.; ^{13}C NMR (C_6D_{12}): δ 21.2 (s, *p*-CH_3), 23.3 (s, *o*-CH_3), 26.8 (s, *o*-CH_3), 32.0 (s, -CH_3), 40.8 (s, -$\underline{C}(CH_3)$), 86.6 (s, Si-$\underline{C}$-O), 128.7 (s, *m*-CH), 129.7 (s, *m*-CH), 135.1 (s, Si-$\underline{C}$-C_2), 139.3 (s, *p*-$\underline{C}(CH_3)C_2$), 142.2 (s, *o*-$\underline{C}(CH_3)C_2$), 144.6 (s, *o*-$\underline{C}(CH_3)C_2$).; ^{29}Si NMR (C_6D_{12}): δ -47.6.

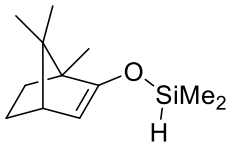

11

Dimethyl(((1S,4S)-1,7,7-trimethylbicyclo[2.2.1]hept-2-en-2-yl)oxy)silane (**11**): ^{1}H NMR (C_6D_{12}): δ 0.22 (dd, 6H), 0.73 (s, 3H), 0.89 (s, 6H), 1.11 (m, 2H), 1.49 (m, 1H), 1.84 (m, 1H), 2.17 (t, 1H), 4.65 (d, 1H), 4.77 (septet, 1H, ^{3}J = 2.8 Hz); ^{13}C NMR (C_6D_{12}): δ -1.5 (s, Si($\underline{C}H_3)_2$), 10.1 (s, -CH_3), 20.1 (s, -CH_3), 20.5 (s, -CH_3), 28.0 (s, -CH_2), 31.9 (s, -CH_2), 50.5 (s, -CH), 54.0 (s, -$\underline{C}(CH_3)(CH_2)(C)_2$), 55.7 (s, -$\underline{C}(CH_3)_2(C)_2$), 103.3 (s, -$\underline{C}$H(CHC2)(COC)), 161.9 (-$\underline{C}$O(CH)(C)); ^{29}Si NMR ($C_6D_{12}$): δ 3.1.

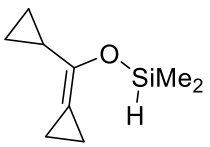

12

(Cyclopropyl(cyclopropylidene)methoxy)dimethylsilane (**12**): ^{1}H NMR (C_6D_{12}): δ 0.18 (m, 6H), 0.45 (m, 4H), 1.00 (m, 4H), 1.60 (m, 1H), 4.87 (septet, 1H, ^{3}J = 2.8 Hz); ^{29}Si NMR (C_6D_{12}): δ 1.6.

2,2,5-Trimethyl-4-hexenal (**13**): ^{1}H NMR (C_6D_{12}): δ 1.58 (s, 6H), 1.68 (s, 6H), 2.10 (d, 2H), 5.06 (t, 1H), 9.38 (s, 1H).

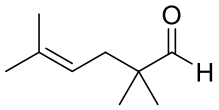

13

5.8. References

1. Dolomanov, O. V.; Bourhis, L. J.; Gildea, R. J.; Howard, J. A. K.; Puschmann, H., *Journal of Applied Crystallography* **2009,** *42* (2), 339-341.
2. Sheldrick, G., *Acta Crystallographica Section A* **2015,** *71* (1), 3-8.
3. Sheldrick, G., *Acta Crystallographica Section A* **2008,** *64* (1), 112-122.
4. Moiseev, A. G.; Leigh, W. J., *Organometallics* **2007,** *26*, 6268-6276.
5. Ishikawa, M.; Yamanaka, T.; Kumada, M., *J. Organomet. Chem.* **1985,** *292*, 167-176.
6. Leigh, W. J.; Harrington, C. R.; Vargas-Baca, I., *J. Am. Chem. Soc.* **2004,** *126*, 16105-16116.
7. Huffman, J. W.; Wallace, R. H., *J. Am. Chem. Soc.* **1989,** *111*, 8691-9698.
8. Langhals, E.; Langhals, H., *Tet. Lett.* **1990,** *31* (6), 859-862.
9. Ando, W.; Hamada, Y.; Sekiguchi, A.; Ueno, K., *Tet. Lett.* **1982,** *23* (50), 5323-5326.
10. Ando, W.; Ikeno, M.; Sekiguchi, A., *J. Am. Chem. Soc.* **1978,** *100* (11), 3613-3615.